

The effect of neutral nonresonant collisions on atomic spectral lines

Nicole Allard

Section d'Astrophysique, Observatoire de Paris, 92190 Meudon, France

John Kielkopf

Department of Physics, University of Louisville, Louisville, Kentucky 40292

The effect of neutral nonresonant collisions on the shape, shift, and intensity of atomic spectral-line profiles is reviewed. A general treatment for the study of an atomic spectral line is developed by establishing reasonable assumptions about the relevant collision processes and by finding an expression for the Fourier transform of the line profile. The authors look at parallel developments of other methods of calculation, consider special limits of practical interest, and illustrate numerical evaluations of complete line profiles. Interatomic potentials for use in line-profile calculations are described, and the problems imposed by nonadditivity and nonadiabaticity are also noted. The observation of line profiles by both conventional and tunable-laser techniques is surveyed. Representative experimental measurements of the widths and shifts of collision-broadened spectral line cores are tabulated, and the phenomena of satellites, oscillations, and power-law behavior of line wings are compared with theoretical expectations. The use of experimental results for the determination of excited atom-atom interactions, the prediction of collision broadening in stellar atmospheres, and the effect of foreign gases on laboratory standard wavelengths are also discussed.

CONTENTS

I. Introduction	1104
II. The Theory of the Broadening of Atomic Spectral Lines by Neutral-Atom Collisions	1105
A. The development of statistical and impact theories	1105
1. Wave trains of infinite extension	1105
2. Wave trains of finite extension	1106
3. Wave trains of finite but mixed extension	1106
4. Inclusion of the phase shift	1106
5. The quasistatic approach	1107
6. A molecular approach to line profiles: statistics and quantum mechanics	1108
7. The synthesis of phase-shift and molecular theories	1110
B. General theory of line broadening in the semiclassical model	1110
C. Quantum theories of line broadening	1112
1. The classical path approximation	1112
a. The spectrum and the correlation function	1112
b. The calculation of the correlation function with time-evolution and density operators	1113
c. Separation of perturbers and the emitter	1113
d. The calculation of $d(s)$	1114
e. The angular average and the calculation of $\Phi(s)$	1114
f. Conditions of validity for the unified theory	1116
g. Breakdown of the classical path approximation	1117
2. An alternative formulation	1118
3. Nonadiabatic processes	1118
a. Fine-structure mixing	1119
b. Symmetry properties of the Hamiltonian and associated operators	1119
c. The choice of representation: Hund's cases	1120
d. An example: Hund's case C applied to the resonance lines of cesium perturbed by xenon	1120
4. Solutions to the general problem of the frequency redistribution of radiation	1123
D. Interatomic potentials for line-broadening calculations	1124
1. Van der Waals interactions	1124
2. Analytic additions to the van der Waals term	1126
3. The Fermi potential	1127
4. Pseudopotentials	1127
E. Evaluation of general line-shape theories	1134
1. Analytical methods and approximations	1134
a. Anderson's analytical formulas	1134
b. Approximate evaluation with the method of Behmenburg	1134
c. Approximate evaluations by Hindmarsh and Farr	1135
2. Numerical methods	1135
a. Atakan, Fox, and Jacobson	1135
b. Takeo	1136
c. Allard	1137
d. Kielkopf	1139
F. Special cases and useful limits	1141
1. JWKB methods	1141
2. Molecular dynamics simulation	1143
3. Density expansions	1143
4. The one-perturber spectrum and line-wing temperature dependence	1144
5. Impact broadening: analytical and tabulated calculations	1145
6. Comments on the validity of limiting approximations	1146
a. On the use of the impact approximation	1147
b. On the use of the static theory	1147
7. Collisional effects on high series members and the effect of high gas density	1147
III. Experiments	1149
A. Conventional spectroscopy	1149
1. Dispersive spectroscopy	1150
2. New developments in detectors	1151
3. Sources for line-shape spectra	1151

a. Absorption spectroscopy	1151
b. Emission spectroscopy	1153
c. Fluorescence spectroscopy	1153
d. Shock-tube spectroscopy	1153
B. Laser spectroscopy and neutral collision broadening	1153
C. Deconvolution	1155
1. Methods of deconvolution	1156
2. Calculation of the Voigt function	1156
3. Deconvolution of Fabry-Perot response	1157
4. Deconvolution of asymmetry	1157
5. Problems concerning the correlation of Doppler and collision broadening	1157
D. Line cores	1158
1. Observations for low foreign-gas density	1159
a. Shift and width	1159
b. Observations of line asymmetries at low density	1159
c. High series members	1159
2. High-density measurements of line cores	1164
a. Low-lying states	1164
b. High Rydberg states	1166
E. Line wings	1166
1. Frequencies near the unperturbed line center	1166
a. The shape of the near wing	1166
b. Intense satellites in binary spectra	1168
c. Multiple-perturber spectra	1169
2. Frequencies far from the line center	1170
3. Observations of oscillations	1172
F. Collision-induced changes in transition probability	1172
1. Effects on allowed transitions	1172
2. Effects on forbidden transitions	1173
G. Radiative redistribution experiments	1174
IV. Applications of Line-Shape Studies to Specific Problems	1174
A. Determination of interatomic potentials	1174
B. Neutral-atom line broadening in stellar atmospheres	1175
C. The problem of practical wavelength standards and pressure shifts	1176
Acknowledgments	1177
References	1177

I. INTRODUCTION

Atomic spectral lines as we actually observe them are rarely sharp, symmetric, or centered on the exact energy-level difference for the isolated atomic states. The causes for the distribution of radiation in an atomic transition have been a subject of study at least since Michelson's work before the turn of the century. Through analyses of spectra of absorption cells, electrical discharges, flames, and the sun and stars it has been possible to distinguish the effects of the Doppler shift due to atomic motion relative to the observer, the influence of external fields and local electric fields due to ions and electrons, the resonant interaction of one atom with another of the same kind, and the collisions with dissimilar perturbers. This review is concerned primarily with this last category: the effect of nonresonant neutral collisions on atomic spectra.

Many reviews of the subject have appeared documenting the progress made since the early visual observations and speculations about competing processes gave way to progressively more elaborate measurements and precise theoretical analyses. The first was written by Weisskopf

(1933), and it was soon followed by the work of Morgenau and Watson (1936). Others of greater interest for us now include the comprehensive treatment of experimental and theoretical work due to Ch'en and Takeo (1957), the theoretical reviews of Breene (1957, 1961), a short book by Traving (1960), and the readable survey by Hindmarsh and Farr (1972). Although recently articles by Schuller and Behmenburg (1974) and Behmenburg (1979) have appeared, the review of Ch'en and Takeo (1957) provides the most thorough coverage of early experimental results. The substantial changes apparent in both theoretical and experimental work of the last decade are not at all completely described in the review literature. We have written this article in order to fill this void and to offer our own view of the present situation in neutral-atom line-broadening problems.

We have made no attempt here to include resonance broadening, an area in which activity is not too great at present, or Stark broadening. The latter is well treated in Griem's books (1964, 1974). Nor do we discuss Doppler broadening except in the context of its combined effect with collision broadening. Our primary emphasis is on the treatment of the complete line profile, both from an experimental and from a theoretical viewpoint. Consequently the subject of impact broadening and depolarization, as treated most recently by Lewis (1980), is not isolated for special consideration.

Our treatment is in part intended to be pedagogical, so that a student or someone who is not currently working in the area can obtain a reasonable overview of recent accomplishments, while an experimentalist can turn to the theoretical discussions to get some practical hints on the comparison of his results with realistic calculations, and the theoretician can get an exposure to interesting experimental techniques and recent results. For more specialized treatments, particularly of the finer points of theoretical discussions, we refer the reader to the original literature. In this regard we point out the existence of a very comprehensive bibliography (Fuhr, Wiese, and Roszman, 1972–1978) that is reasonably well indexed.

Because so many of the earlier reviews have gone through extensive historical surveys [this is particularly true of Breene, (1961)], we would rather begin by looking at the broad interrelationships between the distinctly different ideas that have led to present-day efforts. In Fig. 1 we trace the development of unified line-profile theories, their evaluation through numerical calculation, analytical techniques as in the unified Franck-Condon method, series expansions, or the special limits of the impact core and statistical wing. There is a fairly new technique of molecular dynamics simulation, and also recent work in the closely related area of the collisional redistribution of radiation, that shows some promise. The old controversy between the JWKB methods of Jablonski and the Fourier analyses of Lenz found common ground first in the classical analysis of Anderson (1952) and subsequently in the quantum treatment of Baranger (1958a, 1958b, 1958c, 1962). Since then evaluations by several methods have found general broad agreement with experimental results, although the last step between

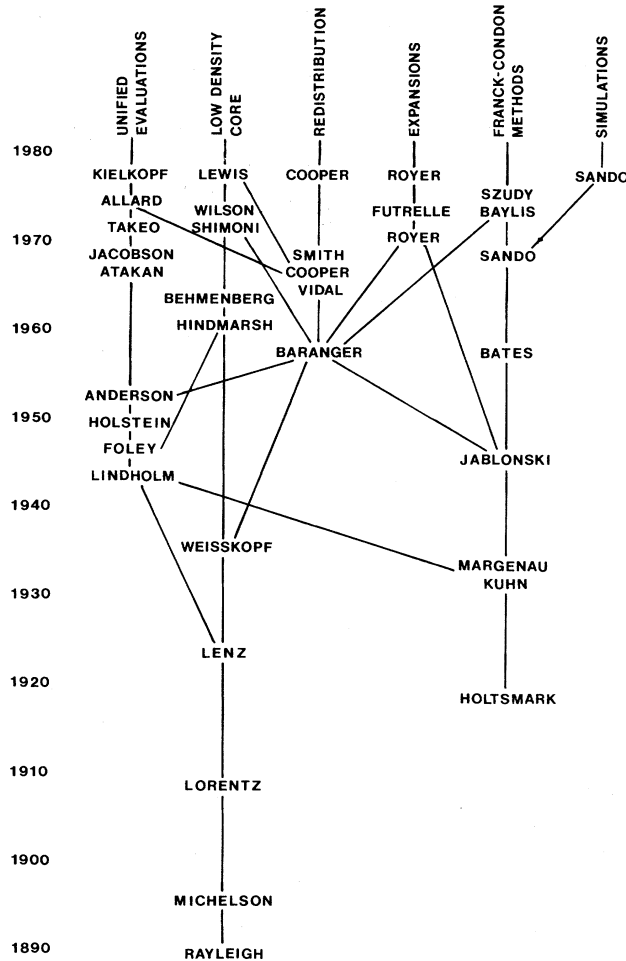


FIG. 1. Historical connections between current trends in theories of neutral-atom line broadening.

the formal theory and its comparison with observation remains the most crucially difficult, with an imposing blockade due to the uncertainty about neutral-atom interaction potentials.

It is our viewpoint that from among the options that are available, albeit some quite elegant, the most suitable for a general treatment is a study of the spectral line through its Fourier transform. So in the calculations of the second section it will be our purpose to establish first of all a set of reasonable assumptions about the collision processes that determine the profile of an atomic line, and from them to find an expression for the Fourier transform of the line profile, that is for the correlation function. Within the limits imposed by our assumptions, the expression we obtain will be exact. With care it can be evaluated in a number of cases of practical interest. At the same time we shall look at parallel developments of other methods of calculating line profiles and examples of some of the results.

In the third section we survey the recent developments in experimental methods, including laser spectroscopy and new technologies in classical spectroscopy. These

methods have made possible the observation of a wealth of phenomena from the line core to the far wing, at high and low densities of foreign gas. In the final section we look at the problems involved in the application of these studies to the determination of interatomic potentials from the observed profiles, and to the measurement of abundances in stellar atmospheres.

In the theoretical discussion that follows we use angular frequency units (radians sec⁻¹), but in the experimental work it is much more convenient to use a wave-number scale (cm⁻¹) for both frequency and potential energy. The conversion factor is $\bar{\nu} = \omega / 2\pi c$. Atomic densities n are usually given in units of atoms cm⁻³, but some of the literature refers to units of relative density (so-called r.d.). A conversion can be made through Loschmidt's number; one r.d. is 2.687×10^{19} atoms cm⁻³. A final problem with nomenclature is in the use of the terms "half-width," "half-width at half maximum," sometimes abbreviated HWHM, and "full width at half maximum," or FWHM. We shall always mean the full width at half maximum intensity when we discuss the linewidth, and the half-width at half maximum intensity when we discuss the line half-width.

II. THE THEORY OF THE BROADENING OF ATOMIC SPECTRAL LINES BY NEUTRAL-ATOM COLLISIONS

... experiment has shown that in every case thus far examined the width of the spectral lines diminish[es] with the pressure in an approximately linear proportion towards a constant limiting value.

—Michelson, 1895

A. The development of statistical and impact theories

1. Wave trains of infinite extension

If we consider the picture of a simplified atom with two levels E_i and E_f between which a radiative transition takes place, we would expect the emission spectrum of this atom to have a single line with frequency ω_0 determined by the energy difference

$$\omega_0 = (E_i - E_f)/\hbar. \quad (1)$$

The radiation will be monochromatic if the radiative process is not terminated, and the time dependence of the emitted light will be given by an amplitude

$$f(t) = \text{Re}[f_0 \exp(-i\omega_0 t)]. \quad (2)$$

The power spectrum

$$I(\omega) \propto |\int f(t) \exp(i\omega t) dt|^2, \quad (3)$$

is the square of the Fourier transform of the amplitude, and is sharply peaked at $\omega = \omega_0$ for the infinite wave train of Eq. (2). This relationship between the time-dependent amplitude and the spectrum is illustrated in

Fig. 2. We never actually observe this behavior, of course, because the wave train is interrupted by collisions between the radiator and other atoms in its environment. It is specifically the effect of these collisions on the time dependence of the radiation and on the power spectrum that is the subject of this review.

2. Wave trains of finite extension

One of the earliest contributions on the subject of line broadening was written by Michelson (1985), and its appearance in the *Astrophysical Journal* illustrates that studies of these processes have useful applications beyond the bounds of fundamental physics. The approach outlined by Michelson also contains the essential elements of most of the modern theories, for he recognized the utility of describing the line profile in terms of its Fourier transform.

Michelson's model was of billiard ball atoms that encounter hard collisions: a collision between the radiator and the perturber was assumed to have taken place when the separation between them had become less than or equal to the sum of their mean atomic diameters. If τ is the time between two collisions, then it is also the time during which radiation continues. Thus we have a wave train of finite length $c\tau$, where c is the speed of light, and the emitted radiation is now described by

$$f(t) = \text{Re}[f_0 \exp(-i\omega_0 t) \Theta(\tau - |t/2|)], \quad (4)$$

where $\Theta(x)$ is a step function equal to unity for $x > 0$, and equal to zero otherwise. The power spectrum given by the square of the Fourier transform is proportional to

$$I(\omega) \propto \left[\frac{\sin[\tau(\omega - \omega_0)/2]}{(\omega - \omega_0)/2} \right]^2. \quad (5)$$

The width of this spectral line is just proportional to the inverse $1/\tau$ of the time between collisions, but the line is unshifted from its natural frequency.

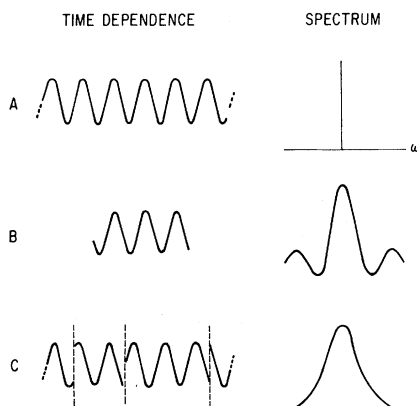


FIG. 2. Line profiles from different wave trains: (a) infinite duration; (b) finite duration; (c) interruption with a Poisson distribution of durations.

3. Wave trains of finite but mixed extension

In this first simple approach all the wave trains had the same length and phase, but Lorentz (1906) considered the atom as a classical charged oscillator in collision with a perturber and investigated the probability distribution for the times between collisions. He imposed a distribution with a mean time between collisions τ_c such that

$$P(\tau)d\tau = \exp(-\tau/\tau_c)d\tau/\tau_c \quad (6)$$

is the probability that the time since the last collision is between τ and $\tau + d\tau$. The spectrum of Eq. (5) is averaged with the weighting probability of Eq. (6) to give an integral proportional to

$$I(\omega) \propto \int_0^\infty \left[\frac{\sin[\tau(\omega - \omega_0)/2]}{(\omega - \omega_0)/2} \right]^2 \exp(-\tau/\tau_c)d\tau \quad (7)$$

or the familiar Lorentzian profile

$$I(\omega) \propto \frac{1}{(\omega - \omega_0)^2 + (1/\tau_c)^2}. \quad (8)$$

4. Inclusion of the phase shift

The radiation emitted from an atom is changed by the force field of a neighboring atom. Frequency and amplitude are therefore no longer constant in time.... The change is so great, however, that the phase of the vibration after the collision is no longer the same as it would have been had there been no collision.

—Weisskopf, 1933

A different interpretation was introduced by Lenz (1924, 1933) and by Weisskopf (1932a, 1932b, 1933) when they recognized that a complete interruption of the wave train was not necessary to produce a broadening of the line. In earlier approaches the frequency of radiation was considered constant and the collision terminated the radiation process. Actually, the perturbers act over a long distance, and the frequency of the emitted radiation gradually changes with the approach of the perturber. The instantaneous frequency may be described by

$$\omega(t) = \omega_0 + \frac{d\eta}{dt} \quad (9)$$

when ω_0 is the frequency in the absence of any perturbing forces, while the remaining term in η is due to the change in phase of the oscillation from the interaction of the radiator with its surroundings. For Weisskopf, the collision starts when the phase of the emitted radiation has changed by unity. This arbitrary definition forms one of the bases for the interruption theory. The line in this case also has a Lorentzian profile with a width determined by $1/\tau_c$, but τ_c is now the mean time between optical collisions, those for which the phase change exceeds one radian.

Following Lenz, Lindholm (1945) took into account the phase shifts in the initial state, considering them to

be linearly increasing functions of time during the collision. He neglected the radiation that occurred during the collision, but included the effects of weak distant collisions that produce a shift as well as broadening of the line, assuming, moreover, that there is no phase correlation before or after the collision. The profile found by Lindholm was a shifted Lorentzian,

$$I(\omega) = \frac{\gamma/\pi}{(\omega - \omega_0 - \sigma)^2 + \gamma^2}, \quad (10)$$

where the shift σ and the half-width γ are determined from the collisional phase shifts. In addition to this dominant term, Lindholm confirmed the result of Lenz that a dispersionlike asymmetry is also present. Such asymmetries have been regarded until recently as of secondary importance within the range of validity of the impact theory.

5. The quasistatic approach

It should therefore be possible to investigate the potential function of the interaction of two atoms (especially of the polarization forces) experimentally by measuring the intensity curve towards the wings of the broadened lines.

—Kuhn, 1934

A conceptually different approach to the problem of the profile developed out of the work of Holtsmark (1919) on Stark broadening, and the application of these ideas to neutral-atom pressure broadening by Kuhn and Margenau. Kuhn (1934, 1937a, 1937b) and Kuhn and London (1934) based their development on the Franck-Condon principle. To a first approximation, they regarded the radiating atom as at rest, emitting a frequency $\omega_0 + \Delta\omega$ that was given by the energy difference between the states of the radiator perturbed by its interaction with nearby atoms,

$$\omega_0 + \Delta\omega = (E_i - E_f)/\hbar = \omega_0 + \Delta V/\hbar, \quad (11)$$

where ΔV is the total difference in perturbations of the initial and final states. The intensity within a frequency interval ω to $\omega + d\omega$ should therefore be proportional to the probability of finding an arrangement of perturbers that would give the frequency specified by Eq. (11). The radiation we observe in the line wing arises from the moment of the actual collision, during a time of the order τ_d marking the duration of the collision, as illustrated by Fig. 3, while the line core comes from the interrupted periods of radiation between collisions.

Kuhn recognized that this result applied when the relative motion in the system of the radiator and its perturbers was infinitely slow; that is, in the static limit. For this reason, these theories are regarded as static theories of line broadening, and perhaps less specifically as statistical theories. With the same approach, Jablonski (1945) was able to incorporate the effects of nuclear motion, as we elaborate in Sec. II.A.6.

Kuhn restricted his approach to single-encounter col-

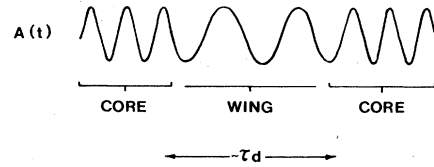


FIG. 3. Radiation and the collision process. During the collision, the emission is primarily in the line wing. The interrupted but otherwise unperturbed radiation is responsible for the line core.

lisions, with the argument that if the probability of finding one perturber near the radiator is small, then the probability of finding more than one is negligible. This means that the resulting line profile will only apply if the perturber is much closer than the mean atomic separation. With difference potentials

$$\hbar\Delta\omega = \Delta V(R), \quad (12)$$

for example, $C_p R^{-p}$, this approach will work when R is small, so that it should describe well the wing of the line.

The intensity of the line for large $\Delta\omega$ is evidently proportional to the probability of finding one perturber between R and $R + dR$,

$$I(\Delta\omega) |d\omega| = n 4\pi R^2 |dR|, \quad (13)$$

where the number density of perturbers is n . If we require one and only one perturber near the radiator, the probability factor on the right-hand side of Eq. (13) must be multiplied by $\exp(-n 4\pi R^3/3)$ in order to exclude the possibility of multiple-perturber interactions (Chandrasekhar, 1943). The nearest-neighbor and binary interaction theories will be equivalent for sufficiently small n or R . This simple formula is the basis even today of analyses of the wings of spectral lines, and in the form

$$I(\Delta\omega) = n 4\pi R^2 \left| \frac{d\omega}{dR} \right|^{-1} = n 4\pi R^2 \left| \frac{d\Delta V}{dR} \right|^{-1} \hbar \quad (14)$$

it shows that in this approximation the intensity is determined by the slope of the difference potential. Figure 4 illustrates the mapping of a perturbation $V(R)$ onto the distribution of radiation about a spectral line.

If we substitute Eq. (12) for the potential into Eq. (14) for the profile and assume a power-law interaction, then we obtain

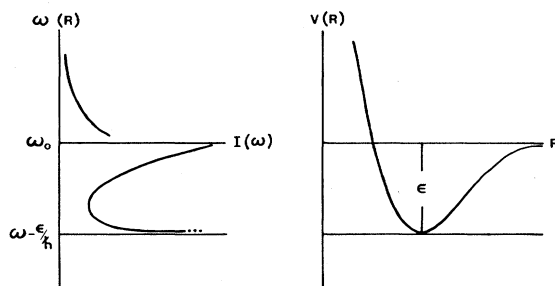


FIG. 4. Mapping the difference potential into the spectrum.

$$I(\Delta\omega) = (4\pi/p)n(C_p/\hbar)^{3/p}(\Delta\omega)^{-(p+3)/p}, \quad (15)$$

which leads, for the van der Waals interaction ($p=6$), to

$$I(\Delta\omega) \propto \Delta\omega^{-3/2}. \quad (16)$$

This calculation fails to describe the center of the line because for large R the intensity is proportional to the probability of the perturbation caused by many perturbers, and because perturber motion has been neglected. Margenau (1932, 1935, 1951) and Margenau and Watson (1936) carried out a statistical calculation, including multiple encounters, that is a generalization of Kuhn's (1934) work, extending slightly the validity of the description of the line towards smaller $\Delta\omega$ and providing the same limiting case for large $\Delta\omega$. Ch'en and Takeo (1957) present a derivation of Margenau's statistical line profiles for power-law potential differences, and additional detail may be found there.

6. A molecular approach to line profiles: statistics and quantum mechanics

(H. G. Kuhn) Does your treatment predict satellite lines? (A. Jablonski) The theory does not predict this mysterious effect.

—Jablonski, 1968

In a series of papers, Jablonski (1931, 1937, 1938, 1939, 1940, 1945, 1948, 1965, 1968) elaborated a quantum-mechanical theory of pressure broadening that, in contradistinction to the phase-shift theories we have discussed so far, treats the intensity distribution in a spectral line as if a radiator and N perturbers formed one giant quasimolecule. This model is the basis of the recently developed unified Franck-Condon theories (Szudy and Baylis, 1975; Szudy, 1979) and of quasistatic temperature-dependent wing-profile theories (Hedges, Drummond, and Gallagher, 1972) that are particularly useful for low foreign-gas densities, and which, in fact, do predict satellites. In this section we shall outline briefly the development of the Jablonski theory for a one-perturber spectrum and show how it reduces to the Kuhn-Margenau result for slow collisions. The use of this to predict the temperature dependence of line wings and its relationship to impact and unified theories will be considered in Sec. II.F. Jablonski's work underlies much of the quantum-based theory of line broadening, having influenced all recent efforts in the branches shown in Fig. 1. The one-perturber approach illustrated here is only given as a representative example.

For purposes of discussion we isolate a single radiator and a single unstructured perturber in a spherical volume of radius R_s . The initial total energy of the perturber is E_i , and as it approaches an excited radiator with energy $\hbar\omega_0$ at some point a photon of energy $\hbar\omega$ is emitted. The perturber leaves with a final translational energy E_f . Equating initial and final energies, we obtain

$$\hbar\omega_0 + E_i = \hbar\omega + E_f, \quad (17)$$

$$\Delta\omega = \xi/\hbar, \quad (18)$$

where ξ is $(E_i - E_f)$ and $\Delta\omega$ is $(\omega - \omega_0)$. When the energy of the perturber increases, the emitted photon has a lowered frequency. The intensity distribution as a function of $\Delta\omega$ is determined by the probability distribution for the required change in translational energy of the perturber, which we call $W(\xi)$.

This distribution is calculated by using the Born-Oppenheimer model and decoupling the electronic and nuclear motions of the molecule. The adiabatic hypothesis in classical pressure-broadening theories results from this picture, in that perturber-radiator collisions are assumed not to induce transitions in the electronic states of the radiator. The total wave functions of the quasimolecule in the one-perturber limit are constructed with the products

$$|\psi\rangle = |\phi\rangle |\chi\rangle, \quad (19)$$

where $|\phi\rangle$ is the electronic wave function of the radiator and $|\chi\rangle$ describes the motion of the perturber.

The electric dipole transition probability of this system is proportional to the square of the matrix element

$$D_{if} = \langle \psi_i | d | \psi_f \rangle \quad (20)$$

of the electric dipole moment operator d , which acts only on radiator wave functions. Consequently,

$$D_{if} = d_{if} A_{if} \quad (21)$$

where

$$d_{if} = \langle \phi_i | d | \phi_f \rangle \equiv \text{dipole transition moment}, \quad (22)$$

$$A_{if}^2 = \langle \chi_i | \chi_f \rangle^2 \equiv \text{Franck-Condon factor}. \quad (23)$$

If d_{if} remains fixed during the collision (refer to Sec. III.F for a discussion of collision-induced transitions), then the probability that the energy of the perturber will change from E_i to E_f , just A_{if}^2 , determines the spectrum.

The perturber states are denoted with quantum numbers ν , the number of nodes in the radial eigenfunction, and l , the angular momentum or rotational quantum number. If $|\chi\rangle$ is a product of radial and rotational eigenfunctions, then the orthogonality of the rotational eigenfunctions requires that only states of nuclear motion $|\nu_i l_i\rangle$ and $|\nu_f l_f\rangle$, for which $l_i = l_f$, have nonzero Franck-Condon factors (Jablonski, 1937; Szudy and Baylis, 1975). As a consequence, the probability of a transition depends only on the quantum numbers ν_i and ν_f and the angular momentum l of the incoming perturber.

The relative intensity distribution on an energy scale is obtained for an incident perturber of energy E_i by multiplying A_{if}^2 by the density of final-state energy levels (dv_f/dE_f) and the probability $Q_l dl$ that an incident perturber has an angular momentum between l and $l+dl$. The intensity is thus a function of l and $\xi = E_i - E_f$. The differential contribution, yet to be integrated over angular momentum (or impact parameter) and the distribution of collision energies, is

$$I(\omega)d\omega = W(\xi)d\xi, \quad (24)$$

$$I(\omega)d\omega = A_{if}^2 \frac{d\nu_f}{dE_f} Q_l dl d\xi. \quad (25)$$

The Franck-Condon factor and the level density are evaluated by using JWKB wave functions as solutions to the Schrödinger equations for the initial and final states of the perturbers. These wave functions are normalized within a sphere of radius R_s to give

$$\chi_{\nu l} = \left[\frac{2}{R_s} \frac{k(\infty)}{k(R)} \right]^{1/2} \cos \left[\int_{R_t}^R k(R) dR + \delta \right], \quad (26)$$

approaching as a limit at large R (with another value of δ)

$$\chi_{\nu l} = (2/R_s)^{1/2} \cos[k(\infty)R + \delta]. \quad (27)$$

R_t is the classical turning point for the state, and the results are valid only when the perturber is far from R_t . The phase constants δ are determined by inspecting the solution for $R < R_t$. The wave number $k(R)$ is p/\hbar , defined for the momentum p by

$$k(r) = [2\mu(E - V(R)) - \hbar^2 l(l+1)/R^2]^{1/2}/\hbar \quad (28)$$

with asymptotic value

$$k(\infty) = (2\mu E)^{1/2}/\hbar, \quad (29)$$

where μ is the reduced mass of the perturber-radiator system.

In terms of these wave functions, the required overlap integral is (Szudy and Baylis, 1975)

$$A_{if} = \frac{[k_i(\infty)k_f(\infty)]^{1/2}}{R_s} \int_{R_t}^{R_s} dR \frac{\cos[\Phi(R)]}{k(r)} \quad (30)$$

and

$$\Phi(r) = \int_{R_t(i)}^R dR k_i(R) - \int_{R_t(f)}^R dR k_f(R). \quad (31)$$

The value of A_{if} is determined for the most part near the distances R_c at which

$$k_i(R_c) = k_f(R_c) \quad (32)$$

or in terms of total energy E and potential energy V

$$E_i - V_i(R_c) = E_f - V_f(R_c). \quad (33)$$

Together with Eq. (18) and the definition of ξ , Eq. (33) yields

$$\hbar\Delta\omega = \xi = V_i(R_c) - V_f(R_c). \quad (34)$$

The most probable frequency is the one corresponding to the classical form of the Franck-Condon principle. The integral for A_{if} in Eq. (30) is evaluated by a quadratic expansion of Φ about these points of stationary phase, so that approximately

$$A_{if}^2 \simeq \frac{k_i(\infty)k_f(\infty)}{k(R_c)} R_s^{-2} \frac{\hbar^2}{(\mu |d\xi/dR|_{R=R_c})} \pi(2\cos^2\phi). \quad (35)$$

Because the phase ϕ in the interference term ($2\cos^2\phi$) is sensitive to the angular momentum and collision energy, this term averages to unity when the distribution of initial states is allowed for.

The density of translational energy levels $d\nu_f/dE_f$ is calculated from the condition that χ is zero on the spherical boundary surface. This gives, from Eq. (27),

$$k_f(\infty)R + \delta = [(2\nu_f + 1)/2]\pi. \quad (36)$$

Differentiation with respect to E_f , noting that k_f depends on E_f , yields

$$\frac{d\nu_f}{dE_f} = \mu R_s / \pi \hbar^2 k_f(\infty). \quad (37)$$

Since our interest centers on large values of l , the factor Q_l is evaluated classically. It is determined by the chance that a classical value of the impact parameter will correspond to angular momentum quantum numbers in the range from l to $l+dl$ and is given by geometrical arguments [Jablonski, 1945, Eq. (28)],

$$Q_l = \frac{3}{2}(2l+1)[k_i(\infty)R_s]^{-2}. \quad (38)$$

This is actually valid only when $l \ll k_i(\infty)R_s$, the largest possible l , but it can be used without error for all l since only values in this range of validity contribute to the profile (Szudy and Baylis, 1975).

The intensity distribution is then found by substituting Eqs. (35), (37), and (38) into Eq. (25) and summing over the Condon points, to obtain

$$I(\omega)d\omega = \sum_c \left[\frac{4\pi R_s^3}{3} \right]^{-1} \left[\frac{\pi(2l+1)dl}{k_i^2} \right] \times \left[\frac{2d\xi}{k(R_c)/k_i |d\xi/dR|_{R_c}} \right]. \quad (39)$$

The grouping of terms here, after Eq. (2) of Hedges, Drummond, and Gallagher (1972), allows us to find a classical analog easily. This equation is also identical with the integrand of Eq. (39) of Jablonski (1945).

Since there is only one perturber in the sphere of radius R_s , the perturber density n is equal to the first term $(4\pi R_s^3/3)^{-1}$. The second term is just $2\pi b db$, where the impact parameter b is related to the angular momentum l by $b^2 = l(l+1)/k_i^2$. The derivative in the denominator of the third term transforms $d\xi$ into a spatial derivative. This term becomes $v_i(\infty)[2dR/v_i(R_c)]$, where $v_i(R_c)$ is the radial velocity at R_c . The third term is thus $v_i(\infty)$ multiplied by the time spent in the increment dR_c . When the variation of perturber velocity as a function of internuclear separation is neglected (a reasonable assumption so long as the perturbation is small compared to the initial kinetic energy), then the right-hand side of Eq. (39) is a differential volume. In spherical coordinates, centered on the radiator, this equation becomes

$$I(\omega)d\omega = n \sum_c 4\pi R_c^2 dR_c, \quad (40)$$

where ω and R_c are related through Eq. (34). This ex-

pression, derived by Jablonski (1945) from quantum-mechanical calculations, is equivalent to the expression of Kuhn and Margenau, Eq. (13), that was arrived at by statistical arguments.

The one-perturber spectrum of Eq. (39) also contains information about the temperature dependence of spectral line wings. That aspect of the theory is discussed in Sec. II.F.4. Other general developments in the evaluation of Eq. (35) are discussed in Sec. II.F.1.

7. The synthesis of phase-shift and molecular theories

Jablonski considers that the fact that the intensity distribution calculated by this method does not agree with the Lorentz-Weisskopf formula indicates that the Fourier integral method is fundamentally incorrect.... The wave-mechanical treatment does, in fact, yield both of these formulas under the assumption of physical conditions proper for each

—Foley, 1946

Early line-broadening theories were characterized by two distinct approaches. On the one hand, theories in which the Fourier series was obviously asserted, what we generally call phase-shift theories, predicted a Lorentzian line core and said very little about the line wing. On the other hand, statistical theories and calculations based on molecular models, which led to quite different expressions did not predict a Lorentzian core, and were difficult to reconcile with the phase-shift theories. Jablonski, for example, offered the opinion that phase-shift theories had not been shown to describe the phenomena rigorously enough, and he presented arguments against the treatments of Weisskopf (1932a, 1932b, 1933) and Foley (1946) [see particularly the exchange between Jablonski (1948) and Foley (1948)].

Foley (1946) presented a proof that the Fourier integral expression for a line profile could be derived from a quantum treatment of the broadening with the approximation of adiabatic collisions, although he did not show that the results of the static theory followed from the Fourier analysis in a systematic way. An early attempt in this direction by Lindholm (1946) had indicated that there was a connection. Holstein (1950) showed how the static theory of Kuhn could be obtained from the Fourier analysis, and he also made an early "antistatic" wing calculation which still stands as correct in the light of more recent work by Szudy and Baylis (1975, 1977). Other contributions by Jablonski (1968) and Szudy and Baylis integrate the molecular method into this general scheme.

B. General theory of line broadening in the semiclassical model

The theory to be developed here is exact when its basic assumptions about intermolecular forces are correct, except insofar as the actual numerical calculations may involve approximations.

—Anderson and Talman, 1956

We consider in this section the generalization by Anderson (1952) and Anderson and Talman (1956) of the line-shape theories developed by Lindholm (1945) and Foley (1946). This theory provided the first unified description of the profile of a pressure-broadened atomic spectral line at any pressure, and for any spectral region around the line. Even though one of the required assumptions is that the interatomic forces are scalar and additive, and there are better ways to treat far line wings in the binary limit, evaluations of this theory to be discussed in Sec. II.E provide the best general interpretations of experimental results possible so far.

From Eq. (9) we describe the time-dependent wave train for a single emitter as

$$f(t) = f_0 \exp(-i\omega_0 t) \exp[-i\eta(t)]. \quad (41)$$

Implicit in this description, in which the oscillator of frequency ω_0 has a time-dependent phase during the collision $\eta(t)$, are two critical assumptions: the perturbers are assumed to travel on classical trajectories, and the oscillator is assumed to be only adiabatically perturbed. To evaluate the power spectrum we use the Wiener-Khintchine theorem [for example, see Cowley (1970) or Papoulis (1962)] and compute the Fourier transform of the autocorrelation function.

The autocorrelation function $\Phi(s)$ measures the average evolution of the wave train over a time interval s from an initial time t . In terms of the complex amplitude $f(t)$,

$$\Phi(s) = \langle f(t)^* f(t+s) \rangle_t. \quad (42)$$

The autocorrelation function is then proportional to

$$\begin{aligned} \Phi(s) &\propto \exp(-i\omega_0 s) \\ &\times \langle \exp\{-i[\eta(t+s) - \eta(t)]\} \rangle_t. \end{aligned} \quad (43)$$

Accordingly, the Fourier transform of this function is the emission line profile

$$\begin{aligned} I(\omega) &\propto \int_{-\infty}^{+\infty} ds \exp[i(\omega - \omega_0)s] \\ &\times \langle \exp\{-i[\eta(t+s) - \eta(t)]\} \rangle_t. \end{aligned} \quad (44)$$

When the spectrum is referred to the unperturbed frequency ω_0 , it is convenient to define the autocorrelation of the phase all along the wave train as

$$\Phi(s) = \langle \exp\{-i[\eta(t+s) - \eta(t)]\} \rangle_t. \quad (45)$$

Then, with frequency measured from the line center,

$$I(\omega) \propto \int_{-\infty}^{+\infty} \Phi(s) \exp(i\omega s) ds \quad (46)$$

gives the desired contour.

An assumption that the ergodic hypothesis is valid allows us to replace the time average of Eq. (45) by an average over different collisions. The phase shifts are evaluated in terms of the potential due to all perturbers,

$$V(t) = \sum_{k=1}^N V_k[R_k(t)], \quad (47)$$

where the R_k 's are the distances of the N different per-

turbers from the radiator, while the V_k 's are the binary interaction potentials. Of course Eq. (47) is true only for isolated s states; we shall encounter this difficulty again in the quantum theories discussed in the following section. As evidence that this assumption is a satisfactory approximation, there have been theoretical analyses (Baylis, 1977; Sando, Erickson, and Binning, 1979) and observations that line-shape spectra appear to be insensitive to nonadditivity. The phase difference is expressed as

$$\eta(t+s) - \eta(t) = \int_t^{t+s} \sum_{k=1}^N \hbar^{-1} V_k [R(t')] dt' , \quad (48)$$

and the correlation function is given by

$$\Phi(s) = \left\langle \exp \left[-i \left(\sum_{k=1}^N \int_t^{t+s} \hbar^{-1} V_k [R(t')] dt' \right) \right] \right\rangle_t . \quad (49)$$

By replacing the average over initial times with an average over all collision geometries at the same initial time, taken to be $t=0$, we obtain

$$\Phi(s) = \left\langle \prod_{k=1}^N \exp \left[-i \int_0^s \hbar^{-1} V_k [R(t')] dt' \right] \right\rangle_{\text{collisions}} . \quad (50)$$

Anderson assumed that the perturbers were independent of one another, so that this average over a product could be replaced by a product of averages,

$$\Phi(s) = \left[\left\langle \exp \left[-i \int_0^s \hbar^{-1} V[R(t')] dt' \right] \right\rangle_{\text{collisions}} \right]^N . \quad (51)$$

To calculate the mean, we suppose that each perturber follows a classical rectilinear trajectory, as illustrated in Fig. 5. If b is the impact parameter, and if $x=x_0+\bar{v}t'$ is the position of the perturber along its trajectory, then the mean can be written in terms of the integral over

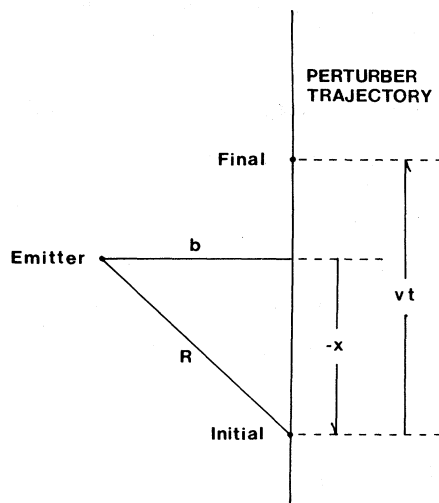


FIG. 5. Rectilinear trajectory of the classical perturber.

possible initial positions of the perturbers within a volume \mathcal{V}

$$\begin{aligned} \Phi(s) = & \left[\frac{1}{\mathcal{V}} \int \int_{\mathcal{V}} 2\pi b db dx_0 \right. \\ & \times \exp \left[-i \int_0^s \hbar V[(b^2 + (x_0 + \bar{v}t')^2)^{1/2}] dt' \right] \left. \right]^N . \end{aligned} \quad (52)$$

We make use of the approximation $(1-\alpha)^N \approx \exp(-N\alpha)$, that is valid when $\alpha \ll 1$ and $N \gg 1$, to simplify this expression for the autocorrelation function. We obtain

$$\begin{aligned} \Phi(s) = & \left\{ 1 - \frac{1}{\mathcal{V}} \int \int_{\mathcal{V}} 2\pi b db dx_0 \right. \\ & \times \left[1 - \exp \left[-i \int_0^s \hbar^{-1} V[(b^2 + x^2)^{1/2}] dt' \right] \right]^N \end{aligned} . \quad (53)$$

Then for a fixed number density n given by the ratio of the number of perturbers N to their occupied volume \mathcal{V} , when \mathcal{V} becomes very large,

$$\Phi(s) = \exp[-ng(s)] \quad (54)$$

and

$$\begin{aligned} g(s) = & 2\pi \int_0^\infty b db \\ & \times \int_{-\infty}^\infty dx_0 \left[1 - \exp \left[-i \int_0^s \hbar^{-1} V[(b^2 + x^2)^{1/2}] dt' \right] \right] . \end{aligned} \quad (55)$$

Equations (54) and (55) are the basis for the Anderson-Talman theory of spectral line broadening by collisions.

The "unified" nature of these equations becomes apparent if we inspect the solutions in the limit of large s and in the limit of zero velocity. As Anderson (1952) showed for the limit $s \rightarrow \infty$, we can write formally for $g(s)$

$$g(s) = (\alpha_0 + i\beta_0) + (\alpha_1 + i\beta_1)s , \quad (56)$$

$$\begin{aligned} \alpha_1 = & \bar{v} \int_0^\infty 2\pi b db \\ & \times \left[1 - \cos \left[(\hbar \bar{v})^{-1} \int_{-\infty}^{+\infty} V[(b^2 + x^2)^{1/2}] dx \right] \right] , \end{aligned} \quad (57)$$

$$\beta_1 = \bar{v} \int_0^\infty 2\pi b db \sin \left[(\hbar \bar{v})^{-1} \int_{-\infty}^{+\infty} V[(b^2 + x^2)^{1/2}] dx \right] . \quad (58)$$

The additive constant $(\alpha_0 + i\beta_0)$ is usually taken as zero, and the profile that results from the Fourier transform of Eq. (54) is a Lorentzian with a half-width $n\alpha_1$ and a shift $n\beta_1$, respectively, the real and the imaginary parts

of the slope of $g(s)$. Thus the assumption that $g(s)$ has the same behavior for all s that it has for $s \rightarrow \infty$ produces the usual impact-theory line profile.

To find an alternative limiting behavior of $g(s)$, we investigate its value when $\bar{v} \rightarrow 0$. In this case the phase-shift integral simplifies, and the volume integration reduces to one variable. This so-called static limit is

$$g(s) = 4\pi \int_0^\infty R^2 dR [1 - \exp(-i\hbar^{-1}V(R)s)], \quad (59)$$

which is in agreement with Margenau (1951) and produces a spectrum given by Kuhn's result, Eq. (13). The static limit is also the limit of $g(s)$ for small s , as is apparent from Eq. (55) and as has been demonstrated numerically (Kielkopf, 1976a).

The general Anderson-Talman theory thus predicts a wide range of observed effects. These include the Lorentzian line core, the asymmetry of the core when $\alpha_0 + i\beta_0$ is not zero, and the line wing. More recently, we have shown that the numerical evaluation of this theory for representative potentials gives a complete explanation of the red satellites that appear in the near wing of alkali lines perturbed by heavy noble gases (Allard, Sahal-Brechot and Biraud, 1974; Kielkopf, 1976; Kielkopf and Allard, 1980). These features were unexplained at the time of the Ch'en and Takeo review (1957). The complete evolution of the line profile with increasing foreign-gas density closely follows the predictions of this theory.

This approach is obviously incomplete, for it allows only for spherically symmetric, adiabatic interactions. A calculation of the line profile through fully quantal treatments of the radiation and collision process will be surveyed in the following sections, where we extend the Anderson-Talman method to include more realistic interactions and nonadiabatic effects.

C. Quantum theories of line broadening

1. The classical path approximation

Our understanding of the role of quantum processes in the broadening of atomic spectral lines by neutral-atom collisions has developed considerably in the decades since the unification by Anderson of impact and statistical theories within a single classical framework. For instance, Fig. 1 shows the many developments from the work of Baranger (1958a, 1958b, 1958c) concerning the quantum theory of collision broadening within the impact approximation. Few papers, however, have dealt with the problem of the complete profile of the line. Only within the context of the assumption of classically described paths for the perturbers has some progress been made. Thus in this section we draw on Baranger and on Smith, Vidal, and Cooper (1969a, 1969b), Smith, Cooper, and Vidal (1969), Sahal-Brechot (1969), and Allard, Sahal-Brechot, and Biraud (1974) to outline a unified generalization of the Anderson-Talman theory that takes into account such important features as the aniso-

tropy of the interaction and the contribution of inelastic collisions. The procedure for computing the line profile that we develop is completely equivalent to the classical theories for a spherically symmetric potential.

Subsequently, we shall look at the relationship of this theory to other recent theories of radiative redistribution, and we shall also examine conditions for the validity of the necessary classical path approximation and the effects that might be expected when this approximation breaks down.

a. The spectrum and the correlation function

We consider a fixed radiating atom with an initial state $|i\rangle$ and a final state $|f\rangle$, surrounded by moving perturbers. The total power emitted in all directions for a dipole transition of this atom is given by

$$P(\omega) = \frac{4\omega^4}{3c^3} I(\omega), \quad (60)$$

where ω_{if} is the frequency of the transition and

$$I(\omega) = \sum_{if} \delta(\omega - \omega_{if}) (\langle f | d | i \rangle)^2 \rho_i. \quad (61)$$

The absorption spectrum can be obtained from the emission spectrum by application of the Einstein relations. The summation extends over all atomic states, each term weighted with a statistical intrinsic probability ρ_i for the initial state. Because we confine our interest to the line spectrum of the radiating atom and exclude the continuum radiation attributable solely to the perturbers, d is the dipole moment of the radiator and not of the entire system.

This, of course, is the complete spectrum of the atom, but often we are interested only in an isolated line. In such a case the summation in Eq. (61) is omitted. Only selected initial and final states enter. For overlapping lines, the sum must extend over all contributing states (Baranger, 1958b).

Although in the classical treatment we obtained the correlation function from its definition, Eq. (42), here we take the direct approach of Fourier-transforming Eq. (61) to obtain

$$\Phi(s) = \int_{-\infty}^{+\infty} I(\omega) \exp(-i\omega s) d\omega, \quad (62)$$

which, together with its converse, Eq. (46),

$$I(\omega) = \frac{1}{2\pi} \int_{-\infty}^{+\infty} \Phi(s) \exp(i\omega s) ds, \quad (63)$$

describes the line profile. Since $I(\omega)$ is real, the correlation function must be computed only for positive s . We have

$$\Phi(-s) = \Phi^*(s) \quad (64)$$

and

$$I(\omega) = \frac{1}{\pi} \operatorname{Re} \left[\int_0^\infty \Phi(s) \exp(i\omega s) ds \right]. \quad (65)$$

For this reason the signs in the exponentials of Eqs. (62)

and (63) are immaterial. From Eq. (62) we obtain Φ by substituting Eq. (61). After integration over ω , Eq. (62) becomes

$$\Phi(s) = \sum_{if} \exp(-i\omega_{if}s) |\langle f | d | i \rangle|^2 \rho_i . \quad (66)$$

b. The calculation of the correlation function with time-evolution and density operators

This fundamental expression for the correlation function can be written in terms of the time-evolution operator $T(s)$, which transforms a state at time 0 into a state at time s . It is given in the Schrödinger representation by

$$T(s) = \exp[-i(H/\hbar)s] , \quad (67)$$

where H is the Hamiltonian of the system of radiator and perturbers,

$$H = H_A + H_P + V . \quad (68)$$

H_A is the atomic Hamiltonian, H_P the Hamiltonian of the perturbers, and V the total interaction potential (Anderson, 1949; Baranger, 1962; Smith, Vidal, and Cooper, 1969; Allard, Sahal-Brechot, and Biraud, 1974). The correlation function of Eq. (66) can be equivalently written

$$\Phi(s) = \text{Tr}[d T^\dagger(s) d T(s) \rho] , \quad (69)$$

where the trace operator Tr acts over all the states of the entire system of the radiating atom and the assembly of perturbers, and ρ is the Boltzmann-Gibbs density matrix for the whole system. This is most readily shown by substituting into Eq. (69) the appropriate matrix elements and explicitly evaluating Eq. (69) to reduce it to Eq. (66). A general discussion of density matrices has been given by Fano (1957). This form for $\Phi(s)$ is useful for separating the statistics of the perturber and emitter spaces.

c. Separation of perturbers and the emitter

We now introduce a few assumptions about the density matrix and the states that will allow a distinction between perturber and emitter statistics, thus making possible a significant reduction in the computation of the correlation function. Following Baranger (1962) and Cooper (1967), we construct the states of the system from the direct product states

$$|\psi(t)\rangle = |\phi(t)\rangle |\chi(t)\rangle , \quad (70)$$

where the wave function of the radiator $|\phi\rangle$ depends on its coordinates, and the wave function $|\chi\rangle$ depends only on the coordinates of the perturbers. The perturber function is assumed to consist of wave packets and obeys a Schrödinger equation which does not depend on the state of the radiating atom. This means we neglect the "back reaction" of the radiator on the perturbers (Smith,

Vidal, and Cooper, 1969). In this approximation [Baranger, 1962, Eqs. (21–22)], the radiator wave function evolves in a time-dependent potential, averaged over the perturber wave packets. For the neutral-atom line-broadening problem, these wave packets are sufficiently small that we picture classical trajectories for the perturbers as they disturb the radiating atom.

The extent of the perturber wave packet is the smallest interval over which the correlation function can be divided in the classical sense, a point we shall return to later. With this understanding, we can adopt a theory of the correlation function calculated with a classical path approximation, and use the factored states to compute $\Phi(s)$. The density matrix also factors into two parts, and for it we write (Fano, 1957)

$$\rho = \rho_A \rho_P \quad (71)$$

with the inherent assumption that perturbers and radiators move independently. This assumption requires that we take a specific form for the density matrix of the radiators. Approximately we have

$$\rho_A \simeq \frac{1}{Z(T)} g_i \exp[-(H_A + \bar{V})/kT] , \quad (72)$$

where $Z(T)$ is the partition function, H_A the radiator free-atom Hamiltonian, and \bar{V} the statistical average of the perturbation over the positions and speeds of the perturbers. Then, to assure separation of the density matrix as in Eq. (71), we must let \bar{V}/kT approach zero in the exponent.

The assumptions that allow the factorization of the density matrix Eq. (71) do not hold rigorously in real cases, but lead to negligible error except in the far line wing, where frequencies are removed from the unperturbed line center by amounts of the order kT/\hbar . The inadequacy of Eq. (71) may be seen particularly in radiative redistribution problems in this domain. In the binary collision approximation, Burnett *et al.* (1980) have presented a method for calculating the density operator in the presence of a driving field and perturbers without restriction to the factorized form. They also discuss conditions under which the approach used here is valid.

We factor the time-evolution operator so that

$$T(s) = T_A(s) T_P(s) , \quad (73)$$

where T_A follows the perturbed atomic Hamiltonian $H_A + \bar{V}$, and T_P follows the perturber Hamiltonian H_P . With this factorization and a few manipulations it is easy to see that the correlation function is given by (Sahal-Brechot, 1969; Allard, Sahal-Brechot, and Biraud, 1974)

$$\Phi(s) = \sum_{if} \left[\frac{1}{Z(T)} g_i \exp(-E_i/kT) \times \langle i | d(s) | f \rangle \langle i | d | f \rangle \right]_{\text{Av}} . \quad (74)$$

Here g_i is the degeneracy of the initial state, E_i the asymptotic initial-state energy, and the potential V is

neglected in the exponent to allow the separation of perturber and emitter spaces. The average symbolized by $\langle \rangle_{Av}$ is over the ensemble of perturber states, now regarded as classical particles. The operator $\mathbf{d}(s) = T^\dagger \mathbf{d} T$ is the dipole moment of the radiator in the Heisenberg representation.

d. The calculation of $\mathbf{d}(s)$

To calculate the required matrix elements of $\mathbf{d}(s)$ from

$$\mathbf{d}(s) = T^\dagger(t+s, t) \mathbf{d} T(t+s, t) \quad (75)$$

we introduce the time-evolution operator $U(t+s, t)$, which is related to T by

$$T(t+s, t) = T_A(s) U(t+s, t), \quad (76)$$

where $T_A(s)$ is the evolution operator of the unperturbed system given by

$$T_A(s) = \exp \left[-\frac{i}{\hbar} H_A s \right]. \quad (77)$$

The evolution operator in the interaction representation, $U(t+s, t)$, is customarily defined by

$$\begin{aligned} U(t+s, t) &= 1 - \frac{i}{\hbar} \int_t^{t+s} dt_1 \tilde{V}_T(t_1) \\ &\quad - \frac{1}{\hbar^2} \int_t^{t+s} dt_1 \tilde{V}_T(t_1) \int_t^{t_1} dt_2 \tilde{V}_T(t_2) \\ &\quad + \dots, \end{aligned} \quad (78)$$

where

$$\tilde{V}_T(t_1) = \exp \left[\frac{i}{\hbar} H_A t_1 \right] V_T(t_1) \exp \left[-\frac{i}{\hbar} H_A t_1 \right] \quad (79)$$

with

$$s > t_1 > t_2 > \dots > t_n. \quad (80)$$

This expansion is symbolically a time-ordered exponential, in which the operator \mathcal{T} maintains the required order. Its use in line-broadening theory is discussed extensively by Smith, Cooper, and Roszman (1973), who derive results similar to those that follow here. The evolution operator becomes

$$U(t+s, t) = \mathcal{T} \exp \left[\frac{1}{\hbar} \int_t^{t+s} \tilde{V}_T(t) dt \right]. \quad (81)$$

These time-ordered integrals cannot, in general, be reduced to an unordered exponential because the terms $\tilde{V}_T(t_i)$ and $\tilde{V}_T(t_j)$ do not always commute. But there are circumstances under which they will; for instance, if strong collisions do not overlap one another. We retain the ordering operator implicitly in the following expressions and consider in the next section criteria for dispensing with this requirement. Then we write from Eqs. (74)–(77) and (81) the correlation function

$$\begin{aligned} \Phi(s) &= \sum_{if} \frac{g_i \exp(-E_i/kT)}{Z(T)} \\ &\quad \times \langle i | \mathbf{d} | f \rangle \langle i | [\mathbf{d}(s)]_{Av} | f \rangle \end{aligned} \quad (82)$$

and for the elements of $\mathbf{d}(s)$

$$\begin{aligned} [\mathbf{d}(s)]_{Av} &= \left[U^{-1}(t+s, t) \exp \left[\frac{i}{\hbar} H_A s \right] \right. \\ &\quad \times \mathbf{d} \exp \left[-\frac{i}{\hbar} H_A s \right] U(t+s, t) \Big]_{Av} \end{aligned} \quad (83)$$

or

$$\begin{aligned} \langle f | [\mathbf{d}(s)]_{Av} | i \rangle &= \sum_{pq} [U_{fp}^{-1}(t+s, t) \langle p | \mathbf{d} | q \rangle \\ &\quad \times U_{qi}(t+s, t) \\ &\quad \times \exp(-i\omega_{qp}s)]_{Av}. \end{aligned} \quad (84)$$

From here on we restrict our consideration to lines which are isolated, either degenerate and unresolved, or well separated (Anderson, 1949). A general theory for overlapping lines has not yet been applied to a neutral-atom problem for which experimental data exist. A discussion of overlapping lines in the impact limit has been given by Baranger (1958b). For an isolated line which is a transition between states designated $|jm\rangle$, we take into account the degeneracy in m to obtain

$$\begin{aligned} \langle j_f m_f | [\mathbf{d}(s)]_{Av} | j_i m_i \rangle &= \sum_{m_1 m_2} [\exp(-i\omega_{if}s) \langle j_f m_f | U^{-1} | j_f m_1 \rangle \\ &\quad \times \langle j_f m_1 | \mathbf{d} | j_i m_2 \rangle \langle j_i m_2 | U | j_i m_i \rangle]_{Av}. \end{aligned} \quad (85)$$

e. The angular average and the calculation of $\Phi(s)$

To obtain a workable form for the correlation function we need to complete the averages in Eq. (85). This process is divided into two parts, the first of which is the problem of averaging over all orientations of a reference frame chosen for the calculation of U by the collision geometry, one in which one axis is along the impact parameter for the collision trajectory (Cooper, 1967). This angular average involves a superposition of all possible Euler angles representing the relative orientation of the frame of the collision to that of the laboratory in which the collision is observed.

It is convenient to regard \mathbf{d} as a tensor operator of rank 1 and to introduce its reduced matrix elements defined by (Judd, 1963; Edmonds, 1968)

$$\langle j_f m_f | \mathbf{d} | j_i m_i \rangle = (-1)^{j_f - m_f} \begin{bmatrix} j_f & 1 & j_i \\ -m_f & 0 & m_i \end{bmatrix} \times \langle j_f | d | j_i \rangle . \quad (86)$$

Then, by explicitly averaging over the Euler angles and making use of the rotational transformation properties of the atomic wave functions, we can express the angular average by (Cooper, 1967; Sahal-Brechot, 1969)

$$\begin{aligned} \langle j_f | [d(s)]_{\text{Ang}} | j_i \rangle &= \langle j_f | d | j_i \rangle \exp(-i\omega_{if}s) \\ &\times [U_{ff}^{-1}(t+s,t) U_{ii}(t+s,t)]_{\text{Ang}} , \end{aligned} \quad (87)$$

where

$$\begin{aligned} [U_{ff}^{-1}(t+s,t) U_{ii}(t+s,t)]_{\text{Ang}} &= \sum_{\substack{m_i m_f \\ m'_i m'_f \\ M}} (-1)^{2j_f + m_i + m'_i} \begin{bmatrix} j_f & 1 & j_i \\ m_f & M & -m'_i \end{bmatrix} \\ &\times \begin{bmatrix} j_f & 1 & j_i \\ m_f & M & -m_i \end{bmatrix} \langle j_i m'_i | U_c | j_i m_i \rangle \\ &\times \langle j_f m_f | U_c^{-1} | j_f m'_f \rangle . \end{aligned} \quad (88)$$

Here we have denoted by U_c the operator U referring to the axes of collision (Cooper, 1967). Only diagonal terms in U (or S for the impact approximation) enter for the angular average of an isolated line.

Deferring momentarily the completion of the averaging process, let us consider the remaining problem, one central to all unified theories of line broadening, namely, to calculate $U(t+s,t)$. It is given by Eq. (81), where the total interaction \tilde{V}_T is equal to the sum of the interactions $\tilde{v}_1, \tilde{v}_2, \dots, \tilde{v}_i, \dots, \tilde{v}_N$ due to the different perturbers $1, 2, \dots, i, \dots, N$, which act during the correlation time s . In terms of these individual interactions we obtain

$$U(t+s,t) = \mathcal{T} \exp \left[-\frac{i}{\hbar} \int_t^{t+s} [\tilde{v}_1(t') + \tilde{v}_2(t') + \dots + \tilde{v}_N(t')] dt' \right] . \quad (89)$$

If we suppose, for example, that the collisions are separated in time so that \tilde{v}_i is equal to zero when \tilde{v}_j is not zero, and reciprocally that \tilde{v}_j is equal to zero when \tilde{v}_i is not zero, then

$$[\tilde{v}_i(t'), \tilde{v}_j(t'')] = 0 \quad (90)$$

for every i, j, t' , and t'' .

With this hypothesis, which is central to unified theories of line broadening (Smith, Cooper, and Roszman, 1973), we can replace the time-ordered expression Eq. (89) by a commutative product of the evolution operators $u_i(t+s,t)$ which are solutions of the Hamiltonian of the atom in the presence of only one perturber. The Hamiltonian in this case is $H = H_A + \tilde{v}_i(t)$, the collisions can be ordered as necessary because the operators commute, and we write

$$\begin{aligned} U(t+s,t) &= \mathcal{T} \left[\exp \left[-\frac{i}{\hbar} \int_t^{t+s} \tilde{v}_1(t') dt' \right] \right. \\ &\quad \times \exp \left[-\frac{i}{\hbar} \int_t^{t+s} \tilde{v}_2(t'') dt'' \right] \dots \left. \right] , \end{aligned} \quad (91)$$

$$\begin{aligned} U(t+s,t) &= \mathcal{T} \left[\exp \left[-\frac{i}{\hbar} \int_t^{t+s} \tilde{v}_1(t') dt' \right] \right] \\ &\quad \times \mathcal{T} \left[\exp \left[-\frac{i}{\hbar} \int_t^{t+s} \tilde{v}_2(t'') dt'' \right] \right] \dots , \end{aligned} \quad (92)$$

$$U(t+s,t) = \prod_{i=1}^N u_i(t+s,t) . \quad (93)$$

Now the calculation involves only the effect of one collision,

$$u_i(t+s,t) = \mathcal{T} \left[\exp \left[-\frac{i}{\hbar} \int_t^{t+s} \tilde{v}_i(t') dt' \right] \right] . \quad (94)$$

Whether we can now remove the time-ordering constraint depends on validity conditions summarized in the following section.

As a consequence of the commutator Eq. (90) and the result Eq. (93), we need to calculate

$$\begin{aligned} [U_{ff}^{-1}(t+s,t) U_{ii}(t+s,t)]_{\text{Av}} &= (u_{1ff}^{-1} u_{1ii} u_{2ff}^{-1} u_{2ii} \dots u_{Nff}^{-1} u_{Nii})_{\text{Av}} . \end{aligned} \quad (95)$$

We have separated the sequence of products from Eq. (93) into one-perturber sets, which, for simplicity, we have designated $u_{ff}^{-1} u_{ii}$. The perturbers are assumed to move independently, and the average of the products in Eq. (95) is replaced by the product of the averages to yield

$$[U_{ff}^{-1}(t+s,t) U_{ii}(t+s,t)]_{\text{Av}} = [(u_{ff}^{-1} u_{ii})_{\text{Av}}]^N . \quad (96)$$

When we evaluate the power in this expression by the approximation used in the Anderson-Talman theory, that $(1-\alpha)^N \approx \exp(-N\alpha)$ for small α and large N , we obtain

$$(U^{-1}U)_{\text{Av}} = \exp[-N(1-u_{ff} u_{ii})_{\text{Av}}] , \quad (97)$$

a workable expression for the average needed in the calculation of the correlation function.

The angular average has been discussed and is given in Eq. (88). The other average we need is over the initial-

perturber velocity and position. As in Sec. II.B, this is obtained by integration over a volume \mathcal{V} of space about the radiator

$$(1 - u_{ff}^{-1} u_{ii})_{\text{Av}} = \frac{1}{\mathcal{V}} \int_0^\infty f(v) dv \int \int_{\mathcal{V}} 2\pi b db v dt \times [1 - (u_{ff}^{-1} u_{ii})_{\text{Ang}}] . \quad (98)$$

Here $f(v)$ is the Maxwellian velocity distribution of mutual perturber-radiator velocities, b is the impact param-

eter, and t is the time of the collision. The integrals extend over the volume, which will become infinitely large with constant number density $n = N/\mathcal{V}$ of perturbers. A more formal treatment of this average is given by Allard (1973).

We now combine Eqs. (86)–(97) and (98), delete factors constant through the line profile, and obtain for isolated lines

$$\Phi(s) = \sum_{if} \exp(-i\omega_{if}s) \exp[-ng(s)] \quad (99)$$

with

$$g(s) = \int_0^\infty f(v) dv \int_0^\infty 2\pi b db \int_{-\infty}^{+\infty} v dt \{ 1 - [u_{ff}^{-1}(t+s,t) u_{ii}(t+s,t)]_{\text{Ang}} \} . \quad (100)$$

In Eq. (100) u_{ff} or u_{ii} refers to a single perturber, the angular average is given by Eq. (88), and the profile for an isolated line defined by this correlation function is normalized to unit area on an angular frequency scale.

In the impact limit as $s \rightarrow \infty$, Eq. (100) simplifies. All collisions are completed, and the evolution operator matrix for U is replaced by the S matrix. We obtain

$$g(s) = \alpha_0 + i\beta_0 + (\alpha_1 + i\beta_1)s \quad (101)$$

and

$$\alpha_1 + i\beta_1 = \int_0^\infty f(v)v dv \int_0^\infty 2\pi b db (1 - S_{ff}^{-1} S_{ii})_{\text{Ang}} . \quad (102)$$

If the diagonal elements of the S matrix are written in the form [Baranger, 1962, Eq. (59)]

$$S_{ff}^{-1} S_{ii} = \exp(-\xi + i\eta) , \quad (103)$$

then the half-width $n\alpha_1$ and the shift $n\beta_1$ become

$$n\alpha_1 = n \int_0^\infty f(v)v dv \times \int_0^\infty 2\pi b db [1 - \exp(-\xi)\cos(\eta)] \quad (104)$$

$$n\beta_1 = n \int_0^\infty f(v)v dv \times \int_0^\infty 2\pi b db \exp(-\xi)\sin(\eta) . \quad (105)$$

In the special case when ξ is infinite, every collision is inelastic, there is no shift, and the width is the collision frequency. This is the Lorentz (1906) theory. On the other hand, if ξ is zero, all collisions are elastic and we obtain the adiabatic theory of Lindholm (1945) and Foley (1946).

These expressions are also equivalent to the formulas given by Lewis (1980) for the impact limit. In the quasistatic limit, Eq. (100) reduces to the results of Margenau (1935, 1951), in just the same way that the Anderson theory reduced to corresponding phase-shift and static theory results in similar limits. The expression given here thus constitutes a generalization of the Anderson-

Talman theory, but as an extension of Baranger (1958) it is a unified theory in the sense discussed by Smith, Cooper, and Roszman (1973).

f. Conditions of validity for the unified theory

This theory, like others of the same sort (Smith, Cooper, and Vidal, 1969; Bezzerezides, 1969a, 1969b; Bottcher, 1971; Lee, 1971; Smith, Cooper, and Roszman, 1973), has a fundamental limitation imposed by the assumption that perturbations by different perturbers acting at different times commute for all perturber pairs and all times, as expressed by Eq. (90). There are several conditions that would be sufficient to make this occur, and since these are often satisfied in experimental studies of neutral-atom broadening, the theory is generally quite useful. The validity conditions are summarized as follows:

(1) Pairs of collisions are well separated in time, so that, as explained prior to Eq. (90), only one v_i is turned on at a time. This condition is equivalent to requiring a low density and, as an approximate criterion, if \bar{b} is an impact parameter which is preponderant in the collision, we must have

$$\bar{b} \ll n^{-1/3} . \quad (106)$$

We shall see that this may be an important limitation on the utility of the theory for the analysis of transitions in highly excited atoms at high gas density. Time ordering following Eq. (94) can be dropped in this case.

(2) The operators v_i are diagonal, for then the potential is rigorously isotropic and Eq. (90) holds exactly. Thus in the case of scalar additive interactions, the profile given by Eqs. (99) and (100) is correct at all densities, but time ordering should be retained in principle. Its neglect, according to Smith *et al.* (1973), approximates the perturbers as statistically independent, ignoring two-body and higher-order correlations that have an uncertain effect on the neutral-atom line profile. Such corrections should be small and are perhaps generally negligible.

(3) The collisions are weak and first-order perturbation theory is valid for all events. If the duration of collision is τ_d , then this condition may be written

$$\frac{V(\bar{b})}{\hbar} \tau_d \ll 1 . \quad (107)$$

The limits of validity on the classical path approximation, required for these results to apply, will be discussed in the following section. In addition, the condition for the separation of density matrices of the radiator and the perturber was that the term V/kT be negligible when the radiator density matrix is computed. For consistency, we must also not include V/kT in the velocity distribution $f(v)$. This point has been discussed by Cooper (1973) in detail, and it has particular bearing on the works of several authors who retain the factor (Schuller and Behmenburg, 1974; Atakan and Jacobson, 1972; Fox and Jacobson, 1969). The errors in any case would not be large unless V were nearly kT . The distribution used for the analysis of far-wing profiles in several experiments (Hedges, Drummond, and Gallagher, 1972) can be recovered from the unified theory in the limit of small correlation time s only if $f(v)$ does not include V/kT , and if the proper perturber dynamics are included in the average, which is to say that curvature of the classical path must be allowed for. Averaging over a curved trajectory in the unified approach would lead to an $\exp(-V/kT)$ weighting in the line wings. In summary, for straight perturber trajectories, $f(v)$ must not include the potential energy. The case of the static limit will be considered in some detail later.

g. Breakdown of the classical path approximation

The classical path approximation (Smith, Vidal, and Cooper, 1969a) that is basic to these calculations is valid under conditions of such wide range that with few exceptions it is used for almost all line-broadening calculations. The precise conditions of validity are, however, of special interest because in unified theories the approximation fails under some conditions that may be of practical significance.

First of all, we restrict our attention here to the possible breakdown of the classical treatment of the wave functions of the perturbers. Another source of difficulty, the separation of perturber and emitted density matrices, was addressed earlier when we imposed the requirement that

$$V/kT \ll 1 \quad (108)$$

for this treatment. When we identify a particular frequency with a particular perturbation, as in the statistical theory, Eq. (108) translates into a frequency-dependence condition $\hbar\omega \ll kT$. Thus at 1000 K the theory is valid only within a region of much less than 700 cm^{-1} from the line center. More recent work on radiative redistribution (Burnett *et al.*, 1980) has dealt with some situations in which this requirement may be relaxed.

For the classical path approximation to be applicable, it is necessary that the de Broglie wavelength of the perturber be smaller than a characteristic distance over which the interatomic potential varies appreciably. A measure of the order of size of this distance is an effective impact parameter \bar{b} . For perturber momentum p we have the condition

$$\bar{b} \gg \lambda/2\pi = \hbar/p . \quad (109)$$

We recognize that the angular momentum l for this impact parameter is

$$\hbar l = p\bar{b} , \quad (110)$$

from which we obtain the condition

$$l \gg 1 . \quad (111)$$

For the line profile to be treated with a classical path, the collisions of significance must have large angular momentum. Such a condition is quite similar to that required to calculate scattering cross sections classically (Mott and Massey, 1965, p. 111).

Another consideration is the assignment of a well-defined position to the perturber, in order that the correlation function may be calculated for different delays along the perturber path. For instance, for a time interval Δs the classical perturber will move a distance $v\Delta s$. The smallest time interval with meaning in the sense of the classical path is one for which

$$v(\Delta s)_{\min} \simeq \lambda/2\pi = \hbar/p \quad (112)$$

or

$$(\Delta s)_{\min} \gg \hbar/(pv) \sim \hbar/kT . \quad (113)$$

Changes in the correlation function over time differences of order Δs map into changes in the spectrum over frequency intervals of order $(\Delta s)^{-1}$. In terms of $\Delta\omega$

$$1/\Delta\omega \gg \hbar/kT \quad (114)$$

or

$$\hbar\Delta\omega \ll kT . \quad (115)$$

This condition appeared earlier, Eq. (108), as a requirement for the separability of the density matrices.

In the far line wing, where spectral energy differences are as great as thermal collisional energies or greater, we see two disparate phenomena working together to alter the classical path spectrum. The effects of deviations from straight-line paths and of perturber wavelength appear under similar conditions. Of course, it is just as we begin to worry about the curvature of the perturber trajectory that we must also assign a particular state to the system in order to define the interaction that determines that trajectory. On the basis of JWKB results, Szudy and Baylis (1975) recommend calculating the path from an average of initial and final states as an adequate approximation to get out of this dilemma. Nevertheless, when the straight-line classical path is invalid, it is surely best to pursue a fully quantal calculation.

2. An alternative formulation

The unified Franck-Condon theory of Szudy and Baylis (1975, 1977) is a molecular approach based on the Franck-Condon principle and developed from the ideas of Jablonski (1945), discussed in Sec. II.A.6, and the work of Baranger (1958a, 1958b, 1962), discussed in the previous section. It is a theory that is useful for the entire line profile, particularly at low densities.

The starting point is Eq. (61) of Sec. II.C.1,

$$I(\omega) = \sum_{if} \delta(\omega - \omega_{if}) (\langle f | d | i \rangle)^2 \rho_i , \quad (116)$$

where ω_{if} is the frequency of the radiator in the presence of all the perturbers, ρ_i is the probability of the initial state of the radiator and its perturbers, and the states of the system are products of single-particle states

$$|i\rangle = |\phi_i\rangle |\chi_i(1)\rangle |\chi_i(2)\rangle \cdots |\chi_i(N)\rangle \quad (117)$$

of the radiator ($|\phi\rangle$) and N perturbers ($|\chi\rangle$). In using the following approach we assume that the potentials are adiabatic, and neglect transitions between different levels of the radiating atoms induced by collisions. Since d operates only on the radiator states, we can make the assumption that its matrix elements are constant terms d_{if} and Fourier-transform $I(\omega)$ [see Eq. (62)] to obtain

$$\Phi(s) = \sum_{if} d_{if}^2 p_i \prod_j [|\langle \chi_i(j) | \chi_f(j) \rangle|^2] \exp(-i\omega_0 s) \times \exp \left[- \sum_j \Delta\omega_{if}(j)s \right] , \quad (118)$$

where ω_0 is the unperturbed frequency, $\Delta\omega_{if}(j)$ is the perturbation due to the j th perturber, and d_{if} is the dipole transition matrix element. Selecting an isolated line for which all d_{if} contributing are equal and constant, we obtain to within a constant factor

$$\Phi(s) = \exp(-i\omega_0 s) [\phi(s)]^N , \quad (119)$$

where $\phi(s)$ is the single-perturber correlation function,

$$\phi(s) = \sum_{if} |\langle \chi_i | \chi_f \rangle|^2 \exp(-i\Delta\omega_{if}s) \rho_i , \quad (120)$$

so that the N -perturber correlation function is proportional to the N th power of a single-perturber correlation function. The spectrum is given entirely in terms of one-perturber quantities.

A more conventional form results by writing

$$\phi(s) = 1 - g(s)/\mathcal{V} , \quad (121)$$

where \mathcal{V} is the volume in which the radiator is isolated. Then as N is increased while N/\mathcal{V} is held constant, the correlation function becomes the same as Eq. (99) of the preceding section,

$$\Phi(s) = \exp(-i\omega_0 s) \exp[-ng(s)] , \quad (122)$$

while $g(s)$ is given by

$$g(s) = \left[\sum_{if} \rho_i |\langle \chi_i'' | \chi_f'' \rangle|^2 [1 - \exp(-i\Delta\omega_{if}s)] \right] . \quad (123)$$

Notice that this form of $g(s)$ neglects possible effects of time ordering. A different normalization for the one-perturber states $|\chi''\rangle$ is introduced explicitly here, to the volume \mathcal{V} . This is common in scattering calculations and is used by Baranger (1958a, Sec. 4).

This is the starting point for Szudy and Baylis [1975, Eq. (2.5)], from which they construct their unified Franck-Condon line shape. The line shape is determined by the values of the free-free Franck-Condon factors $|\langle \chi_i | \chi_f \rangle|^2$ along the lines drawn in our discussion of Jablonski's work. These integrals can be calculated if certain assumptions about the wave functions are made, and we shall consider those results in Sec. II.F.1. An evaluation by these methods of the spectrum of the line wing in the limit where only one perturber is significant at a time, the nearest-neighbor approximation, has been given recently by Herman and Sando (1977).

3. Nonadiabatic processes

As we saw in the previous sections, the quantum treatment of line broadening depends on an evaluation of the evolution operator U for the radiator-perturber system. The problem is nontrivial in all but two-level atoms because of fine-structure transitions between excited states that occur during the collision. The complete calculations of U thus depends upon the evolution of the composition of an atomic state, expressed mathematically as a sequence of coupled differential equations. The exact solution of these coupled equations is so time consuming, even in high-speed numerical calculations, that it has not been feasible to apply it to a complete unified-theory profile calculation.

In 1965 Nikitin introduced the idea of using a molecular model of the collision itself, in such a way that each stage of the collision could be described by the appropriate Hund's coupling case (Nikitin, 1965; Masnou-Seeuws and McCarroll, 1974; Herzberg, 1950; Judd, 1975). This approach has found recent application to line broadening, particularly in the impact region (Lewis, McNamara, and Michels, 1971; Lewis and McNamara, 1972; Lwin, McCartan, and Lewis, 1976; Kielkopf and Allard, 1980). A comparison of different methods of calculating the broadening rate for the sodium D -line core has shown that this method produces broadening rates in agreement both with the solution of coupled equations and with experimental observation (Kielkopf, 1980). In the following, we outline the use of Hund's cases in collision problems, using the treatment given by Masnou-Seeuws and McCarroll (1974). In addition to Nikitin's (1965) original paper, there is also a good survey in a recent review by Nikitin and Smirnov (1978), particularly their Sec. 4. The application of symmetry considerations to the calculation of the S matrix, the

evolution operator for a completed collision, is discussed in a recent review of impact broadening by Lewis (1980).

a. Fine-structure mixing

We reconsider a radiating atom A in collision with a perturber P , separated from A by the distance R , in order to illustrate fine-structure mixing as an example of more general inelastic transitions. The system Hamiltonian is computed in a semiclassical treatment, with the presumption that the trajectories of the atoms are described classically. Usually these trajectories are also assumed to be rectilinear, although this is not a necessary constraint, since nonrectilinear trajectories are unimportant when $|V(R) - V(\infty)| \ll kT$. Then, in the usual way, we separate the Hamiltonian into the free-atom Hamiltonian H_A and the perturber Hamiltonian H_P plus the interaction V between the atoms,

$$H = H_A + H_P + V. \quad (124)$$

We assume that the perturber remains unexcited and that the structure of the perturber is not a consideration in the following calculations. The radiator Hamiltonian, however, is divided into core (H_C) and spin-orbit (H_{LS}) parts. Then

$$H = H_C + H_{LS} + H_P + V \quad (125)$$

is the system Hamiltonian. The problem of calculating the interaction V will be considered in Sec. II.D. Since the evolution operator U is the formal solution of the Schrödinger equation in the interaction representation, the problem is to solve

$$i\hbar \frac{\partial |\Psi\rangle}{\partial t} = H |\Psi\rangle. \quad (126)$$

b. Symmetry properties of the Hamiltonian and associated operators

To describe the collision, we introduce two reference frames with common origin at the center of mass of atom A , as illustrated in Fig. 6:

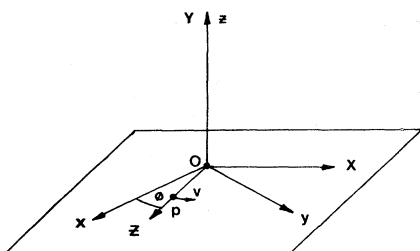


FIG. 6. Two coordinate systems for describing an atomic collision. The $OXYZ$ system has an internuclear Z axis that rotates during the collision; the $Oxyz$ system is fixed in space with the z axis out of the collision plane (Masnou-Seeuws and McCarroll, 1974).

(i) A fixed-frame $oxyz$ has the z axis perpendicular to the collision plane.

(ii) A rotating-frame $OXYZ$ has an internuclear axis OZ between A and B , with the y axis perpendicular to the collision plane.

The passage from the fixed to the rotating frame is described by the Euler angles $(\alpha, \beta, \gamma) = (\phi, \pi/2, \pi/2)$ and can be carried through with the operators $\mathcal{D}(\alpha, \beta, \gamma)$, as described by Edmonds (1968, Chap. 4).

We then introduce three possible bases:

- (i) the atomic basis $|Jm\rangle$ with quantization axis oz ;
- (ii) the atomic basis $|JM\rangle$ with quantization axis OZ ; and
- (iii) the molecular basis $|\Lambda M_L\rangle |SM_S\rangle$.

In case (iii) the axis of quantization is also OZ , the rotating internuclear axis, and $\Lambda = |M_L|$ is defined as in molecular structure calculations (Judd, 1975; Herzberg, 1950).

For our purposes there are three useful symmetry operations on the Hamiltonian:

- (i) $\mathcal{R}_z(\alpha)$ defining rotation about the fixed axis oz ;
- (ii) $\mathcal{R}_Z(\alpha)$ defining rotation about the internuclear axis OZ ; and
- (iii) σ_c defining reflection through the collision plane.

The basis states are to be restricted to sets of a given parity $(-1)^P$ with respect to an inversion through the origin. The eigenstates of the reflection σ_c are constructed from (Masnou-Seeuws and McCarroll, 1974; Shakeshaft, 1972)

$$|JM; \pm\rangle = [|JM\rangle \pm (-1)^M |J-M\rangle]/\sqrt{2} \quad (M \neq 0), \quad (127)$$

$$|J0; \pm\rangle = |J0\rangle, \quad (128)$$

$$\sigma_c |JM; \pm\rangle = \pm (-1)^{P+J+2M} |JM; \pm\rangle, \quad (129)$$

$$\sigma_c |Jm; \pm\rangle = (-1)^P \exp(-i\pi m) |Jm\rangle. \quad (130)$$

Because the interaction potential V is electrostatic in origin, it is cylindrically symmetric about the internuclear axis. In a system that does not rotate, this will mean that the potential will not depend on the sign of M , although its effect may depend on the M value of the state of the system. In the general case, V commutes with σ_c . The potential V also commutes with S^2 and L_z , so consequently it is diagonal in the molecular basis. However, when a rotating axis is used as the axis of quantization, off-diagonal elements in the Hamiltonian will appear due to the time dependence of the basis set (Masnou-Seeuws, 1973; Allard, 1973).

The state $|\Psi(t+s)\rangle$ is obtained from the earlier state $|\Psi(t)\rangle$ through the evolution operator $U(t+s, t)$. We write the result in terms of $|\Psi(t)\rangle$ as

$$|\Psi(t+s)\rangle = U(t+s, t) |\Psi(t)\rangle \quad (131)$$

or in terms of the chosen basis states $|\Phi_j(t)\rangle$ as

$$|\Psi(t+s)\rangle = \sum_j a_j(t+s) |\Phi_j(0)\rangle. \quad (132)$$

The right-hand sides of these two equations must thus be equal, that is,

$$\sum_j a_j(t+s) |\Phi_j(0)\rangle = U(t+s,t) \sum_j a_j(t) |\Phi_j(0)\rangle. \quad (133)$$

From this we obtain a relationship between the matrix elements of U and the coefficients a_j ,

$$a_k(t+s) = \sum_j \langle k | U(t+s,t) | j \rangle a_j(t). \quad (134)$$

Thus, if at the instant "t" the state is $|\Phi_j\rangle$, then the initial conditions $a_j(t)=1$ and $a_{n\neq j}(t)=0$ are sufficient to define

$$U_{kj}(t+s,t) = a_k(t+s,t), \quad (135)$$

which is quite enough to give us the required evolution-operator matrix elements needed for a profile calculation (Callaway and Bauer, 1961; Stacey and Cooper, 1971).

Consider, for example, the expansion of a state in terms of the basis states $|JM\rangle$ in the rotating frame. These states have rotated an angle ϕ from the state at the initiation of the collision for which $t=-\infty$. If these initial states are denoted $|JM\rangle_0$, then the states develop from the initial state according to the rotation about the Y axis in Fig. 6,

$$|JM\rangle = \exp(-i\phi J_Y) |JM\rangle_0. \quad (136)$$

The implicit dependence on $\phi(t)$ for this basis means that the expansion of a general state of the system

$$|\Psi\rangle = \sum_{M=-J}^M a_M |JM\rangle \quad (137)$$

has a time derivative

$$\frac{\partial |\Psi\rangle}{\partial t} = \sum_{M=-J}^M (\dot{a}_M |JM\rangle - i\dot{\phi} J_Y a_M |JM\rangle). \quad (138)$$

Thus the Schrödinger equation [Eq. (126)] becomes

$$i\hbar \sum_{M=-J}^J \dot{a}_M |JM\rangle = \sum_{M=-J}^J (H - \hbar\dot{\phi} J_Y) |JM\rangle a_M. \quad (139)$$

The rotation of the basis states can be simulated by using an effective Hamiltonian $H' = H - \hbar\dot{\phi} J_Y$ for this choice of initial basis. In the Schrödinger representation we ob-

tain a set of coupled equations for the coefficients a_M ,

$$i\hbar \dot{a}_M = \sum_{M'=-J}^J \langle JM | H' | JM' \rangle a_{M'}. \quad (140)$$

Should the system Hamiltonian couple states of other J , then the summation would be extended as necessary. The solution of these equations, according to Eq. (135), yields the time evolution of the system, and thereby the required evolution-operator matrix elements. The effective Hamiltonian H' depends on the basis chosen, and the matrix elements in these coupled equations are never diagonal.

c. The choice of representation: Hund's cases

As shown in Table I, the different terms of the Hamiltonian do not always commute. In order to resolve the time evolution, it is often useful to choose a basis in which the off-diagonal terms are the smallest. In this optimal case, it is sometimes possible to neglect the off-diagonal elements entirely. In such an instance we say that the system is described by a Hund's coupling case (Hund, 1926, 1927; Herzberg, 1950; Roueff, 1972; Masnou-Seeuws, 1973; Allard, 1973; Judd, 1975). The different Hund's cases are summarized in Table II, together with an approximate validity condition for the use of that case.

d. An example: Hund's case C applied to the resonance lines of cesium perturbed by xenon

Although the appropriate Hund's case may change through a collision, or with impact parameter, in some instances the solution for U can be exact, and in other cases it may be well approximated by a single Hund's case for the entire calculation. An example of changing Hund's cases thorough a collision trajectory was given by Lewis, McNamara, and Michels (1971) in their calculation of impact broadening of the sodium D lines. Here we consider the simpler example of the resonance lines of cesium perturbed by xenon. The validity of our calculation rests on assumptions of low density and perturbations much less than kT . The treatment given here was summarized briefly in Allard, Sahal-Brechot, and Biraud (1974) and treated more completely in Allard (1973).

We consider the solution of the problem in basis states

TABLE I. Symmetry properties of the collision Hamiltonian.^a

Terms in the collision Hamiltonian $H' = H - \hbar\dot{\phi} J_Y$	Spin-orbit H_{LS}			Electrostatic V		Rotation	
Symmetry	$\mathcal{R}_Z(\alpha)$	$\mathcal{R}_z(\alpha)$	σ_c	$\mathcal{R}_Z(\alpha)$	σ_c	L_y	J_y
Commuting operators	$J^2 J_Z$	$J^2 J_z$	$J^2 J_z$	$L_Z S^2 S_Z$	$S^2 S_z$	$L^2 L_z$	$J^2 J_z$
Diagonal representation	$ JM\rangle$	$ Jm\rangle$	$ Jm\rangle$	$ \Lambda M_L\rangle SM_S\rangle$	$ \Lambda M_L; \pm\rangle Sm_S\rangle$	$ Lm_L\rangle Sm_s\rangle$	$ Jm\rangle$
			$ JM; \pm\rangle$		$ \Lambda M_L; \pm\rangle SM_S; \pm\rangle$		

^aMasnou-Seeuws and McCarroll (1974).

TABLE II. Hund's cases.^a

Hund's case	Representation	Validity ^b
A	$ \Lambda M_L\rangle SM_S\rangle$ or $ \Lambda M_L; \pm\rangle SM; \pm\rangle$	$V \gg E_{LS} \gg \hbar\dot{\phi}$
B	$ \Lambda M_L; \pm\rangle Sm_s\rangle$	$V \gg \hbar\dot{\phi} \gg E_{LS}$
C	$ JM\rangle$ or $ JM; \pm\rangle$	$E_{LS} \gg V \gg \hbar\dot{\phi}$
D	$ Lm_L\rangle Sm_S\rangle$	$\hbar\dot{\phi} \gg E_{LS} \gg V$
E	$ Jm\rangle$	$E_{LS} \gg \hbar\dot{\phi} \gg V$

^aMasnou-Seeuws and McCarroll (1974).^bThe fine-structure separation is E_{LS} , the matrix element of the perturbation responsible for recoupling the state in question is V .

$|JM\rangle$ for both initial and final states of the transition $6s^2S_{1/2}-6p^2P_{1/2,3/2}$. Except for very close collisions that are not of interest for the optical problem, the ground state remains very well isolated, and the potential energy is diagonal in the basis $|\frac{1}{2} \pm \frac{1}{2}\rangle$. The coupling coefficient in the interaction representation has the simple differential equation

$$i\hbar\dot{a}_f = \langle f | V | f \rangle = V_f a_f \quad (141)$$

that has the solution

$$\begin{aligned} a_f(t+s,t) &= \exp \left[-i \int_t^{t+s} (V_f / \hbar) dt \right] \\ &= \exp[-i\delta(t+s,t)], \end{aligned} \quad (142)$$

$$U_{ff} = \exp(-\delta) \quad (143)$$

for the final ground state.

For the initial state we need to distinguish diagonal potential-energy matrix elements

$$V(^2\Pi_{1/2}) = \langle \frac{1}{2} \pm \frac{1}{2} | V | \frac{1}{2} \pm \frac{1}{2} \rangle, \quad (144)$$

$$V(^2\Sigma_{1/2}) = \langle \frac{3}{2} \pm \frac{1}{2} | V | \frac{3}{2} \pm \frac{1}{2} \rangle, \quad (145)$$

$$V(^2\Pi_{3/2}) = \langle \frac{3}{2} \pm \frac{3}{2} | V | \frac{3}{2} \pm \frac{3}{2} \rangle. \quad (146)$$

$ JM\rangle$	$ \frac{1}{2} - \frac{1}{2}\rangle$	$ \frac{1}{2} + \frac{1}{2}\rangle$	$ \frac{3}{2} - \frac{3}{2}\rangle$	$ \frac{3}{2} - \frac{1}{2}\rangle$	$ \frac{3}{2} + \frac{1}{2}\rangle$	$ \frac{3}{2} + \frac{3}{2}\rangle$
$\langle \frac{1}{2} - \frac{1}{2} $	$V(\Pi_{1/2})$	$+i\frac{\hbar\dot{\phi}}{2}$		$V(\Sigma\Pi)$		
$\langle \frac{1}{2} + \frac{1}{2} $	$-i\frac{\hbar\dot{\phi}}{2}$	$V(\Pi_{1/2})$			$V(\Sigma\Pi)$	
$\langle \frac{3}{2} - \frac{3}{2} $			E_{LS} $+ V(\Pi_{3/2})$	$+i\frac{\hbar\dot{\phi}}{2}\sqrt{3}$		
$\langle \frac{3}{2} - \frac{1}{2} $	$V(\Sigma\Pi)$		$-i\frac{\hbar\dot{\phi}}{2}\sqrt{3}$	E_{LS} $+ V(\Sigma_{1/2})$	$+i\hbar\dot{\phi}$	
$\langle \frac{3}{2} + \frac{1}{2} $		$V(\Sigma\Pi)$		$-i\hbar\dot{\phi}$	E_{LS} $+ V(\Sigma_{1/2})$	$+i\frac{\hbar\dot{\phi}}{2}\sqrt{3}$
$\langle \frac{3}{2} + \frac{3}{2} $				$-i\frac{\hbar\dot{\phi}}{2}\sqrt{3}$	E_{LS} $+ V(\Pi_{3/2})$	

(153)

The designations Σ and Π refer to the molecular states for which M_L is 0 or ± 1 , respectively, and the subscripts refer to M_J . We also need to consider the effect of off-diagonal potential terms such as

$$V(\Sigma\Pi) = \langle \frac{3}{2} \pm \frac{1}{2} | V | \frac{1}{2} \pm \frac{1}{2} \rangle \quad (147)$$

connecting states of different J with the same M . Although $V(\Sigma\Pi)$ may be as large as a diagonal term, for this example we assume it to be small in comparison to the spin-orbit interaction E_{LS} that separates $|^2P_{1/2}\rangle$ and $|^2P_{3/2}\rangle$.

H' also included the rotational coupling operator $-\hbar\dot{\phi}J_Y$, which, for these basis states $|JM\rangle$, has matrix elements

$$\begin{aligned} \langle J'M' | -\hbar\dot{\phi}J_Y | JM \rangle \\ = \left\langle J'M' \left| -\frac{\hbar\dot{\phi}}{2i}(J_+ - J_-) \right| JM \right\rangle, \end{aligned} \quad (148)$$

where

$$J_+ = J_X + iJ_Y \quad (149)$$

and

$$J_- = J_X - iJ_Y. \quad (150)$$

Thus, since

$$J_\pm |JM\rangle = [J(J+1) - M(M \pm 1)]^{1/2} |JM \pm 1\rangle, \quad (151)$$

$$\begin{aligned} \langle J'M' | -\hbar\dot{\phi}J_Y | JM \rangle \\ = \pm \frac{i\hbar\dot{\phi}}{2} \delta_{JJ'} \delta_{M', M \pm 1} [J(J+1) - M(M \pm 1)]^{1/2}. \end{aligned} \quad (152)$$

So the complete matrix of H' for the six substates of the 2P multiplet is

The term $\dot{\phi}$ in the effective Hamiltonian introduces off-diagonal contributions due to rotation into the time-evolution equations. The $^2P_{1/2}$ and $^2P_{3/2}$ states are not coupled by rotation, but the substates of each level are mixed. Whether the degree of nonadiabaticity introduced in this way is significant for the line profile depends on the relative magnitudes of $\hbar\dot{\phi}$ and the interaction potential. We make the assumption that Hund's case C is valid throughout the collision, or, following Table II, that $E_{LS} \gg V \gg \hbar\dot{\phi}$. This is reasonable for the perturbation of a heavy alkali by a heavy noble gas at typical laboratory temperatures of the order of 500 K. For the resonance lines of Cs perturbed by Xe, the $6p$ state has a spin-orbit interaction of 554 cm^{-1} , V is of the order 100 cm^{-1} at $R=5 \text{ \AA}$, and $\hbar\dot{\phi}$ is of the order v/R , about 4 cm^{-1} . Even for high doublets in Cs, the approximation is still good because, as the fine structure decreases with increasing excitation, so does the typical perturbation, and the larger impact parameters of interest yield smaller $\dot{\phi}$. For the $9p$ state E_{LS} is 45 cm^{-1} , V is of the order 10 cm^{-1} for $R=25 \text{ \AA}$, and $\hbar\dot{\phi}$ is less than 1 cm^{-1} . This approximation would not be good, however, for light alkalies with smaller fine structure.

An appropriate expansion including all the terms in $\langle JM | H' | J'M' \rangle$ is quite complex, but when Hund's case C is valid the terms in $\dot{\phi}$ can be neglected. Furthermore, the remaining off-diagonal potential terms $V(\Sigma\Pi)$ couple $^2P_{1/2}$ and $^2P_{3/2}$, introducing a first-order correction of magnitude $[V(\Sigma\Pi)]^2/E_{LS}$ to the zero-order result, smaller by a factor V/E_{LS} than the diagonal terms. It is feasible then to regard the $^2P_{1/2}$ and $^2P_{3/2}$ states as uncoupled so long as only spectral regions for which $V(R) \ll E_{LS}$ are considered. In the sense of the coupled equations, the spin-orbit interaction is so large that the terms linking $^2P_{1/2}$ and $^2P_{3/2}$ oscillate strongly, making the fine-structure cross section negligible compared to the total one.

Appropriate expansions in terms of the $|JM\rangle$ basis are

$$|^2P_{1/2}\rangle = a_1 |^{\frac{1}{2}} + \frac{1}{2}\rangle + a_2 |^{\frac{1}{2}} - \frac{1}{2}\rangle \quad (154)$$

and

$$\begin{aligned} |^2P_{3/2}\rangle &= b_1 |^{\frac{3}{2}} + \frac{3}{2}\rangle + b_2 |^{\frac{3}{2}} + \frac{1}{2}\rangle \\ &\quad + b_3 |^{\frac{3}{2}} - \frac{1}{2}\rangle + b_4 |^{\frac{3}{2}} - \frac{3}{2}\rangle. \end{aligned} \quad (155)$$

The coupled equations are found by application of Eq. (140) explicitly, but as a consequence of the arguments presented, no off-diagonal terms in H' appear. The coupled equations then reduce to two simple soluble systems,

$$i\hbar\dot{a} = V(^2\Pi_{1/2})a \quad (156)$$

for the $J=1/2$ state and

$$i\hbar\dot{b}_1 = V(^2\Pi_{3/2})b_1 \quad (157)$$

and

$$i\hbar\dot{b}_2 = V(^2\Sigma_{1/2})b_2 \quad (158)$$

for the $J=\frac{3}{2}$, $M_J=\frac{3}{2}$, and $M_J=\frac{1}{2}$ states, respectively.

In the $J=\frac{1}{2}$ case the matrix element of U , as it was for the ground state, is given by a single phase shift,

$$\begin{aligned} \langle 6p \ ^2P_{1/2}M_J | U(t+s,t) | 6p \ ^2P_{1/2}M'_J \rangle \\ = \delta_{M_J M'_J} \exp(-i\eta), \end{aligned} \quad (159)$$

with η given by

$$\eta = \frac{1}{\hbar} \int_t^{t+s} V(^2\Pi_{1/2}) dt. \quad (160)$$

Because this level is well isolated by the spin-orbit interaction, it evolves as if the interaction were spherically symmetric. It follows that the isolated transition $6s \ ^2S_{1/2}-6p \ ^2P_{1/2}$ has a spectrum that can be accounted for by a scalar phase-shift line-broadening theory.

The $J=\frac{3}{2}$ case has two noninteracting sublevels with $M_J=\frac{3}{2}$ and $\frac{1}{2}$. The evolution operator is given by

$$\begin{aligned} \langle 6p \ ^2P_{3/2}M_J | U(t+s,t) | 6p \ ^2P_{3/2}M'_J \rangle \\ = \delta_{M_J M'_J} \times \begin{cases} \exp(-i\eta_1) (M_J \pm \frac{3}{2}) \\ \exp(-i\eta_2) (M_J = \pm \frac{1}{2}), \end{cases} \end{aligned} \quad (161)$$

with η_1 and η_2 given by

$$\eta_1 = \int_t^{t+s} [V(^2\Pi_{3/2})/\hbar] dt \quad (162)$$

and

$$\eta_2 = \int_t^{t+s} [V(^2\Sigma_{1/2})/\hbar] dt. \quad (163)$$

The final steps in the calculation of the correlation consist of performing the angular average and the sum in Eqs. (99) and (100). In this case the angular average in Eq. (100) reduces to a simple average on M_J , while the sum adds the spectra of two doublet components, which, since the fine structure has been regarded as large in comparison to the perturbation on collision, behave as if they were isolated. We obtain for $J=\frac{1}{2}$

$$g(s) = 2\pi \int_0^\infty b db \int_{-\infty}^{+\infty} \bar{v} dt \{1 - \exp[i(\delta - \eta)]\}, \quad (164)$$

and for $J=\frac{3}{2}$

$$\begin{aligned} g(s) &= 2\pi \int_0^\infty b db \int_{-\infty}^{+\infty} \bar{v} dt (1 - \frac{1}{2} \{\exp[i(\delta - \eta_1)] \\ &\quad + \exp[i(\delta - \eta_2)]\}). \end{aligned} \quad (165)$$

We shall see subsequently how these equations can be used to interpret the observed spectra of the cesium principal series perturbed by xenon.

Such models allow a determination of the profile differences between the D_1 and D_2 lines of the alkalies to

be made without having to resolve coupled equations. In the case where the anisotropy is neglected, the potentials for each of the states are the same and $\eta = \eta_1 = \eta_2$. Both lines are broadened identically. The distinction in the broadening of the two components of an alkali doublet arises when the anisotropy is not neglected; that is, has its physical basis in the different potentials of the $^2P_{1/2}$ and $^2P_{3/2}$ states.

The impact broadening of the sodium *D* lines by helium and atomic hydrogen has been calculated using this approach (Lewis, McNamara, and Michels, 1971; Lewis and McNamara, 1972). In those analyses the collisions are divided into two regions. In the inner zone, near the point of closest approach, Hund's case B is assumed to be valid, and electron spin and orbital angular momentum of the sodium atom decouple, with the orbital angular momentum following the rotation of the molecular axis. In the outer zone, Hund's case C is assumed to be valid, and rotation of the atomic system is neglected. The results of these calculations for the Na-He case are in good agreement with experiments (Kielkopf, 1980) and with fully quantal calculations (Wilson and Shimon, 1975).

4. Solutions to the general problem of the frequency redistribution of radiation

The profile that we have been calculating gives the frequency dependence of the absorption coefficient of an atom exposed to a low-intensity radiation field, or of the emission probability of a single photon. However, this is only part of a much more complex problem of predicting the probability of the emission of a photon of one frequency and polarization, after the atom has absorbed a photon of another frequency and polarization. The radiative redistribution function $F(\omega_1, \omega_2)$ describes this process. This redistribution problem is central to the formation of spectral lines in optically thick sources, in the sun, for instance, because a change in radiation frequency can effectively shift a photon from the optically thick core of a spectral line to the optically thin line wing, allowing it to escape from the source. Line-formation processes as applied to stellar atmosphere have been reviewed by Hummer and Rybicki (1971). Here we survey only what has been found out recently about the relationship between the redistribution function and the unified-theory profile, and about depolarization of line-wing fluorescence. Experiments on redistribution are discussed more fully in Sec. III.G.

A typical radiative redistribution experiment would introduce light of frequency ω_1 , as shown in Fig. 7, exciting an atom in state $|i\rangle$ to state $|e\rangle$. The atom subsequently undergoes a transition from $|e\rangle$ to $|f\rangle$, radiating at ω_2 . Because of collisions and the Doppler effect, ω_1 is not necessarily equal to ω_{ei} , and similarly ω_2 is not necessarily ω_{ef} . The evaluation of the redistribution function involves intricate considerations of the timing of events that can contribute to the evolution operators, as graphically illustrated by Omont, Smith, and Cooper

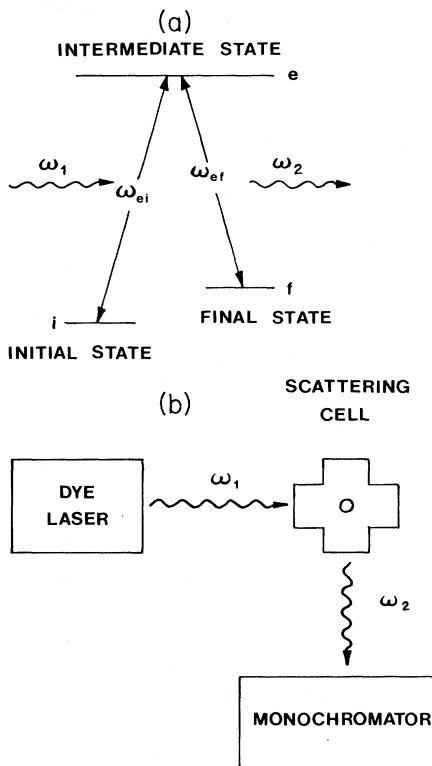


FIG. 7. Radiative redistribution.

(1972). The redistribution of radiation in the limit of the impact approximation near the center of the atomic line was first studied by Huber (1969a, 1969b), who investigated the dependence of the spectrum on the scattering angle and the combined effect with Doppler broadening. With the Baranger theory, Omont, Smith, and Cooper (1972) subsequently extended this approach using techniques similar to those we have applied here to line profiles. They concluded that redistribution near the line is entirely due to elastic collisions because the inelastic collisions cause fluorescence to appear out of the terminating level. Such transitions are usually far from the line under study, particularly in the impact limit, so that inelastic effects are manifested only by a renormalization of the frequency redistribution function. The work of Omont *et al.* also included a consideration of degenerate levels.

The general situation shown in Fig. 7 is simplified if we assume that the initial and final states are the same, so that ω_0 is the frequency corresponding to the energy difference between the two unperturbed levels. Then, if we neglect inelastic collisions,

$$F(\omega_1, \omega_2) = Cf(\omega_1)p(\omega_1, \omega_2), \quad (166)$$

$$p(\omega_1, \omega_2) = \left[\frac{\gamma_e}{\gamma_c + \gamma_e} \delta(\omega_1 - \omega_2) + \frac{\gamma_c}{\gamma_c + \gamma_e} f(\omega_2) \right], \quad (167)$$

and

$$f(\omega) = \frac{(\gamma_c + \gamma_e)/\pi}{(\omega - \omega_0 - \sigma_c)^2 + (\gamma_c + \gamma_e)^2}, \quad (168)$$

where C is a normalization constant, γ_c is the collisional broadening of the transition, γ_e is the radiative width of the intermediate level, and σ_c is the collisional shift. Here we also neglect collisional and radiative broadening of the lower state. The redistribution function is the product of the probability of absorption of a photon of frequency ω_1 and the probability of the emission of a photon of frequency ω_2 . The Rayleigh term given by the delta function in Eq. (167) is a coherent effect that gives the probability of radiation before a collision, while the $f(\omega_2)$ term represents the effect of an elastic collision. This result can also be given in more general form for the impact limit [Eqs. (45), (46), and (53) of Omont, Smith, and Cooper, (1972)], including degeneracy and polarization effects, although its basic physical interpretation remains the same. In the impact region, where radiation during the collision is neglected, the spectrum and the polarization of fluorescence depend only on collisional rates for the relevant atomic multipoles (Thomann, Burnett, and Cooper, 1980).

Related studies of line broadening and collisional depolarization in a magnetic field for the impact approximation have also been reported (Omont, Smith, and Cooper, 1973; Happer, 1972; House, 1970). In that case the dependence of the scattered light intensity on magnetic field strength should allow a determination of both inelastic and elastic cross sections.

The results achieved by these and other efforts (for example, Yelnik and Voslamber, 1979) have given us a reliable understanding of collisional redistribution in the impact limit for low-incident-light flux, but the more general case, particularly for nonimpact regions of the profile, is still a matter of theoretical investigation for which there is a marked paucity of experimental data (Cooper, 1979; Lewis, Salter, and Harris, 1981; Thomann, Burnett, and Cooper, 1980; Burnett and Cooper, 1980a, 1980b; Burnett *et al.*, 1980). There is experimental evidence, however, that the polarization of redistributed radiation in the far wing is high, of the order of 50%, when the gas pressure is sufficiently low that multiple depolarizing collisions are improbable. In these experiments absorption occurs during a collision at the frequency of the incident radiation. This absorption must be correlated with the collision event, for which the perturbation corresponds to ω_1 . The fluorescence spectrum is then described by two components, as in Eq. (167), with a Rayleigh peak at the incident frequency and a fluorescence profile that is sensitive to the collision dynamics. Cooper (1979) concludes that, for isolated nonhydrogenic lines in the absence of inelastic collisions, $f(\omega)$ is just the unified-theory line profile. Burnett *et al.* (1980) have looked into the use of density-matrix methods to evaluate the correlation function and the scattered spectrum when both initial and final levels interact with the perturber. They give expressions [see, for

example, Burnett and Cooper (1980b), Eq. (5.3)] that include corrections to our Eqs. (166)–(168) evaluated in the binary collision, i.e., low-density approximation.

An alternative description of the depolarizing process has been formulated by Lewis, Salter, and Harris (1981) in terms of a molecular coupling model of the sort used to compute impact linewidths in sodium (Lewis and McNamara, 1972). They assume that collisions for a 1P state closer than a cutoff radius are coupled as a molecule, so that the rotation of the molecular axis during the collision for this part of the trajectory is responsible for the observed depolarization. Straightforward geometrical calculation yields expressions that can be analyzed once a potential is chosen. Thus, with a specific choice of $C_6 R^{-6}$ for the long-range interaction, they were able to demonstrate a limiting far-wing polarization determined largely by the collision geometry. This type of information, while possibly present in features of exact far-wing contours from absorption spectra, could be extracted directly only if a unified evaluation of the profile, taking into account nonadiabatic processes, were carried through. Thus the low-density limit of the polarization in the fluorescence spectrum, analyzed with a molecular collision model, complements the conventional static analysis in the binary collision approximation to the absorption spectrum.

D. Interatomic potentials for line-broadening calculations

The concept that a perturber-emitter interaction, defined as a function of their separation, could be related directly to the shape of the emitter's spectral lines was introduced by Weisskopf (1932a, 1932b, 1933) into phase-shift theories of the line core, and by Kuhn and London (1934) and Kuhn (1934, 1937a, 1937b, 1937c) into statistical theories of the line wing. Since those developments, a part of the theory of line shapes has been the determination of the potential, for the purpose of predicting the broadening and shape of spectral lines. Potentials also can be deduced from observed line shapes, although the process is usually not unique and therefore requires some knowledge beforehand of what interactions to expect. This aspect of the problem, an area in which statistical theories of line broadening have found considerable use, will be treated in Sec. IV.A.

Early attempts at potential estimates to find a Weisskopf radius or an optical collision diameter turned to the van der Waals interactions. But even for simple cases, there is no physical justification for the internuclear separations of optical interest. In the case of the broadening of the sodium D lines, the impact width is determined around separations of the order of 5 Å, while the excited-state valence-electron wave-function peaks around 3 Å from the nucleus and has a substantial value out beyond 5 Å. The van der Waals interaction, as the first term of a multipole expansion, could hardly be adequate in this case, and the situation is worse for higher excited states. The purpose of this section is to deal

with potentials that might be inferred from detailed considerations of the atomic interactions. This is not to say that other types, such as the square-well, Morse, Buckingham, and Lennard-Jones potentials, would not be realistic estimates in some instances.

The ultimate problem is, however, to predict the observable effects on spectral lines with a small number of *a priori* or systematic parameters. So we consider here just those potentials that have been shown to be much more useful in this regard than the simplest empirical potentials. In the following sections we shall look at estimates of van der Waals interactions for long-range interactions of low-lying states; scattering-length-type potentials useful for the near-Rydberg states; pseudo, model, and *ab initio* potentials that span a wide range of excitations and internuclear separations with detail and improving accuracy.

There have been several recent reviews of excited-state potential calculations. Particularly useful ones are given by Baylis (1978), Bardsley (1974), and Düren (1980). A discussion in Lewis (1980) is also concerned with potentials for impact broadening.

1. Van der Waals interactions

... that force which gives rise to the constant a in van der Waals' equation.

—Margenau, 1939

The van der Waals interaction between unexcited atoms was introduced originally to account for the behavior of compressed gases. London (1930a, 1930b) evaluated the long-range interaction in the form

$$V(R) = \sum_p C_p R^{-p} \quad (169)$$

with quantum-mechanical expressions for C_p . Of special interest to us is the behavior when the two interacting atoms are not alike. In that case only the second- and higher-order interactions are nonzero, and the first nonzero term is

$$C_6 = -\frac{3e^2\hbar^4}{2m^2} \times \sum_{\substack{K' \neq K \\ L' \neq L}} \frac{f_{KK'}f_{LL'}}{(E_{K'}-E_K)(E_{L'}-E_L)(E_{K'}-E_K+E_{L'}-E_L)} \quad (170)$$

(Hindmarsh and Farr, 1972; Margenau and Watson, 1936; London, 1930a, 1930b). Here $f_{KK'}$ and $f_{LL'}$ are the oscillator strengths for transitions from the state K of the perturbed atom to state K' and from state L for the perturber to state L' ; the E_K are the energies of the respective states. The sign of C_6 depends on the sign of $E_{K'}-E_K+E_{L'}-E_L$. If the radiating atom is a metal perturbed by a rare gas in the ground state, this term is dominated by $E_{L'}-E_L$, which will always be positive. Long-range alkali-rare-gas interactions are attractive. In rare-gas-rare-gas or alkali-alkali interactions the sign

of C_6 is not obvious.

The case of interest is this one of the perturbation of an excited metal atom by a noble-gas atom or by neutral atomic hydrogen. Unsöld (1968) has given a simplification that is very useful. Terms in this sum are identified as the gas dipole polarizability α and the expectation value $\langle r^2 \rangle$ for the metal-atom valence electron. The force constant then becomes

$$C_6 = -\alpha e^2 \langle r^2 \rangle. \quad (171)$$

This form of the van der Waals interaction can be interpreted physically as the self-energy of the gas-atom-induced dipole moment in the instantaneous oscillating electric field of the metal atom. Such an interaction is given by

$$\langle V(R) \rangle = -\frac{1}{2} \alpha \langle E(\mathbf{R})^2 \rangle, \quad (172)$$

where $E(\mathbf{R})$ is the total electric field at the gas atom due both to the alkali valence electron and the ion core. When \mathbf{R} is the vector from the alkali nucleus to the perturbing gas atom, \mathbf{r} the vector from the nucleus to the valence electron, and $\mathbf{r}' = \mathbf{r} - \mathbf{R}$ the vector from the perturber to the alkali valence electron, the electric field is given by

$$\mathbf{E} = e \left[\frac{\mathbf{R}}{R^3} + \frac{\mathbf{r}'}{r'^3} \right]. \quad (173)$$

Equation (172) for $V(R)$ is crucial for the pseudopotential and model-potential methods to follow, but in the limit $R \gg r$ the spherical average of E^2 , given by Eq. (173), reduces $V(R)$ to a van der Waals interaction, with C_6 given by Eq. (171).

For excited states of alkalies, and possibly for iron and other transition elements, the diagonal matrix element $\langle r^2 \rangle$ can be calculated from (Condon and Shortley, 1964)

$$\langle r^2 \rangle = \frac{1}{2} a_0^2 n^{*2} [5n^{*2} + 1 - 3l(l+1)]. \quad (174)$$

An alternative expression is given by Hindmarsh, DuPlessis, and Farr (1970). Equation (174) is equivalent to assuming Bates-Damgaard radial wave functions (Bates and Damgaard, 1949). For reference we note that n^* is given by

$$n_K^{*2} = \frac{\mathcal{R}_M}{E_\infty - E_K}, \quad (175)$$

$$\mathcal{R}_M = \frac{\mathcal{R}_\infty}{1 + m/M}, \quad (176)$$

where E_∞ is the ionization energy of the atom, \mathcal{R}_∞ the Rydberg constant, m the electron mass, and M the atomic mass. The mass correction is not significant for most uses of C_6 in this context. Values of the dipole polarizability are given in Table III.

Mahan (1968, 1969) has evaluated C_6 from these expressions for alkali-noble-gas ground states and the first excited p states. His tabulations also include the angular dependence of the interaction (Sec. II.E.4), al-

TABLE III. Dipole and quadrupole polarizabilities.

Noble gas	Dipole polarizability	Quadrupole polarizability
	α (a_0^3)	β (a_0^5)
He	1.384 ^a	2.4 ^b
Ne	2.663 ^a	6.3 ^b
Ar	11.08 ^a	53.0 ^c
Kr	16.73 ^a	101.0 ^c
Xe	27.29 ^a	205.0 ^c

^aTeachout and Pack (1971).^bLanghoff and Hurst (1965).^cDavison (1968).

though for line profiles, when such effects are significant, more detailed calculations that use the full molecular potential should be pursued. Unsöld (1968) applies this form of C_6 to line-core shift and width for metal atoms in an atomic hydrogen gas. A word of caution, however, is in order. There is now ample evidence (Hindmarsh, Petford, and Smith, 1967; Hindmarsh, DuPlessis, and Farr, 1970) that C_6 by itself does not describe the potential adequately for atomic distances that determine the line core. In view of the observations of Baylis (1969) regarding his pseudopotential calculations that the term C_6R^{-6} does not represent the asymptotic interaction except when the potentials are less than a few cm⁻¹ deep, it is doubtful that the near line wings would be accurately given by this potential. Some measurements do, however, show a dependence of intensity on $(\Delta\omega)^{-3/2}$, as expected for an R^{-6} interaction from Eq. (16) (see Sec. III.E.1.a).

2. Analytic additions to the van der Waals term

Analyses of line-core shift and width, primarily by Hindmarsh and colleagues at Oxford and Newcastle (Hindmarsh, Petford, and Smith, 1967; Hindmarsh, DuPlessis, and Farr, 1970; Smith, 1972, 1975), have demonstrated that the van der Waals term alone does not account for the observed effects. This was noticed most markedly in observed shift-to-width ratios, which for an R^{-6} interaction should always be 0.73, but usually were not. Of course, unfortunately, many transitions studied involve degenerate levels for which nonadiabatic mixing is not included in the shift and width calculations. Nevertheless, an observation of line broadening and wing spectra in Tl involving nondegenerate states ($6s^26p^2P_{1/2}-6s^27s^2S_{1/2}$) could not be accounted for solely by an R^{-6} interaction (Cheron, Scheps, and Gallagher, 1977). Hindmarsh (1963) and Behmenburg (1964) were prompted to add a repulsive interaction to make a Lennard-Jones potential,

$$V(R) = C_6 R^{-6} + C_{12} R^{-12}. \quad (177)$$

Fits to observed shifts and widths with this potential give values of C_6 and C_{12} , although not unambiguously. Even the best values of C_6 determined in this way differ from theoretical values by factors of 2 or more.

The repulsive interactions of this scheme are, of course, empirical. Nevertheless, Hindmarsh found a systematic behavior in C_{12} that showed an increase in repulsive interaction with excitation of the atom. He proposed that C_{12} should be calculated by

$$C_{12} = q(|\mathbf{r}| + |\mathbf{r}'|)^{12}, \quad (178)$$

where r and r' are the distances from the alkali and noble gas, respectively, for which the probability density is 0.012 a.u., and q is a constant $0.9 \pm 0.3 \times 10^{-16}$ erg. Kielkopf (1972) showed that for Ar, Kr, and Xe perturbers C_{12} could be calculated from

$$C_{12} = An^{*B}, \quad (179)$$

where A is 8.6×10^{-105} erg cm¹² and B is 10.2, with an accuracy of about 25%.

Other important long-range effects should be added to these empirical approximations. Several calculations have included the next order in the multipole expansion, a term C_8R^{-8} , with C_8 given by

$$C_8 = -\frac{3}{2}\alpha e^2 \langle r^4 \rangle - \frac{5}{2}\beta e^2 \langle r^2 \rangle \quad (180)$$

and with $\langle r^4 \rangle$ given by

$$\begin{aligned} \langle r^4 \rangle = & \frac{1}{8}a_0^{4n^*4} \\ & \times [63n^{*4} - 35n^{*2}(2l^2 + 2l - 3) \\ & + 5l(l+1)(3l^2 + 3l - 10) + 12], \end{aligned} \quad (181)$$

where β is the foreign-gas-atom quadrupole polarizability. The terms represent, respectively, the interaction of the alkali quadrupole with the dipole of the gas induced by the alkali quadrupole, and the interaction of the dipole of the alkali with the quadrupole of the gas induced by the alkali dipole. Useful values for β are included in Table III (Kielkopf, 1974; Hindmarsh, DuPlessis, and Farr, 1970).

Finally, we note that a potential of the form

$$V(R) = \frac{C_6}{R_0^6 + R^6} + \frac{C_8}{R_0^8 + R^8} + \frac{C_{10}}{R^{10}} \quad (182)$$

has been proposed as a reasonable estimate of the average long-range interaction of excited alkalies with noble gases (Kielkopf, 1974). Here a cutoff parameter R_0 is set equal to $(\langle r^2 \rangle / 2)^{1/2}$, and C_{10} is given by the empirical formula

$$C_{10} = 2.8 \times 10^4 \tau n^{*-11.34} R_0^{10}, \quad (183)$$

where a repulsive scaling factor τ is 1.0 for Ar, Kr, and Xe and 0.3 for He and Ne. This potential was used to calculate the impact broadening and shift of the first three doublets of the alkali principal series perturbed by noble gases (Kielkopf, 1976b). These broadening calculations seem to be accurate to about 20% (Lwin and McCartan, 1978).

3. The Fermi potential

As an example of the severe problems that can arise with the use of a van der Waals or similar power-series potential, consider an atom in a highly excited state. For foreign-gas densities of the order of 10^{19} atoms cm^{-3} or greater, excited atoms with radii greater than 40 Å have a substantial probability of having a perturber within the outer antinode of the valence-electron charge distribution. Clearly, the long-range multipole expansion will not work for these states at all (see Fig. 37 below).

This difficulty was first encountered by Fermi (1934) in his analysis of the pressure shifts on high series members of alkali spectra. He proposed an interaction between an excited alkali atom and a noble-gas perturber that has the effective diagonal value

$$\langle V(R) \rangle = 2\pi \frac{\hbar^2}{m} A \Psi^2(R), \quad (184)$$

where A is a parameter called the scattering length, and $\Psi^2(R)$ is the valence-electron probability density at R . While Ψ^2 is readily calculated with a Bates-Damgaard wave function for excited alkalies at large R , the value of A must either be derived from the line-shift measurements, low-energy electron scattering, or *a priori* electron-noble-gas scattering calculations. The systematic values tabulated by O'Malley (1963) for the limit of zero kinetic energy of the valence electron are quoted here for reference in Table IV. Negative values of the scattering length mean that the interaction energy is attractive and that the electron wave function near the noble-gas atom is modified to increase the probability of finding the valence electron there.

The use of this potential in line-shape studies, apart from the application to transitions from very excited states, is restricted by the dependence of electron scattering on the kinetic energy of the electron, and thereby on n^* , as well as by the fact that the very-long-range interactions are not explicitly contained in Eq. (184). The form of the variation of A with n^* has been considered by Roueff (1970), Smirnov (1967), and Nikitin (1965). There does seem to be a discrepancy between various expressions in the literature, but the value (in atomic units)

$$A = \left[\frac{1}{A_0} - \frac{\pi\alpha}{3n^*A_0^2} - \frac{4\alpha[\ln(\alpha^{1/2}/4n^*)]}{3n^*A_0} \right]^{-1} - \frac{\pi\alpha}{5n^*} \quad (185)$$

adapted from Lewis (1980) gives fairly good agreement between computed width and shift for K ($4p-7s$) lines

TABLE IV. Scattering lengths.^a

Noble gas	A_0 (bohr)
He	+ 1.06
Ne	+ 0.18
Ar	- 1.86
Kr	- 3.8
Xe	- 6.9

^aO'Malley (1963).

broadened by He and Ar and experimental measurements (Kielkopf and Knollenberg, 1981). Although this potential may be useful for Rydberg atom transitions, and perhaps other highly excited states, the scattering length should be determined from independent calculations of the electron-gas-atom collision process. Omont (1977) has reviewed this potential for its application to neutral-atom line broadening. A method of including the long-range interactions in a flexible extension from this sort of calculation is discussed in the following section.

4. Pseudopotentials

We have discussed the general problem of alkali-noble-gas diatomic systems because, as we shall see later, many line-shape experiments have been done for these atoms. A major advance in the computation of excited-state potentials on such systems came from the application of pseudopotential methods (Bardsley, 1974) to the problem by Baylis (1969). Here we outline the method and give an example of the results. For other detailed potentials in alkali-noble-gas systems, parameters are given in Baylis (1969) or in the work of Pascale and Vandeplanque (1974), an extension of Baylis' calculations to higher excited states. There are also recent calculations for some of the lower-lying alkali states using a different radial wave function (Czuchaj and Sienkiewicz, 1979) and a modified polarization cutoff without approximation in the numerical integration (Düren and Moritz, 1980).

The calculations are, first of all, done in an atomic basis set $|nl(SL)JM\rangle$. The value M is a good quantum number for each resulting molecular state, and states $\pm M$ are not split by the interaction. The specification of M and the parent atomic state of the separated alkali labels any molecular level, although when alkali fine structure can be neglected, the projection of L on the internuclear axis allows states to be labeled $\Sigma, \Pi, \Delta, \dots$. The molecular arrangement for Σ or Π states has a simple geometry illustrated in Fig. 8. Such labels are not

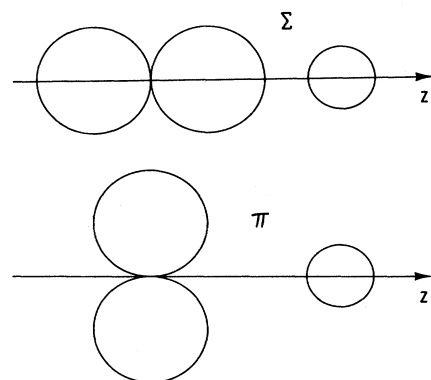


FIG. 8. Two geometries for an alkali p state-noble-gas collision. The Π state, with electronic orbital angular momentum along the internuclear axis, is not repulsive because there is no valence-electron charge along the axis. The Σ state, by contrast, has a stronger repulsive contribution.

rigorous designations for real atoms and can be misleading. The basis $|nl(SL)JM\rangle$ is expanded in terms of one-electron states $|nlm_lsm_s\rangle$, and in that basis we actually calculate matrix elements of an effective Hamiltonian,

$$H_{\text{interaction}} = F(\mathbf{r}, \mathbf{R}) + G(\mathbf{r}, \mathbf{R}) + W(R). \quad (186)$$

The terms in the Hamiltonian are, respectively, the interaction F of the valence electron and the ion core of the alkali with the induced dipole moment of the noble-gas atom, the pseudopotential G representing the Pauli pressure of the valence electron interacting with the noble-gas electrons, and the pseudopotential W for the Pauli pressure in the core-core interaction.

a. The calculation of the valence-electron–noble-gas electrostatic interaction $F(\mathbf{r}, \mathbf{R})$

The interaction of a one-electron atom with a perturber of known dipole polarizability can be calculated from Eqs. (172) and (173) if we neglect high-order polarization of the perturber. This electrostatic expression for F would be valid as long as the valence electron of the atom did not penetrate the perturber, for in that case the polarizability of the perturber would no longer be known, and the concept loses its physical justification. We have to define a region about the perturber of radius r_0 inside of which the electrostatic interaction is determined by some other method. Baylis (1969), for instance, proposes that when the valence electron is within r_0 the interaction is constant and equal to the average value at r_0 . Otherwise, F is expressed in terms of $\Theta(r' - r_0)$, a step function that is one when $r' \geq r_0$ and zero otherwise. We expand Θ in terms of Legendre polynomials so that the matrix elements can be easily evaluated in the atomic basis states:

$$r'^{2q} \Theta(r' - r_0) = \sum_{l=0}^{\infty} f_q^{(l)} P_l(\xi), \quad (187)$$

where $\xi = \cos(\mathbf{r}, \mathbf{R})$, and the $f_q^{(l)}$ are defined by (Baylis, 1969) the recursion relation

$$\begin{aligned} \chi f_q^{(l)} &= \frac{r_0^{2q+2}}{4rR} [P_{l+1}(\xi_0) - P_{l-1}(\xi_0)] \\ &+ \frac{q+l+2}{2l+3} f_q^{(l+1)} + \frac{l-q-1}{2l-1} f_q^{(l-1)}, \end{aligned} \quad (188)$$

where the variable $\chi = (r^2 + R^2)/2rR$, is the value of $\cos(\mathbf{r}, \mathbf{R})$ for $r' = r_0$. Since $f_q^{(0)}$ and $f_q^{(1)}$ are defined by the simple analytical integrals

$$f_q^{(0)} = \frac{1}{2} \int_{-1}^{\xi_0} d\xi (r^2 + R^2 - 2rR\xi)^q \quad (189)$$

and

$$f_q^{(1)} = \frac{3}{2} \int_{-1}^{\xi_0} \xi d\xi (r^2 + R^2 - 2rR\xi)^q \quad (190)$$

[see Eqs. (A8) and (A9) of Baylis, (1969) for evaluations], we can use the recursion formulas to find any $f_q^{(l)}$.

So from Eqs. (172) and (173) we write for F

$$\begin{aligned} F &= -\frac{\alpha e^2}{2R^4} (1 + 2rR^2 r'^{-3} \xi - 2R^3 r'^{-3} \\ &\quad + R^4 r'^{-4}) \Theta(r' - r_0), \end{aligned} \quad (191)$$

or, with substitution for Θ and use of a recursion relation for P_l ,

$$\begin{aligned} F &= -\frac{\alpha e^2}{2R^4} \sum_{l=0}^{\infty} \left[f_0^{(l)} - 2R^3 f_{-3/2}^{(l)} + R^4 f_{-2}^{(l)} \right. \\ &\quad + 2rR^2 \left[\frac{l}{2l-1} f_{-3/2}^{(l-1)} \right. \\ &\quad \left. \left. + \frac{l+1}{2l+3} f_{-3/2}^{(l+1)} \right] \right] P_l(\xi). \end{aligned} \quad (192)$$

This is Baylis' Eq. (A10) without the constant small r' interaction and corrected for a typographical error. Clearly, the $F(\mathbf{r}, \mathbf{R})$ has a very simple expansion,

$$F = \sum_{l=0}^{\infty} F_l(r, R) P_l(\xi), \quad (193)$$

which greatly simplifies the calculation of matrix elements since it separates the angular and radial integrations. Equation (183) for F is valid for all r and R , but will give zero for $r' < r_0$. We need to add to this F a contribution from the region of small r' . Baylis, for instance, includes a constant average interaction, zero for $r' > r_0$,

$$\begin{aligned} F'(R, \xi) &= -\frac{\alpha e^2}{2R^4} \sum_{l=0}^{\infty} [(1 + R^4 r_0^{-4}) \\ &\quad \times (\delta_{l,0} - f_0^{(l)})] P_l(\xi), \end{aligned} \quad (194)$$

which allows the same general form for F to be used for all r .

The eigenvalues of F are calculated from the series equation (193), and the F_l are taken from Eq. (192) or the series expressions given by Baylis. Regardless of the method used to evaluate the F_l or the short-range electrostatic interaction proposed, the parameter r_0 is empirical and must be adjusted by some comparison with experiment or *a priori* calculations. It can therefore be used to compensate to some degree for the inadequacies in the short-range interaction model and the extreme sensitivity of the potential to computation errors in G . This parameter may also be used to compensate for the absence of higher-order polarizabilities of the perturbing gas atom in the assumed electrostatic interaction.

b. The calculation of the valence-electron–noble-gas Pauli pressure repulsion $G(\mathbf{r}, \mathbf{R})$

The subject of pseudopotentials in atomic systems has been reviewed recently by Bardsley (1974). Here we con-

sider a pseudopotential introduced by Gombas (1967) and used by Baylis (1969) for the molecular problem to represent the interaction that repels an alkali valence electron from the noble-gas atom. We impose on the state of a multielectron system the condition that, in accordance with the Pauli exclusion principle, it be represented by a product of mutually orthogonal one-electron states. Because of this condition, the last electron added to the system occupies a state of minimal energy above the ground state, spatially correlated with the lower states. We represent this behavior with a pseudopotential in which the electron distribution is treated as a free-electron gas, as in the Thomas-Fermi statistical method. The total kinetic energy of this system of electrons is

$$E_F = \frac{3}{10} \frac{\hbar^2}{m} (3\pi^2)^{2/3} \int d\mathcal{V} \rho^{5/3}, \quad (195)$$

where ρ is the electron number density. If we apply this expression to the separated and combined systems consisting of an atom A and perturber P , and then take a difference to obtain an interaction energy, we obtain a repulsive Pauli interaction

$$\begin{aligned} V_P(R) &= \frac{3}{10} \frac{\hbar^2}{m} (3\pi^2)^{2/3} \\ &\times \int d\mathcal{V} [(\rho_A + \rho_P)^{5/3} - \rho_A^{5/3} - \rho_P^{5/3}]. \end{aligned} \quad (196)$$

In the limit that $\rho_A \ll \rho_P$ this expression would represent the valence-electron interaction with the high-density portion of the perturbing gas electron density. The expression simplifies to

$$\begin{aligned} V_P(R) &= \frac{\hbar^2}{2m} (3\pi^2)^{2/3} \int d\mathcal{V} \rho_A (\rho_P)^{2/3} \\ &= \int d\mathcal{V} \rho_A G, \end{aligned} \quad (197)$$

which gives us a pseudopotential operator

$$G(\mathbf{r}, \mathbf{R}) = \frac{\hbar^2}{2m} (3\pi^2)^{2/3} \rho_P^{2/3}. \quad (198)$$

This operator depends explicitly on the coordinates r' centered on the perturber, but the integral can be centered on the atom and expanded so that, in analogy with Eq. (193) for $F(\mathbf{r}, \mathbf{R})$,

$$G(\mathbf{r}, \mathbf{R}) = \sum_{l=0}^{\infty} G_l(r, R) P_l(\xi). \quad (199)$$

The terms of this Legendre series have coefficients

$$G_l(r, R) = \frac{2l+1}{2} \int_{-1}^{+1} d\xi G(\mathbf{r}, \mathbf{R}) P_l(\xi). \quad (200)$$

The two difficulties with this calculation are, first, finding appropriate expressions for the perturber charge density and, second, actually evaluating expressions for G_l . Once these expressions are known, the resulting numerical integration on r required to evaluate a matrix element of G has a sharply peaked integrand about the

perturbing gas atom. Baylis (1969) suggested the use of an expansion in derivatives of the three-dimensional delta function as a possible simplification for this calculation, but Pascale and Vandeplanque (1974) and Czuchaj and Sienkiewicz (1979) have suggested that this is not sufficiently accurate. Indeed, the contribution from G in the region $r' < r_0$ is very large and partially cancels the attractive contribution from F . The choice of r_0 is critical, for it governs a precise balance between attractive and repulsive short-range interactions.

Vallée *et al.* (1977) point out the close relationship between this pseudopotential and the Fermi potential. They demonstrate that the first term of the delta-function expansion of Eq. (198) is of the same form as the Fermi interaction, and they identify the relationship between the coefficients in the two expressions. They do not, however, consider the similar short-range polarization contribution of F to the potential of the Baylis model, an interaction effectively included by the empirical adjustment of the scattering length in the Fermi method. This separate treatment of the polarization effects in the Baylis model yields improved accuracies for low-lying states.

c. The calculation of the core-core interaction $W(R)$

When the perturber and the atom are close there may be a significant overlap of the core of the atom with the perturber charge distribution that gives an interaction $W(R)$ analogous to $G(\mathbf{r}, \mathbf{R})$ for the valence-electron overlap. In many cases of spectroscopic interest $W(R)$ is not important, because the line broadening is determined at such long range that W is negligible, and because W makes identical contributions to initial and final states of a transition. W is important in interpreting far wings of resonance lines of alkalies perturbed by noble gases, however, because of the effect of initial-state potential on perturber motion and bound-state formation rates.

$W(R)$ is given by Eq. (196). This result may be reexpressed in terms of simple integrals, as discussed in Appendix B to Baylis (1969), although to preserve short-range accuracy W should be evaluated numerically from Eq. (196) whenever possible. This was the approach used in the recent paper by Czuchaj and Sienkiewicz (1979) and extensive calculations by Snow (1976).

d. Wave functions, basis states, and evaluation of the potential

For the calculation of the interaction of alkali doublets with noble-gas perturbers we use a basis

$$|(SL)JM\rangle = \sum_{M_S, M_L} ((SL)JM | SM_S LM_L) | SM_S LM_L \rangle, \quad (201)$$

where the summation is performed over all M_S and M_L for which $M_S + M_L = M_J$. It then follows that a matrix element of an operator A that commutes with J_Z is given by

$$\begin{aligned} \langle (SL')J'M' | A | (SL)JM \rangle = & \delta(M, M') [(\frac{1}{2}, +\frac{1}{2}, L', M - \frac{1}{2} | J'M)(\frac{1}{2}, +\frac{1}{2}, L, M - \frac{1}{2} | JM) \langle L', M - \frac{1}{2} | A | L, M - \frac{1}{2} \rangle \\ & + (\frac{1}{2}, -\frac{1}{2}, L, M + \frac{1}{2} | J'M)(\frac{1}{2}, -\frac{1}{2}, L, M + \frac{1}{2} | JM) \langle L', M + \frac{1}{2} | A | L, M + \frac{1}{2} \rangle] \end{aligned} \quad (202)$$

so that we must evaluate just two integrals in an $|LM_L\rangle$ basis, or, for a single valence electron, in the one-electron states $|nlm_l\rangle$. Whenever the operator A can be represented as a Legendre series, this evaluation reduces to a numerical integration on r and an angular integration that is given by a Gaunt factor.

We write, for example,

$$A = \sum_{l''} A_{l''} P_{l''} \quad (203)$$

to reduce

$$U(n', l', m'_l; n, l, m_l) = \langle n', l', m'_l | A | n, l, m_l \rangle$$

to

$$\begin{aligned} U = & \sum_{l''} \delta(m'_l, m_l) \left[\int_0^\infty F^*(n', l') F(n, l) A_{l''} dr \right] \\ & \times \langle l'm'_l | P_{l''} | lm_l \rangle, \end{aligned} \quad (204)$$

$$\begin{aligned} \langle l'm'_l | P_{l''} | lm_l \rangle = & \delta(m_l, m'_l) (-1)^{l''} (l, m_l, l'', 0 | l'm_l) \\ & \times (l', 0, l'', 0 | l0). \end{aligned} \quad (205)$$

The $F(n, l)$ are radial wave functions. Although the numerical integration is straightforward, in the region of the noble-gas perturber the large contributions to G can be troublesome and require special attention (Snow, 1976). Recent work by Düren and Moritz (1980) has shown conclusively that the radial integrals should be evaluated exactly and not approximated by expansions. A remaining problem is the selection of an appropriate radial wave function.

The usual choice is the Bates-Damgaard (1949) wave function, which is defined in terms of the effective principal quantum number n^* and the one-electron orbital angular momentum l . The wave function has very good asymptotic behavior, but at small r it diverges, and there is also a question of its normalization. The divergence problem is commonly solved by a truncation, and the wave functions may be normalized with the method of Seaton (1958). Czuchaj and Sienkiewicz (1979) have suggested the use of wave functions of Simons (1974). Their results show an improvement in the agreement of the calculated potentials with available experiments when Simons wave functions are used, but other modifications may be responsible. Simons wave functions have incorrect nodal positions outside the core, features to which the potentials are quite sensitive. The noble-gas wave functions required for the calculation of G and W are usually taken to be analytical functions adjusted to represent Thomas-Fermi or Hartree-Fock calculations of the outer noble-gas shell. The parameters for such wave functions are discussed by Gombas (1967), Baylis (1969), and Pascale and Vandeplanque (1974).

e. Results

In Fig. 9 we show the excited-state potentials for Na-Ar, and in Fig. 10 the potentials for Cs-Xe found by various authors. *Ab initio* results are discussed in the following section and shown for comparison in Fig. 12. Although there are some differences in the results of the calculations, the basic features are uniformly reproduced. Na-Ar shows a weak potential well in the ground state that has been intentionally matched by the calculations to adjust r_0 . This well is only 44-cm^{-1} deep in the Pascale-Vandeplanque calculation. The $3p\ 2P_{1/2}$ state has a much deeper well, 276 cm^{-1} , that is at somewhat shorter range. There are similar deep, short-range wells for many excited states, particularly those for which the corresponding spatial configuration allows penetration along a node in the angular charge distribution of the alkali. The longer-range interaction of higher excited

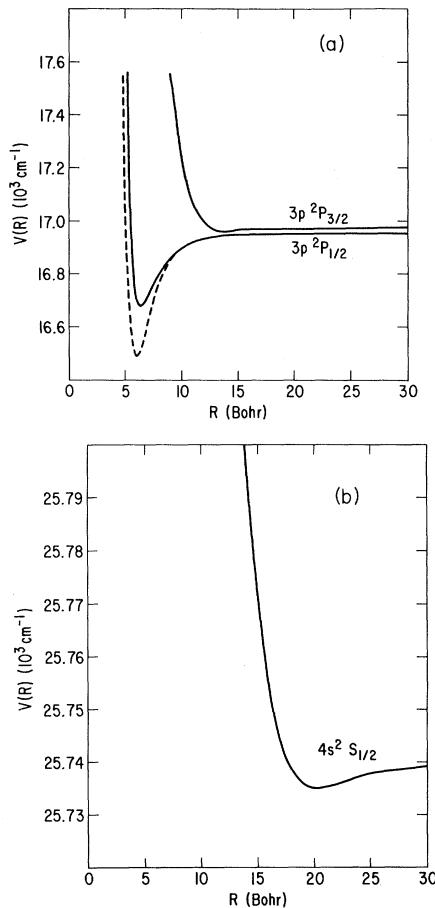


FIG. 9. Potentials for the $3p$ and $4s$ states of Na-Ar: (—) from Pascale and Vandeplanque (1974); (---) from Baylis (1969).

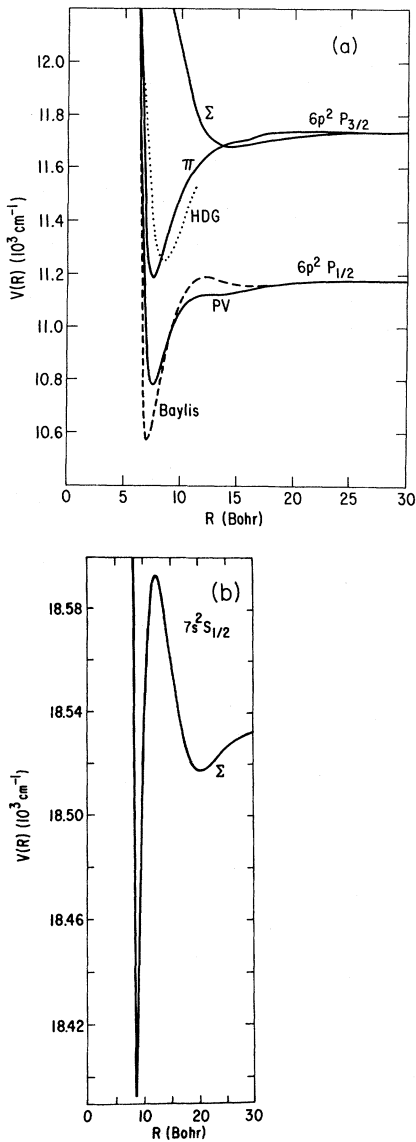


FIG. 10. Potentials for the $6p$ and $7s$ states of Cs-Xe: (—) calculated by Pascale and Vandeplanque (1974); (---) by Baylis (1969); (...) from the experiment of Hedges *et al.* (1972).

states often shows an undulation which follows the valence-electron probability density, as is shown by the $7s^2 S_{1/2}$ Cs-Xe state in Fig. 10.

The interactions in the Cs-Xe example are more prominent than those in Cs-Ar, as a consequence of the larger polarizability of Xe. Like the $7s$ state in the figure, the $9s$ state shows wells of depths 9 cm^{-1} at 12 \AA and 765 cm^{-1} at 4 \AA , separated by an undulation maximum at 10 \AA , at which the perturbation is nearly zero. This complexity of a typical potential is what defeats attempts to use simpler potentials such as power-law or Lennard-Jones interactions to systematically explain all features in a given spectrum. For this example, the long-range interaction beyond the outer 9-cm^{-1} minimum would in

large part determine the broadening and shift of the line core at low pressure, while the details of the short-range interaction would determine the position and intensity of features in the far line wings.

One result of the calculations, pointed out by Baylis (1969) and illustrated in Fig. 37, is that the long-range interaction approaches $C_6 R^{-6}$ only very slowly. Since this might be simulated by taking an empirical C_6 larger than the theoretical value, the line-core observations discussed by Hindmarsh, Petford, and Smith (1967) and Unsöld (1968) that point to a larger than expected empirical C_6 find a natural explanation in the importance of higher-order terms of the multipole expansion, included, for example, in Eq. (192).

Both the power of the pseudopotential method and its greatest weakness rest in the parameter r_0 , which controls the short-range cutoff of F near the noble-gas atom. While W and G are determined in principle for known wave functions of the alkali and noble-gas atoms, the interaction F would be infinite for constant polarizability and small electron-noble-gas separations. At small r' the term $F+G$ behaves like the Fermi potential, and the net size of the interaction is governed by r_0 . Although it is desirable to hold r_0 constant, fixed by the ground-state potential from scattering experiments or *a priori* calculations, the potentials that result often compare poorly to excited-state measurements, while the forms of the potentials are reasonable. The effect of changing the cutoff function at small r' and the choice of r_0 were also investigated by Düren and Moritz (1980). While we defer general comparisons to experiments until later, note in Fig. 10 that the resonance line measurements of Hedges, Drummond, and Gallagher (1972) follow the theoretical curves rather closely.

Line-profile observations by Kielkopf and Allard (1980) probe the long-range interaction for excited Cs in the region of the outermost antinode of the wave function, and line-core observations in K spectra by Spielfield *et al.* (1979) are sensitive primarily to very-long-range interactions. As a general rule the potentials that have been derived experimentally for the interactions of alkalis and heavy noble gases seem to be stronger at long range than the calculations. For example, where a 10-cm^{-1} well is indicated by an experiment on Cs ($9p$)-Xe, the pseudopotential might only show a dip of 1 cm^{-1} . The valence-electron terms F and G are not balanced exactly by fitting the short-range calculation to the observed ground-state well. A remedy would be to make r_0 adjustable as an independent parameter for each state, but such parametrization reduces the predictive power of the potentials, and the method would not be self-consistent, since the conceptual model depends on the physical interpretation of r_0 as a cutoff for any electron near the noble-gas atom.

Bardsley (1974) and Masnou-Seeuws (1981) have pointed out that the Gombas pseudopotential employed in the Baylis model is only one of several possible pseudopotentials. It is independent of l and strictly valid only for s -wave scattering, although all partial waves in the Baylis model use this same pseudopotential. Thus while some

authors have advocated an l -dependent pseudopotential, none have investigated systematically the benefits or difficulties such a treatment might introduce.

At this time pseudopotentials are accurate at long range for the first excited p states of alkalis perturbed by Ar, Kr, and Xe to about 10 cm^{-1} . The short-range behavior may be quantitatively in error to a much greater degree, although the general behavior is expected to be reliable. Error estimates of 30% in the well depths with Ar, Kr, and Xe perturbers are given by Düren and Moritz (1980).

5. Model potentials

Another method of computing alkali–noble-gas potentials was proposed by Bottcher (1973), Bottcher, Dalgarno, and Wright (1973), and Bottcher and Dalgarno (1974). It has been developed by Peach (1978) and Masnou-Seeuws, Phillippe, and Valiron (1978) for extensive application to alkali–noble-gas systems. Known generically as a model potential method, this technique differs from the pseudopotential method discussed in the previous section through the choice of adjustable terms included in the effective Hamiltonian and in the treatment of the electronic wave functions. The general methods are discussed by Bardsley (1974) and by Dalgarno (1975) as applied to many different calculations of atomic and molecular properties. Phillippe, Masnou-Seeuws, and Valiron (1979) and Masnou-Seeuws (1981) exhibit detailed results for such systems as Na-He, Na-Ne, K-Ne, and H-He, but other light-alkali–light-noble-gas calculations are in progress.

The electronic energy of the alkali–noble-gas molecule is computed by direct solution of the Schrödinger equation,

$$(T + V_1 + V_2 + V_3)\Psi(r, r', R) = E\Psi(r, r', R). \quad (206)$$

The interactions $V_1(r)$, $V_2(r')$, and $V_3(r, r', R)$ are defined by semiempirical considerations. In order to appreciate the structure of the calculation and its possible accuracy we need to look at the origin of these terms, as described by Masnou-Seeuws (1981).

The electron-alkali core $V_1(r)$ is based on a multiparameter model potential of Klapisch (1969),

$$V_1(r) = [(z-1)\exp(-a_1r) + b_1r\exp(-c_1r) + 1] \frac{e^2}{r}, \quad (207)$$

in which z is the nuclear charge and r the electron-nucleus separation. This potential is Coulombic at large r as required, but shows an interaction with a bare alkali core at small r . The parameters are adjusted so that for large R the Schrödinger equation has eigenvalues that are close to the energies of the free alkali atom derived from optical spectra. Of course these energies are known to better than 0.01 cm^{-1} , but it is enough to have a fitting accuracy of only about 10 cm^{-1} because for potential calculations we are interested only in the change of

energy as a function of R . One difficulty with this procedure is that the match in energy may not produce a correct wave function; that is, the ground-state $3s$ wave function of Na may be nodeless. Again, the correct amplitude and form of the valence-electron wave function is important for the asymptotic behavior of the potential.

The electron–noble-gas interaction $V_2(r')$ is determined by studying the scattering of the electron by the noble-gas atom. The potential is adjusted to fit experimental low-energy phase shifts and dependable calculated phase shifts at specific selected kinetic energies corresponding to the alkali states in question. The long-range part of this interaction is

$$V_2(r') = -\frac{\alpha e^2}{2r'^4}, \quad (208)$$

where r' is the electron–noble-gas separation and α is the noble-gas dipole polarizability that is either independently computed or measured experimentally. Higher-order terms of the induced multipole interaction are negligible far from the noble-gas atom, but at short range a screened Coulomb potential for the noble-gas nuclear charge $z_{ng}e$ is added,

$$V_2(r') = -\frac{\alpha e^2}{2r'^4} \{1 - \exp[-(a_2 r')^6]\} - \frac{z_{ng}e^2}{r'} \exp(-b_2 r'), \quad (209)$$

with adjustable constants a_2 and b_2 . When the s -wave phase shifts are computed with this local potential, the parameters can be chosen to obtain agreement with known values. The phase shifts are computed with the constraint that the partial-wave radial wave function is orthogonal to the outer rare-gas orbital of the same symmetry.

The three-body term $V_3(r, r', R)$ can be computed exactly only at large R . It is effectively then the part of $-\frac{1}{2}\alpha E^2$ that is not included in V_2 , and is given by

$$V_3(r, r', R) = -\frac{\alpha e^2}{2R^4} + \frac{\alpha \xi'}{r'^2 R^4} \approx -\frac{\alpha e^2}{2R^4} - 2V_2 \frac{\alpha \xi'}{R^2} \quad (210)$$

where $\cos(r', R) = \xi'$. This last approximation is made to provide a cutoff at small r' .

Finally, we add to the eigenvalues of $E(R)$ a value $\varepsilon_0(R)$ to take into account the exponential repulsion due to the long-range overlap of the alkali core and the noble-gas atom. For Na-Ne this function is simply

$$\varepsilon_0(R) = a_0 \exp(-b_0 R). \quad (211)$$

The parameters are chosen to give the alkali-ion–noble-gas system selected properties in accord with available *ab initio* or electron-gas calculations.

The final molecular energies are

$$\epsilon(R) = \varepsilon_0(R) + E(R). \quad (212)$$

For the Na-Ne system the values $E(R)$ were calculated

using Slater orbitals on both centers in prolate spheroidal coordinates. For the alkali valence electron, only orbitals explicitly orthogonal to the rare-gas orbitals are included. The potential curves for K-Ne and Na-Ne have been compared with a number of experiments, many related to line broadening (Phillipe, Masnou-Seeuws, and Valiron, 1979). Comparisons with experimental spectra (Delhoume *et al.*, 1981) indicate a well-depth accuracy of the order of 10 cm^{-1} , an estimate dependent on the line-shape analysis.

It does appear that where potentials of this sort are available they may be a better option than currently available pseudopotentials at small R for light perturbers. For instance, in Fig. 11 the agreement of the model potential for Na-Ne in the ground state is very good, especially considering that the plotted experimental result was not a criterion for the adjustment of the model parameters. We note, though, that these potentials are not useful for large R (greater than about 7.5 \AA) because the asymptotic atomic basis states are not used for the calculation. This means that excited-state interactions from model potentials may fail to give correct line-core width and shift, or near line wings, particularly for transitions other than the resonance lines. Far-line-wing spectra, however, should be calculable from such potentials. In addition, these potentials may be added to more satisfactory long-range calculations to provide a complete interaction curve.

6. *Ab initio* potentials

All of the potentials described thus far are semiempirical and depend in the very least on known atomic energy levels and perturber polarizabilities, and on experimental electron-noble-gas scattering cross sections, or measured alkali-noble-gas potential-well depths. The reason is that the details of the interactions are extraordinarily complex, and with current techniques it is unreasonable to suppose we could calculate the energies of a molecule such as Cs-Xe with its 111 electrons without some nor-

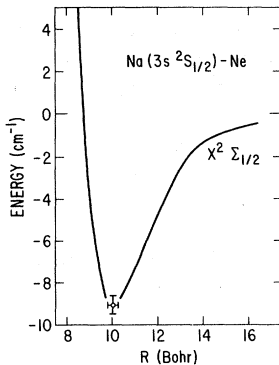


FIG. 11. A potential calculation for Na ($3s\ ^2S_{1/2}$)-Ne from Phillippe, Masnou-Seeuws, and Valiron (1979) compared with a determination of the position of the well minimum in a molecular-beam experiment (Ahmad-Bitar, Lapatovitch, and Pritchard, 1977).

malization to observations. The most complex system of this sort for which *a priori* calculations of excited states with 1-cm^{-1} accuracy have been made is Na-Ar (Saxon, Olson, and Liu, 1977).

These calculations were motivated primarily to compare to Na-Ar pseudopotentials and experiments, in order to see how much of an improvement could be made with the more rigorous calculations. Quasistatic spectra were computed from the calculated potentials and compared to the experiments of York, Scheps, and Gallagher (1975).

Such *ab initio* calculations assume the Born-Oppenheimer approximation and separate nuclear and electronic wave functions. They also neglect spin-dependent interactions. The electronic wave functions and energies were calculated with a configuration interaction method. Each electronic-state wave function was defined by a combination of Slater determinants so that the symmetry and multiplicity of each wave function was properly represented. These Slater determinants were themselves expanded in terms of a one-particle basis set of Slater functions centered on the nuclei. The details of this basis set and its construction are discussed by Saxon, Olson, and Liu (1977), and we note here only that the final calculations used over 7800 orthonormal configuration-state functions!

For comparison we reproduce a sample of the results for Na-Ar in Fig. 12, a potential derived from the Na D-line profile, and a pseudopotential calculation. The ground-state well depths (not shown) in the pseudopotential calculation are only about 15-cm^{-1} shallower than the configuration interaction calculation, but of course the pseudopotential has been adjusted to fit a scattering experiment (Düren, Raabe, and Schlüter, 1968). For the $^2\Pi$ state illustrated, the agreement with the experiment is dramatically better than the pseudopotential. Potentials such as these, although difficult to calculate, serve to adjust pseudopotential calculations that may be more readily applied to excited states.

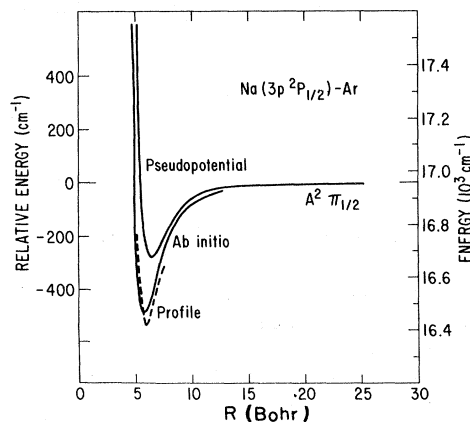


FIG. 12. The potential for Na ($3p\ ^2P_{1/2}$)-Ar determined by *ab initio* methods (Saxon, Olson, and Liu, 1977) compared to a pseudopotential calculation (Pascale and Vandeplanque, 1974) and profile measurements (York, Scheps, and Gallagher, 1975). Compare with Fig. 43.

E. Evaluation of general line-shape theories

Two obstacles have impeded our understanding of collision-broadened neutral atomic spectral line profiles—the problems, first, of finding the correct interatomic interaction and, second, of actually evaluating the profile in a usable form. The latter has markedly influenced the way in which the theory has developed. Before large computers were applied to the problem, it was necessary to reduce the formal theory to a practical analytical expression. Such reduction was often accomplished by sacrificing exactness, so as a consequence we had results that did not work very well, in spite of good basic physics in the original theory. In this section, then, we devote our attention to recent improvements in this interface between the formal logic of the theory and its application as a probe of the physical processes we observe in the laboratory. Section II.F to follow will deal with specific limiting cases that often can be applied instead of the general evaluation.

1. Analytical methods and approximations

a. Anderson's analytical formulas

The unpublished paper of Anderson and Talman (1956) extends the synthesis of the impact and statistical theories discussed in Anderson (1952) by extensively investigating analytical evaluations of the general scalar theory we presented in Sec. II.B. That material is reproduced in large part in Ch'en and Takeo (1957, Sec. II.D), and here we indicate just the essential results of that work.

First of all, Anderson and Talman assumed that the correlation function could be approximated from two calculations, one for small s , and the other in the limit of large s . These were joined to produce an analytical approximation to the function. They found that for a van der Waals interaction the integrals for these two limiting cases could be reduced to one-dimensional numerical calculations. They obtain functions

$$g(s) = As^{1/2} + Bs^{13/6} \quad (s \rightarrow 0), \quad (213)$$

$$g(s) = C + Ds \quad (s \rightarrow \infty), \quad (214)$$

where A , B , C , and D are complex constants. Their results compare rather well with an approximation by Lindholm (1945) in which the phase shift during the collision was considered to be constant. This agreement thus supports a subsequent approximate evaluation by Behmenburg (Sec. II.1.b) for Lennard-Jones potentials that uses the Lindholm method.

Anderson and Talman continued with an evaluation of the Fourier transform for $g(s)$ given by Eqs. (213) and (214), with specific limits on the value of density and frequency. They obtained for high density a result identical with the statistical theory of Margenau (1935), and showed that on the red wing for all densities the $\Delta\omega^{-3/2}$ intensity law [Eq. (16)] is recovered as expected. They

also investigated the validity conditions for the statistical theory. While they found the results useful if $\hbar|\Delta\omega| \ll |V(R_s)|$ for the red wing of a van der Waals interaction-broadened spectral line, where R_s is the average atomic spacing $n^{-1/3}$, they also pointed out that the full statistical profile, obtained by replacing $g(s)$ by its limit for small s , is valid only when the density is high.

For both low density and frequency they obtained a Lorentzian line profile with an asymmetry factor, but with the provision that the impact theory is valid only when the asymmetry is small. We shall look at the problem of core asymmetry in more detail in Sec. III.D.1.b.

b. Approximate evaluation with the method of Behmenburg

The difficulties of performing the numerical calculation and the favorable agreement of the Anderson-Talman analytical methods for a van der Waals potential with the method of Lindholm, prompted Behmenburg (Behmenburg, 1968; Schuller and Behmenburg, 1974; Behmenburg, 1979) to do a similar evaluation for a Lennard-Jones potential.

In order to simplify the calculation, two assumptions were made in addition to those of the general scalar theory described in Sec. II.B. These new assumptions were that the duration of collision is proportional to the impact parameter, and that the phase change during a collision is a linear function of time through the collision; that is, that there is a constant frequency change during the collision (Hindmarsh and Farr, 1972). The important parameter introduced is the duration of collision τ , which is written as equal to $\chi(2b/\bar{v})$ for impact parameter b , mean velocity \bar{v} , and an adjustable parameter χ selected so that the calculated profiles best match the experiments. The advantage to this approach is that the calculation of $g(s)$ can be performed analytically for all but a final one-dimensional integration. The spectrum is the Fourier transform of a numerical function that can be computed rather quickly.

With this model Behmenburg investigated the effect of adding the C_{12} term to the interaction on the predicted shift, width, and asymmetry of a line at high pressure. With some adjustment of parameters he found that he could obtain rather good agreement between the observations and his calculations, as shown in Fig. 13. In a sense this result is surprising because for such high gas densities the profile is determined in large part by the behavior of $g(s)$ for small s . This behavior in turn is very sensitive to the two *ad hoc* assumptions introduced to speed the calculation. The profiles of this model should be reasonably good for the line core at low pressure, but because of the assumption of constant frequency shift during the collision time, the theory will only be an approximation to the spectral intensity distribution radiated during the collision. At high pressure this radiation dominates the line profile. Nevertheless, the work

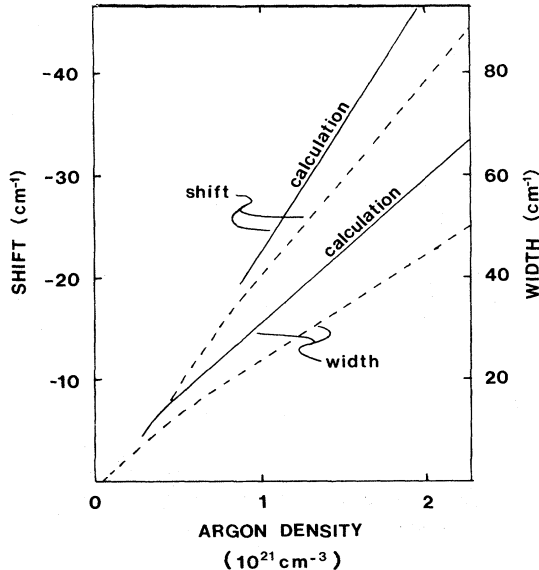


FIG. 13. Width and shift of the Cs ($6s\ 2S_{1/2}$ - $6p\ 2P_{1/2}$) transition perturbed by Ar as calculated with a Lennard-Jones potential by Behmenburg (Schuller and Behmenburg, 1974), compared with data from Ch'en and Garrett (1966).

shows clearly the importance of including details of the short-range potential when a profile is calculated.

c. Approximate evaluations by Hindmarsh and Farr

The quasistatic theory of Kuhn and Margenau (Sec. II.A.5) was applied by Bergeon (1954), Bergeon, Robin, and Vodar (1952), and Hindmarsh and Farr (1969) to the case of a Lennard-Jones potential. The static-theory spectra developed from these calculations displayed enhancements in the low-frequency wing that are associated with the minimum of the potential, the so-called red satellite bands. While the static-theory spectra are in reasonable accord with the actual appearance of spectra at high foreign-gas density, at low density the red satellites are far too sharp, tending to an infinite singularity in the limit of binary interactions and zero velocity.

In an effort to give a more realistic representation of the low-density profiles, Hindmarsh and Farr (1969, 1972) proposed that

$$g(s) = \frac{2M}{kT} \int_0^\infty R^2 dR \int_{-\infty}^{+\infty} dv_R \int_{-\infty}^{+\infty} dv_\phi \exp \left[-\frac{M}{2kT} \left[v_R^2 + v_\phi^2 + \frac{2V_i(R)}{M} \right] \right] [1 - \exp(-i\eta)], \quad (216)$$

$$\eta(s) = \frac{1}{\hbar} \int_0^s (V_i - V_f) dt. \quad (217)$$

These integrals are evaluated with a trajectory that is not rectilinear, but is determined instead by the initial-state interaction so that the actual orbit of the perturber is correctly computed for the classical case. Cooper (1973) has pointed out that $V(R)$ cannot be included in the

$$I(\omega) = \int_0^\infty \frac{\gamma(\omega')/\pi}{(\omega - \omega')^2 + \gamma(\omega')^2} I_{\text{static}}(\omega') d\omega', \quad (215)$$

where the half-width of the impact profile $\gamma(\omega')$ is dependent on the frequency of the corresponding static profile I_{static} . The effect of this integration is to remove the singularity from the static spectrum. The calculations indicate that the finite duration of a collision might smear the line-wing red satellites, and in this the model provides valuable physical insight.

In the representative calculations reported by Hindmarsh and Farr, γ was estimated on the basis of an effective lifetime appropriate for each frequency ω' . The method by which these lifetimes are calculated, however, is not unlike the *ad hoc* assumption of the Weisskopf theory that divides collisions into types, depending on whether their phase shifts are greater or less than one radian. Consequently it is difficult to assess the accuracy or applicability of a detailed profile of this type. Cooper (1973) has noted that it is possible to write an expression for the profile analogous to Eq. (215), but in which the Lorentzian term is a much more complex function. Unfortunately, there is no rigorous mathematical justification for Eq. (215), and there is no simple method by which $\gamma(\omega')$ can be defined to make Eq. (215) comparable in accuracy to an evaluation of the Anderson theory, for example.

2. Numerical methods

The analytical difficulties of completely evaluating a profile without recourse to numerical calculations are overwhelming, and in recent times most efforts have concentrated on translating the formal theory into computer programs with, in some cases, necessary approximations to maintain acceptable execution times. In this section we look at the results of four such independent evaluations.

a. Atakan, Fox, and Jacobson

Fox and Jacobson (1969) evaluated $g(s)$ by averaging in spherical coordinates over the initial radial separation of the perturber and the radiator, and over the magnitude and direction of the initial velocity. They used for $g(s)$ the expressions

Boltzmann factor when rectilinear trajectories of the perturbers are used. We have mentioned this problem in Sec. II.C.1.f. It is not obvious that the inclusion of $V(R)$ in the velocity distribution and the use of curved perturber paths is consistent with the factorization of the

density matrix as required by the theory. For perturbations much less than kT for which the theory should be valid, the inclusion of this term in the average will not be significant anyway.

Fox and Jacobson proceeded by expanding the potentials in a power series in time and integrating to obtain the phase shift, term by term. The series was truncated to include up to terms $O(t^3)$ in the phase shift, the angular integrations were done analytically, and the integral on R was completed with ten-point Gaussian quadrature. It is not possible to directly assess the truncation errors in the series approximation to η , but at high density, for which the theory was particularly intended, only small correlation times s are of interest, and the results should be reasonably good. We illustrate in Fig. 14 a shift calculated for Cs $6s\ 2S_{1/2}$ - $6p\ 2P_{1/2}$ perturbed by argon, and reported by Fox and Jacobson (1969). The coefficients of a Lennard-Jones potential were adjusted to fit the data of Ch'en and Garrett (1966). Other calculations by Atakan and Jacobson (1972), illustrated in Fig. 15, compare computed and experimental spectra at high density. While the calculated profile has about the same shape, width, and shift as the line, the remaining disagreement is significant and indicates a need for additional improvements in the calculations or in the assumed potentials.

b. Takeo

Takeo (1970) reported an evaluation of the Anderson-Talman theory with a Lennard-Jones potential. His work differed from that of Atakan and Jacobson (1972) and Fox and Jacobson (1969) in that he did not expand the phase-shift integral in a truncated power series. He also did not include the potential in the Boltzmann factor and, in fact, did not actually perform a velocity average, but rather substituted \bar{v} instead. Except for the approximations he employed in order to compute the correlation function in a reasonable time, his evaluation is the first fully numerical calculation of the Anderson theory as it was conceived for a potential that should approximately represent the interaction of an observable system.

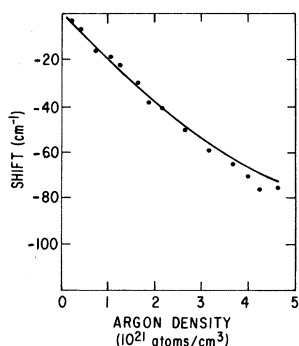


FIG. 14. Shift of the Cs ($6s\ 2S_{1/2}$ - $6p\ 2P_{1/2}$) transition perturbed by Ar as calculated with a Lennard-Jones potential by Fox and Jacobson (1969), compared with data from Ch'en and Garrett (1966). Figure 13 shows an alternative calculation.

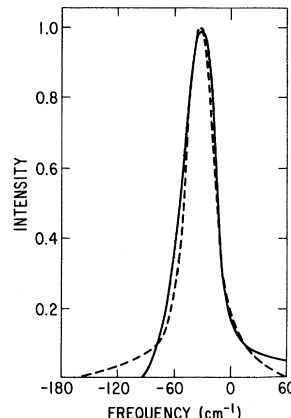


FIG. 15. Profile of the transition for Fig. 14 at 1.6×10^{21} atoms cm^{-3} and 410 K calculated by Atakan and Jacobson (1972) with a Lennard-Jones potential having a well 48-cm^{-1} deep at 5.5 \AA , compared with an experimental profile from Ch'en.

His calculations were to be compared with the observations of the resonance lines ($6s\ 2S_{1/2}$ - $6p\ 2P_{1/2,3/2}$) of cesium perturbed by xenon, as reported by Gilbert and Ch'en (1969) and Ch'en, Gilbert, and Tan (1969). For this purpose he chose a Lennard-Jones difference potential with a theoretical value of C_6 from Mahan (1969), and calculated according to Eq. (171). He established a value for C_{12} appropriate to a potential well 32-cm^{-1} deep, so that the red satellite that is found on the $2P_{3/2}$ component of the resonance line would be reproduced at the correct frequency in a statistical-theory calculation. For this potential he then computed profiles from Eqs. (46), (54), and (55) at the two experimental temperatures 666 and 800 K, and at several xenon gas densities.

The computational procedure he employed was to evaluate the correlation function by averaging in spherical coordinates. The integrand for $g(s)$ was expanded as a series in terms of the variable $\bar{v}s/R$. For values of this variable near unity the integration was performed numerically, but for large or small values the integration was performed analytically and simplified before the numerical integration in order to minimize possible numerical error from subtracting two numbers of nearly equal magnitude. There was no assessment of the overall errors of this computational procedure.

The computed spectra show one red satellite and two violet satellites, as experimentally observed by Gilbert and Ch'en (1969). Figure 16 shows for comparison a profile calculated for densities of 2.7×10^{20} atoms cm^{-3} and 4.3×10^{20} atoms cm^{-3} , and an experimental profile at 3.1×10^{20} atoms cm^{-3} . The calculated red satellite grows with increasing density, and at 1.1×10^{21} atoms cm^{-3} most of the profile is in the red satellite region. The violet satellites are not obvious in these calculated profiles, and are much too weak compared to the observed violet satellites. Takeo also notes that the secondary satellite, thought to be due to interactions of two perturbers with a cesium atom, was stronger in the

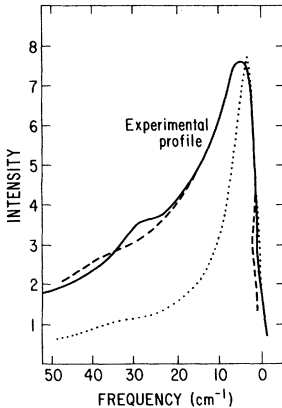


FIG. 16. Profiles calculated by Takeo (1970) for a Lennard-Jones potential: (—) for Xe density of 4.3×10^{10} atoms cm^{-3} ; (···) for Xe density of 2.7×10^{20} atoms cm^{-3} ; both at 666 K compared to experimental profile (—) at 3.0×10^{20} atoms cm^{-3} and 418 K for Cs ($6s^2S_{1/2}-6p^2P_{3/2}$) (Gilbert and Ch'en, 1969).

experiment than in the calculation. Insofar as the potential is capable of representing the interactions responsible for the red wing of the line, the agreement with experiments is encouraging.

c. Allard

The unified theory described in Sec. II.C.1 has been applied to the case of the cesium resonance lines perturbed by xenon (Allard, 1973; Allard, Sahal-Brechot, and Biraud, 1974). Hund's case C was shown to be valid for this problem, so that the methods of Sec. II.C.3.d could be applied. This made it unnecessary to solve coupled equations in order to describe the evolution operator. The potentials used for this calculation were a Lennard-Jones potential for the molecular Σ state and a van der Waals potential for the molecular Π , chosen in such a way that the results of Sec. II.C.3.d for the $^2P_{1/2}$ line were identical to the scalar-theory formulation used by Takeo (1970). In this example, a mean velocity was introduced to avoid numerical integration over a Maxwellian distribution.

As with other evaluations discussed here, this calculation involves first the computation of the autocorrelation function, and then the Fourier transform in order to obtain the spectrum. This evaluation was the first not to rely in any way on series expansions or approximations to speed the computation, but to follow an exact numerical evaluation. The method is potentially powerful, but demands a detailed consideration of the Fourier transform, with attention to the sampling theorem and the use of apodization to extract poorly contrasted features (Allard, Sahal-Brechot, and Biraud, 1974).

These theoretical calculations were performed for the same conditions as the experiments of Gilbert and Ch'en (1969). An example, presented in Fig. 17 for comparison to Takeo's calculation and an experiment, shows a series

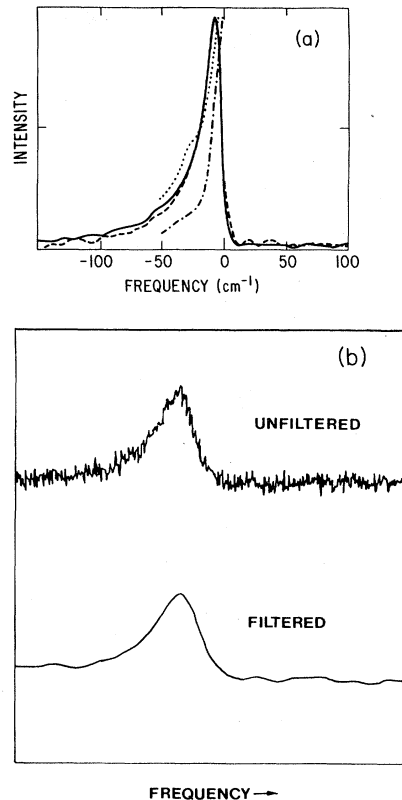


FIG. 17. (a) Unified-theory profiles calculated for the Cs ($6s^2S_{1/2}-6p^2P_{1/2}$) (—) and ($6s^2S_{1/2}-6p^2P_{3/2}$) (—) transitions compared with an experimental profile (●) and a calculation by Takeo (—··—) from Fig. 16. The xenon gas density was 6×10^{20} atoms cm^{-3} and the temperature was 418 K. (b) Densitometer tracing of a photographic spectrum (R. Granier, unpublished) of the Cs ($6s^2S_{1/2}-6p^2P_{3/2}$) line with a xenon density of 1.4×10^{20} atoms cm^{-3} at 870 K shown filtered and apodized for comparison to the calculation in (a) (Allard, Sahal-Brechot, and Biraud, 1974).

of satellites all along the profile. A photographic spectrum, filtered to remove high-frequency noise present in the background away from the line, shows features analogous to the computed ones. These may originate in interference effects, as discussed in Sec. III.E.3.

Calculations of the Anderson-Talman theory for a square-well potential

$$V(R) = V (R \leq a), \quad (218)$$

$$V(R) = 0 (R > a) \quad (219)$$

were reported by Allard (1978) and by Allard and Biraud (1980). Perturbers were assumed to follow rectilinear trajectories with a uniform velocity \bar{v} , and the autocorrelation function was completely analytical, resulting in a fast and precise calculation. The dependence of the profiles on temperature, with a Maxwellian velocity distribution explicitly included in the average, has also been reported (Allard and Biraud, 1982).

Only two parameters, the range of the potential a and

the depth of the well V , are now required. Although this model for a potential can be regarded as physically unrealistic, its interpretation is clear. The profiles which are obtained have a series of red satellites periodically centered at multiples of the depth of the well, as shown in Fig. 18. These are examples (Allard, 1978) with well depths sufficiently large to give satellites well separated from the main line. This allows a study of the properties of the satellites with different potential parameters and perturber densities. It was shown that the number of perturbers in the interaction volume

$$h = \frac{4}{3} \pi a^3 n \quad (220)$$

is the determining parameter for the amplitude of the satellites. For increasing h the satellites become more and more important and can be stronger than the line, as in Fig. 20. This is in agreement with experimental results of Gilbert and Ch'en (1969) and Kielkopf and Allard (1980). In Fig. 19 the amplitudes of the first and second satellites are plotted against foreign-gas density. Both curves exhibit maxima at, respectively, $h=1$ and $h=2$. Notice that when the peak of the first satellite begins to decrease, the strengths of the other satellites are still increasing. The shape of the curves plotted in Fig. 19 for the first and second satellites are similar, and the same behavior will appear for sequential satellites, but at higher densities. This general behavior is expected on the basis of the Poisson distribution, which gives the probability of finding a select number of perturbers closer to the radiator than a , and it has been reported experimentally (Kielkopf and Allard, 1979). Observations of the phenomena are discussed in Sec. III.E.1. Only the analyticity of the square-well autocorrelation function, which permits the calculation of a great number of profiles, allows the theoretical study of this interesting phenomenon.

In addition to the satellite peaks, the profile for this potential also shows oscillations due to the square-well geometry. These oscillations are artifacts analogous to optical diffraction, and they have a period that depends on \bar{v} . As a consequence they nearly disappear when the correlation function is averaged over velocities.

These variations, established for large V with a

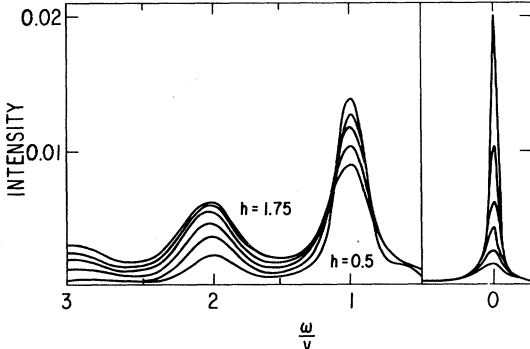


FIG. 18. The variation with density of line profiles and satellites as calculated for a square-well potential of depth V and radius a , for different values of $h = n(4\pi a^3/3)$.

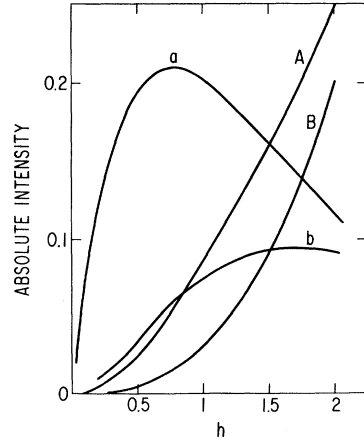


FIG. 19. The variation of the amplitude of satellites with density for a square-well potential: (a) the amplitude of the first satellite relative to the main line; (b) the amplitude of the second satellite relative to the main line; (A) the amplitude of the first satellite on an absolute scale; (B) the amplitude of the second satellite on an absolute scale (Allard, 1978).

resolved satellite, extrapolate well to small V where the satellite is embedded in the line center. A complete explanation of the variation of width, shift, and asymmetry with density is given by applying results established for the case of well-resolved satellites to the case of unresolved satellites (Allard and Biraud, 1980; Gilbert, Allard, and Ch'en, 1980). The apparent variations of the parameters of the line have been studied for several different potential-well depths. These results can be subdivided into three domains:

(i) The satellite is well separated from the line core, as in Figs. 20 and 21(a). The width, shift, and asymmetry of the computed profiles show discontinuities as a function of density similar to those known to appear in ex-

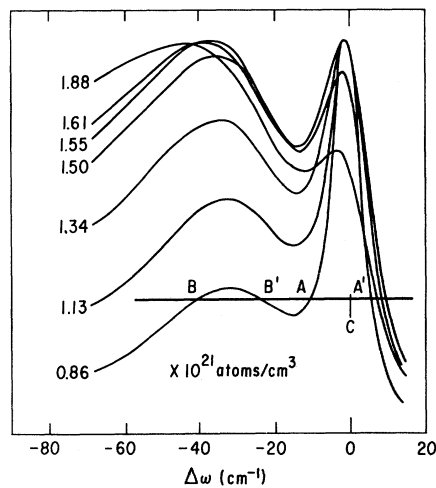


FIG. 20. The variation of the calculated profiles for a square-well potential with density. All of the profiles have their maxima set to one. These calculations and those of Figs. 18 and 19 are for a well 39.8-cm^{-1} deep with a radius of 6 Å (Allard and Biraud, 1980).

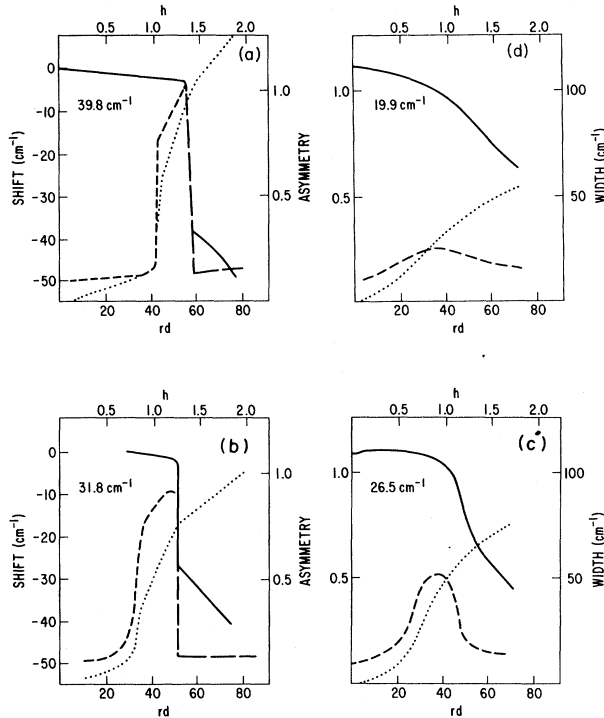


FIG. 21. The variation of width, shift, and asymmetry for a square-well potential of radius 6 Å with different depths: (—) width; (···) asymmetry; (—) shift (Allard and Biraud, 1980).

perimentally measured profiles. These features should be compared with experiments discussed in Sec. III.D.2.

The origin of these discontinuities lies in the relative positions and intensities of the satellites and the main line. Figure 20 shows that the first satellite remains almost at the same frequency, but that its amplitude increases with density. The discontinuity in shift and asymmetry occurs when the satellite becomes stronger than the line core. The linewidth is measured at half the peak amplitude of the profile. The discontinuity in width occurs when the dip between the line and the satellite has an intensity greater than half the line-peak intensity. This is illustrated in Fig. 20 by the horizontal line $BB'A'CA'$. When the dip rises above the half intensity point, the width is measured from B to A' , but when the dip is less than half the line peak, the width is measured from A to A' . The discontinuity in the asymmetry curve occurs for the same reason.

(ii) The satellite is no longer clearly resolved. With increasing density the satellite becomes a shoulder which climbs up along the red side of the main line and distorts the line shape. A dip does not appear between the line core and the satellite, and distinct discontinuities no longer appear. The same phenomena do occur, but the effects are smoothed as shown in Figs. 21(b) and 21(c). This is a transition between cases (i) and (iii).

(iii) The satellite is completely blended into the line core. The satellite does not cause a distinct red shoulder, but instead sums with the line core to form an un-

resolved contour. This gives rise to very smooth profiles and prevents any discontinuity from appearing in the plots of the width, shift, and asymmetry versus density, as shown in Fig. 21(d).

When these curves are compared with the experimental results of high-density observations, to be discussed in the following sections, it is apparent that they reproduce well the S shape of the width curve, the Z shape of the shift curve, and the bell shape of the asymmetry curve. It is remarkable that the simple square-well potential yields computed spectral line-profile characteristics that are in satisfactory agreement with experimental data.

d. Kielkopf

With the view that the only way to test unified theories of line broadening is to compare the computed line shape for well-known interatomic potentials with a wide range of experimental data on the same system at different pressures and temperatures, Kielkopf (1976a, 1978, 1982) and Kielkopf and Allard (1980) studied the problem of precise evaluation of the semiclassical line profile for potentials somewhat more general than the Lennard-Jones. The computed width, shift, asymmetry, and profiles have been compared with principal series transitions in cesium and barium perturbed by xenon, and sharp series transitions in potassium.

The calculations reported in these papers evaluate the Fourier transform $I(\bar{v})$ for a frequency \bar{v} (cm^{-1}) from the unperturbed line center with the real integral

$$I(\bar{v}) = 2 \frac{c}{\bar{v}} \int_0^\infty \exp[-n\alpha(u)] \times \cos[2\pi\bar{v}uc/\bar{v} - n\beta(u)] du , \quad (221)$$

where $u = \bar{v}s$ measures the distance along a rectilinear trajectory instead of the time of travel. This form of Eq. (65) is particularly convenient for numerical calculation. The functions $\alpha(u)$ and $\beta(u)$ are the real and imaginary parts of $g(s)$,

$$g(s) = \alpha(\bar{v}s) + i\beta(\bar{v}s) , \quad (222)$$

which are determined in cylindrical coordinates by Eq. (55) or Eqs. (99) and (100). In order to avoid the infinite upper limit of the Fourier transform equation (221), the calculation takes advantage of the fact that, for large u , $g(s)$ is a linear function of s . There exists some value u_0 such that for $u \geq u_0$ both $\alpha(u)$ and $\beta(u)$ can be described by

$$\alpha(u) = \alpha_0 + \alpha_1 u , \quad (223)$$

$$\beta(u) = \beta_0 + \beta_1 u \quad (224)$$

to an accuracy that exceeds the established accuracy of the numerical calculation for smaller u . In the computations reported in these papers, this accuracy is of the order of 3 to 4 decimal places. Once this is recognized, the integral from u_0 to ∞ can be done analytically. The

spectrum is first calculated as if Eqs. (223) and (224) were valid for all u . This can be done exactly and gives a Lorentzian plus an asymmetric dispersion term. The difference between the real behavior for $u < u_0$ and the linear terms is then added. The advantage of this procedure is that, once the linear region has been identified

the correlation function does not need to be calculated for $u \geq u_0$, and as a consequence it is not necessary to apodize the Fourier transform. The profile is given by

$$I(\bar{v}) = I_L(\bar{v}) + I_A(\bar{v}) + I_W(\bar{v}) \quad (225)$$

with

$$I_L(\bar{v}) = 2(c/\bar{v}) \exp(-n\alpha_0) \cos(n\beta_0) \frac{n\alpha_1}{(n\alpha_1)^2 + (2\pi c \bar{v}/\bar{v} - n\beta_1)^2}, \quad (226)$$

$$I_A(\bar{v}) = 2(c/\bar{v}) \exp(-n\alpha_0) \sin(n\beta_0) \frac{2\pi c \bar{v}/\bar{v} - n\beta_1}{(n\alpha_1)^2 + (2\pi c \bar{v}/\bar{v} - n\beta_1)^2}, \quad (227)$$

$$I_W(\bar{v}) = 2(c/\bar{v}) \int_0^{u_0} du \{ \exp[-n\alpha(u)] \cos[2\pi c \bar{v}u/\bar{v} - n\beta(u)] \\ - \exp[-n(\alpha_0 + \alpha_1 u)] \cos[2\pi c \bar{v}u/\bar{v} - n(\beta_0 + \beta_1 u)] \}. \quad (228)$$

The asymmetric line-core character and its mathematical origin as the nonzero intercept of the slope of the imaginary part of $g(s)$ is clear from this formalism.

The actual evaluation is of course speeded considerably by choosing potentials for which the phase-shift integral can be analytically calculated. The choice in the first paper (Kielkopf, 1976a) was a power series in R^{-p} with even p

$$V = \sum_{p=6}^{12} C_p R^{-p}. \quad (229)$$

But it is not possible to fit such a potential to the pseudopotentials available for alkali-noble-gas interactions, and spectra computed from Eq. (229) were found not to agree very well with experiments that produced very sharp satellites in the line wings. In later work, while this form was used for large R , for small R another power series,

$$V = \sum_{p=0}^6 B_p R^p, \quad (230)$$

was introduced. The inner and outer regions were matched in slope and magnitude at a suitable point.

The profiles from these calculations illustrate first of all that satellites appear near the frequency from the line center that corresponds to the difference-potential well depth. The satellite may not be a distinct peak, but rather a shoulder on the main line, as illustrated in Fig. 22. The position of the edge of this shoulder is always closer to the line than the well depth, and the shape of the computed satellite is never as sharp as predicted by the unified Franck-Condon theory or statistical theories. The calculations demonstrate clearly that the position of the satellite in the spectrum is determined by the difference-potential well depth.

The computed spectra also show that the shape of the satellite depends on the curvature of the potential. A potential of low curvature around the extremum produces a very sharp satellite, such as that shown for low density

in Fig. 23. The overall strength of the satellite as a fraction of the total energy in the line is a function of the internuclear separation corresponding to the formation of the satellite feature. Thus larger separations with higher probabilities of collision produce stronger satellites.

In the sequence of calculations shown here we see the growth of an isolated line with increasing gas density for a selected potential. Many of the features encountered in other evaluations are found here: the intrinsic low-pressure core asymmetry, a red satellite, and, with higher densities, a very broad and shifted profile that includes frequencies covered by the red satellite and core at lower densities. The first satellite initially grows in strength, but so do contributions at frequencies farther from the line than the satellite. The calculations shown in Fig. 23 also display the development of higher-order satellites that we interpret as satellites-on-satellites; that is, as

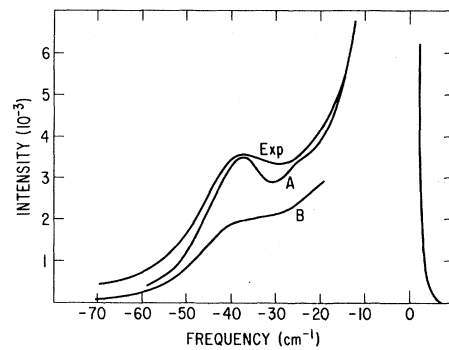


FIG. 22. An experimental profile for Cs ($6s\ ^2S_{1/2}-7p\ ^2P_{1/2}$) perturbed by Xe at 1.1×10^{19} atoms cm^{-3} at 546 K compared to two unified-theory calculations: (a) a multiparameter potential with a well at 14.1 \AA and a depth of 46.0 cm^{-1} with a reduced curvature of 30; (b) a 6-8 potential with a 47 cm^{-1} well at 11.2 \AA and a reduced curvature of 48. The sharper well produces a less distinct satellite. All profiles are normalized to unit area; the density for calculation (b) is 0.64×10^{19} atoms cm^{-3} and the temperature is 500 K (Kielkopf and Allard, 1980).

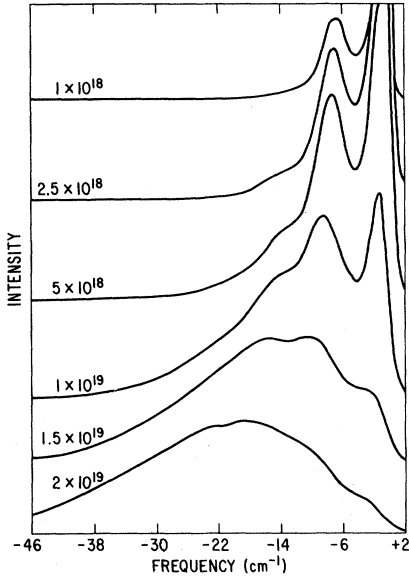


FIG. 23. Calculated profiles for Cs ($6s\ 2S_{1/2}$ - $9p\ 2P_{1/2}$) perturbed by Xe at 500 K and different densities.

satellites due to many-perturber interactions. At very high density the profile assumes a Gaussian character, with minor undulations corresponding to high-order multiple-perturber interactions.

These illustrations show that the computed spectra have an appearance very similar to those observed. Analyses of the line core that allow for the asymmetry shown are also in good agreement with recent experiments of Kielkopf (1980) and Walkup, Spielfiedel, and Pritchard (1980). While these predictions of the line-shape theories have been observed, no calculated potentials are as yet sufficiently accurate to predict spectra in the near line wing. All the evaluation procedures we have discussed use some type of semiempirical potential, adjusted so that the computed and observed spectra have some features in common, but the fact that the density dependence of the spectral contours and width, shift, and asymmetry are also accounted for without such fitting in recent work (Kielkopf and Allard, 1980; Gilbert, Allard, and Ch'en, 1980), lends support to the essential basis of the line-shape theory.

In spite of the obvious successes of these methods in explaining many features of observed profiles, we are drawing comparisons between theories applicable to isolated adiabatic levels and experiments that involve levels that are not fully isolated and are described by potentials more complex than a scalarly additive function of internuclear separation. Thus there is much yet to be done, particularly along the lines of including nonadiabatic effects and nonadditivity at high density.

F. Special cases and useful limits

1. JWKB methods

In Sec. II.C.2 we showed how single-perturber wave functions could be explicitly introduced into the calcula-

tion of $g(s)$ in such a way that the line shape is determined by the Franck-Condon factors $|\langle \chi_i | \chi_f \rangle|^2$. A low-density unified approximation to adiabatic, additive line profiles has been derived from this result, which contains only quantities already present in the impact and one-perturber expansions, and yet describes the complete frequency range with a single expression.

The unified Franck-Condon (UFC) line shape (Szudy and Baylis, 1975, 1977; Szudy, 1979) can be written as

$$I(\omega) = \frac{1}{\pi} \frac{F(x)}{(\omega - \omega_0 - \sigma)^2 + (\gamma)^2}, \quad (231)$$

where γ and σ are the impact line-shape width and shift given by

$$\gamma + i\sigma = \frac{\pi n \hbar}{\mu} \left(\frac{1}{k_i} \sum_{l=0}^{\infty} (2l+1) \times \{1 - \exp[2i(\delta_i - \delta_f)]\} \right). \quad (232)$$

This expression is in the form given by Szudy (1979). The calculation of the impact width and shift has been discussed in Szudy and Baylis (1977). In Eq. (232) the reduced mass of the binary system is μ , the initial wave number of the perturber is k_i , the brackets $\langle \dots \rangle$ indicate an average over k_i , the sum is on the quantum number l of the relative angular momentum of the collision pair, and δ_i and δ_f are the scattering phase shifts for the initial and final levels of the radiating atom.

The line-shape function $F(x)$ is defined in terms of the variable x given as

$$x = \omega - \omega_0 - M_1, \quad (233)$$

where

$$M_1 = \frac{\int_{-\infty}^{+\infty} (\omega - \omega_0) I(\omega) d\omega}{\int_{-\infty}^{+\infty} I(\omega) d\omega} \quad (234)$$

is the first moment of the line profile. It is given by

$$F(x) = \frac{n}{2} \int_{-\infty}^{+\infty} ds \exp(ixs) g''(s), \quad (235)$$

where $g(s)$ is calculated from Eq. (123). These expressions would also be valid at low density for $g(s)$ calculated from either a classical path unified theory or a scalar phase-shift theory, with appropriate limitations for each case.

The particularly useful result of this method arises if JWKB wave functions are used to evaluate $g(s)$ in Eq. (123). Then in the notation of Szudy and Baylis (1977), the line-shape function is given by

$$F(x) = \left(\frac{\pi m v_i}{2 k_i^2} \sum_l (2l+1) |H_l(x)|^2 \right), \quad (236)$$

where v_i is the initial relative velocity, $v_i = \hbar k_i / \mu$, and H_l is the reduced free-free Franck-Condon factor. This overlap integral has the simple form

$$H_l(x) = 2x \int_0^{\infty} ds \cos[sx - \eta(s)]. \quad (237)$$

The phase difference between initial and final states is $\eta(s)$. The low-density line core, which is often called the impact limit, is recovered when $x \rightarrow 0$. In that case, to lowest order in x ,

$$F(x) = \gamma, \quad (238)$$

which gives a Lorentzian profile. The next-order term adds a slight asymmetry.

To investigate the line shape in the wings, the overlap integrals $H_l(x)$ have to be calculated at large x . In this case it turns out that the main contribution comes from the regions of stationary phase; that is, from the vicinity of Condon points which are the solutions of

$$\hbar x = \Delta V(R_c) \quad (239)$$

when $\Delta V = V_i - V_f$, the difference between the interaction potential for the initial and final states of the transition. If the solutions R_c of this equation are real, then they represent the transition points that obey the Franck-Condon principle; that is, vertical transitions. These real Condon points are the basis of the quasistatic theory.

We can, on the other hand, have complex solutions to Eq. (239). Frequency regions which correspond to such complex Condon points are called antistatic regions. For a line originating with a difference potential that has a minimum, as in a Lennard-Jones type of curve, frequencies farther removed from the line on the red side than the well depth correspond to complex Condon points interpreted with antistatic solutions for $F(x)$.

The contributions to the integral for $H_l(x)$ have to be evaluated for each possible Condon point. In the case of isolated Condon points, the phase shift is expanded as a quadratic function of s , and the resulting intensity is the usual quasistatic line profile. When two Condon points are close, it is necessary to expand the difference potential as a quadratic function so that the phase carries terms of the order s^3 . With use of the method of steepest descent (Holstein, 1950) the resulting integral can be approximated with an Airy function. This is exactly the procedure used in the work of Sando and Wormhoudt (1973) and Sando (1974), in which observed and calculated satellite band shapes were compared. Szudy and Baylis (1975), however, expect the method to work well only when the potential can be accurately represented by a quadratic expansion.

In order to get a more satisfactory description of the profile, they expand the phase shift as a cubic function of a new variable chosen to give a profile that varies smoothly from the Sando-Wormhoudt expression in terms of an Airy function when the Condon points are far apart. The method has the advantage over other techniques, in that it allows the explicit inclusion of an average over initial energies and that it gives useful, easily evaluated expressions for line-wing profiles. Without giving details of the calculations, we simply quote the following results.

In the line wings when $|x| \gg \gamma$ the UFC profile is

$$I(\omega) = 24\pi n \hbar \sum_c |D(R_c)|^2 \frac{|\pi z_c|^{1/2} R_c^2 L(z_c)}{|\Delta V'(R_c)|} \times \exp[-V_i(R_c)/kT]. \quad (240)$$

The reduced frequency z_c is a dimensionless parameter given by

$$z_c = \frac{1}{2} \left[\frac{\mu}{2kT} \right]^{1/3} \left[\frac{\Delta V'(R_c)}{\hbar} \right]^2 \left[\frac{\Delta V''(R_c)}{\hbar} \right]^{-4/3}, \quad (241)$$

and the primes indicate differentiation with respect to R . $L(z)$ is a "universal" line-shape function, in the sense that the shape of the line wing is determined in large part by this function, regardless of the line being considered. $L(z)$ is the integral

$$L(z) = \int_0^\infty dy y^{-2} |\mathcal{A}_i(-zy)|^2 \exp(-y^3), \quad (242)$$

where \mathcal{A}_i denotes the Airy function. The universal line-shape function is illustrated by the solid line in Fig. 24. A tabulation is also given by Szudy and Baylis (1975).

For large positive z_c , $L(z)$ is approximated by

$$L(z_c) \approx \frac{1}{6\sqrt{\pi z_c}} \quad (243)$$

and $I(\omega)$ is given approximately by the quasistatic profile

$$I(\omega) \approx 4\pi n \hbar \sum_c |D(R_c)|^2 \frac{|\pi z_c|^{1/2} R_c^2 L(z_c)}{|V'(R_c)|} \times \exp[-V_i(R_c)/kT]. \quad (244)$$

This expression is singular for Condon points R_0 corre-

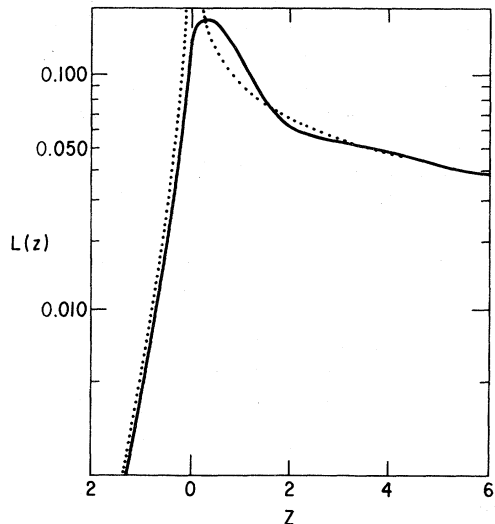


FIG. 24. The universal line-shape function $L(z)$ (—) and asymptotic approximation (···) (Szudy and Baylis, 1975).

sponding to extrema in the difference potential. These singularities occur in the regions where potential curves for the upper and lower states run parallel. The red satellites observed for years in alkali spectra perturbed by noble gases (see Sec. III.E.1) are interpreted as the real manifestation of these theoretical singularities. These classical satellites have a position given by

$$x_s = \frac{\Delta V(R_0)}{\hbar} = \omega_s - \omega_0 - M_1 \quad (245)$$

that corresponds to the value $z_c = 0$ for the reduced frequency.

Negative values of the reduced frequency correspond to complex Condon points. For $z_c \ll -1$ the asymptotic form of $L(z_c)$ is given by

$$L(z_c) \simeq (108\pi |z_c|)^{-1/2} \exp(-12^{1/3} |z_c|). \quad (246)$$

The intensity in this far antistatic region decreases exponentially.

In a recent paper, Royer (1978) reports a numerical test of the accuracy of the UFC formula and compares the UFC profile with other approximations used in the low-density regime. By reference to a numerical evaluation of the Anderson theory, he concludes that the Szudy-Baylis approximation is the most accurate, in addition to being the simplest, low-density approximation available for an adiabatic, scalarly additive, line-broadening theory. Because these theories are thus limited, agreement with the Anderson-Talman theory does not necessarily indicate a best theory.

2. Molecular dynamics simulation

Rather than compute the autocorrelation function from the formulas of Anderson and Talman or from one of the other additive or unified theories, Erickson and Sando (1979, 1980) have computed absorption line shapes with numerical simulations of the molecular dynamics of a system of an absorber and many perturbers. They studied a particular system consisting of one sodium atom and 255 argon atoms in a box with volume and initial velocities chosen to correspond to an argon density of 2×10^{21} atoms cm^{-3} and a temperature of 450 K. They let the argon atoms move on classical paths determined by the Na-Ar ground-state potential, and computed the dipole autocorrelation function and its Fourier transform to obtain the line shape. For a single excited-state potential the molecular dynamics simulation spectra are reported to be in remarkable agreement with Anderson-theory calculations, but for multiple adiabatic excited states the Anderson theory gave a narrower line, and one less intense in the blue wing than the simulation.

A method such as this offers the interesting possibility of testing the expressions developed for the autocorrelation functions in the various unified theories. It also offers means of taking into account effects such as perturber-perturber correlations that seem to influence

very-high-density spectra as deduced from analyses of width, shift, and asymmetry by Royer (1980).

3. Density expansions

Clearly, unified theories, even the simplest ones such as the Anderson-Talman theory with a square-well potential, offer the best available method for understanding, at least qualitatively, the full development of line profiles with increasing gas density. But we have also seen that in the low-density limit, a condition encountered most often experimentally, there are two extreme approximations often used: the impact approximation for the core of the line, and the statistical theory for the wings. These approximations reproduce, often quantitatively, the observed behavior of line profiles. Some of the features of these low-density approximations, as well as characteristics of high-density spectra, can be treated by expanding the spectrum in powers of the density (Royer, 1971a, 1978).

Of course we deal with the Fourier transform of the autocorrelation function discussed previously, with $g(s)$ given by Eq. (55), (100), or (123), depending on whether the Anderson-Talman, unified, or Franck-Condon theory is in use. The natural procedure is then to expand the autocorrelation function in powers of n and Fourier transform term by term, but this yields a divergent spectrum in the limit $\omega \rightarrow 0$ because $g(s)$ is unbounded for large s (Royer, 1978). Instead, it is necessary to separate $g(s)$ into a locally averaged part that gives an impact line core and an oscillating part that produces the line wing.

Following the discussion after Eq. (222), we separate the correlation function into two parts,

$$g(s) = [(\alpha_0 + i\beta_0) + (\alpha_1 + i\beta_1)s] + \tilde{g}(s), \quad (247)$$

the linear part of which we associate with the low-density line core, and the second part $\tilde{g}(s)$ with the line wing. The correlation function with the $g(s)$ can be written

$$\Phi(s) = \exp\{-n[(\alpha_0 + i\beta_0) + (\alpha_1 + i\beta_1)s]\} \times [1 + n\tilde{g} + (n^2/2!)\tilde{g}^2 + \dots]. \quad (248)$$

The Fourier transform of this series does not have divergent terms if the constants in Eq. (247) are chosen to reproduce the asymptotic behavior of $g(s)$:

$$g(s) = (\alpha_0 + i\beta_0) + (\alpha_1 + i\beta_1)s \quad (s \rightarrow \infty), \quad (249)$$

$$\tilde{g}(\infty) = 0. \quad (250)$$

As a consequence the term-by-term Fourier transform gives a density expansion for the spectrum, * symbolizing convolution,

$$I(\omega) = I_c(\omega) * [\delta(\omega) + nI_w(\omega) + (n^2/2!)I_w(\omega)*I_w(\omega) + \dots], \quad (251)$$

where I_c is the core distribution at low density. I_w is in-

terpreted as the wing of the one-perturber distribution (Baranger, 1962; Royer, 1971a), although the intensity distributions labeled I_c and I_w are not normalized in the sense that their frequency-integrated area is unity. Royer introduces a normalization factor \mathcal{V} into the one-perturber spectrum,

$$I_{wN}(\omega) = \mathcal{V}^{-1} I_w(\omega), \quad (252)$$

and a related factor $\exp(n\mathcal{V})$ into the core spectrum,

$$I_{cN}(\omega) = \exp(n\mathcal{V}) I_c(\omega), \quad (253)$$

and rewrites Eq. (241) as

$$I(\omega) = I_{cN}(\omega) * \sum_{k=0}^{\infty} \exp(-n\mathcal{V}) \frac{(n\mathcal{V})^k}{k!} I_{wN}^{*k}(\omega). \quad (254)$$

I_{wN}^{*k} is the intensity distribution due to the combined effects of k perturbers. It is weighted by the Poisson distribution, which is the probability that those perturbers will be in a volume \mathcal{V} if the number density is n .

The structure which we see in Eqs. (251) and (254) shows that at low density the core distribution is most important, and that as the density increases, higher-order multiple-perturber effects become more prominent, just as they show up in the numerical evaluations of the unified theories. The convolution theorem appears explicitly here with the spectrum of N perturbers given by the convolution of many one-perturber distributions. These convolutions exhibit satellites at frequencies $N(\Delta\omega_s)$ if $\Delta\omega_s$ is the satellite frequency for a single perturber. The intensity of each of these multiple-perturber features is determined by the corresponding Poisson distribution factor in the series. This expansion is thus a very physical one, because it decomposes the spectrum into individual spectra from elementary collision processes. Royer (1978) cautions that this interpretation should not be taken too literally, since the terms of the series are not always positive. The use of such expansions to explain multiple-perturber spectra will be taken up in Sec. III.E.1.c.

It may be worthwhile to compare Eq. (254) with the Hindmarsh and Farr (1969) expression, Eq. (215), which is rather similar. The two results would be equivalent if I_{wN} were evaluated as a static-theory spectrum, and if I_{cN} were a Lorentzian with frequency-dependent width, but generally Eq. (254) cannot be taken as a basis for using the methods of Eq. (215).

4. The one-perturber spectrum and line-wing temperature dependence

In many cases of experimental interest the foreign-gas density is low enough that the one-perturber spectrum is a useful approximation to the data. From Eq. (254) this occurs when the probability of finding more than one perturber near the radiator is negligible. Furthermore, we have seen that when the initial-state potential is small in comparison to thermal energies the Kuhn-Margenau

statistical distribution of Eq. (14) describes this spectrum if duration of collision effects are neglected. Experiments have demonstrated, however, that in regions removed from the center of the line strong dependence on temperature is observed (Gallagher, 1968; Hedges, Drummond, and Gallagher, 1972).

Let us look again at the spectrum derived by Jablonski (1945) and given in Eq. (39),

$$I(\omega) \propto \int f(v) dv \int 2\pi b db \frac{2v_i(\infty)}{v_i(R_c)} \left| \frac{dR}{d\xi} \right|, \quad (255)$$

where we have substituted for the terms given there as discussed in the paragraph following that equation. Here $v_i(R)$ is the radial velocity of the perturber for the initial state of the system, b the impact parameter, R_c the internuclear separation at which the transition is most probable according to Eq. (34), and $f(v)$ the Maxwellian velocity distribution. We have integrated over allowed values of the impact parameter and averaged over velocities in this expression. Notice that the average is performed over velocities at infinity. The radial velocity is

$$v_i(R) = v_i(\infty) \left[\frac{E_i - V_i(R)}{E_i} - \frac{b^2}{R^2} \right]^{1/2}. \quad (256)$$

The integral over b can extend only up to b_{\max} for which a particular R is accessible; that is, where $v(R)$ is zero. Thus

$$b_{\max}^2 = R^2 \frac{E_i - V_i(R)}{E_i}. \quad (257)$$

The impact-parameter integration gives

$$\int_0^{b_{\max}} 2\pi b db \frac{2v_i(\infty)}{v_i(R_c)} = 4\pi R_c^2 \frac{[E_i - V_i(R_c)]^{1/2}}{E_i^{1/2}}. \quad (258)$$

In terms of the total kinetic energy of the perturber at infinity E_i , the velocity distribution is

$$f(v)dv = 2\pi(\pi kT)^{-3/2} \exp(-E_i/kT) E_i^{1/2} dE_i. \quad (259)$$

The velocity integral in Eq. (245) becomes an energy integral, giving for $I(\omega)$

$$\begin{aligned} I(\omega) &\propto 2\pi(\pi kT)^{-3/2} \\ &\times \int_{\epsilon}^{\infty} \exp(-E_i/kT) [E_i - V_i(R_c)]^{1/2} \\ &\times 4\pi R_c^2 \left| \frac{dR_c}{d\xi} \right| dE_i \end{aligned} \quad (260)$$

with a lower limit ϵ that depends on whether the potential $V_i(R)$ is repulsive or attractive. The limit for a positive, repulsive potential is just $V(R_c)$, since energies lower than this cannot reach R_c . For an attractive potential, the lower limit is $\epsilon=0$. To evaluate the integral, we substitute $x=(E - V)/kT$ to obtain, in these two cases,

$$I(\omega) = \sum_c \left[4\pi R_c^2 \left| \frac{dR_c}{d\xi} \right|^{-1} \right] \exp[-V_i(R_c)/kT] \quad [V_i(R_c) > 0], \quad (261)$$

and

$$I(\omega) = \sum_c \left[4\pi r_c^2 \left| \frac{dR_c}{d\xi} \right|^{-1} \right] \exp[-V_i(R_c)/kT] \times \frac{(\pi)^{1/2}}{2} \int_{-V_i/kT}^{\infty} \exp(-x)x^{1/2}dx \quad [V_i(R_c) < 0], \quad (262)$$

where the sum is over all Condon points contributing to the spectrum.

The differences in the temperature factors of these equations are illustrated in Fig. 25. In the case of an attractive potential this distribution corresponds only to free particles. The portion of the momentum space corresponding to bound particles has been excluded (Hedges, Drummond, and Gallagher, 1972). If both bound and free perturbers are included, then the distribution is given by $\exp(-V_i/kT)$ even when the potential is attractive.

The results of this analysis in Eqs. (261) and (262) have been used in several instances for the determination of interatomic potentials from spectral line-wing intensities. These results are discussed in Sec. III.E.2 and IV.A. Here we point out the essential feature, that the Boltzmann factor is used to obtain information about the initial state, while the derivative dependence gives information about the difference potential. Some problems have been encountered with uniqueness in this inversion. Other limitations to the validity of the treatment, dependent as it is on static line-broadening theory, are discussed in the following sections.

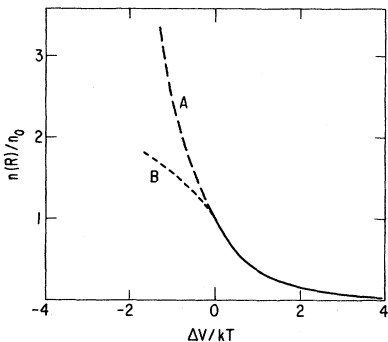


FIG. 25. The distribution functions for an equilibrium ensemble (a) including all states both bound and free, and (b) including only free-particle collisions (Hedges, Drummond, and Gallagher, 1972).

5. Impact broadening: analytical and tabulated calculations

It is believed that the ratio of shift to broadening is sufficiently sensitive to the form of the force law to permit its determination of the law by careful experiments.

—Foley, 1946

We return once again to the question of the central core of the line at low density. This, we have seen from the density expansion discussed in Sec. II.F.3, is determined for the most part by the asymptotic correlation function for large s . The correlation function given by

$$\Phi(s) = \exp\{-n[(\alpha_0 + i\beta_0) + (\alpha_1 + i\beta_1)s]\}, \quad (263)$$

as we have seen [Eqs. (216)–(218)], yields for the area-normalized Fourier transform

$$I(\omega) = \exp(-n\alpha_0)\cos(n\beta_0) \frac{\gamma/\pi}{(\omega - \sigma)^2 + \gamma^2} + \exp(-n\alpha_0)\sin(n\beta_0) \frac{(\omega - \sigma)/\pi}{(\omega - \sigma)^2 + \gamma^2}, \quad (264)$$

where the half-width at half maximum intensity is $\gamma = n\alpha_1$ and the shift is $\sigma = n\beta_1$. When the constant intercept of $g(s)$ is neglected, $I(\omega)$ is a Lorentzian. In fact, in most cases the asymmetry is so small it is difficult to observe within a few half-widths of the line center. The width and shift are given in terms of α_1 and β_1 either by Eqs. (57) and (58), for a scalar interaction in the Anderson theory, or by Eq. (102) in the Baranger theory. For spherically symmetric interactions in the adiabatic approximation the results are equivalent. Replacing v with \bar{v} to perform the velocity average in the unified theory, we obtain

$$\gamma = n\bar{v} \int_0^\infty 2\pi b db [1 - \cos(\eta)], \quad (265)$$

$$\sigma = n\bar{v} \int_0^\infty 2\pi b db \sin(\eta), \quad (266)$$

$$\eta = \int_{-\infty}^{+\infty} dt \Delta V [(b^2 + \bar{v}^2 t^2)^{1/2}] / \hbar, \quad (267)$$

for a difference potential $\Delta V(R)$.

While the general problem of impact broadening has recently been reviewed (Lewis, 1980), we want to summarize here a few results in closed and graphical form that have proven to be useful, particularly for simple analyses of the relationship between linewidths and interatomic difference potentials. For this purpose we consider first the case where ΔV is a square well [Eqs. (218) and (219)] of depth V and radius a . The half-width and shift parameters are, respectively,

$$\gamma = n\bar{v}\pi a^2 \left\{ 1 + \frac{1}{2}x^{-1}[1 - \cos(x) - x \sin(x)] \right\} \quad (268)$$

and

$$\sigma = n\bar{v}\pi a^2 \left[x^{-1}\cos(x) - \frac{1}{2}x^{-2}\sin(x) \right], \quad (269)$$

where x is the maximum phase shift for a central collision $2aV/\hbar\bar{v}$ (Allard, 1978). For a deep square well, $x \rightarrow \infty$ and the Lorentz result is obtained: a width proportional to the collision cross section and no shift.

The other case for which an analytical evaluation of the width and shift is possible is a potential

$$V = \pm C_p R^{-p}. \quad (270)$$

The result has been given by several authors (Unsöld, 1968; Szudy and Baylis, 1977; Hindmarsh and Farr, 1972) for $p > 3$:

$$\gamma = n\bar{v}\pi a_w^2 \Gamma[(p-3)/(p-1)] \cos[\pi/(p-1)], \quad (271)$$

$$\sigma = \pm n\bar{v}\pi a_w^2 \Gamma[(p-3)/(p-1)] \sin[\pi/(p-1)], \quad (272)$$

$$a_w = \left[\frac{C_p}{v\hbar} (\pi)^{1/2} \frac{\Gamma[(p-1)/2]}{\Gamma(p/2)} \right]^{1/(p-1)}. \quad (273)$$

The quantity a_w is the Weisskopf radius, the impact parameter for which the collisional phase shift is one radian. Its value determines the scale of the width and shift, while the shift-to-width ratio is given by

$$\sigma/\gamma = \pm \tan[\pi/(p-1)]. \quad (274)$$

This ratio decreases with increasing p . An interaction which sets in rapidly as a function of decreasing R generates a small line shift. Notice that in principle this potential can be used to account for any shift-to-width ratio, but that for fixed p the ratio can have only one value. If p is 6, for instance, a van der Waals potential yields $\sigma/\gamma = -0.73$. Historically, the observation that many lines did not exhibit this ratio was one major reason for incorporating other possible potentials into neutral-atom line-broadening calculations.

The Lennard-Jones potential

$$V(R) = C_6 R^{-6} + C_{12} R^{-12} \quad (275)$$

(Sec. II.D.1) was independently applied to line broadening by Hindmarsh, Petford, and Smith (1967) and Behmenberg (1968). The methods were extended to include 6-8-12 potentials by Hindmarsh, DuPlessis, and Farr (1970). Although the phase-shift integral for this potential is in closed form, the width and shift have to be computed numerically. The calculations yield tabular or graphical data that can be used to predict or interpret width and shift observations. The half-width and shift are shown to be given by

$$\gamma = n\bar{v}a_{LJ}^2 B(\alpha), \quad (276)$$

$$\sigma = n\bar{v}a_{LJ}^2 S(\alpha), \quad (277)$$

$$a_{LJ} = 2^{1/2} [3\pi |C_6| / (8\hbar\bar{v})]^{1/5}, \quad (278)$$

and

$$\alpha = 0.536(\bar{v}\hbar)^{6/5} C_{12} / |C_6|^{11/5}. \quad (279)$$

The functions $S(\alpha)$ and $B(\alpha)$ are displayed in Fig. 26 for negative C_6 .

One thing that we can learn immediately from such graphs is that the observed shift and width at a single temperature do not always give a unique determination of the interatomic potential. This is a consequence of the oscillations in both S and B for small α . We might conclude that, in general, the measurement of linewidth

and shift in the impact limit is not a good method for obtaining the interaction potentials. On the other hand, in some cases the width and shift can be uniquely related to the potential or the nonuniqueness can be overcome by additional experimental data. Such data might come from the line wing or from temperature dependence of the line-core broadening. An example of the former possibility has been given by Kielkopf and Allard (1980). Temperature dependence measurements have been reported by Vaughan and Smith (1968) and Kreye (1982) for this purpose. A further difficulty arises in that in many cases the broadening yields potentials on the assumption of adiabaticity, an assumption not necessarily valid. In spite of these shortcomings, there is a large body of data on potentials derived by these methods that we shall discuss in Sec. IV.A.

6. Comments on the validity of limiting approximations

At low pressures the statistical theory is certainly valid on the wings of the line, the impact theory in the center, while at high pressures the statistical theory is valid if its fundamental assumption that the frequency perturbation for a given atom is the sum of that due to all others in the gas is not too seriously incorrect.

—Anderson, 1952

Both the impact and static approximations are useful by themselves under certain conditions determined by such factors as spectral resolution, gas density and temperature, the difference potential for the interaction, and the spectral region under study. Particularly for the case of the impact approximation there are rather well-defined limits of validity that are approximately complementary to the conditions for the one-perturber limit of the static theory at low perturber density. In this section we provide guidelines on the use of limiting cases of the unified theory.

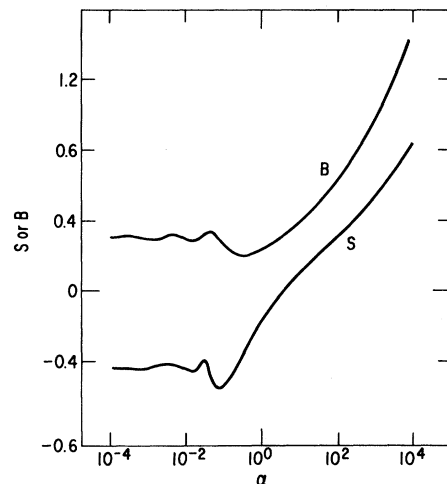


FIG. 26. Shift and width integrals for a Lennard-Jones potential with an attractive R^{-6} coefficient and a repulsive R^{-12} coefficient (Hindmarsh, Petford, and Smith, 1967).

a. On the use of the impact approximation

Baranger (1962, Sec. 5.1) has considered the validity conditions for the impact approximation. Following his discussion, and in reference to Fig. 3, we define τ_d as a representative duration of collision, and τ_c as a mean time between collisions. The impact approximation is valid, according to Baranger, when $\tau_d \ll \tau_c$, implying that the total energy radiated comes mostly from the intervals between collisions. For regions near the line center this is actually a condition on perturber density n . We estimate

$$\tau_d \approx b/v \quad (280)$$

for impact parameter b and velocity v , and from Eq. (271)

$$\tau_c \approx 1/nv\pi a_w^2, \quad (281)$$

so that the Baranger criterion can be expressed as

$$n \ll 1/\pi b a_w^2 \approx 1/\pi a_w^3, \quad (282)$$

where typical impact parameters for emission in the line core are of the order a_w .

Spitzer (1940) and Hindmarsh and Farr (1972) have treated frequency-dependent criteria for the impact approximation. The latter authors find a frequency $\Delta\omega$ measured from the line center at which the Lorentzian of the impact core is comparable in strength to the emission that occurs during the collision. Spitzer, on the other hand, evaluates a correction to the impact approximation to find the frequency at which a preassigned relative error may occur. The results in both cases are the same and depend on the potential chosen for the evaluation. With a power potential such as Eq. (270), the validity condition is

$$\Delta\omega < P \frac{\bar{v}}{a_w}, \quad (283)$$

where P is the preassigned error and a_w is given by Eq. (273). So $\Delta\omega$ can be related to the line half-width, Eq. (271), by

$$\Delta\omega < \gamma(P/\{n\pi a_w^3 \Gamma[(p-3)/(p-1)] \times \cos[\pi/(p-1)]\}). \quad (284)$$

Thus under the Baranger criterion, Eq. (282), the impact theory is useful within a few half-widths of the line center.

b. On the use of the static theory

Baranger (1962) discusses the validity of the static theory in terms of the correlation function, giving as a condition the requirement that the correlation function go to zero before a single collision is completed. A sufficient condition for this has been given by Royer (1980, Sec. V.B.2) in the context of the Anderson-Talman theory,

$$n \gg 1/(4\pi R_0^3/3), \quad (285)$$

where R_0 is the radius of an "interaction volume" about the radiator.

A specific validity condition for the static theory in the wing of a line broadened by a power-law interaction [Eq. (270)] has also been given by Holstein (1950). It is complementary to the condition for the validity of the impact theory, Eq. (283),

$$\Delta\omega > 1/\tau_d, \quad (286)$$

where $\tau_d \approx b/v$, and b is found from Eqs. (273) and (283) to yield

$$\Delta\omega > v^{p/(p-1)} / (C_p/\hbar)^{1/(p-1)}. \quad (287)$$

Equations (286) and (287) are used to justify the application of the static theory to far-line-wing analyses.

7. Collisional effects on high series members and the effect of high gas density

Quite often nannies and kids are pastured separately for reasons which need not concern us. In the evening when the kids and their maternal ancestors are again placed in the same corral it is most impressive to watch a nanny rapidly and unerringly pick her offspring from among hundreds of other and apparently identical kids while refusing to be cozened by the younger members of other families. Although impressive, we must admit that this cannot hold a candle to the selectivity of the electron and the nucleus to which we refer.

—Breene, 1961

In the survey of experimental results to follow we shall see that the large body of data that line-shape theories have been devised to treat is derived from measurements of strong spectral lines which originate in low-lying atomic transitions. Historically, however, one of the first connections between spectral line broadening and atomic collisions treated quantum-mechanically was made by Fermi (1934) in his study of the broadening and shift of high series members of alkali spectra, involving the Rydberg states to which the above quotation refers. In the light of the developments of the generalized theories we have discussed here, we look again at this aspect of line broadening.

The distinguishing characteristic of high series member transitions is that the excited valence electron has a significant probability distribution encompassing a very large volume. A state with $n^* = 10$, for example, has an atomic volume more than 10^4 times larger than a state with $n^* = 2$. This means that phenomena that are important only at very high densities in transitions between low-lying states become equally important at relatively low densities in transitions from a very excited atomic state. Obviously, the condition for the validity of the impact theory, Eq. (272), is satisfied only for low densities in such cases, and whenever the interaction perturbations are significant, the statistical approach to line shapes may well be adequate to describe the observations.

We consider in the following only the case where the probability of multiple-perturber interactions is very high. Densities must be sufficiently great for several perturbers to be simultaneously present within the radiating atom; in practice, for Rydberg atoms the required densities are much less than one atmosphere.

Neutral-atom-Rydberg-atom collisions have been reviewed recently by Omont (1977), who surveyed shifts and broadening in the impact approximations. Here we look, instead, at behavior for higher densities, with consideration of the correlation function in the limit of small time delay.

The expansion in densities derived by Royer (1971a) and discussed in Sec. II.F.3 shows that the profile is simply related to the probability $W(m,h)$ of finding m and no more than m perturbers in a volume \mathcal{V} near the perturbed atom. For a perturber density n , $W(m,h)$ is given by the Poisson distribution for $h=n\mathcal{V}$

$$W(m,h) = \frac{1}{m!} h^m \exp(-h). \quad (288)$$

Some of the statistical properties of this distribution have been described by Chandrasekhar (1943). The changing form of $W(m,h)$ is shown in Fig. 27. As expected, the probability of finding one perturber within \mathcal{V} , $W(1,h)$, is maximum when $h=1$, and greater than the probabilities of finding two or more perturbers simultaneously within \mathcal{V} . Generally, the probability $W(m,h)$ is greatest when $h=m$. With increasing h there is a steady movement of the maximum probability toward larger numbers of perturbers within \mathcal{V} .

This changing distribution is reflected in the calculated profiles discussed in Sec. II.E.2. The effect of two or more perturbers becomes quite significant at higher densities, where the peak of the line profile corresponds to the most intense satellite, and thereby to the most probable distribution of perturbers. The peak comprising the line core at low densities, a region usually described by the impact approximation, disappears completely when the probability of finding more than one perturber interacting at a time is large. In that case the profile of

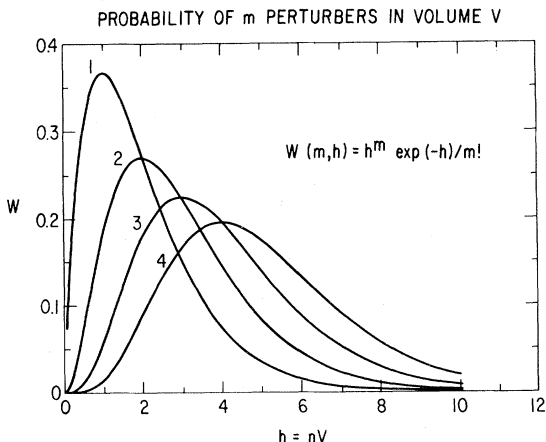


FIG. 27. Poisson distribution $W(m,h)$ of the probability of finding m perturbers in a volume \mathcal{V} such that $h=n\mathcal{V}$.

the line shifts as its oscillator strength is redistributed among higher-order satellites, a phenomenon quite different from the shift of the line core in the impact approximation. When the probability of finding m perturbers interacting with the atom is maximum, the corresponding spectrum of m perturbers dominates the profile and determines the linewidth and shift.

For a qualitative explanation of observed spectra, consider an additive interaction yielding an angular frequency shift ϵ , localized within a volume \mathcal{V} about the radiator. The phenomena may be semiquantitatively described by saying that the radiation is only at ω_0 when all perturbers are out of the volume, is $\omega_0+\epsilon$ if one perturber is in the volume, and so on. For arbitrary ω we require $m=(\omega-\omega_0)/\epsilon$ perturbers in the volume. The intensity is then proportional to the probability of finding only this many perturbers in \mathcal{V} :

$$\begin{aligned} I(\omega) &= W[(\omega-\omega_0)/\epsilon, n\mathcal{V}] \\ &= \frac{(n\mathcal{V})^{(\Delta\omega/\epsilon)}}{(\Delta\omega/\epsilon)!} \exp(-n\mathcal{V}). \end{aligned} \quad (289)$$

For obvious reasons it is very convenient to define ω_m

$$\omega_m = n\mathcal{V}\epsilon + \omega_0 \quad (290)$$

as the line center. Then, with substitutions $\xi=\Delta\omega/\epsilon$ and $\xi_0=n\mathcal{V}$, the intensity is given by

$$I(\xi) = \frac{(\xi_0)^\xi}{\xi!} \exp(-\xi_0). \quad (291)$$

This is of course discrete, defined only for the integral ξ , but for $\xi \gg 1$, the limit of high density, it becomes practically continuous. Then, since

$$\xi! \simeq (2\pi\xi)^{1/2} \xi^\xi \exp(-\xi), \quad (292)$$

Eq. (291) can also be written

$$I(\xi) \simeq (2\pi\xi_0)^{1/2} (\xi_0/\xi)^{\xi+1/2} \exp(\xi-\xi_0). \quad (293)$$

For large ξ it is not difficult to show that this expression is approximately equivalent to

$$I(\xi) \simeq (2\pi\xi_0)^{1/2} \exp[-(\xi-\xi_0)^2/(2\xi_0)]. \quad (294)$$

This is a Gaussian line profile with a peak at $\xi=\xi_0$, or a shift

$$\sigma = n\mathcal{V}\epsilon \quad (295)$$

and a half-width at half maximum intensity $[(2\ln 2)\xi_0]^{1/2}$ or

$$\gamma = n^{1/2} [(2\ln 2)\mathcal{V}]^{1/2} \epsilon. \quad (296)$$

While the shift increases linearly as n at high density, the width of the line grows only as $n^{1/2}$.

The Gaussian profile in the high-density limit was predicted for all lines, not just Rydberg series, by Royer (1980), noting that, at high n , $\Phi(s)$ must go to zero rapidly as s increases in Eq. (54). By expanding $g(s)$ in time and retaining lowest-order terms we are left with

$$\lim_{s \rightarrow 0} \operatorname{Re} g(s) \sim s^2, \quad (297)$$

$$\lim_{s \rightarrow 0} \operatorname{Im} g(s) \sim s . \quad (298)$$

The Fourier transform of such $\Phi(s) = \exp[-ng(s)]$ is a Gaussian line, as indicated by Eqs. (294)–(296). This result is not dependent on any particular potential model, although actual values of widths and shifts are.

It is well known (Omont, 1977) that the impact-limit shift of a Rydberg line is given by (in angular frequency units)

$$\sigma = n 2\pi A \frac{\hbar}{m} , \quad (299)$$

where A is the scattering length [see Eq. (184)] for the valence electron on a foreign-gas atom. This result, first derived by Fermi (1934; see also Massey and Burhop, 1952) without the use of line-broadening theory, explains the observations of Amaldi and Segre (1934a, 1934b) and others (Füchtbauer and Gössler, 1935; Füchtbauer and Reimers, 1935; Füchtbauer and Schulz, 1935). It is from such data that scattering lengths for low-energy electrons have been extracted (O'Malley, 1963) that compare favorably with values from other experiments. It is interesting that this shift can also be obtained from the considerations leading to Eq. (294).

The static approximation to $g(s)$ is, from Eq. (59),

$$g(s) = 4\pi \int_0^\infty R^2 dR \left[1 - \exp \left(-\frac{i}{\hbar} V(R)s \right) \right] , \quad (300)$$

which, for

$$g(s) = \alpha(s) + i\beta(s) , \quad (301)$$

yields

$$\alpha(s) = 4\pi \int_0^\infty R^2 dR \left[1 - \cos \left(\frac{V(R)}{\hbar} s \right) \right] \quad (302)$$

and

$$\beta(s) = 4\pi \int_0^\infty R^2 dR \sin \left(\frac{V(R)}{\hbar} s \right) . \quad (303)$$

Again we note that, when n is large, since $\Phi(s) \rightarrow 0$ for s not near 0, we can expand α and β as functions of s and retain just the leading terms:

$$\alpha(s) \simeq \left[4\pi \int_0^\infty \frac{[V(R)/\hbar]^2}{2} R^2 dR \right] s^2 , \quad (304)$$

$$\beta(s) \simeq \left[4\pi \int_0^\infty \frac{V(R)}{\hbar} R^2 dR \right] s . \quad (305)$$

The shift term, given by the integral in $\beta(s)$, is easily evaluated for the Fermi potential of Eq. (174):

$$V(R) = 2\pi \frac{\hbar^2}{m} A \Psi^2(R) , \quad (306)$$

$$\beta(s) \simeq 2\pi \frac{\hbar}{m} A \left[4\pi \int_0^\infty \Psi^2(R) R^2 dR \right] s . \quad (307)$$

The bracketed term is just unity, yielding

$$\beta(s) \simeq 2\pi \frac{\hbar}{m} As \quad (308)$$

or

$$\sigma = n 2\pi A \frac{\hbar}{m} , \quad (309)$$

just the Fermi shift.

Consequently the shift of Rydberg transitions from the low-density impact regime to the high-density limit follows the same linear relationship for all members of the series. The width, evaluated similarly from $\alpha(s)$, is

$$\gamma = n^{1/2} \left[4\pi \int_0^\infty \left(\frac{V(R)}{\hbar} \right)^2 R^2 dR \right]^{1/2} (2 \ln 2)^{1/2} . \quad (310)$$

For $V(R)$ given by the Fermi potential, the half-width at half maximum of the Gaussian line is

$$\gamma = n^{1/2} \left[2\pi \frac{\hbar}{m} A \right] (2 \ln 2)^{1/2} \langle \Psi^2 \rangle^{1/2} , \quad (311)$$

where $\langle \Psi^2 \rangle$ is a mean value of the probability density for finding the valence electron at R . A comparison of Eqs. (310) and (311) with Eqs. (295) and (296) demonstrates that the qualitative volume of interaction \mathcal{V} in that discussion is actually $\langle \Psi^2 \rangle^{-1}$. Further, the width-to-shift ratio should depend on the gas density n and the atomic state, but not on the properties of the foreign-gas perturbers in this high-density limit.

Experimental profiles with reliable photometric quality have not been explored systematically for high series member spectra, but available results are discussed in Sec. III.D.2.b. A recent experiment by Brillet and Gallagher (1980) on rubidium 5s-ns and 5s-nd Doppler-free spectra for noble-gas perturbers, for example, reports that profiles from 0.2 to 30 torr were Lorentzian, but details of the analysis were not given. The shifts were found to be independent of series member from $n = 15$ to 35, while the broadening decreased by an order of magnitude over the same range. The considerable body of width, shift, and asymmetry measurements in the literature (Sec. III.D.3) has been used by Royer (1980) to confirm the anticipated dependence on density. His work also includes the additional possibility of perturber-perturber correlations at very high density; analyses of resonance line spectra for pressures as great as 30 atmospheres support the existence of such effects.

III. EXPERIMENTS

But the last word belongs, of course, to experiment. This word, however, seems not yet to have been pronounced.

—Jablonski, 1945

A. Conventional spectroscopy

While the observation of pressure effects on spectral lines is an old art, dating at least to Michelson's visual

measurements of line visibility (Michelson, 1895), the considerable body of data accumulated prior to the review of Ch'en and Takeo (1957) was derived from photographic observations of line shifts, positions of maxima, and approximate widths. The development of precise photoelectric photometry and the improvements in grating spectrometers and interferometers, as well as recent developments in related electronic technology, have had a substantial effect on the quality of available data and on types of observations possible. In this section we provide a brief overview of the application of these by now conventional techniques to the study of neutral-atom line broadening and of new methods and devices that promise future improvements.

1. Dispersive spectroscopy

As in most cases the width of the spectral lines at low pressure is so small that it is usually masked by imperfections of the spectroscopes employed, this question must be attacked by interference methods.

—Michelson, 1895

An impact-broadened spectral line core from a typical light source or absorption cell at pressures less than an atmosphere is usually less than 1 cm^{-1} full width at half maximum, with a broadening rate of the order of $10^{-3} \text{ cm}^{-1} \text{ Torr}^{-1}$ for noble-gas perturbations of the resonance lines of the alkali metals. Thus, for spectral lines in the visible and gas pressures of the order of 100 torr, it is necessary to have an instrumental resolution in excess of 10^5 in order to resolve the line profile. Sufficient resolution can be achieved with large-grating spectrometers or with Fabry-Perot interferometers, and both types of instrumentation have found wide use. The possibility of using Fourier-transform spectroscopy (Thorne, 1974), first introduced by Michelson (1895), which would yield the spectral correlation function directly, does not seem to have been considered since his time for broadening studies in atomic spectra.

Recent developments in grating technology are reviewed by Palmer, *et al.*, (1975). In order to achieve a resolution of 500 000, several laboratories have employed echelle spectrometers with 20 cm or larger gratings, ruled with approximately $300 \text{ grooves mm}^{-1}$. Since these instruments operate in high order, e.g., the 10th for green light, predispersion or prefiltering is also necessary. While ghost intensity from interferometrically ruled gratings is of the order of 10^{-6} of the line-peak intensity, parasitic scattered light from unwanted orders can be a problem, particularly in absorption spectroscopy, where the scattered-light level may be several percent of the continuum. An improvement of orders of magnitude in scattered-light level with some increase in resolution is possible with high-groove-density holographically manufactured gratings, particularly since these gratings operate with high resolution in the first order. Dravins (1978) has demonstrated how quantitative photometry in absorption spectroscopy is improved with the use of these gratings, which should therefore see considerable

use in the future for observations in the ultraviolet; for instance, in studies of highly excited states (Kielkopf, 1981a). The improvement in scattered-light level possible with a large holographic grating is illustrated in the data from Dravins shown in Fig. 28. Other examples are shown in Kielkopf (1981b).

Techniques of spectroscopy with large-grating instruments have been discussed by de Sa and McCartan (1972), Lorenzen and Niemax (1977), and Kielkopf (1980, 1981b). Current instrumentation in this regard almost invariably features some type of scanned detector, rather than rotation of the grating itself, which often imposes problems of stability. Indeed temperature stability is an important consideration for line-shift measurements, and use of fused silica or Zerodur for new grating blanks has improved these measurements markedly. For studies of emission sources the scattered-light problem of single-grating instruments is overwhelming, because line-wing features of interest are often of the same level of intensity as the unwanted background. A solution employed recently (Ottinger *et al.*, 1975) has been to use a double monochromator for observations far from the line center. This allows the measurement of features as weak as 10^{-9} of the line peak, which is a practical limit due solely to light flux anyway.

For line-core measurements, the single Fabry-Perot etalon is often used. An example of its application to emission spectra is given by Kielkopf and Knollenberg (1981), and to absorption spectra by Deleage *et al.*, (1973). The well-defined instrumental characteristics of the Fabry-Perot interferometer are a practical advantage for precise line-core shape measurements (Roesler, 1974; Lewis, 1980). Improvements in active stabilization (Ramsey, 1970) and the ease of implementing signal-averaging techniques for piezoelectrically scanned instruments could yield much-improved line-core shifts and widths. The rather high off-band leakage of the single Fabry-Perot can be reduced by triple passing, or by the use of several interferometers in series (Drummond and Gallagher, 1973). This type of instrument has been employed in an extensive set of line-wing measurements (Sec. III.E) of the fluorescence of alkali resonance lines perturbed by the noble gases. In this application the

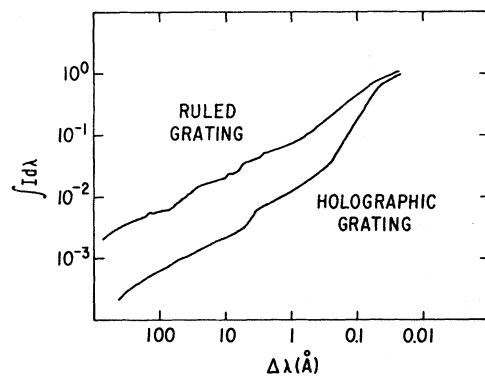


FIG. 28. Accumulated energy in the instrumental profile for classically ruled and holographic gratings (Dravins, 1978).

great luminosity advantage of the Fabry-Perot over a grating instrument of comparable spectral resolution was put to practical use (Jacquinot, 1960).

2. New developments in detectors

Just as the introduction of the photomultiplier revolutionized the determination of line profiles in the 1950's and has been the experimental basis for most of the new measurements reported in this article, new developments in imaging detector technology promise equally impressive gains in the future. These devices have been introduced into very-low-light-level spectroscopy, particularly for astronomical applications, but their use for studies of weak far-line-wing fluorescence, rapid absorption spectroscopy, and measurements of transient profiles is a natural extension of these early applications. Since a number of laboratories have such experiments underway, we give a brief review of the essential information here.

A useful review of digital imaging detectors has been given by Ford (1979). Digital imaging techniques are divided there into four categories: television camera tubes, silicon arrays, hybrid systems involving image intensifiers, and digital image tubes. We shall look here at recent applications of devices in these categories to low-light-level or high-resolution spectroscopy as appropriate for spectral line profile studies.

Television camera tubes have been commercially available for spectroscopic applications for a number of years, and an example of their use is given by Speer *et al.*, (1980). Particularly useful, because of their linear response, are vidicons. These tubes have a photoconductive target, and the most useful in stability and sensitivity are silicon vidicons (Hunten, Nelson, and Stump, 1976; McCord and Frankston, 1975), which have a diode array target. Improved low-light-level sensitivity is obtained with tubes that have internal gain, either SEC vidicons (Chiu, 1977) or SIT vidicons (Weller, Herbst, and Jeffers, 1977). These devices are not completely satisfactory for spectroscopy because of their physical bulk and complexity, nonlinearity of response, and sensitivity to microphonics. The electron-beam readout also results in adjacency effect, making the determination of a weak signal near a strong one difficult and introducing an uncertainty in readout position on the photosensitive target.

Potentially more practical are silicon photodiode arrays, solid-state detectors on a single substrate that are read out electronically. Two principal advantages for these devices are the high spatial stability, equivalent to that of a photographic plate, and the high quantum efficiency, which approaches 100% in some spectral regions. For spectroscopy the most useful devices are self-scanned photodiode arrays called "Reticons." These are now available with up to 2048 elements, typically $25\text{ }\mu\text{m}$ on a side in a linear array. Cooled to liquid-nitrogen temperatures, the arrays can be exposed for up to several hours to accumulate signals and reduce the effect of readout noise. Since saturation signals are typically of the order of 10^7 photons pixel $^{-1}$, and readout noise is of the order

of 10^3 photons pixel $^{-1}$, signal-to-noise ratios in excess of 100:1 have been reported (Vogt, Tull, and Kelton, 1978). Two gains over the use of photomultipliers are significant. The first is the advantage of multiplexity, since up to 2048 spectral channels can be observed simultaneously. The second is the higher quantum efficiency, particularly in the red. Typically a few seconds of exposure are equivalent to 30 min of scanned observation, as illustrated in Fig. 29. Improved sensitivity in the ultraviolet is achieved by using fluorescent coatings such as coronene (Blouke *et al.*, 1980). For very-low-light-level and transient signals, such as would be encountered in shock-tube experiments, a combination of Reticon and image intensifier may be useful (Lemaire, 1980). Integral devices of this sort, known as Digicons (Tull, Choisser, and Snow, 1975), that may be used for spectroscopy are now commercially available. Laboratory use of uncooled Reticons has been reported by Morris and McIlrath (1979) and, in line-shape measurements, by Harima, Tachibana and Urano (1980).

Another form of silicon diode array, differing from the Reticon in the method of charge readout, is the charge-coupled device or CCD. In these detectors the charge in each pixel is transferred from pixel to pixel until it reaches a preamplifier on the chip. This allows the construction of very large arrays, with sizes up to 800×800 elements available. Smaller-area arrays with 128×128 pixels and a slightly different charge-injection device (CID) construction have been available in commercial cameras since 1978. Area arrays promise utility in combination with Fabry-Perot interferometers (Roesler, 1980) and echelle spectrographs.

As improvements in array detectors rapidly become commonplace, we can expect applications to low-light-level line-wing spectroscopy, which would benefit from the advantage of multiplexity these detectors provide. Similarly, measurements of small line shifts, limited in the past by problems of grating rotation or slit scanning, are now more feasible.

3. Sources for line-shape spectra

Specific sources of atomic spectra have found individual applications in studies of neutral-atom line broadening dependent on the region of the line profile, the excitation of the line, and the pressure and temperature range required. A comparison of different examples will illustrate these limitations on experimental line-profile measurements.

a. Absorption spectroscopy

Except for laser-excited cells, absorption spectroscopy is used to study transitions with an atomic ground state for the lowest level. This complements emission spectroscopy, which cannot be used for such transitions because of problems with reversal and self-absorption. There are practical limitations to absorption spectro-

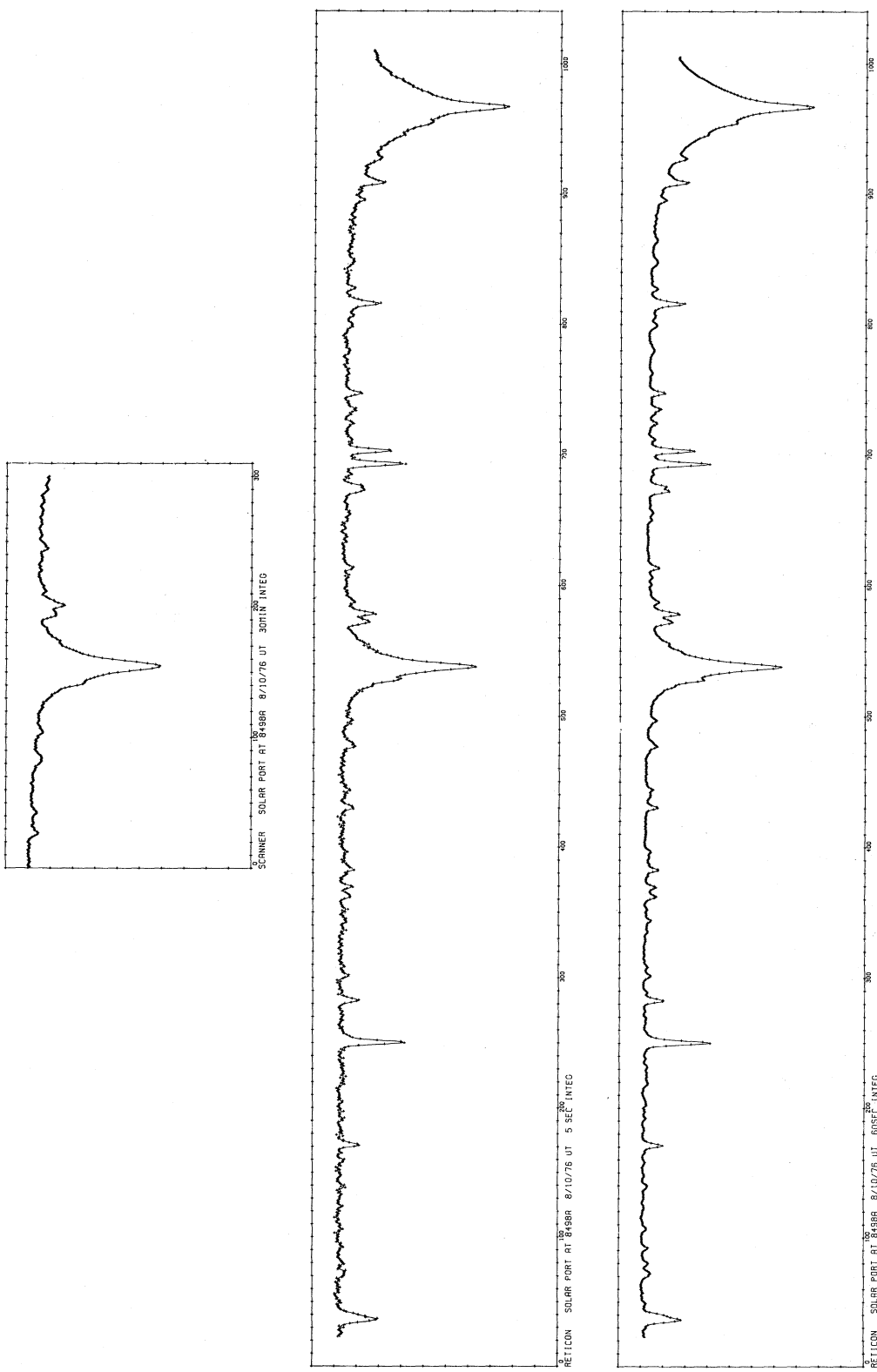


FIG. 29. A comparison of a 30-min observation (top) with a scanned photomultiplier, a 5-sec exposure with a Reticon detector (center), and a 60-sec Reticon exposure (bottom) for the solar spectrum near 8500 \AA (Vogt, Tull, and Kelton, 1978).

copy that are not easy to overcome. If low temperatures are desired, then a very long path length is required for weak transitions (Exton, 1976). On the other hand, if high temperatures are required, then there are problems with cell wall materials (Collins, Petford, and Blackwell, 1970). The maximum temperature range possible is from about 300 K (long-path cesium) to 3000 K (carbon tube furnace with iron) at cell pressures up to one atmosphere. With reactive materials, alkali metals in particular, there are difficulties with window seals at high temperatures (West, Shuker, and Gallagher, 1978), and with reactivity with fused silica and glass wall and window materials as well. Very-high-pressure cell designs have been reported by Ch'en and Parker (1955) that allow cell pressures of 10 atm or more, but at temperatures limited to hot regions only in the center of the cell. The use of heat-pipe absorption cells for pressure-broadening studies is not recommended because of the metal—foreign-gas separation produced by the diffusion of the metal. As a result there are often problems with condensation on windows due to nonuniform cell temperatures.

Absorption spectroscopy requires an intense flat-background continuum. For wavelengths longer than 5000 Å the tungsten-iodide lamp is usually employed. For shorter wavelengths, down to 2000 Å, the compact xenon arc lamp is ideal. With an intense continuum, high-resolution spectroscopy can still achieve signal-to-noise ratios in excess of 100:1. These methods have been used to measure small line asymmetries and deviations from Lorentzian behavior in the impact region, to make high-precision determinations of line shifts and widths, and to observe quantum oscillations and multiplet-perturber effects in line-wing spectra (McCartan and Farr, 1976; Spielfiedel *et al.*, 1979; Kielkopf and Allard, 1980; Kielkopf, 1980; Chen and Phelps, 1973; Lorenzen and Niemax, 1977).

b. Emission spectroscopy

Although electrical discharges introduce the additional problem of broadening by electrons and ions and of self-reversal and self-absorption of resonance lines, for studies of excited states they can be particularly useful. Gwinn, Thomas, and Kielkopf (1968) have used electrodeless microwave sources to survey the appearance of satellites on cesium lines, and Tam and Moe (1976) have made similar emission observations of excimer transitions *s-s* and *s-d* in potassium—and sodium—noble-gas spectra. High-current, high-gas-density discharges also have been used by Schuhmann, Wildman, and Gallagher (1980) for measurements of MgXe excimers. The technique appears particularly appropriate for studies of high-gain laser transitions. Precise measurements of line-core shift and width on excited states have been made on specially designed alkali lamps in potassium—and sodium—noble-gas broadening (Kielkopf and Knollenberg, 1975; Kielkopf and Knollenberg, 1981). Even hollow cathode discharges, which operate only at low pressures, have been used to look for temperature depen-

dence of satellite profiles (McCartan, Farr, and Hindmarsh, 1974).

c. Fluorescence spectroscopy

The advantage of fluorescence is that the source is free of significant electron broadening and that the conditions can be controlled and measured exactly, so that profiles can be normalized with precision. This is clearly illustrated in the measurements by Niemax (1980) of three-body effects in cesium spectra. Further, it is often possible to identify particular far wings with the state excited, without the disturbing influence of unwanted overlapping radiation that would appear in a typical electrical discharge. With resonance lamp excitation Gallagher and co-workers (Sec. III.E) have studied far wings of alkali resonance lines broadened by noble gases. In conventional use of fluorescence, only transitions directly connected to the ground state can be studied this way. Stepwise or multiphoton excitation with lasers is possible for other transitions.

d. Shock-tube spectroscopy

Laboratory absorption and fluorescence sources are limited significantly in temperature because of materials problems. For many theoretical comparisons, one temperature is as good as another, and this is not a serious obstacle, but for the determination of line-broadening rates for use in stellar atmosphere models, studies with temperatures of the order of 5000 K or higher are desired. Such extreme conditions are necessary both to duplicate stellar atmosphere temperatures and to insure dissociation of molecular hydrogen for the determination of broadening by atomic hydrogen. These problems are by no means unambiguously solved, but some recent results have been reported on shock-tube experiments that reached densities of the order of 10^{20} atoms cm $^{-3}$ at temperatures of 5000–10 000 K in compressed-gas shocks. Diagnostic problems remain in such devices, for the gas temperature, pressure, and degree of dissociation must be measured for each shock cycle, and the entire transient profile must also be recorded. In spite of these difficulties, devices of this sort are the only way now available to simulate the conditions of stellar atmospheres in the laboratory (Baird, Eckart, and Sandeman, 1979; Burgess and Grindlay, 1970).

B. Laser spectroscopy and neutral collision broadening

In classical spectroscopy the use of large high-resolution gratings, scanning multietalon Fabry-Perot interferometers, improved absorption cells and emission sources, and new families of detectors have led to stimulating new measurements of collisional effects. On the other hand, recent developments in the use of tunable lasers have made possible both improved experimental precision and the acquisition of information unobtainable

by other methods. The basic techniques of high-resolution laser spectroscopy have been reviewed recently (Demtröder, 1973, 1981), and here we survey only their application to line-shape problems.

The tuned nature of laser excitation is a powerful tool for fluorescence studies; observations of time-resolved near-line-wing fluorescence have been reported by Kielkopf (1975a) and by Marek and Niemax (1976a, 1976b) for cesium spectra perturbed by xenon. In these results, which describe observations of radiation from excited p states also accessible by conventional absorption spectroscopy, the new information gained concerns primarily excitation transfer processes in foreign-gas collisions. West, Shuker, and Gallagher (1978) have used cw laser excitation of pressure-shifted sodium resonance lines to study the fluorescence spectrum of far-wing profiles at densities in excess of 10^{20} cm^{-3} . In previous experiments with Na fluorescence (York, Scheps, and Gallagher, 1975) resonance lamp excitation was used, but at high noble-gas pressures the absorption profiles of the sodium D lines shifted compared to spectral lines of the unperturbed resonance lamp. Tunable-laser techniques can also be applied to higher states, and still develop measurable signals. Marek and Niemax (1976a, 1976b) and Niemax (1980) have observed spectra from states up to $9p$ in cesium and from other nearby states that are collisionally populated by excitation transfer. This offers the possibility of studying near-wing and line-core broadening in transitions from excited states that do not connect directly with the ground state. The series of ns states in cesium are populated by collisional transfer from nearby np levels, and the $6p-ns$ transitions are observable in fluorescence, as are $6s-ns$ collision-induced bands. The latter features were found to correspond to electrical discharge emission studies of Tam and Moe (1976) and laser fluorescence studies of Happer, Moe, and Tam (1975). Of course multiphoton ionization processes take hold rapidly for incident radiation with photon energy greater than half the ionization potential, so that to obtain high-intensity fluorescence signals from excited states not perturbed by ionization in the cell requires control of incident laser intensity and stepwise excitation. Sayer, Ferray, and Lozingot (1979) have observed absorption spectra of Cs—noble-gas $6s-7s$ transitions by tuning the laser through the transition and detecting the infrared $6s-6p$ fluorescence resulting from cascade decay. This method yields highly sensitive detection of otherwise very weak effects. Webster and Rostas (1978) and Delhoume *et al.*, (1981) have studied K—noble-gas $4s-5p$ line profiles both by observing the spectrum of the fluorescence when the unperturbed lines are pumped, and by observing the total fluorescence as the laser is scanned through the profile. An example of their observations for broadening by neon is shown in Fig. 30.

A study of the sodium D -line cores broadened by noble gases with laser fluorescence techniques has been made by Chatham, Gallagher, and Lewis (1980). In their investigation the line wings were measured by observing the total fluorescence from a cell with

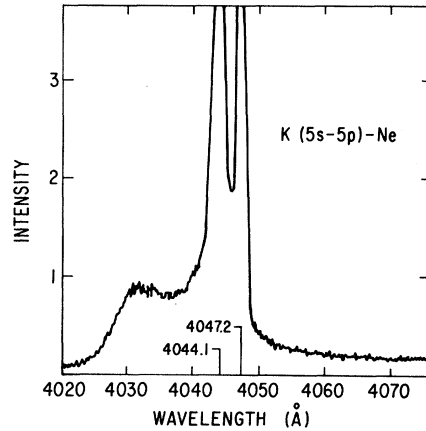


FIG. 30. Blue satellite on the K ($5s-5p$) transition perturbed by Ne at 700 torr and 508 K from Delhoume *et al.* (1981). The feature is particularly interesting because it is predicted by model potential calculations.

sodium—rare-gas mixtures as a dye laser was tuned across the line profile. The method gave high signal-to-noise ratio and linewidths with uncertainties of the order of 2%. Corrections were necessary to compensate for the attenuation of the laser in the line centers that were not optically thin, and although the results compared reasonably well with high-precision conventional absorption spectroscopy (Kielkopf, 1980), remaining discrepancies exceeded the expected errors.

Doppler-free two-photon spectroscopy (Grynberg and Cagnac, 1977) of the broadening of the Balmer-alpha line by helium (Weber, 1979, 1981) has been used to avoid the large thermal broadening in atomic hydrogen spectra. The shift and broadening of individual fine-structure transitions were measured in the very-low-density range from 4×10^{15} to $4 \times 10^{16} \text{ atoms cm}^{-3}$, and the effect of inelastic fine-structure transfer collisions could be seen in exceptionally large linewidths and shifts of anomalous sign. Similar effects on the sodium D lines have also recently been reported (Weber and Jungman, 1981).

The broadening and shift of ns and nd high Rydberg states can also be measured by Doppler-free two-photon spectroscopy in alkali metals; results on self-broadening in Rb $s-s$ transitions have been reported by Stoicheff and Weinberger (1980). In their method the excited atom, ionized in an axial electric field, neutralizes the space charge in the detector and changes bias current to yield a measurement. Reported results cover the density range of 1×10^{14} to $4 \times 10^{15} \text{ atoms cm}^{-3}$, and measurements beyond $n=120$ are given. As shown in Fig. 31, there is a striking oscillation along the series that may mark the influence of the detection process on the apparent widths of the lines. Brillet and Gallagher (1980) have measured broadening in Rydberg states of Rb caused by noble gases by detecting the fluorescence after two-photon Doppler-free excitation of $5s-ns$ and $5s-nd$ transitions. Related experiments on lower-lying states are described by Biraben *et al.* (1977).

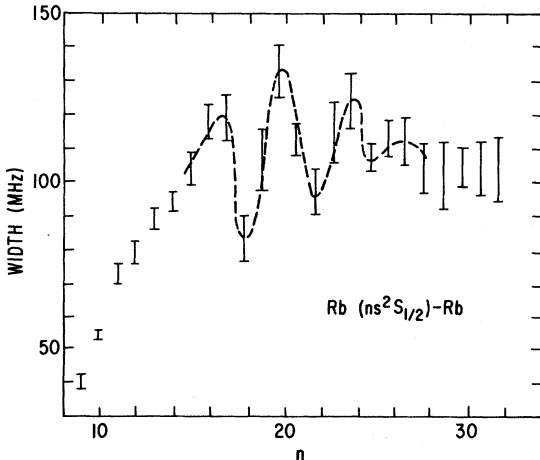


FIG. 31. Width of the Rb (5s-ns) transitions perturbed by unexcited Rb at 0.060 torr, observed with Doppler-free two-photon spectroscopy by Stoicheff and Weinberger (1980).

Trilevel echos provide another detection method for the observation of broadening of excited ns and nd states in alkalis. Flusberg *et al.*, (1979) and Mossberg, Kachru, and Hartmann (1981) report the broadening of d states up to $n = 34$ for foreign-gas pressures less than 4×10^{16} atoms cm^{-3} . The technique effectively determines the correlation function for a macroscopic oscillating electric dipole moment in the sample through the appearance of a delayed coherent emission from an intermediate state, in this case the $3s-3p$ resonance transition. The intensity of this echo depends on the delay between the initial two-step excitation pulses and an excitation transfer pulse, and is directly a measure of the correlation function in the sample. At low densities the Lorentzian linewidths can be determined from the dependence of the correlation function on time delay. Collisional cross sections derived for broadening by argon are illustrated in Fig. 32.

New techniques available through laser spectroscopy thus correlate well with improvements in conventional methods. Laser spectroscopy alone provides access to the impact cores of excited ns and nd alkali states and to Doppler-free impact broadening in atomic hydrogen. On the other hand, it also provides a very efficient excitation mechanism for studies of regions outside the impact profile through tuned-laser absorption spectroscopy, with detection of the fluorescence of excited atom-foreign-gas mixtures. In this context, the radiative redistribution experiments discussed in Sec. III.G are unique to laser spectroscopy. In many respects, continued interest in line-shape phenomena stems from this vital new technology.

C. Deconvolution

To extract the effect of atomic collisions on spectral lines from the observed spectra it is necessary to remove the instrumental effects and any other causes of line

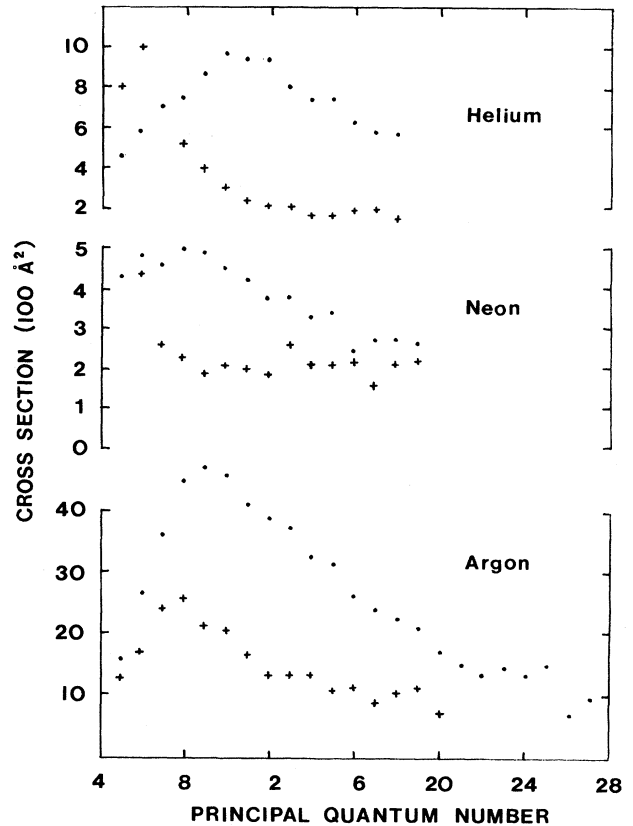


FIG. 32. Collision cross sections for transitions from the Na $3s\ 2S_{1/2}$ state to $ns\ 2S_{1/2}$ (+) and to $nd\ 2D_{3/2}$ (●) perturbed by noble gases, as determined with the trilevel echo technique (Flusberg *et al.*, 1979).

broadening from the measurements. In some cases, as a practical matter, no corrections are necessary. This occurs, for instance, if line wings are observed with an instrument of spectral passband so narrow that no appreciable change in wing strength occurs within the passband. Even then, however, the extremely weak far wing of the instrument, say 10^{-5} of peak response for a typical high-quality spectrometer, or even higher off-peak broadband fluorescence in tuned dye lasers, may overlap the line peak and produce a signal just as strong as the line wing being observed. The problem is most severe for far-wing fluorescence observations, whether conventional or with tuned lasers, and least significant for absorption spectroscopy.

Corrections for instrumental response and Doppler broadening are almost always necessary in measurements of impact broadening and of small deviations from Lorentzian profiles in the near line wing. Unless very narrow-band lasers are used in Doppler-free experiments, the corrections can be a large fraction of the observed linewidth, and it is not surprising that accurate results depend sensitively on how the deconvolution is performed. Here we consider techniques recently developed for deconvolution, for the evaluation of Voigt profiles and instrumental response of interferometers, and for the

detection of small asymmetries and the removal of inherent instrumental asymmetry. Needless to say, these methods have evolved significantly since the review of Ch'en and Takeo (1957), when the only technique available required the comparison of measured strip-chart records with tabulated profiles.

1. Methods of deconvolution

Suppose that the true profile is given by the function $f''(x)$, and the apparatus function is $f'(x)$. Then the observed distribution is given by the convolution

$$f(x) = \int_{-\infty}^{+\infty} f''(x-y)f'(y)dy , \quad (312)$$

as all spectral elements in the true profile contribute to any observed frequency with a weight given by the instrumental response. If we presume that the instrumental response is known, and this may not always be true, then the problem is to determine the true distribution f'' from the apparent distribution f by solution of the integral equation.

General methods of solution have been discussed by Jansson (1970), who studied iterative techniques, while other authors have utilized the equivalence of this integral to the product of infinite-order square and column matrices to seek solutions by matrix inversion (Herget *et al.*, 1962). The basic problem with these approaches is the effect of errors in the experimental curve, because such errors, if real, imply unresolved detail in the true profile. Thus all deconvolution methods are basically unstable and can lead to unreasonable errors in the deduction of the true profile if some limits are not imposed in the deconvolution process. Deconvolution error has been discussed by Jones and Misell (1970), who point out that all methods in use involve some degree of approximation, not the least of which is that the experiment can never determine the entire observed profile, but only a section of it. In any case, the limiting factor in general deconvolution is noise in the observed spectra (Lorre, 1973).

One way to overcome these limitations is to presume some form for the functions f , f' , and f'' , or their Fourier transforms. For instance, Ottlinger *et al.* (1975), in observations of rubidium resonance line impact broadening, assumed that the true profile f'' was a Lorentzian of unknown width. The instrumental profile f' was taken from the observation of a Doppler-broadened, but not collision-broadened, line of nearby wavelength. Then the convolution calculated with Eq. (312) was compared to the observed profile to select a best value for the Lorentzian width. An advantage of this technique is that it provides an immediate indication of non-Lorentzian behavior in the impact core, although it cannot provide a quantitative deconvoluted profile.

The most commonly used solution is to assume that the functions f have Fourier transforms proportional to (Unsöld, 1968)

$$\phi(t) = \exp[-(\alpha_0 + \alpha_1 t + \alpha_2 t^2 + \dots)] , \quad (313)$$

which means that they are themselves convolutions of Gaussian and Lorentzian lines

$$f_g(x) = \frac{1}{\pi^{1/2} \alpha_2} \exp[-(x/\alpha_2)^2] \quad (314)$$

and

$$f_l(x) = \frac{\alpha_1/\pi}{x^2 + \alpha_1^2} , \quad (315)$$

such that

$$f(x) = \int_{-\infty}^{+\infty} f_l(x-y) f_g(y) dy \quad (316)$$

defines the instrumental, source, and observed profiles. This convolution of Gaussian and Lorentzian functions is known as a Voigt profile. If the parameters of the Voigt profile describing the lines can be determined, then convolution is achieved simply by multiplying the Fourier transforms; that is, by adding the coefficients in the exponent of Eq. (313):

$$\alpha_1 = \alpha'_1 + \alpha''_1 , \quad (317)$$

$$\alpha_2^2 = \alpha'^2_2 + \alpha''^2_2 . \quad (318)$$

Although the method is restricted to symmetric instrumental functions and true profiles that are Doppler-broadened Lorentzians, it provides a direct technique for the determination of linewidths. In current use the actual fitting of the Voigt function to the observed and instrumental profiles is achieved through least-squares iterative procedures (Bevington, 1969) for which standard programs are available. The possibility of fitting the Fourier transform has also been considered by Ivanov and Fishman (1973).

2. Calculation of the Voigt function

There has been considerable work in recent years on the development of fast and accurate methods for computing or approximating Voigt functions. Mathematical properties of the function have been reviewed by Armstrong (1967). Methods of computing the function to accuracies exceeding one part in 10^4 are given there and in several recent papers that are concerned particularly with the problem of computational speed (Reichel, 1968; Drayson, 1976; Pierluissi, Vanderwood, and Gomez, 1977; Hui, Armstrong, and Wray, 1978). All of these papers report useful FORTRAN computer programs.

Several rapid approximative procedures have also been proposed. Simple rational approximations that can be implemented with limited computing power have been given by Whiting (1968) and Kielkopf (1973). In the latter, the Voigt function is represented by the sum of a Gaussian and a Lorentzian function plus a correction term. An accuracy of seven significant figures is achieved for lines which deviate only slightly from pure Gaussian or Lorentzian, and for intermediate values the approximation is good to three figures within a few half-widths of the line center (Hui, Armstrong, and

Wray, 1978). Hui also gives a method of rapid computation that achieves accuracies of the order of ten significant figures, with computation times as short as 10 msec, on an IBM S370/145. In any case, it is necessary to have a rapidly computed function in order to proceed with iterative, nonlinear, least-squares fitting. The availability of suitable codes for Voigt-function generation no longer seems to be a problem.

3. Deconvolution of Fabry-Perot response

The response of a Fabry-Perot interferometer to a single spectral line is a more difficult matter than the evaluation of the convolution Eq. (316) with Voigt functions. The complexity of the problem is increased by the periodic apparatus response, which means that the instrument samples many frequencies in the line wing simultaneously. Solutions for the convolution in this case have been given graphically by Ballik (1966) and Day (1970), and in tabular form by Hernandez (1966, 1970). More general solutions in terms of Fourier series have been given by Larson and Andrew (1967) for a multiple-etalon Fabry-Perot, and by Kielkopf (1979) for the response to asymmetric lines.

4. Deconvolution of asymmetry

The general class of correlation functions

$$\phi(t) = \exp\{-[\alpha(t) + i\beta(t)]\}, \quad (319)$$

$$\alpha(t) = \alpha_0 + \alpha_1 t + \alpha_2 t^2 + \dots, \quad (320)$$

$$\beta(t) = \beta_0 + \beta_1 t + \beta_2 t^2 + \dots \quad (321)$$

includes Voigt profiles ($\alpha_0 = \beta_0 = \beta_2 = 0$), the asymmetric lines of impact line-broadening theory ($\beta_2 = 0$), and the general pressure-broadened line profiles of Eq. (99). The intensity of the spectral line is given by the Fourier transform

$$I(\omega) = \frac{1}{2\pi} \int_{-\infty}^{+\infty} \phi(t) \exp(i\omega t) dt. \quad (322)$$

The ideal interferometer has the infinitely sharp but periodic response

$$F(\omega) = \sum_{m=-\infty}^{\infty} I(\omega + m\sigma) \quad (323)$$

for a free spectral range σ . The function has the Fourier series representation with $t_m = 2\pi m / \sigma$ (Kielkopf, 1979)

$$F(\omega) = \frac{\exp(-\alpha_0)}{\sigma} + \frac{2}{\sigma} \sum_{m=1}^{\infty} \exp[-\alpha(t_m)] \times \cos[\omega t_m - \beta(t_m)] \quad (324)$$

that can be rapidly evaluated numerically.

This function can be adapted to least-squares deconvolu-

tion in two ways. One is to assume that the instrumental response is given by a set of innate α and β parameters. This is a good assumption for a Fabry-Perot, since the reflectivity of the plates determines the Lorentzian width of the profile, the plate defects determine the Gaussian width (Hernandez, 1966), and the effect of the scanning aperture can be approximated adequately by additional Gaussian terms. This procedure is also adequate for the representation of spectrometer response by assuming that σ is much larger than the spectral region of interest. A second more general method is to represent the instrumental response by a set of empirically determined Fourier coefficients (Larson and Andrew, 1967), a procedure useful for multiple-etalon systems. In either case the actual evaluation of the series is possible with fast Fourier-transform methods (Cooley and Tukey, 1965; Brigham, 1974). An example of the use of this function in line fitting is shown in Fig. 33.

5. Problems concerning the correlation of Doppler and collision broadening

The motion of the radiator alters the spectrum we observe through the Doppler effect, but it also determines the relative perturber-radiator velocity distribution, and through that the collision broadening. Consequently, Doppler and collisional effects on spectral lines are not independent. Yet, the removal of thermal Doppler broadening from an experimental observation of collision broadening by deconvolution methods depends on the as-

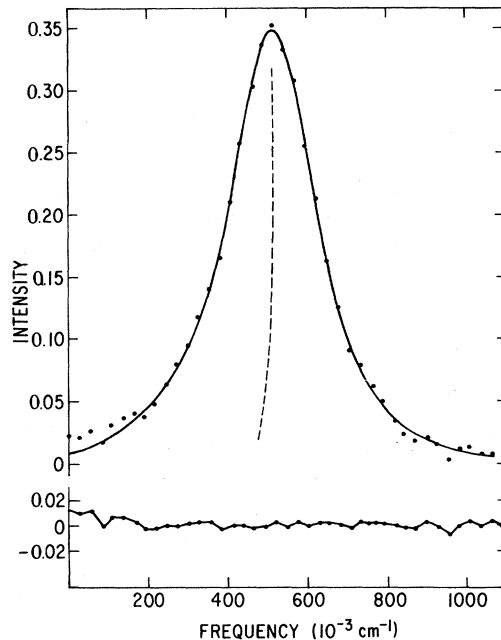


FIG. 33. The sodium ($3s\ 2S_{1/2}-3p\ 2P_{1/2}$) line perturbed by 6.4×10^{18} atoms cm^{-3} of xenon at 445 K and fitted with the profile of Eq. (301), including the superposition of the two hyperfine components of the line. The bisector indicated by the dashed line illustrates the inherent asymmetry of the line.

sumption that collision broadening and Doppler broadening are not correlated. How significant is this correlation, and how would it be manifested in an observable spectrum?

Combined Doppler and collision broadening have been investigated theoretically in many papers (Dicke, 1953; Gersten and Foley, 1968; Berman, 1975; Ward, Cooper, and Smith, 1974; Czuchaj, 1976) and experimentally for alkali-noble-gas spectra in at least one instance (McCartan and Lwin, 1977). The conclusion of all these studies is qualitatively that, when the collisional mean-free path and the wavelength of the radiation are of the same order, the combined effect may be a purely Lorentzian profile, and that under some circumstances the combined linewidth may actually decrease with increasing pressure, as the Doppler shift from one phase in the radiator cycle is cancelled by the shift from another phase (Hindmarsh and Farr, 1972).

The work of Ward, Cooper, and Smith (1974) is a study of the impact core for the case of interaction in only one level of the radiating system, within the context of the Baranger (1958a) theory. The problem centers on the calculation of the velocity average and the Doppler shift simultaneously. With the equations we have used before,

$$\Phi(s) = \langle \exp[-i\xi(s)] \rangle, \quad (325)$$

$$\xi(s) = \eta(s) + \kappa \cdot [\mathbf{R}(s) - \mathbf{R}(0)], \quad (326)$$

the usual phase shift $\eta(s)$ has been augmented with a correction for the translation of the radiator that will generate a Doppler shift in the nonrelativistic limit. The average for $\Phi(s)$ is evaluated with Poisson statistics, and in the one-interacting-level approximation, the correlation function is

$$\begin{aligned} \Phi(s) &= \int d^3v f(v) \exp(-i\kappa \cdot vs) \\ &\times \exp\{-[\Gamma(v) + i\Delta(v)]\}, \end{aligned} \quad (3.27)$$

where $f(v)$ is a Maxwellian velocity distribution. $\Gamma(v)$ and $\Delta(v)$ are the speed-dependent width and shift functions. Consequently, Doppler broadening and pressure broadening are not independent processes.

The Fourier transform of this correlation function is a spectrum that is the average over a Maxwellian velocity distribution of a Doppler-shifted pressure-broadened profile. These functions are also described by Berman (1975) as speed-dependent Voigt profiles. For power-law potentials it is possible to do an evaluation of the speed-dependent width and shift. The results are those given by Eqs. (271) and (272), but must be averaged over a shifted Maxwellian, a calculation that is done numerically. In Fig. 34 we show two results from the paper of Ward, Cooper, and Smith (1974) that illustrate how the speed-dependent profiles depart from Voigt behavior. The critical parameter is the ratio of perturber to emitter mass, and when this value is large the Doppler Gaussian component disappears completely, resulting in a Doppler narrowing of the line at the appropriate pressure.

For a perturber-emitter mass ratio of 1.0, the reduc-

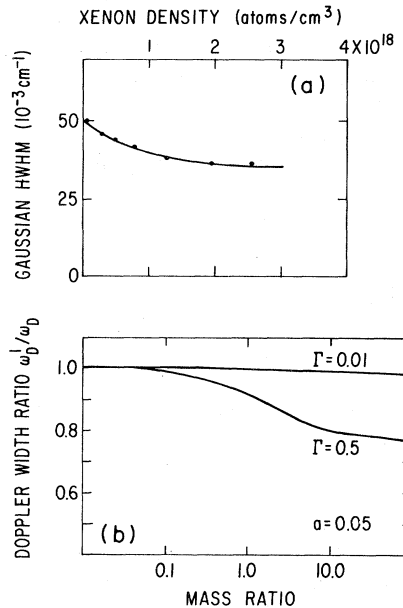


FIG. 34. (a) An observation of the apparent reduction of the Gaussian linewidth with increasing xenon density in the broadening of the lithium ($2s-2p$) transition reported by McCartan and Lwin (1977). (b) The predicted Doppler width dependence as a function of collisional linewidth Γ (for a Voigt parameter $a = 0.05$) calculated by Ward, Cooper, and Smith (1974). When the perturber is more massive than the emitter, the apparent Doppler width decreases with increasing collision broadening.

tion of the Gaussian component of a Voigt analysis is about 10% in the region beyond the half-width of the line; given typical measurement errors of the same order, this is not a very large effect. The phenomenon has been observed in lithium perturbed by xenon by McCartan and Lwin (1977). They recorded the ${}^7\text{Li}$ resonance line for a temperature of the order of 600 K and gas densities less than 3×10^{18} atoms cm^{-3} . Under these conditions they could resolve the fine structure of the line and fit the profile with a Voigt function. When helium was used as the perturbing gas they found an excellent fit, but when xenon was used the Gaussian component deduced from the fitting was dependent on pressure, decreasing with increasing pressure exactly as predicted.

In addition to these effects there should also be an asymmetry of the line that comes about because, in the Maxwellian average of the profile, the line shift is velocity dependent. The asymmetry will be small and will correlate with the size of the shift. While asymmetries have been observed in collision-broadened lines (Sec. III.D.1.b), they have been attributed to the intrinsic asymmetry of the impact line core, rather than to this smaller velocity effect.

D. Line cores

Many experimental results are inconsistent even with the linear dependence of half-width on density obtained

by the phase-shift approximation. This discrepancy seems to be more prominent at higher densities, where multiple interactions may dominate binary ones.

—Ch'en and Takeo, 1957

For the purposes of summarizing and discussing the body of recent experimental results, we divide available measurements into two broad categories: line cores, the region near the maximum in the line intensity, and line wings, the regions removed from this maximum. Although this division is somewhat artificial, it does allow us to separate wing observations, conventionally interpreted with unified line-shape theories and with the statistical theory, from low-pressure line-center measurements that are interpreted with the impact theory. But we also include in this category of line cores the line-center observations at high density that obviously cannot be interpreted with impact theories, and recent determinations of deviations of low-pressure profiles from the expected Lorentzian form.

1. Observations for low foreign-gas density

a. Shift and width

This general subject is summarized in Lewis' review of impact broadening (Lewis, 1980). In Table V we list the measurements of line half-widths and shifts known to us without restriction on the combination of radiating atom and foreign gas. The data given are selected from literature searches based on Lewis (1980) and on Fuhr, Wiese, and Roszman (1972, 1973, 1975, and 1978) and recent abstracting journals. For compactness, some restrictions have been made, however. Only data for states with effective principal quantum numbers less than five are included; only data of high photometric precision are included, that is, no photographic measurements are listed; only measurements for which instrumental effects and other possible sources of broadening have been subtracted are given. The table differs from Table 6.2 of Lewis (1980) in that it includes transitions other than the resonance lines, and perturbers other than noble gases, and that it does not include calculated values.

With few exceptions the data presented are for alkali and alkaline-earth transitions to the first few excited states perturbed by noble gases. Only very few values are known for transitions other than the resonance lines. Values for line broadening due to relatively inert molecular gases such as N₂ and CO₂, and for the astrophysically crucial atomic H and H₂ are rare. Almost all experiments are restricted to temperatures less than 1000 K for the reasons discussed in Sec. III.A.

b. Observations of line asymmetries at low density

As we have seen in Secs. II.B and II.F.5, predictions of an asymmetrizing dispersion component in the impact line core can be made on the basis of simple arguments about the correlation function, and must appear when

the duration of atomic collisions is allowed for. Quantitative methods of calculation have been presented by Kielkopf (1976a) and by Szudy and Baylis (1977).

The first indication that such effects were experimentally observable was seen by McCartan (1972) in the absorption and emission spectra of the potassium 4s-4p doublet perturbed by argon and krypton. He reported that the red wing was more intense than it should be if the line core were a symmetric Lorentzian. Qualitative estimates of the asymmetry in broadening of calcium and cesium lines were given by Smith (1972, 1975), but the exact shape of the asymmetry was not determined because it was such a small effect (an increase in intensity of a few percent over the Lorentzian extrapolation) and was influenced by instrumental asymmetries as well.

A quantitative determination of the nature and magnitude of these effects is dependent on fitting the observed profiles with the expected form, and searching for evidence that the inclusion of a dispersion-type asymmetry reduces χ^2 in the fit to the data. This has now been done for the cesium 6s-7p and 6s-8p transitions perturbed by xenon (Kielkopf and Allard, 1980) and the sodium 3s-3p transitions perturbed by He, Ne, Ar, Kr, and Xe (Kielkopf, 1980; Walkup, Spielfiedel, and Pritchard, 1980). The most precise determination of the asymmetry yet is the laser-fluorescence measurement by Walkup *et al.*, for which there are no significant instrumental corrections, and for which estimated errors are less than 10%. A tabulation for the Na D lines is given in Table VI.

Clearly impact-broadened lines are asymmetric, and the amount of asymmetry depends in some detail on the interatomic potential. Asymmetries calculated with the methods of Szudy and Baylis (1977) and Kielkopf (1976a) are in agreement with each other and with the observations for sodium (Walkup, Spielfiedel, and Pritchard, 1980).

c. High series members

Until, recently, the broadening of high Rydberg states has been measured under conditions of such high density (Sec. III.D.3) that the effect of overlapping multiple collisions of the excited atom and perturbers is significant. This occurs because of the extremely large size of such excited atoms, as noted in Sec. II.F.7. These conditions raise questions about the validity of line-broadening theories intended, for instance, to explain impact broadening of the resonance lines.

We have seen that recent Doppler-free laser experiments by Stoicheff and Weinberger (1980), Flusberg *et al.* (1979), and Brillet and Gallagher (1980) are yielding data for highly excited states at low gas density (see Figs. 31 and 32). The ionization or photon echo detection schemes involve processes in addition to the interaction of radiation and collisionally perturbed atoms, although Stoicheff's ionization detection does provide a direct measure of line profile and shift. Low-density data represents only a small part of the overall behavior

TABLE V. Observations of line cores at low densities.

Transition	Perturber	Half-width γ/n (10^{-20} cm $^{-1}$ /cm $^{-3}$)	Shift σ/n	Temperature (K)	Reference
H ($2p-3d$)	He	2.4 ± 0.5	0.12 ± 0.05	800	Kielkopf (1975b)
	Ne	2.9 ± 0.6	-0.07 ± 0.50	800	
	Ar	5.6 ± 1.1	-2.70 ± 0.80	800	
Li ($2s-2p$)	He	1.1 ± 0.6	-0.08 ± 0.04	400	Gallagher (1975)
		0.92 ± 0.05	0.00 ± 0.002	520	Smith and Collins (1976)
		1.01	0.03	600	Lwin <i>et al.</i> (1977)
	Ne	0.76 ± 0.04	-0.30 ± 0.06	400	Gallagher (1975)
		0.80	-0.10	600	Lwin <i>et al.</i> (1977)
	Ar	1.19 ± 0.62	-0.72 ± 0.08	400	Gallagher (1975)
		1.10	-0.38	600	Lwin <i>et al.</i> (1977)
	Kr	1.47 ± 0.08	-0.82 ± 0.08	400	Gallagher (1975)
		1.45	-0.35	600	Lwin <i>et al.</i> (1977)
	Xe	1.66 ± 0.08	-1.06 ± 0.12	400	Gallagher (1975)
		1.65	-0.36	600	Lwin <i>et al.</i> (1977)
Na ($3s\ ^2S_{1/2}-3p\ ^2P_{1/2}$)	He	0.81 ± 0.05	0.00 ± 0.03	450	Deleage <i>et al.</i> (1973)
		1.01 ± 0.05	0.00 ± 0.03	475	McCartan and Farr (1976)
		0.94 ± 0.02		450	Chatham <i>et al.</i> (1980)
		1.02 ± 0.01	0.16 ± 0.05	450	Kielkopf (1980)
	Ne	0.60 ± 0.05	-0.33 ± 0.02	475	McCartan and Farr (1976)
		0.74 ± 0.01		450	Chatham <i>et al.</i> (1980)
		0.506 ± 0.013	-0.267 ± 0.023	450	Kielkopf (1980)
	Ar	1.47 ± 0.10	-0.75 ± 0.02	475	McCartan and Farr (1976)
		1.47 ± 0.01		450	Chatham <i>et al.</i> (1980)
		1.29 ± 0.01	-0.603 ± 0.040	450	Kielkopf (1980)
	Kr	1.28 ± 0.02		450	Chatham <i>et al.</i> (1980)
		1.44 ± 0.04	-0.625 ± 0.031	450	Kielkopf (1980)
	Xe	1.40 ± 0.11	-0.585 ± 0.04	475	McCartan and Farr (1976)
		1.55 ± 0.03		450	Chatham <i>et al.</i> (1980)
		1.58 ± 0.07	-0.542 ± 0.036	450	Kielkopf (1980)
Na ($3s\ ^2S_{1/2}-3p\ ^2P_{3/2}$)	H	4.41		8100	Baird <i>et al.</i> (1979)
		4.69		9800	Baird <i>et al.</i> (1979)
	He	8.3		4000	Burgess and Grindlay (1970)
		0.859 ± 0.027	0.0 ± 0.027	450	Deleage <i>et al.</i> (1973)
		1.16 ± 0.10	-0.037 ± 0.035	475	McCartan and Farr (1976)
		1.30 ± 0.52		7500	Baur and Cooper (1977)
		2.22		5000	Baird <i>et al.</i> (1979)
		5.50		10400	Baird <i>et al.</i> (1979)
		1.14 ± 0.01		450	Chatham <i>et al.</i> (1980)
		1.06 ± 0.02	0.059 ± 0.045	450	Kielkopf (1980)
	Ne	0.765 ± 0.05	-0.34 ± 0.015	475	McCartan and Farr (1976)
		3.05		9100	Baird <i>et al.</i> (1979)
		2.53		10500	Baird <i>et al.</i> (1979)
		0.671 ± 0.016		450	Chatham <i>et al.</i> (1980)
Na ($3s-4d$)	Ar	0.565 ± 0.092	-0.376 ± 0.023	450	Kielkopf (1980)
		1.20 ± 0.1	-0.805 ± 0.04	475	McCartan and Farr (1976)
		1.12 ± 0.03		450	Chatham <i>et al.</i> (1980)
		1.18 ± 0.03	-0.698 ± 0.064	450	Kielkopf (1980)
	Kr	1.25 ± 0.03		450	Chatham <i>et al.</i> (1980)
		1.33 ± 0.02	-0.698 ± 0.018	450	Kielkopf (1980)
	Xe	1.23 ± 0.12	-0.746 ± 0.04	475	McCartan and Farr (1976)
Na ($3s-5s$)		1.31 ± 0.03		450	Chatham <i>et al.</i> (1980)
		1.52 ± 0.05	-0.604 ± 0.019	450	Kielkopf (1980)
	He	4.08 ± 0.48	0.90 ± 0.2	563	Biraben <i>et al.</i> (1977)
	Ne	2.3 ± 0.16	-0.64 ± 0.11	563	Biraben <i>et al.</i> (1977)
	Ar	5.1 ± 0.53	-3.1 ± 0.42	563	Biraben <i>et al.</i> (1977)
Na ($3s-5s$)	Kr	5.0 ± 0.69	-2.7 ± 0.16	563	Biraben <i>et al.</i> (1977)
	Xe	5.1 ± 0.42	-3.2 ± 0.16	563	Biraben <i>et al.</i> (1977)
	He	7.27 ± 0.32	3.3 ± 0.48	563	Biraben <i>et al.</i> (1977)
	Ne	2.8 ± 0.21	1.3 ± 0.21	563	Biraben <i>et al.</i> (1977)

TABLE V. (Continued.)

Transition	Perturber	Half-width		Shift σ/n (10^{-20} cm $^{-1}$ /cm $^{-3}$)	Temperature (K)	Reference
		γ/n	(10 $^{-20}$ cm $^{-1}$)			
Na ($3p\ ^2P_{1/2}$ - $4d\ ^2D_{3/2}$)	Ar	5.73	± 0.42	-3.6 ± 0.32	563	Biraben <i>et al.</i> (1977)
	Kr	5.1	± 0.37	-2.6 ± 0.37	563	Biraben <i>et al.</i> (1977)
	Xe	5.73	± 0.58	-3.1 ± 0.21	563	Biraben <i>et al.</i> (1977)
	He	3.6	± 0.2	0.4 ± 0.3	500	Kielkopf and Knollenberg (1975)
	Ne	1.9	± 0.2	-1.8 ± 0.2	500	Kielkopf and Knollenberg (1975)
	Ar	4.3	± 0.3	-2.6 ± 0.3	500	Kielkopf and Knollenberg (1975)
Si ($4s\ ^3P_1$ - $3p\ ^1S_0$)	Kr	4.6	± 0.5	-3.0 ± 0.4	500	Kielkopf and Knollenberg (1975)
	Xe	6.1	± 0.6	-3.8 ± 0.3	500	Kielkopf and Knollenberg (1975)
	Ar	3.33	± 0.35	-3.56 ± 0.95	6000	Evans and Cooper (1972)
	Si ($5p\ ^1D_2$ - $4s\ ^1P_1$)	Ar	6.65	± 1.78	6000	Evans and Cooper (1972)
	K ($4s\ ^2S_{1/2}$ - $4p\ ^2P_{1/2}$)	He	0.822	± 0.016	410	Lwin and McCartan (1978)
	Ne	0.45	± 0.01	-0.22 ± 0.01	410	Lwin and McCartan (1978)
K ($4s\ ^2S_{1/2}$ - $4p\ ^2P_{3/2}$)	Ar	1.30	± 0.02	-1.23 ± 0.03	410	Lwin and McCartan (1978)
	Kr	1.23	± 0.03	-0.875 ± 0.546	410	Lwin and McCartan (1978)
	Xe	1.47	± 0.02	-0.950 ± 0.032	410	Lwin and McCartan (1978)
	N ₂	1.30	± 0.02	-0.971 ± 0.021	410	Lwin and McCartan (1978)
	He	1.09	± 0.02	0.13 ± 0.02	410	Lwin and McCartan (1978)
	Ne	0.615	± 0.01	-0.33 ± 0.01	410	Lwin and McCartan (1978)
K ($4s\ ^2S_{1/2}$ - $5p\ ^2P_{1/2}$)	Ar	1.05	± 0.02	-0.806 ± 0.021	410	Lwin and McCartan (1978)
	Kr	1.23	± 0.03	-0.615 ± 0.021	410	Lwin and McCartan (1978)
	Xe	1.46	± 0.02	-0.950 ± 0.032	410	Lwin and McCartan (1978)
	N ₂	1.30	± 0.02	-0.700 ± 0.021	410	Lwin and McCartan (1978)
	He	1.91	± 0.21	0.74 ± 0.27	450	Spielfiedel <i>et al.</i> (1979)
	Ne	0.80	± 0.27	0.0 ± 0.5	450	Spielfiedel <i>et al.</i> (1979)
K ($4s\ ^2S_{1/2}$ - $5p\ ^2P_{3/2}$)	Ar	3.61	± 0.32	-2.0 ± 0.05	450	Spielfiedel <i>et al.</i> (1979)
	Kr	3.3	± 0.1	-1.97 ± 0.05	474	McCartan and Hindmarsh (1969)
	Xe	3.3	± 0.3		450	Spielfiedel <i>et al.</i> (1979)
	He	2.7	± 0.3	1.06 ± 0.27	450	Spielfiedel <i>et al.</i> (1979)
	Ne	1.3	± 0.1	0.0 ± 0.5	450	Spielfiedel <i>et al.</i> (1979)
	Ar	3.2	± 0.3	-2.4 ± 0.1	450	Spielfiedel <i>et al.</i> (1979)
K ($4p\ ^2P_{1/2}$ - $7s\ ^2S_{1/2}$)	Xe	3.7	± 0.3		450	Spielfiedel <i>et al.</i> (1979)
	He	11.9	± 0.4	9.7 ± 1.4	450	Kielkopf and Knollenberg (1981)
	Ar	9.0	± 1.0	-6.4 ± 0.1	450	Kielkopf and Knollenberg (1981)
	He	11.1	± 0.7	10.5 ± 0.5	450	Kielkopf and Knollenberg (1981)
		9.1	± 0.7	-6.4 ± 0.1	450	Kielkopf and Knollenberg (1981)
	Ar	9.5	± 0.35	-7.4 ± 0.28	478	Kreye (1982)
		11.1	± 0.41	-8.4 ± 0.34	760	Kreye (1982)
Ca ($4s^2\ ^1S_0$ - $4s\ ^4p\ ^1P_1$)	He	1.25	± 0.03	-0.080 ± 0.004	735	Smith (1972)
	Ne	1.18	± 0.03	-0.083 ± 0.009	665	Bowman and Lewis (1978)
	Ar	0.69	± 0.03	-0.366 ± 0.002	735	Smith (1972)
	Ar	1.85	± 0.20	-0.903 ± 0.006	735	Smith (1972)
		0.940	± 0.025	-0.44 ± 0.2	640	Bowman and Lewis (1978)
	Kr	1.98	± 0.1		410	Myint <i>et al.</i> (1979)
		1.45	± 1.2	-0.836 ± 0.009	735	Smith (1972)
Ca ($4s\ ^4p\ ^3P_1$ - $4s\ ^5S\ ^3S_1$)	Xe	1.62	± 0.15	-0.958 ± 0.008	735	Smith (1972)
	He	3.74	± 0.11	1.1 ± 0.2	2080	O'Neill and Smith (1980a)
Ca ($4s\ ^4p\ ^3P_1$ - $4s\ ^5S\ ^3S_1$)	Ne	1.6	± 0.2	-0.15 ± 0.16	2300	O'Neill and Smith (1980a)
	Ar	3.58	± 0.21	-2.1 ± 0.2	2700	O'Neill and Smith (1980a)
Ca ($4s\ ^4p\ ^3P_1$ - $4s\ ^5S\ ^3S_1$)	He	3.74	± 0.11	1.1 ± 0.2	1970	O'Neill and Smith (1980a)
	Ne	1.60	± 0.11	-0.24 ± 0.16	2210	O'Neill and Smith (1980a)
Ca ($4s\ ^4p\ ^3P_1$ - $4s\ ^5S\ ^3S_1$)	Ar	3.31	± 0.11	-2.1 ± 0.16	2530	O'Neill and Smith (1980a)
	He	3.71	± 0.11	1.1 ± 0.16	1970	O'Neill and Smith (1980a)
Ca ($4s\ ^4p\ ^3P_1$ - $4s\ ^5S\ ^3S_1$)	Ne	1.70	± 0.11	-0.34 ± 0.16	2180	O'Neill and Smith (1980a)
	Ar	3.13	± 0.11	-2.2 ± 0.16	2460	O'Neill and Smith (1980a)
Ca ($3d\ ^4s\ ^3D$ - $3d\ ^4p\ ^3F$)	He	1.66	$\pm 0.08^a$		2500	Smith and Raggett (1981)
Ca ($3d\ ^4s\ ^3D$ - $3d\ ^4p\ ^3D)$		1.87	$\pm 0.09^a$			
Ca ($3d\ ^4s\ ^3D_1$ - $3d\ ^4p\ ^1D_2$)		1.88	± 0.09			
Ca ($3d\ ^4s\ ^1D_2$ - $3d\ ^4p\ ^1D_2$)		1.70	± 0.08			
Ca ($3d\ ^4s\ ^1D_2$ - $3d\ ^4p\ ^3P_1$)		3.18	± 0.16			

TABLE V. (Continued.)

Transition	Perturber	Half-width γ/n (10^{-20} cm $^{-1}$ /cm $^{-3}$)	Shift σ/n	Temperature (K)	Reference
Ca ($3d4s^3D_3$ - $4s5p^3P_2$)		4.67 ± 0.21			
Ca ($3d4s^1D_2$ - $4s5p^1P_1$)		4.27 ± 0.11			
Ca ($3d4s^1D_2$ - $3d4p^1P_1$)		6.79 ± 0.34			
Ca ($3d4s^1D_2$ - $4s6p^1P_1$)		7.61 ± 0.40			
Ca ($3d4s^1D_2$ - $4s4f^1F_3$)		5.73 ± 0.24			
Ca ($4s4p^1P_1$ - $4p^21D_2$)		4.14 ± 0.21			
Ca ($4s4p^1P_1$ - $4s5d^1D_2$)		8.51 ± 0.40			
Ca II ($4s^2S_{1/2}$ - $4p^2P_{1/2}$)	He	1.40 ± 0.38		7466	Baur and Cooper (1977)
		0.55 ± 0.03	-0.19 ± 0.06	655	Bowman and Lewis (1978)
	Ar	0.78 ± 0.02	-0.11 ± 0.02	765	Bowman and Lewis (1978)
Ca II ($4s^2S_{1/2}$ - $4p^2P_{3/2}$)	He	0.78 ± 0.08	-0.06 ± 0.06	655	Bowman and Lewis (1978)
	Ar	0.81 ± 0.04	-0.59 ± 0.02	765	Bowman and Lewis (1978)
Ca II ($3d^2D_{3/2}$ - $4p^2P_{1/2}$)	He	0.42 ± 0.05		655	Bowman and Lewis (1978)
	Ar	0.75 ± 0.03		765	Bowman and Lewis (1978)
Ca II ($3d^2D_{5/2}$ - $4p^2P_{3/2}$)	He	0.68 ± 0.05		655	Bowman and Lewis (1978)
	Ar	0.77 ± 0.04		765	Bowman and Lewis (1978)
Fe (a^5D_2 - z^7D_3)	He	1.04		2534	O'Neill and Smith (1980b)
Fe (a^5D_4 - z^7F_5)	He	1.69 ± 0.25		573	Copley and Camm (1973)
Fe (a^5D_2 - z^7F_3)	He	1.15		2060	O'Neill and Smith (1980b)
Fe (a^5D_3 - z^5D_3)	He	0.806		1631	
Fe (a^5D_2 - z^5D_3)	He	0.838		1677	
Fe (a^5D_1 - z^5D_1)	He	1.17		1882	
Fe (a^5F - z^5D)	He	0.976 ^a		2072	
Fe (a^5D_4 - z^5F_5)	He	1.80 ± 0.27		573	Copley and Camm (1973)
		1.38 ± 0.21	2.6 ± 0.6	4000	Driver and Lombardi (1977)
		0.93		1466	O'Neill and Smith (1980b)
Fe (a^5D_3 - z^5P_3)	He	1.11		1659	
Fe (a^5D_2 - z^5F_3)	He	1.08		1755	
Fe (a^5D_3 - z^5F_3)	He	1.02		1669	
Fe (a^5D_2 - z^5F_3)	He	1.00		1575	
Fe (a^5D_1 - z^5F_1)	He	1.03		1716	
Fe (a^5D_1 - z^5P_1)	He	1.16		1707	
Fe (a^5D_2 - z^7P_3)	He	1.17		2379	
Fe (a^5D_2 - z^3D_3)	He	1.11		2120	
Fe (a^5D_2 - z^3D_2)	He	1.31		2431	
Fe (a^5D_2 - z^3F_3)	He	1.12		1990	
Fe (a^5D_2 - z^3F_2)	He	1.16		2123	
Fe (a^5D_2 - z^3P_2)	He	1.24		1743	
Fe (a^5F_4 - y^5F_4)	He	1.99 ± 0.29		573	Copley and Camm (1973)
Fe (a^5F - y^5D)	He	1.14 ^a		2042	O'Neill and Smith (1980b)
Fe (z^7F_6 - e^7D_5)	He	2.80 ± 0.56		573	Copley and Camm (1973)
Fe (a^3F_4 - z^5G_5)	He	1.88 ± 0.28		573	
Kr ($4p^5(^2P_{3/2})5s[3/2]_2$ - $4p^5(^2P_{3/2})5p[3/2]_2$)	He	0.690	0.108	80	Vaughan and Smith (1968)
		1.29	0.283	295	
	Ne	0.342	-0.227	80	
		0.770	-0.211	295	
	Ar	0.590	-0.321	80	
		1.22	-0.735	295	
	Kr	0.652	-0.445	80	
		0.963	-0.652	295	
Kr ($4p^5(^2P_{3/2})5s[3/2]_1$ - $4p^5(^2P_{3/2})5p[1/2]_0$)	He	0.720	0.141	80	
		1.37	0.350	295	
	Ne	0.368	-0.237	80	
		0.600	-0.226	295	
	Ar	0.623	-0.321	80	
		1.33	-0.755	295	
	Kr	6.40	0.200	90	
		6.55	0.200	90	
Rb ($5s^2S_{1/2}$ - $5p^2P_{1/2}$)	He	1.02 ± 0.19		320	Ottinger <i>et al.</i> (1975)

TABLE V. (Continued.)

Transition	Perturber	Half-width	Shift	Temperature	Reference
		γ/n (10^{-20} cm $^{-1}/\text{cm}^{-3}$)	σ/n	(K)	
Rb ($5s^2S_{1/2}-5p^2P_{3/2}$)	Ne	0.52 ± 0.07	-0.041 ± 0.037	320	
	Ar	1.00 ± 0.13	-0.78 ± 0.07	320	
	Kr	1.00 ± 0.09	-0.800 ± 0.056	320	
	Xe	1.15 ± 0.13	-0.836 ± 0.074	320	
	He	1.02 ± 0.19	-0.082 ± 0.037	320	
	Ne	0.54 ± 0.09	-0.22 ± 0.037	320	
	Ar	1.02 ± 0.13	-0.89 ± 0.13	320	
	Kr	0.89 ± 0.07	-0.89 ± 0.06	320	
Sr ($5s^1S_0-5p^1P_1$)	Xe	1.17	-1.00 ± 0.07	320	
	He	1.31 ± 0.03	0.0 ± 0.03	700	Farr and Hindmarsh (1971)
	Ar	1.30 ± 0.03	-0.76 ± 0.03	680	
	He	0.498 ± 0.034	-0.043 ± 0.020	573	Schuessler <i>et al.</i> (1981)
Cd ($5s^21S_0-5s5p^3P_1$)	Ar	0.405 ± 0.067	-0.367 ± 0.157	573	
	He	0.98 ± 0.07	0.67 ± 0.10	295	Bernabeu and Alvarez (1980)
	Ne	0.51 ± 0.04	-0.29 ± 0.01		
	Ar	1.00 ± 0.11	-0.89 ± 0.04		
	Kr	1.01 ± 0.12	-0.27 ± 0.01		
	Xe	1.09 ± 0.13	-0.84 ± 0.11		
	H ₂	2.05 ± 0.32	0.23 ± 0.02		
	N ₂	1.55 ± 0.29	-0.74 ± 0.01		
Cs ($6s^2S_{1/2}-6p^2P_{3/2}$)	He	1.36 ± 0.09	0.39 ± 0.17		
	Ne	0.53 ± 0.11	-0.43 ± 0.03		
	Ar	1.16 ± 0.01	-0.75 ± 0.03		
	Kr	0.55 ± 0.05	-0.81 ± 0.11		
	Xe	2.93 ± 0.31	-0.91 ± 0.08		
	H ₂	2.37 ± 0.41	0.18 ± 0.03		
	N ₂	1.97 ± 0.49	-0.73 ± 0.02		
	He	4.1 ± 1.1		400	Evdokimov (1968)
Cs ($6s^2S_{1/2}-7p^2P_{1/2}$)		4.4 ± 0.25	1.5 ± 0.1	400	Rostas Lemaire (1971)
	Ne	1.75 ± 0.10	0.0 ± 0.03	395	Smith (1975)
		4.1 ± 0.8		4500	Evans and Cooper (1972)
	Ar	4.3 ± 0.6		400	Evdokimov (1968)
		3.35 ± 0.25	-1.63 ± 0.05	400	Rostas and Lemaire (1971)
		4.74 ± 1.04		4500	Evans and Cooper (1972)
		3.42 ± 0.15	-1.29 ± 0.04	395	Smith (1975)
	Xe	3.14 ± 0.20	-1.66 ± 0.05	395	Smith (1975)
Cs ($6s^2S_{1/2}-7p^2P_{3/2}$)		2.80 ± 0.10	-1.48 ± 0.05	380	Kielkopf and Allard (1980)
	He	2.97 ± 0.37		400	Evdokimov (1968)
		3.45 ± 0.20	0.73 ± 0.05	400	Rostas and Lemaire (1971)
	Ne	1.62 ± 0.10	-0.56 ± 0.07	380	Smith (1975)
	Ar	3.3 ± 0.37		400	Evdokimov (1968)
		2.8 ± 0.35		363	Ch'en <i>et al.</i> (1969)
		2.9 ± 0.15	-1.55 ± 0.06	400	Rostas and Lemaire (1971)
		3.18 ± 0.15	-1.46 ± 0.06	380	Smith (1975)
Cs ($6s^2S_{1/2}-8p^2P_{1/2}$)	Xe	2.60 ± 0.05	-1.67 ± 0.07	380	Kielkopf and Allard (1980)
	H ₂	33 ± 3		623	Ferry <i>et al.</i> (1981)
	Xe	5.43 ± 0.61	-1.80 ± 0.30	450	
	Xe	5.41 ± 0.40	-2.56 ± 0.28	450	
	He	0.408 ± 0.015	0.045 ± 0.002		Butaux and Lennuier (1965)
	Ne	0.260 ± 0.015	-0.078 ± 0.004		
	H ₂	0.836 ± 0.019	-0.149 ± 0.006		
	He	0.632 ± 0.074	-0.078 ± 0.022	280	Bosquet and Bras (1977)
Hg ($6s^21S_0-6s6p^1P_1$)	Ne	0.465 ± 0.056	-0.342 ± 0.048	280	
	Ar	0.669 ± 0.074	-0.416 ± 0.056	280	
	Kr	0.669 ± 0.084	-0.416 ± 0.048	280	
	Xe	0.654 ± 0.056	-0.413 ± 0.045	280	
	He	1.69 ± 0.11	0.242 ± 0.056	743	Cheron <i>et al.</i> (1977)
	Ne	0.743 ± 0.074	-0.316 ± 0.074	743	
	Ar	1.56 ± 0.11	-1.00 ± 0.07	743	
Tl ($6s^26p^2P_{3/2}-6s7s^2S_{1/2}$)					

TABLE V. (Continued.)

Transition	Perturber	Half-width γ/n (10^{-20} cm $^{-1}/\text{cm}^{-3}$)	Shift σ/n	Temperature (K)	Reference
Tl ($6s^2 6p \ ^2P_{1/2}-6s \ ^2S_{1/2}$)	Kr	1.34 ± 0.07	-0.93 ± 0.07	743	
	Xe	1.34 ± 0.04	-1.04 ± 0.07	743	
	He	1.97 ± 0.19	0.48 ± 0.11	720	
	Ne	0.82 ± 0.09	-0.26 ± 0.07	720	
	Ar	1.88 ± 0.11	-1.00 ± 0.15	720	
	Kr	1.69 ± 0.13	-0.85 ± 0.19	720	
	Xe	1.82 ± 0.19	-1.00 ± 0.19	720	

^aAverage for the multiplet. Consult the reference for a full list of lines.

pattern that is to be investigated, and most of the extant information dates from the work of Füchtbauer and co-workers (Füchtbauer and Gössler, 1935; Füchtbauer and Reimers, 1935; Füchtbauer and Schulz, 1935) and Amaldi and Segre (1934a, 1934b), which was done at high density, i.e., where pressure broadening is much greater than Doppler broadening. For a discussion of these and related results, see Sec. III.D.3.

Table VII summarizes measurements now available of the broadening of transitions to excited states with an effective principal quantum number greater than 5. These measurements were made under conditions of sufficiently low density to insure the dominance of single encounters in the determination of the line profile. In no case have actual profiles been reported. Only derived parameters such as shift and broadening cross sections are given in the literature.

2. High-density measurements of line cores

a. Low-lying states

For observations of transitions to the first two excited p states of cesium and rubidium, data on shift, width, and asymmetry have been reported by Ch'en, Granier, and co-workers, as indicated in Table VIII. The width and asymmetry measurements of Ch'en are photoelectric, but all other measurements are photographic. Densities of up to 40 atm were used for some experiments. All of

TABLE VI. Asymmetry of the sodium D lines at atmospheric pressure.^a

	$3s \ ^2S_{1/2}-3p \ ^2P_{1/2}$ D 1	$3s \ ^2S_{1/2}-3p \ ^2P_{3/2}$ D 2
He	1.002	1.01
Ne	1.01	1.02
Ar	1.11	1.12
Kr	1.12	1.14
Xe	1.16	1.20

^aGiven here is the ratio of half-width on the low-frequency side to half-width on the high-frequency side, computed from the data of Walkup, Spielfiedel, and Pritchard (1980) and of Kielkopf (1980). The deviation from unity is proportional to gas density.

the data refer to high-pressure absorption measurements for temperatures typically around 500 K. Normalized core profiles have not been reported for densities above one atmosphere, with the exception of the cesium resonance doublet perturbed by xenon, for which limited data appear in Gilbert and Ch'en (1969) and in Gilbert, Allard, and Ch'en (1980).

Shift and width curves for the broadening of the cesium $6s-6p$ transition by neon and by xenon are shown in Fig. 35. Most of the qualitative features of these curves were presented in the paper of Gilbert, Allard, and Ch'en (1980) and explained by Allard and Biraud (1980) using the Anderson-Talman theory and a square-well potential. These characteristics were discussed at length in Sec. II.E.2c. Royer (1980) has been able to fit the shift and width curves with a parametrized correlation function, and has deduced the appearance of perturber-perturber correlations in the high-density data. The $6s-7p$ cesium observations for densities of the order of one atmosphere of xenon appear to be explained by unified-theory calculations based on potentials determined by fitting to low-density observations of the core and near wings. Nevertheless, complete calculations of the entire profile from core to far wing that include high-density shifts and widths are lacking (Kielkopf and Allard, 1980).

The most striking features in the curves are caused by extrema in the interatomic difference potentials. These produce resolvable shoulders or satellites on the lines at low density. At higher densities, as the satellites grow in strength to intensities comparable to the low-pressure line core, the new line profile shifts suddenly to the satellite peak. This behavior causes sudden dramatic changes in the width and shift, as illustrated for xenon in Fig. 35(a). The experimental behavior with neon is not so striking, presumably because the difference potentials for the transition are less extreme, and the satellites are unresolved even at low density. The shift with neon is puzzling, because for the $^2P_{1/2}$ component it is first to the red for densities less than about 24 atm, but for higher densities it is to the blue. This would also indicate unresolved red and violet satellites on the line if the interpretations applied to xenon are universal. Unified-theory calculations for these cases, with good theoretical potentials, would be very useful in the interpretation of these results.

TABLE VII. Low-density observations of high series members.^a

States	Width	Shift	Gases	Reference
Na $3p-6d$		×	He, Ne, Ar, Kr, Xe	Kielkopf and Knollenberg (1975)
3s-7s to 20s			He, Ne, Ar, Kr, Xe,	Flusberg <i>et al.</i> (1979)
3s-6d to 34d	×		CO, N ₂	
K			K	Mazing and Serapinas (1971)
Rb $5s-11s$ to $60s$	×	×	Rb	Weber and Niemax (1979b)
Rb $5s-10s$ to $50s$	×		Rb	Stoicheff and Weinberger (1980)
$5s-10d$ to $50d$	×			
$5s-15s$ to $34s$	×	×	He, Ne, Ar, Kr, Xe	Brillet and Gallagher (1980)
$5s-19d$	×	×	He, Ne, Ar, Kr, Xe	
Cs			Ar	Mazing and Vrublevskaya (1966)
Cs			Cs	Mazing and Serapinas (1971)
Cs $6s-11d$ to $40d$	×	×	Cs	Weber and Niemax (1979a)
Cs $6s-9p$ to $20p$		×	Ne	Garrett, Ch'en, and Looi (1967)
$6s-9p$		×	Ar	Tan and Ch'en (1970)
$6s-9p$ to $10p$		×	Kr	Ch'en, Looi, and Garrett (1967)
$6s-9p$ to $11p$		×	Xe	Ch'en, Gilbert, and Tan (1969)

^aOnly data with observations at pressures much less than one atmosphere ($2.7 \times 10^{19} \text{ cm}^{-3}$) for states with $n^* > 5$ are included.

TABLE VIII. High-density observations of line cores.

States	Width	Shift	Gases	Maximum density	References
				(rd)	
H $2p-3d$	×	×	He	63	Sidell and Ch'en (1977)
			Ar	61	
H $2p-4d$	×	×	He	63	
Li $2s-2p$	×	×	Ar	75	Ch'en and Henry (1973)
Li $2p-3d$	×	×	Ar	75	
Al $2p \ ^2P_{1/2}-3d \ ^2D_{3/2}$	×		Ar	50	Holmes <i>et al.</i> (1969b)
Al $2p \ ^2P_{1/2}-4s \ ^2S_{1/2}$	×		Ar	50	
Na $3s-3p$			Ar	100	
	×	×	Kr	11	West and Gallagher (1978)
	×	×	Xe	11	
Ca II $4s \ ^2S_{1/2}-4p \ ^2P_{1/2}$	×		He	120	Ch'en and Henry (1973)
			Ar	75	
Ca $4s \ ^1S_0-4s \ ^1P_1$	×		Ar	100	
Cr $a \ ^5S_2-y \ ^5P_J$	×		He	100	Holmes <i>et al.</i> (1969a)
Cr $a \ ^7S_3-z \ ^7P_J$	×		He	100	
			Ar	100	
Cr $a \ ^7S_3-y \ ^7P_J$	×		Ar	100	
Mn $a \ ^6S_{5/2}-z \ ^6P_J$	×		He	10	Ch'en and Bennett (1960)
	×	×	Ar	30	
			Ar	75	Holmes <i>et al.</i> (1969b)
Fe (see footnote a)	×		He	102	Holmes, Ch'en, and Takeo (1969)
			Ar	108	
Ni $a \ ^1D_2-z \ ^1P_1$	×		Ar	100	Holmes <i>et al.</i> (1969a)
Ni $a \ ^3F_2-y \ ^3F_2$	×		Ar	100	
Cu $4s \ ^2S_{1/2}-4p \ ^2P_J$	×		Ar	100	Holmes <i>et al.</i> (1969b)
Rb $5s \ ^2S_{1/2}-5p \ ^2P_J$	×		Ne	40	Granier, Granier, and Vodar (1966)
			Ne	35	Granier and Granier (1966c)
	×	×	Ar	60	Granier, Granier, and DeCroutte (1963b)
	×	×	Ar	30	Grainer and Granier (1966b)
	×	×	Xe	3	Ch'en and Fountain (1964)
	×	×	H ₂	30	Granier, Granier, and Vodar (1966)
	×	×	D ₂	30	
Rb $5s \ ^2S_{1/2}-6p \ ^2P_J$	×		Kr	7	Granier and Granier (1966a)
	×	×	Xe	3	Ch'en and Fountain (1964)
Rb $5s \ ^2S_{1/2}-7p \ ^2P_J$	×		Xe	1.5	

TABLE VIII. (Continued.)

	States	Width	Shift	Gases	Maximum density (rd)	References
Rb	$5s^2 S_{1/2}-8p^2 P_J$	×	×	Xe	2.5	
Sr	$5s^2 1S_0-5s 5p^1 P_1$	×	×	He	60	Wang and Ch'en (1979)
		×	×	Xe	3.5	
Sr II	$5s^2 S_{1/2}-5p^2 P_{1/2}$	×	×	He	120	Ch'en and Henry (1973)
		×	×	Ar	45	
Mo	$a^5 D_2-y^5 F_3$		×	Ar	75	Holmes <i>et al.</i> (1969b)
In	$5s 5p^2 P_J-6s^2 2S_{1/2}$	×	×	He	26	Ch'en <i>et al.</i> (1960)
		×	×	Ar	30	
Cs	$6s^2 S_{1/2}-6p^2 P_J$	×	×	He	200	Garrett and Ch'en (1966)
		×	×	Ne	70	Garrett, Ch'en, and Looi (1967)
		×	×	Ar	160	Ch'en and Garrett (1966)
		×	×	Kr	58	Ch'en, Looi, and Garrett (1967)
		×	×	Xe	47	Ch'en, Gilbert, and Tan (1969)
		×	×	CF ₄	2.5	
Cs	$6s^2 S_{1/2}-7p^2 P_J$	×	×	He	11	Garrett and Ch'en (1966)
		×	×	Ne	50	Garrett, Ch'en, and Looi (1967)
		×	×	Ar	18	Ch'en and Garrett (1966)
		×	×	Kr	11	Ch'en, Looi, and Garrett (1967)
		×	×	Xe	5.5	Ch'en, Gilbert, and Tan (1969)
Cs	$6s^2 S_{1/2}-8p^2 P_J$	×	×	Ne	24	Garrett, Ch'en, and Looi (1967)
		×	×	Ar	5.5	Tan and Ch'en (1970)
		×	×	Kr	2	Ch'en, Looi, and Garrett (1967)
		×	×	Kr	5	Tan and Ch'en (1970)
		×	×	Xe	2.5	
		×	×	Xe	5	
Ba II	$6s^2 S_{1/2}-6p^2 P_{1/2}$	×	×	He	120	Ch'en, Gilbert, and Tan (1969)
		×	×	Ar	45	Ch'en and Henry (1973)
Ba II	$6s^2 S_{1/2}-6p^2 P_{3/2}$	×	×	He	120	
		×	×	Ar	60	
Hg	$6s^2 1S_0-6s 6p^3 P_1$	×	He	580	Granier and Granier (1965a, 1965b)	
		×	He	200	Granier, Granier, and Vodar (1966)	
		×	H ₂	625	Granier, Granier, and DeCroutte (1963a)	
		×	D ₂	625		

^aConsult the reference for a full list of lines.

b. High Rydberg states

Table IX summarizes currently available high-density observations for large n^* . As an example, we illustrate in Fig. 36 the behavior, as a function of series member, of cesium spectra broadened by noble gases (Tan and Ch'en, 1970). The behavior is that predicted by the Fermi theory: for highly excited states the shifts are independent of the state. Regrettably, similar results for the widths are not available, and the expectation that the widths should increase only as $n^{1/2}$ (see Sec. II.F.7) has not been verified. Tan and Ch'en (1970) also feel that the Fermi theory does not correctly predict the behavior of the shift with gas density for densities greater than 2 atm. Thus there is no question but that additional measurements of widths, shifts, and indeed profiles of these lines at high density would be very desirable.

The line-core profile for these transitions is expected to be Gaussian for very high densities, but that expectation is contingent upon the absence of significant far-wing satellite features on Rydberg series transitions, as well as on the constancy of the oscillator strength during

the collision (Royer, 1980). There have been no experimental studies of either point as yet.

E. Line wings

Today nobody really worries about the spectra of alkali atoms.

—Parsons and Weisskopf, 1967

1. Frequencies near the unperturbed line center

a. The shape of the near wing

Among the earliest reported observations of near-wing intensities were attempts to verify the predictions of Eq. (16) that under the influence of van der Waals potentials the red wing of collision-broadened lines would vary as $(\Delta\omega)^{-3/2}$. As described by Kuhn (1961), observations by Minkowski (1935), Kuhn (1937a, 1937b), Ruhmkorf (1938), Huldt and Knall (1954), and Robin and Robin

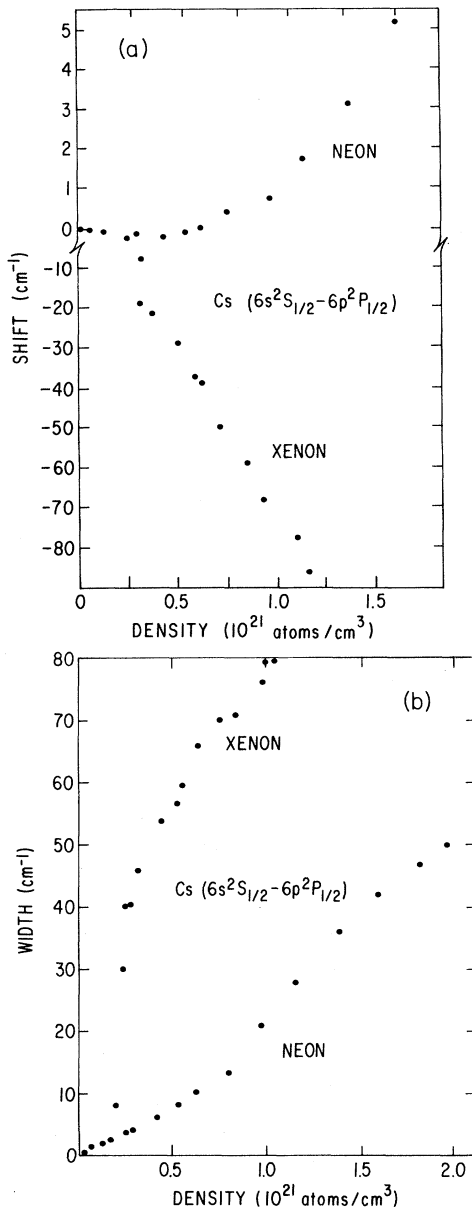


FIG. 35. Shift and width of $\text{Cs} (6s^2 S_{1/2} - 6p^2 P_{1/2})$ perturbed by xenon and neon as a function of gas density for temperatures of about 400 K (Ch'en, Gilbert, and Tan, 1969; Garrett, Ch'en, and Looi, 1967).

(1957a, 1957b) have all confirmed that, when the line wing is no longer Lorentzian on the red side, it behaves in agreement with this expectation over a range of a factor of 10 in intensity. In the light of current thinking about the significance of higher-order multipole terms in the interaction, and indeed of interactions that do not resemble van der Waals potentials at all, the agreement of these observations with simple static theory is more a problem than a solution. For instance, in Fig. 37 we show the potential of the $5p^2 P_{1/2}(^2\Pi_{1/2})$ state of Rb perturbed by Xe from the tabulations of Pascale and Vandeplanque (1974), and compare that potential to the van

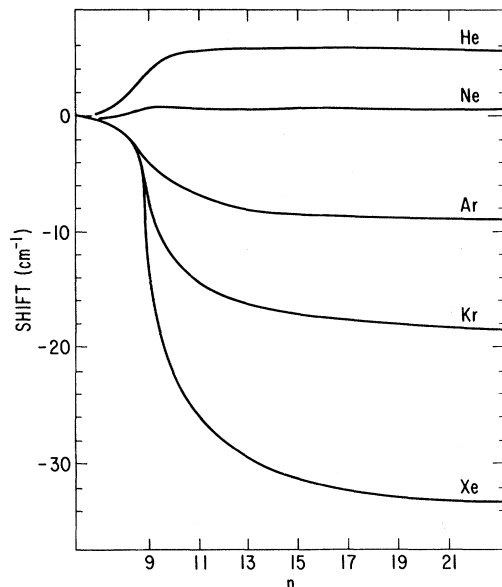


FIG. 36. Shift of $\text{Cs} (6s^2 S_{1/2} - np^2 P_{3/2})$ transitions for the series up to $n = 25$ for different noble gases at the same density, about 2.5×10^{19} atoms cm^{-3} and 550 K (Tan and Ch'en, 1970).

der Waals term $C_6 R^{-6}$ expected for that state. The two potentials, while of nearly the same form for weak interactions of order 1 cm^{-1} , are not at all of the same magnitude.

Near wings have recently been remeasured for power-law dependence, and high-resolution results of pho-

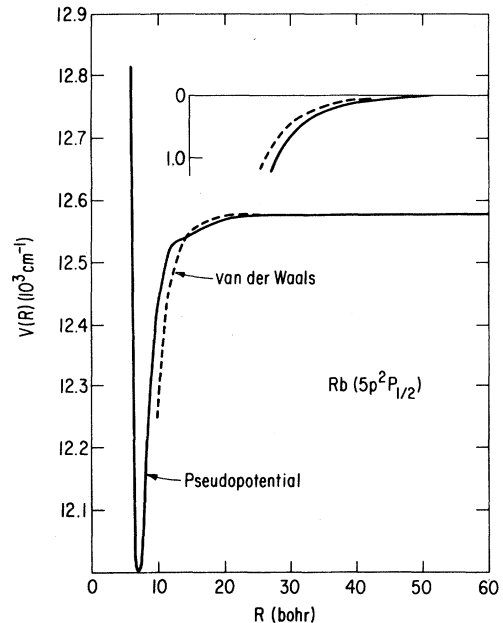


FIG. 37. Comparison of the van der Waals and pseudopotential (Pascale and Vandeplanque, 1974) calculations for the Rb ($5p^2 P_{1/2}$) state perturbed by Xe, illustrating that the van der Waals potential is weaker than the interaction at long range where the near line wing is formed.

TABLE IX. High-density observations of high series members.

Element	Foreign gases	Reference
Na	He, Ar, H ₂ , N ₂	Amaldi and Segre (1934a, 1934b)
	He, Ne, Ar	Füchtbauer (1934)
	He, Ne, Ar, H ₂ , N ₂	Füchtbauer and Schulz (1935)
K	He, Ar, H ₂ , N ₂	Amaldi and Segre (1934a, 1934b)
	He, Ne, Ar	Füchtbauer (1934)
	H ₂	Ny and Ch'en (1937a, 1937b)
Rb	He, Ne, Ar	Ny and Ch'en (1938)
	H ₂	Füchtbauer (1934)
	He, Ne, Ar, Hg	Füchtbauer (1934)
Cs	Xe, Hg	Füchtbauer (1934)
	Kr	Füchtbauer and Reimers (1935)
	He, Ne, Ar, Kr, Xe	Tan and Ch'en (1970)

tometric quality now are known for Li, Rb, and Tl lines broadened by noble gases (Gallagher, 1975; Ottinger *et al.*, 1975; Cheron, Scheps, and Gallagher, 1977). In Table X we summarize red-wing dependences from those papers. For Ar, Kr, and Xe perturbers, all of which have high polarizabilities and consequently large van der Waals interactions, red wings vary in the range from $(\Delta\omega)^{-1.3}$ to $(\Delta\omega)^{-1.7}$ over an intensity change of about 20, but it seems safer to conclude that near line wings do not vary as $(\Delta\omega)^{-1.5}$ in general, and that the presence of near-wing red satellites disturbs the monotonic behavior of the wing in many cases. When $(\Delta\omega)^{-1.5}$ is observed almost exactly, it is only over a limited intensity range.

b. Intense satellites in binary spectra

This work has removed any serious doubt as to the nature of the alkali-rare-gas low-frequency bands.

—Hindmarsh and Farr, 1972

The existence of abnormally intense regions in spectral line wings was first noted about 50 years ago (Oldenberg,

1928, 1929; Kuhn and Oldenberg, 1932; Ch'en and Takeo, 1957). A summary of photographically discovered features was given by Ch'en and Wilson (1961). It was clear then that many satellites could be qualitatively grouped, the simplest categories being red and violet satellites, with other classifications added to distinguish shape and strength. The complexity of this categorization, as well as the absence of reliable unified-theory line-shape calculations, led to considerable speculation about the origin of the features indexed in Table XI.

The problem of the origin and calculation of the shape of satellites was surveyed most recently by Cooper (1973). The unified-theory calculations (Sando, 1974; Szudy and Baylis, 1975; Allard, Sahal-Brechot, and Biraud, 1974; Kielkopf, 1976a, 1978; Kielkopf and Allard, 1980) have all demonstrated by rather successful comparison with available profiles that these satellites originate in extrema on interatomic difference potentials, and as such are very analogous to rainbow scattering in atomic collision experiments (Royer, 1971b; Mott and Massey, 1965). These satellites are essentially static phenomena, and explanations in terms of the static theory have been given by Hindmarsh and Farr (1969) and Kielkopf and Gwinn (1968). The more recent, elaborate profile calculations have served to demonstrate that collision dynamics do not remove the expected intensity enhancements. Thus we have no reason to think that any of the satellite features listed here are due to anything but such processes: for alkali-rare-gas spectra the near-red satellites originate from distant difference-potential wells, while the weaker violet satellites come from potential extrema that, at closer separations, imply weaker features. The varying probability that statistical equilibrium provides can also produce shoulders in the far-red wing, as illustrated in the data shown in Fig. 39 of Sec. III.E.2. Changes in the transition probability may also affect profiles, particularly for otherwise forbidden lines.

Although earlier we discussed the success of the unified theory in explaining the behavior of these features (Secs. II.E and II.F), a glance again at Fig. 22 will illustrate the typical agreement that can be achieved at present. Residual discrepancies might be due to the inflexibility of the fitting-potential function. Future calculations based upon accurate numerical potentials should

TABLE X. Power-law behavior of line wings.^a

Transitions	Gas	Red wing ^b	Range (cm ⁻¹)
Li 2s 2S _{1/2} -2p 2P _{1/2,3/2}	He	2.0	2-22
	Ne	2.0	2-15
	Ar	2.1	3-33
	Kr	2.35	4-33
	Xe	2.4	4-33
Rb 5s 2S _{1/2} -5p 2P _{1/2}	He	2.0	2-19
	Ne	2.5	2-5
	Ar	1.6	1-4
	Xe	1.5	2-11
Tl 6s 6p 2P _{1/2} -6s 7s 2S _{1/2}	He	2.0	0-30
	Ne	2.0	0-15
	Ar	1.4	3-10
	Kr	1.3	3.5-9
	Xe	1.3	3.5-15

^aData are from Li: Gallagher (1975); Rb: Ottinger *et al.* (1975); and Tl: Cheron *et al.* (1977).

^bThe power dependence $(\Delta\omega)^{-x}$ is listed in this column.

TABLE XI. Intense binary satellites.^a

Transition	Krypton (cm ⁻¹)	Xenon (cm ⁻¹)	Transition	Krypton (cm ⁻¹)	Xenon (cm ⁻¹)	
K 4s 2S _{1/2}	-4p 2P _{1/2}	-16	-31	-8d 2D _{3/2}	-11	-16
	-4p 2P _{3/2}	-13	-29	-7d 2D _{5/2}	-15	-26
	-5p 2P _{1/2}	-24	-60	-7d 2D _{3/2}	-15	-37
	-6p 2P _{1/2}	-20	-41	-8d 2D _{5/2}	-5	-7
	-7p 2P _{1/2}	-14		-8d 2D _{3/2}	-7	-15
Rb 5s 2S _{1/2}	-5p 2P _{1/2}	-7	-18	-9d 2D _{3/2}		-8
	-5p 2P _{3/2}	-18	-32	Cs 6p 2P _{1/2}	-8s 2S _{1/2}	-13
	-6p 2P _{1/2}	-20	-46		-9s 2S _{1/2}	-8
	-6p 2P _{3/2}	-28	-42	Cs 6p 2P _{3/2}	-8s 2S _{1/2}	-13
	-7p 2P _{1/2}	-18			-9s 2S _{1/2}	-23
	-7p 2P _{3/2}	-17			-10s 2S _{1/2}	-27
Rb 5p 2P _{1/2}	-8s 2S _{1/2}	-5	-10	Cs 6d 2D _{5/2}	-5f 2F _{5/2}	-24
	-9s 2S _{1/2}		-4		-6f 2F _{5/2}	-18
Rb 5p 2P _{3/2}	-8s 2S _{1/2}	-5	-10		-7f 2F _{5/2}	-13
	-9s 2S _{1/2}		-4		-8f 2F _{5/2}	-27
Rb 5p 2P _{1/2}	-6d 2D _{3/2}	-21	-45		-9f 2F _{5/2}	-22
	-7d 2D _{3/2}	-9		Cs 6d 2D _{3/2}	-5f 2F _{5/2}	-24
	-8d 2D _{3/2}		-7		-6f 2F _{5/2}	-18
Rb 5p 2P _{3/2}	-6d 2D _{5/2}	-23	-47		-7f 2F _{5/2}	-13
	-7d 2D _{5/2}	-8	-23		-9f 2F _{5/2}	-18
	-8d 2D _{5/2}		-9	Cs 6s 2S _{1/2}	-5d 2D _{3/2}	-8
Rb 5p 2P _{1/2}	-8s 2S _{1/2}	-5	-10		-5d 2D _{5/2}	-6
	-9s 2S _{1/2}		-4		-6d 2D _{3/2}	-18
Rb 5p 2P _{3/2}	-8s 2S _{1/2}	-5	-10		-6d 2D _{5/2}	-19
	-9s 2S _{1/2}		-4		-7d 2D _{3/2}	-14
Sr 5s 2 ¹ S ₀	-5s 5p 1P ₀		-50		-7d 2D _{5/2}	-11
Cs 6s 2S _{1/2}	-6p 2P _{1/2}	-5	-12	Cs 6s 2S _{1/2}	-8d 2D _{3/2}	-7
	-6p 2P _{3/2}	-17	-40	Ba 6s 2 ¹ S ₀	-6s 7p 1P ₁	-29
Cs 6s 2S _{1/2}	-7p 2P _{1/2}	-19	-39		-6s 8p 1P ₁	-12
	-7p 2P _{3/2}	-29	-55		-6s 9p 1P ₁	-8
	-8p 2P _{1/2}	-14	-29		-6s 10p 1P ₁	-3
	-8p 2P _{3/2}	-17	-31		-6s 11p 1P ₁	-2
	-9p 2P _{1/2}	-6	-10	Hg 6s 2 ¹ S ₀	-6s 6p 3P ₁	+70, +138
	-9p 2P _{3/2}	-6	-13	Tl 6s 2 ² p 2P _{1/2} -6s 2 ⁷ s 2S _{1/2}		-14, +91
Cs 6p 2P _{1/2}	-6d 2D _{3/2}	-12	-35	Tl 6s 2 ² p 2P _{3/2} -6s 2 ⁷ s 2S _{1/2}	-21, +35, +84	-48, +35
	-7d 2D _{3/2}	-19	-37			-35, +53

^aThis table includes most known "red satellites" that appear close to the atomic line and that are easily recognized on photographic spectra for foreign-gas densities of the order 10¹⁹ cm⁻³. References for the entries given are: K: Jefimenko and Williams (1965); Rb: Jefimenko and Curtis (1957); Sr: Wang and Ch'en (1979); Cs: Gwinn, Thomas, and Kielkopf (1968); Ba: Kielkopf (1978); Hg: Kielkopf and Miller (1974); Tl: Cheron, Scheps, and Gallagher (1977). The values given in (cm⁻¹) are the displacements from the atomic lines. All values are rounded to the nearest (cm⁻¹), but accuracies are typically not as good as ±1 cm⁻¹, since the features listed here are rather diffuse and sometimes do not show a pronounced maximum. However, in many cases these satellites appear as distinct lines in photographic spectra near the unperturbed atomic transition.

eventually bring out problems in the line-shape theory it-self.

c. Multiple-perturber spectra

The possibility that the effect of more than one simultaneously acting perturber would be uniquely discernable in line-wing spectra was recognized by Hindmarsh and Farr (1969) in their application of the static theory to satellite profiles. The effect may have been seen by McCartan and Hindmarsh (1969) in the wing of the 4s-5p potassium transition perturbed by krypton. In that case they reported a discontinuity in the monotonic de-

crease of the absorption coefficient beyond the red satellite that appeared 24 cm⁻¹ from the line. This unusual region in the neighborhood of 50 cm⁻¹ may have indicated the effect of two perturbers acting simultaneously in the satellite-forming region of an additive potential. There were, however, no observations of density dependence for the profile to confirm the hypothesis, and the possibility that it was due to a feature in the binary interatomic potential cannot be discounted. A similar effect seen in Na (3s-3p)-Xe (McCartan and Farr, 1976) is almost certainly part of the far-wing system reported by West and Gallagher (1978).

Some evidence of two-perturber effects is apparent in

the density dependence of wing intensities reported for Cs (6s-7p,8p)-Xe by Lorenzen and Niemax (1977) and by Exton and Snow (1978). West, Shuker, and Gallagher (1978) studied the effect of multiple-perturber interactions on the sodium-noble-gas excimer bands, and observed a feature at about 3200 cm^{-1} , twice the 1600 cm^{-1} of the excimer band, that exhibited density dependence evidently due to the presence of two xenon perturbers simultaneously. In addition, they verified that the convolution character expected for line wings [Eq. (254)] existed for their measurements when the identified feature due to two xenon perturbers fit the convolution of two one-perturber spectra.

Similar effects, but on forbidden transitions, were noted by Yabuzaki *et al.* (1978) in K-Xe fluorescence excited by a krypton-ion laser. For their experiments potassium spectra were measured in the region from 4500 to 6000 Å, and the observed features were identified as the 4s-5s transition of K-Xe, but the distribution of radiation among the observed peaks and the development of the spectra with density followed that expected for K-Xe_n polyatomic system with a bound excited state.

Observations of line broadening involving more than two perturbers in the wing, but for which bound states were not significant, were reported by Kielkopf and Allard (1979, 1980) for Cs (6s-9p)-Xe lines and by Kielkopf (1981a) for Cs (6s-8p,9p,10p)-Kr and -Xe transitions. An example is shown in Fig. 38. The observed development of the profile is exactly that predicted in the calculations discussed in Sec. II.E. It is apparent from this as yet limited set of observational data that the presence of identifiable multiple-perturber effects in line-wing spectra is probably universal, dependent only on the existence of difference-potential extrema at ranges suitable for the chosen gas density. It is for this reason that, the higher the excitation of the atomic state, the larger the effects of multiple perturbers appear to be at a given gas density.

Of course, on states which are not spherically symmetric—indeed, all known examples are *p* states—potentials depend on angle and are not exactly additive. The observed spectra seem to be evidence that, averaged over collisions, additivity of interactions is an adequate approximation.

2. Frequencies far from the line center

In spite of these rather useful properties, we feel compelled to add a warning that constructing and aligning such an instrument is a job for patient men.

—Hedges, Drummond, and Gallagher, 1972

The far line wing is observable at densities less than one atmosphere for the resonance lines only when the line center is very saturated in optical absorption experiments, because the wing absorption coefficient is of the order of 1×10^{-6} of the line-center strength. In fluorescence, special techniques, instruments, and perseverance (as noted in the quotation above) are required to obtain meaningful quantitative results. Ch'en and Takeo (1957)

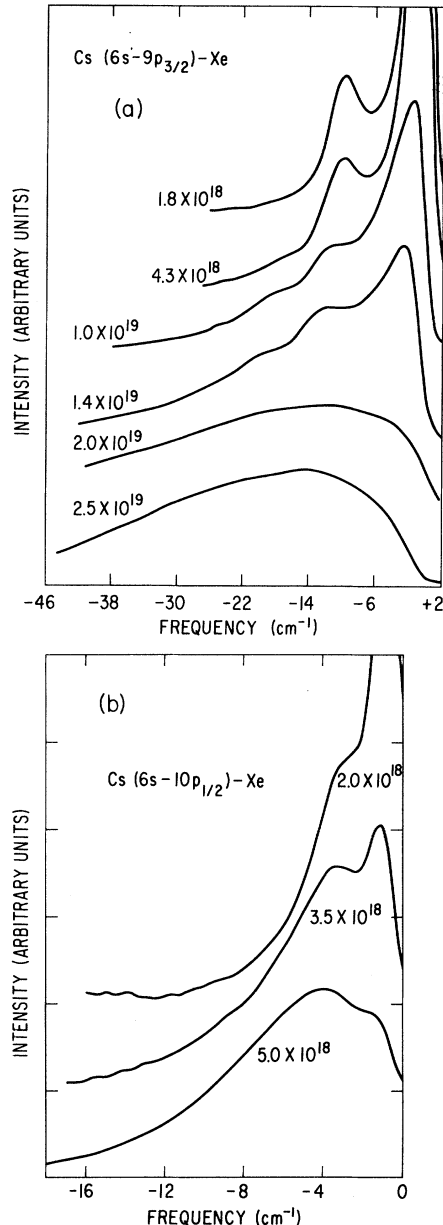


FIG. 38. Observation of the Cs ($6s\ ^2S_{1/2}$ - $9p\ ^2P_{3/2}$) line perturbed by Xe for different densities at about 550 K, and the Cs ($6s\ ^2S_{1/2}$ - $10p\ ^2P_{1/2}$) with Xe at about 575 K. Notice on the $9p$ spectra the secondary satellite prominent at $1.4 \times 10^{19} \text{ atoms cm}^{-3}$, while at much lower densities in the $10p$ spectra the primary satellite overtakes the main line (Kielkopf, 1981a).

identify the far red wing and the violet satellites as essentially high-temperature phenomena, although it is apparent from the more recent fluorescence data that temperature is not the controlling factor in their existence.

Table XII summarizes published observations of line-wing spectra that extend more than 100 cm^{-1} from the line center. Noble-gas broadening of Li, Na, Rb, Cs, and Tl has been reported in an extensive series of papers, the

TABLE XII. Available data on far line wings.^a

Transitions	Gases	Range (cm ⁻¹)	Reference
Li 2s-2p	He, Ne, Ar, Kr, Xe	-3500—2000	Scheps <i>et al.</i> (1975)
Na 3s-3p	He, Ne, Ar, Kr, Xe	-3500—2000	York <i>et al.</i> (1975)
Rb 5s-5p	He, Ne, Ar, Kr, Xe	-1600—500	Drummond and Gallagher (1974)
Rb 5s 2S _{1/2} -5p 2P _{3/2}	Ne, Ar, Kr, Xe	0—500	Carrington and Gallagher (1974)
Cs 6s-6p	He, Ne, Ar, Kr, Xe	-1000—500	Hedges <i>et al.</i> (1972)
Tl 6s-6p	He, Ne, Ar, Kr, Xe	-4500—800	Cheron <i>et al.</i> (1977)

^aOnly allowed transitions are included.

experimental basis of which is the observation of line-wing fluorescence following resonance excitation. Figure 39 shows the typical behavior of the Rb (5s-6p) line wings broadened by noble gases; on the 2P_{1/2} component they have a red shoulder that progresses from about 600 cm⁻¹ from the line center, for neon, outward to about 1100 cm⁻¹, for xenon. There is a similar red shoulder on the 2P_{3/2} component. This component also shows a blue satellite which is displaced about 400 cm⁻¹ from the center of the line. Features such as these can be interpreted by statistical theories to yield the interatomic difference potentials for the systems, and with such analyses these data provide the most extensive set of such measurements available. The temperature dependence of line-wing spectra was discussed in Sec. II.F.4, and the

determination of potentials from line-profile spectra is reviewed in Sec. IV.A.

It is worthwhile noting that the 2P_{1/2} wings are attributed to the X²Σ_{1/2}-A²Π_{1/2} difference potential, and the 2P_{3/2} red wing is similarly ascribed to the X²Σ_{1/2}-A²Π_{3/2} potential. The blue wing on this line is due to the other state, B²Σ_{1/2}, into which the atomic 2P_{3/2} state proceeds with equal probability upon collision. The 2P_{3/2} red wing is about half the comparable strength of the 2P_{1/2} wing because of this splitting. The effect has also been noticed in near wings on Cs lines (Kielkopf and Allard, 1980), and can be explained within the context of the unified-theory profiles given by Eqs. (164) and (165). In the near line wing the 2P_{3/2} spectrum has the character of the convolution of Π and Σ spectra, each at a density of n/2. Consequently the red (Π) wing on 2P_{3/2} is half the strength of the red wing on 2P_{1/2}.

The distinction between "satellite" and "shoulder" here is intentional. The far-wing red shoulders form from an essentially monotonically decreasing difference potential in the statistical interpretation. The shoulder arises from the enhanced probability associated with the excited-state potential well, and is very temperature sensitive in strength. This temperature dependence was used whenever possible to extract the excited-state potential from the difference potential. The violet satellite must arise from a potential extremum, and it is a satellite in the sense of the statistical theory we discussed earlier: the slope of the difference potential goes through zero near the peak of this feature. These satellites are also sensitive to temperature because as the temperature increases, the perturbers are more likely to climb the excited-state potential barrier that generates the difference-potential maximum.

An interesting and still puzzling feature of these far-wing observations is the behavior of the line profiles with helium. Drummond and Gallagher (1974) discuss the problem extensively, and their analysis points out that the helium results are affected experimentally both by increased off-band leakage in the spectrometer and by the need for excitation transfer corrections of greater importance than for the data with other gases. In spite of allowance for these factors, the helium data do not generally submit to statistical-theory analysis as it is used for the other gases. For helium, such analyses lead to unacceptable potentials.

The authors attribute this to the breakdown of semi-

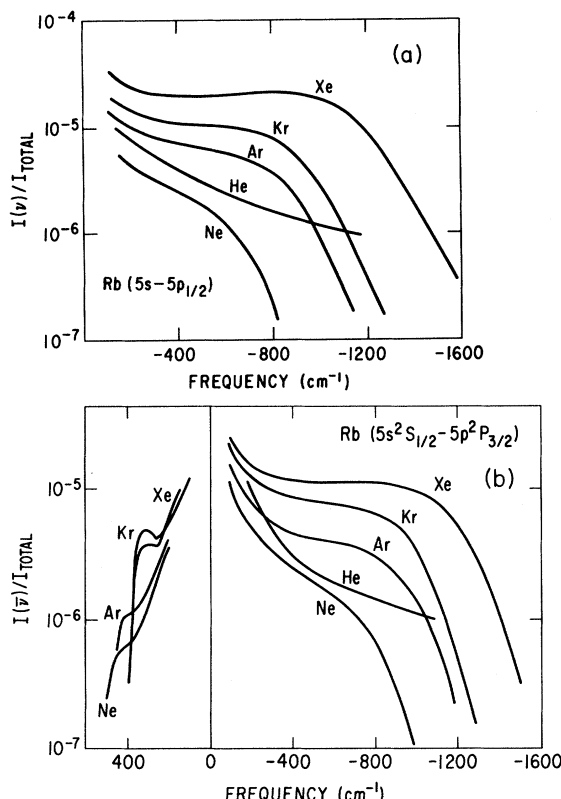


FIG. 39. Far-line-wing spectra of Rb (5s 2S_{1/2}-5p 2P_{1/2,3/2}) for various noble gases at low density (Drummond and Gallagher, 1974).

classical line-broadening theory due to the finite wavelength of the perturber, an effect most prominent for the lightest perturber, helium. The limitation of the classical path approximation imposed by this effect was brought out in Sec. II.C.1.g. Also seen are evidences of failure in the far red wing, which are attributed to quantum-mechanical barrier penetration that smears the classical spectrum.

We note in the list of observations the absence of measurements for potassium and for most of the alkaline earths. There are also not any measurements for lines other than the resonance transitions. Of course, there are obvious problems for states of higher excitation, including increased excitation transfer, interference from other transitions, the influence of diatomic alkali molecular lines, and rapidly declining oscillator strengths. We have yet to see, however, a verification of the expectations that develop from the Pascale-Vandeplanque (1974) potential calculations, which predict deep, short-range wells on almost all the excited states analogous to the potentials that produce the extreme-wing features on the resonance lines. For these transitions the intense near-wing satellites we discussed earlier arise for internuclear separations of the order of 20 Å for the Cs (6s-9p)-Xe line, for example. The potential calculations predict very deep wells in the 3–4 Å range, that should generate features hundreds of cm⁻¹ from the line center, but be weaker by several orders of magnitude than the near-wing features that have already been observed. Studies of the far line wing are an exciting domain in which line broadening overlaps the physics of diatomic molecules, and in which we can observe failures in line-broadening theory as it is conventionally formulated.

3. Observations of oscillations

In photoelectric observations of the red wing of the Cs (6s ²S_{1/2}-6p ²P_{3/2})-Ar transition, Chen and Phelps (1973) observed a series of seven or more weak undulations that had also been noticed photographically by Jefimenko and Ch'en (1957). We show a section of that spectrum in Fig. 40.

These oscillations were interpreted by Carrington *et al.* (1973) as due to contributions from bound-free transitions in which excited-state vibrational levels provide an oscillating component in the spectrum. Calculated spectra produced features with about the same intensity and spacing as those observed.

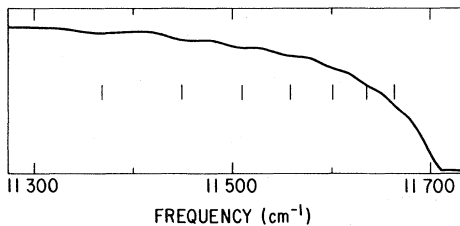


FIG. 40. Oscillations in the red wing of Cs (6s ²S_{1/2}-6p ²P_{3/2}) perturbed by Ar (Chen and Phelps, 1973).

Another type of oscillation shows up in some spectra between a satellite and the central line. Such features appear in the photographic data of Jefimenko and Curtis (1957), and in the photometric measurements of Carrington and Gallagher (1974) on blue satellites in rubidium spectra; we reproduce an example in Fig. 41. These satellites seem to be interference features that are due to the coherent addition of two contributions to the same region of the profile during the course of collision. Such oscillations also result from unified-theory calculations, as we illustrated in Fig. 22, and as was reported by Allard (1978), Kielkopf (1976a), and Kielkopf and Allard (1980). One might expect that the calculated spectra would show more interference than the experiments, since such spectra do not involve a true velocity average. Other calculations predicting these effects have been given by Royer (1971b), Sando and Wormhoudt (1973), Dalgarno and Sando (1973), Mies and Smith (1966), and Mies (1968). As Royer points out, these interference features may be very sensitive to the potential.

F. Collision-induced changes in transition probability

1. Effects on allowed transitions

... the amplitude [of vibration] is nearly independent of the distance between the molecules; ... such a [collisional] variation of intensity is not an important factor in broadening the spectral lines.

—Michelson, 1895

One of the fundamental suppositions that must be made to do line-profile calculations as we have outlined

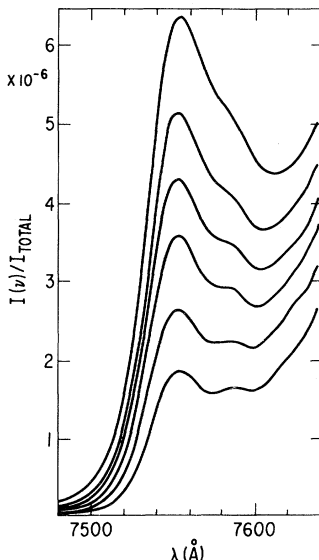


FIG. 41. Blue satellite on the Rb (5s ²S_{1/2}-5p ²P_{3/2}) transition perturbed by Ar as a function of cell temperature, illustrating an interference oscillation between the satellite and the main line (Carrington and Gallagher, 1974).

is that the probability of a radiative transition is not a function of the separation of the radiator and the perturber. This postulate may be traced back at least to the reasoning of Michelson (1895), noted above. In this section we want to review some of the evidence available from experiments that defines the circumstances under which collision-induced absorption or fluorescence might produce measurable effects in line profiles.

For the most part, experimental spectroscopists usually presume that there are no substantial effects of foreign-gas pressure on the transition probabilities of allowed lines, and it is very common to find high-precision *f*-value measurements based on absorption spectroscopy of the species of interest in the presence of some buffer gas. Some early experiments on mercury resonance radiation were discussed by Mitchell and Zemansky (1934), who concluded that uncertainties regarding foreign-gas effects on atomic vapor pressure complicate the interpretation of results that may evidence a decrease in transition probability at high gas density for the integrated line profile.

Gilbert and Ch'en (1969) studied the total integrated absorption intensity of the cesium resonance lines and all satellites due to He, Ar, Kr, and Xe foreign gases at temperatures of the order of 440 K and densities from 11 to 65 atm. Over this range for all gases they found a very definite decrease in total integrated strength with increase in density; for xenon, for instance, they observed a factor of about 2 between 11 and 43 atm. Nevertheless, they also noted that the observed effect may well have been due to a change in cesium vapor pressure. This question is not resolved as yet, but it does point out that comparisons of absolute measurements of profiles at different foreign-gas densities that depend on the calculation of total integrated absorption from measured temperatures, known oscillator strengths, and thermodynamic formulas must be regarded with caution.

Recently, Exton and Snow (1978) studied absorption coefficients of cesium principal-series lines broadened by xenon and looked into the question of the total integrated absorption for several members of the series. They report that, for the fourth member (6s-9p), the total absorption appeared to increase when the wings gained appreciable strength relative to the central core. The observed effect may be related to the instrument resolution. Other measurements (Kielkopf and Allard, 1980) at higher resolution do not confirm this behavior for the allowed principal-series lines.

2. Effects on forbidden transitions

In contrast to the allowed lines, the forbidden or only weakly allowed transitions appear to be very sensitive to collision-induced effects. The first point of evidence is in the extensive series of measurements reported by Mack (1950, 1952) primarily of precise excited alkali *s*- and *d*-state energy levels from forbidden *s-s* and *s-d* absorption transitions enhanced by foreign gases. Many others have noticed that *s-d* transitions in particular

show unusual satellites and line profiles; we give an example in Fig. 42. Notice the very sharp lines at the 6s-6d transitions frequencies, and the diffuse, almost unconnected, underlying satellites centered at 8.4 Å to the red of each line. The satellite associated with $^2D_{5/2}$ underlies the $^2D_{3/2}$ line. Such features were seen on the Cs (6s-6d)-Xe transitions (Lapp, 1966) and on 6s-6d, 7d, 8d transitions perturbed by Xe and Kr (Gwinn, Thomas, and Kielkopf, 1968). Similar effects have also been seen in Rb spectra perturbed by Kr (Besombes, Granier, and Granier, 1969). In a few cases precise measurements have been made (Sayer, Ferray, and Lozingot, 1979; Sayer *et al.*, 1980; Niemax, 1977). The expected collision-induced dipole transition probability is of the same order as the experimentally observed intensities (Granier, Granier, and Schuller, 1975). A calculation of the profile of such transitions (Gallagher and Holstein, 1977; J. Pascale, 1977; Sayer, Visticot, and Pascale, 1978) that allows for collision-enforced phenomena produces profiles of about the right form. A detailed comparison of normalized profiles (such as those in Niemax, 1977) with calculations not restricted to the static limit, and based on independently determined theoretical potentials, seems to be needed.

Niemax (1977) does demonstrate that for the Cs (6s-nd) transitions the oscillator strengths for the entire integrated profiles do increase with xenon gas density if the satellites (i.e., the "quasistatic" wing) are included in the integration. Dakhil and Kielkopf (1977) found 6s-ns transitions in absorption spectra of cesium with xenon at densities of the order of 5×10^{18} atoms cm⁻³ for *n* = 11–19. At these foreign-gas densities they noted that the 6s-nd transitions occurred with most of the line strength in identifiable features due to perturbations of the nd levels by collisions when *n* was greater than ten. The 6s-ns transitions disappeared when helium was substituted for xenon.

The available evidence is thus inconclusive about the importance of collision-induced effects on allowed transitions. On forbidden transitions the effects can be very pronounced, so that at high gas density the entire *s-s* or *s-d* transition is collision induced, with an oscillator strength determined by the presence of the buffer gas, a profile dependent on the changing dipole moment with internuclear separation, and a line position strongly dependent on the value of the difference potential for which the transition probability is maximum.

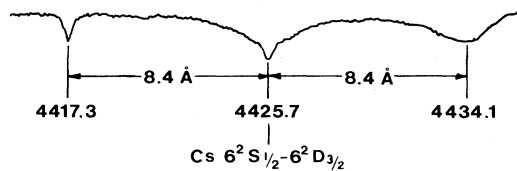


FIG. 42. Broad and unusually strong satellites on the forbidden Cs (6s-6d) multiplet perturbed by xenon (Lapp, 1966).

G. Radiative redistribution experiments

In Sec. II.C.3 we discussed the redistribution by frequency of radiation when it is absorbed and then reemitted by collisionally perturbed atoms. There we showed that recent theoretical developments conclude that the absorption, emission, and radiative redistribution profiles are closely related, but that the polarization of the redistributed radiation may carry more information about the transfer of excitation between excited-state sublevels than we could obtain through more conventional experiments. Although all of the experiments we have discussed that involve fluorescence of optically excited vapors fall into this category, we want to point out here those experiments that were particularly designed to reveal information about the redistribution process.

Carlsten, Szöke, and Raymer (1977) and Carlsten and Szöke (1976a, 1976b) reported measurements of the spectrum of redistributed fluorescent radiation with nitrogen laser-pumped dye laser excitation of Sr (1S_0 - 1P_1) in Ar at densities of the order of 4×10^{17} atoms cm^{-3} to 2×10^{19} atoms cm^{-3} . They observed that the Rayleigh fluorescence signal was Lorentzian as a function of detuning from the unperturbed line frequency, and they were able to measure the ratio of intensities of the total Rayleigh and redistributed fluorescence.

Raymer and Carlsten (1977) observed Raman and collision-induced fluorescence from Tl ($6p$ $^2P_{1/2,3/2}$ - $7s$ $^2S_{1/2}$) perturbed by Ar. In addition to detecting stimulated emission in the forward direction, they also measured the ratio of collision-induced fluorescence to Raman scattering for a right-angle geometry. According to the results we have discussed, in particular those of Nienhuis and Schuller (1977), the ratio as a function of detuning should be the same as the emission line shape, yet they report a discrepancy in shape, increasing with $\Delta\nu$, in comparison to the conventional measurements of Cheron, Scheps, and Gallagher (1976). The population factors in these two experiments may be different, however.

Recently, a measurement of the collision-induced fluorescence spectrum for the Tl-Ar system was made by Raymer, Carlsten, and Pichler (1979). They obtained the total fluorescence intensity as a function of laser detuning and used the ratio with the Raman intensity at each frequency to compare with conventional Tl emission experiments. The shape of the spectral distributions were exactly identical except in the extreme red wing, where population effects must be taken into account. The absolute strength was uncertain, although apparently within a factor of 2 of the absolute strength obtained from the emission spectrum.

The degree of depolarization in the redistribution spectrum of Tl, as a function of Ar density, has been studied by Thomann, Burnett, and Cooper (1980). They found high polarization in the low-pressure limit for the line wings, agreeing with the trend in the molecular collision predictions of Lewis, Salter, and Harris (1981). Comprehensive experimental studies for other transitions

or atom pairs of the spectra and polarization of redistributed radiation have not been reported.

IV. APPLICATIONS OF LINE-SHAPE STUDIES TO SPECIFIC PROBLEMS

A. Determination of interatomic potentials

We cannot foresee any basic limitation which should prevent major improvements of accuracy in the immediate future. If this can be realized we believe this will be the most accurate method presently available for learning these interaction potentials and perhaps many others as well.

—Hedges, Drummond, and Gallagher, 1972

On both empirical and theoretical grounds spectral line broadening depends on the statistics of gaseous mixtures, the classical and quantum mechanics of atomic collisions, and the interactions between the radiating atom and one or more perturbers. When all other factors can be regarded as well understood, then experimental observations of width, shift, and asymmetry, or of complete line profiles, can be used to determine the potentials. The details of the analyses required were presented in Sec. II.F.5 for impact broadening, and in Sec. II.F.4 for line-wing spectra.

The use of impact broadening has had the widest application, usually with an interpretation based on the assumption of a Lennard-Jones differences potential. As we noted, without temperature dependence or line-wing spectra, such determinations are ambiguous and certainly sensitive only to interactions at very long range. Nevertheless, they produce for excited states additional information about the interactions. Many of the papers referred to in Table V provide Lennard-Jones potential constants determined in this way.

An observation of the line wing is in principle a more effective way of determining the interaction. For example, the extensive measurements of Hedges, Drummond, and Gallagher (1972) for Cs ($6s$ - $6p$)-Xe illustrate how the individual potentials can be traced without assumptions on the analytic form of the potential. Again, we summarize in Table XIII some systems for which wing spectra have yielded molecular potentials. The measurements are confined generally to interactions with noble gases.

There remains a question of the reliability of these far-wing results. In the case of the sodium $3s$ - $3p$ resonance transition, York, Scheps, and Gallagher (1975) have measured the fluorescence spectrum to determine potentials for interactions with noble gases. The potentials also have been determined from laser fluorescence experiments by Smalley *et al.* (1977) for Na-Ar and by Ahmad-Bitar, Lapatovich, and Pritchard (1977) for Na-Ne in which molecular spectra of bound states for the $A^2\Pi$ - $X^2\Sigma$ transitions were detected. The molecules were created by supersonic expansion of the gas into sodium vapor, which gives a molecular excitation temperature of less than 1 K. In the Na-Ne case the line-wing spectra

TABLE XIII. Potentials from line wings.

States	Gases	Separation (Å)	Reference
Li 2s and 2p	Ar,Kr,Xe	2–5	Scheps <i>et al.</i> (1975)
Na 3s and 3p	Ar,Kr,Xe	2.6–4.4	York, Scheps, and Gallagher (1975)
Rb 5s and 5p	Ne,Ar,Kr,Xe	2.8–5.5	Drummond and Gallagher (1974)
Sr 5p 1P_0	Ar,Xe	5–10	Harima <i>et al.</i> (1981)
Cs 6s and 6p	He,Ne,Ar,Kr,Xe	3.5–6	Hedges, Drummond, and Gallagher (1972)
Cs 7p $^2P_{1/2}$	Xe	7–20	Kielkopf and Allard (1980)
8p $^2P_{1/2}$	Xe	7–30	
9p $^2P_{1/2}$	Xe	12–40	
Ba 7p 1P_1	Xe	8–20	Kielkopf (1978)
8p 1P_1	Xe	12–25	
9p 1P_1	Xe	10–30	
10p 1P_1	Xe	10–35	
11p 1P_1	Xe	10–40	
Tl 7s and 7p	He,Ne,Ar,Kr,Xe	2.8–5.2	Cheron, Scheps, and Gallagher (1976)

did not show pressure dependence other than linear scaling, and there was no measurement of temperature dependence. Consequently, no potential was deduced, and no direct comparison can be drawn with the well depth and radius found by Ahmad-Bitar, Lapatovich, and Pritchard.

For argon broadening a more positive comparison can be drawn. The molecular-beam observations of Smalley *et al.* (1977) were fitted by Goble and Winn (1979) to obtain an analytical potential as illustrated in Fig. 43 for $A^2\Pi_{1/2}$. The discrepancy is only of the order of 30 cm^{-1} out of a well depth of about 572 cm^{-1} , which is within the expected error of the line-shape data due to the validity limit of the statistical theory. The more recent scattering measurements of Düren and Gröger (1978, 1979) give excited-state well depth of 559 cm^{-1} , in excellent concurrence with the other two measurements.

The line-wing experiments also did not independently determine the position of the potential-well minimum, but rather fitted calculated ground-state potentials. So the horizontal displacement in Fig. 43 might be attributed to an uncertainty in the calculated ground state.

It is probably safe to conclude that for broadening by argon, krypton, and xenon the potentials derived from analyses of far line wings are reliable within about 30 cm^{-1} . For helium there are problems, which we have already discussed in Sec. III.E.2. Broadening by neon, as an intermediate case, yields potentials of unproven reliability.

Ahmad-Bitar, Lapatovich, and Pritchard draw a comparison between the molecular-beam results for Na-Ne $B^2\Sigma$, the analysis of sodium-neon line-core broadening by Lwin, McCartan, and Lewis (1976), and the near-wing and core observations of McCartan and Farr (1976). In this case the beam experiment indicated a level bound by $2.4 \pm 0.8 \text{ cm}^{-1}$. This observation was inconsistent with the conclusion of Lwin and co-workers that the actual potential is more repulsive than the calculated pseudopotentials of Baylis (1969) and of Pascale and Vandenplanque (1974), and with the conclusion of McCartan and Farr (1976) that the potential well was less than 0.5- cm^{-1} deep. If anything, these comparisons point out the uncertainty involved in interpreting line-core observations in terms of interatomic potentials.

Spectroscopically determined potentials for diatomic excimer molecules, systems such as Cs-Xe or Tl-Hg, are useful for the determination of the properties of electrical-discharge excimer lasers. The subject is surveyed by Rhodes (1979) and in the article by Gallagher (1979) which deals specifically with the study of such excimer system by line-shape spectroscopy. Rostas (1981) also presents a summary of work on alkali-rare-gas excimers in which almost all the physical information is derived from studies of the line profiles.

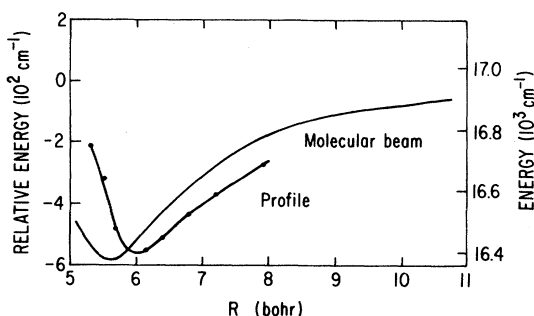


FIG. 43. Comparison of potentials for Na ($3p\ ^2P_{1/2}$)-Ar determined by molecular beam (Goble and Winn, 1979) and line profile (York, Scheps, and Gallagher, 1975). Also compare to Fig. 12.

B. Neutral-atom line broadening in stellar atmospheres

A strong metallic line in the solar spectrum will be saturated at the center, and as a consequence the line wings determine the apparent width of the absorption line,

which also depends on the oscillator strength of the transition and the abundance of the element in the solar atmosphere. The line wings are determined in large part by collision broadening by neutral hydrogen. In a typical solar-model atmosphere (Gingerich *et al.*, 1971) at an optical depth of 1.0, the temperature is 6390 K and the gas density is $3.2 \times 10^{-7} \text{ gm cm}^{-3}$, or about $1.9 \times 10^{17} \text{ atoms cm}^{-3}$. The effect of the relatively small density is offset in large part by the high temperature. Similar conditions occur in all late-type stars, and the analysis of metallic element abundances in these stars depends on knowledge of the collision broadening. Indeed, uncertainty over the magnitude of the broadening is still a major handicap for the use of stellar line profiles in the study of physical processes in stellar atmospheres and the determination of chemical abundances (O'Neill and Smith, 1980a, 1980b; Cowley, 1970; Smith and Raggett, 1981).

In our discussion of shock tubes for neutral-atom studies in Sec. III.A.4.d we saw how few measurements there are under conditions that promote the total dissociation of molecular hydrogen and that maintain a high gas temperature. As a consequence, our laboratory empirical knowledge of the required line-broadening rates is extremely limited. The problem has recently been surveyed by Pagel (1971), who considers the general measurement of stellar line profiles as a source of astrophysically significant information, and Lwin, McCartan, and Lewis (1977), who consider the extrapolation of temperature-dependent broadening by atomic hydrogen from available data. Although, it is still not uncommon to use some type of scaled van der Waal's interaction to predict broadening in the stellar case, both authors point out that there is considerable evidence that this is simply an unreliable approximation.

To offset this problem there have been a number of theoretical efforts to calculate the broadening, particularly of iron by atomic hydrogen. Some recent papers are Brueckner's (1971) theory and tables as a function of n^* , the extensive tabulations of Deridder and Rensbergen (1974, 1976) based on the Fermi-Roueff potential, the calculations of Roueff for sodium lines (1974, 1975), and the analytical formulas given by Edmunds (1975) and by Irwin (1979). The agreement of any of these theories with empirically deduced damping constants for solar iron lines does not seem to be exceptional, and errors of an order of magnitude are possible.

There is certainly a very strong need for laboratory measurements of some sort and for additional calculations, particularly with regard to the determination of hydrogen-metal atom potentials. One possibility for the near future is the systematic study of pressure broadening in hydrogen shock tubes with the assistance of array detectors such as the Reticon. Recently, O'Neill and Smith (1980a, 1980b) have looked into the usefulness of an analogy between broadening by helium and broadening by hydrogen. Helium is of course much easier to work with in the laboratory, and in appropriately designed absorption cells adequately high temperatures

can be obtained to simulate late-type stars. They use observed helium broadening to deduce C_{12} for a Lennard-Jones potential, which they then apply to hydrogen broadening. For example, they predict a half-width of the 6102 Å calcium line broadened by hydrogen at 5000 K of $1.03 \times 10^{-19} \text{ cm}^{-1}/\text{cm}^{-3}$, compared to O'Mara (1976) with a value of $1.35 \times 10^{-19} \text{ cm}^2$, and to Deridder and Rensbergen (1976) with $0.80 \times 10^{-19} \text{ cm}^2$. The best empirical solar value is $1.27 \times 10^{-19} \text{ cm}^2$. The O'Neill-Smith semiempirical value and O'Mara's calculation both agree with the solar value, but the Deridder-Rensbergen calculation does not. The van der Waal's interaction in this case predicts a broadening of only $0.56 \times 10^{-19} \text{ cm}^2$, almost three times too small. In addition to obtaining reasonable scaled values of the broadening rates, they have been successful in recognizing cases where impurities in configuration assignments lead to unexpected broadening rates (Smith and Raggett, 1981).

Since observations of laboratory spectra, even for systems such as cesium-xenon that do not have direct astrophysical application, can be used to perfect broadening calculation methods and to study the process of radiative redistribution, which is of even greater astrophysical usefulness, the solution of the hydrogen-broadening problem would follow from reliable potential calculations such as those of Lewis, McNamara, and Michels (1971) for Na-H. Direct observation of hydrogen broadening in the laboratory at temperatures of the order of 5000 K is still needed.

C. The problem of practical wavelength standards and pressure shifts

Practical light sources for wavelength standards, such as the iron hollow cathode (Crosswhite, 1975), the uranium hollow cathode (Palmer, Keller, and Engleman, 1980), and the thorium electrodeless source (Giachetti, Stanley, and Zalubas, 1970) must always contain some buffer gas to carry the initial electrical discharge and to insure stable operation. Filling pressures of helium, neon, or argon at room temperature may be as low as 1 or 2 torr, or as high as 20 torr. Since these secondary standards are referenced to the primary length standard, they become effectively the tool by which wavelengths, and hence energy levels and ionization potentials, are measured in atomic spectra, and possible shifts in these standard wavelengths due to foreign-gas pressure are very important.

Some expected characteristics of the pressure shifts can be gleaned from the known behavior of alkali-metal lines. Sodium (for instance, the $3s^2S_{1/2}-3p^2P_{1/2}$ transition) shows shifts of +0.0006, -0.0009, and +0.0021 cm^{-1} for helium, neon, and argon, respectively, at 450 K and 10 torr. These would be small but significant effects for standard lines, and similar shifts can be expected in other atomic transitions between low-lying levels. Giachetti, Stanley, and Zalubas found shifts in thorium spectra of the order of 0.0025 cm^{-1} between different

light sources. They concluded that the effects were consistent with different filling pressures. From the alkali results in Table V we can see that shifts for argon are often larger than shifts for helium and neon. Argon shifts are also usually to lower energy, while helium shifts are usually to higher energy. Of these gases, argon with a large red shift is the worst choice, and neon is a satisfactory compromise, but the sign of its shift is not very predictable. For low-lying transitions we expect that filling pressures less than 10 torr will produce line shifts less than 0.001 cm^{-1} . Nevertheless, there are no studies of the effect of foreign-gas pressure on the most commonly used wavelength standards.

The recent iodine atlas (Gerstenkorn and Luc, 1978) reports standard spectra for I_2 with no filling gas at its own very low vapor pressure. Although the determination of the reference wavelengths reported there depended on the transfer of standardization with a uranium hollow-cathode source and krypton fill gas, no significant systematic errors are expected above the $\pm 0.006 \text{ cm}^{-1}$ accuracy of the tables. The uranium standards, now also of interest for laser spectroscopy because of their use with optogalvanic detection, are based on commercial uranium hollow-cathode lamps filled with about 5 torr of neon. With the possibility of different buffer pressures caused, for instance, by cleanup as the lamps age, or of different fill gases in lamps of other manufacture, some dependence of the wavelengths may be expected. The upper levels in question are usually less than halfway to the ionization limit, so the effects should hardly be larger than the quoted accuracy of $\pm 0.003 \text{ cm}^{-1}$.

Pressure shifts are much more significant for higher transitions. Highly excited atoms are more easily perturbed by collision, and when n^* is as large as five, the shifts may be an order of magnitude larger than the example given above (Kielkopf and Knollenberg, 1981). Consequently wavelength measurements of transitions for high series members must be made at very low pressure. An example of the effect of 10 torr of helium on the determination of $np\ 2P_{3/2}$ levels in cesium for n from 7 to 27 has been given by Lorenzen and Niemax (1979). They compared their low-pressure spectra (referenced to an iron hollow cathode) with those obtained by Kratz (1949), who reported measurements at a pressure of 10 torr. Discrepancies as large as 0.2 cm^{-1} were found, large enough they felt to infer that Kratz' absorption cell was actually filled at 19 torr instead of 10. These energy-level errors and corresponding ionization potential discrepancies carry through to the 1971 revision of the NBS Atomic Energy Levels (Moore, 1971), and probably are also important for other alkali and alkaline-earth elements for which many excited energy levels have been measured under similar conditions.

ACKNOWLEDGMENTS

We are indebted to Drs. W. Baylis, Y. Biraud, N. Feautrier, F. Masnou-Seeuws, and S. Sahal-Brechot for

helpful discussions and for the interest they have shown in this review. One of us (J.K.) acknowledges the support of the National Science Foundation through Grants Nos. PHY78-18862 and PHY80-13655. Travel support was provided through NSF and NATO.

REFERENCES

- Ahmad-Bitar, R., W. P. Lapatovich, and D. E. Pritchard, 1977, Phys. Rev. Lett. **39**, 1657.
- Allard, N. F., 1973, These de 3^e Cycle (University of Paris) (unpublished).
- Allard, N. F., 1978, J. Phys. B **11**, 1383.
- Allard, N. F., and Y. G. Biraud, 1980, J. Quant. Spectrosc. Radiat. Transfer **23**, 253.
- Allard, N. F., and Y. G. Biraud, 1982, J. Phys. (Paris) **43**, 501.
- Allard, N. F., S. Sahal-Brechot, and Y. G. Biraud, 1974, J. Phys. B **7**, 2158.
- Amaldi, E., and E. Segrè, 1934a, Nature (London) **133**, 141.
- Amaldi, E., and E. Segrè, 1934b, Nuovo Cimento **11**, 145.
- Anderson, P. W., 1949, Phys. Rev. **76**, 647.
- Anderson, P. W., 1952, Phys. Rev. **86**, 809.
- Anderson, P. W., and J. D. Talman, 1956, "Pressure broadening of spectral lines at general pressures," Bell System Technical Publication No. 3117 (New Jersey).
- Armstrong, B. H., 1967, J. Quant. Spectrosc. Radiat. Transfer **7**, 61.
- Atakan, A. K., and H. C. Jacobson, 1972, J. Quant. Spectrosc. Radiat. Transfer **12**, 289.
- Baird, J. P., M. J. Eckart, and R. J. Sandeman, 1979, J. Phys. B **12**, 355.
- Ballik, E. A., 1966, Appl. Opt. **5**, 170.
- Baranger, M., 1958a, Phys. Rev. **111**, 481.
- Baranger, M., 1958b, Phys. Rev. **111**, 494.
- Baranger, M., 1958c, Phys. Rev. **112**, 855.
- Baranger, M., 1962, "Spectral line broadening in plasmas" in *Atomic and Molecular Processes*, edited by D. R. Bates (Academic, New York), p. 493.
- Bardsley, J., 1974, Case Stud. At. Phys. **4**, 299.
- Bates, D. R., 1951, Mon. Not. R. Astron. Soc. **111**, 303.
- Bates, W. R. and A. Damgaard, 1949, Philos. Trans. R. Soc. London, Ser. A **242**, 101.
- Baur, J. F., and J. Cooper, 1977, J. Quant. Spectrosc. Radiat. Transfer **17**, 311.
- Baylis, W. E., 1969, J. Chem. Phys. **51**, 2665. Also JILA Report No. 100 (Joint Institute for Laboratory Astrophysics, University of Colorado, Boulder).
- Baylis, W. E., 1977, J. Phys. B **10**, L477.
- Baylis, W. E., 1978, "Interaction potentials for collisions of excited atoms" in *Progress in Atomic Spectroscopy*, edited by W. Hanle and H. Kleinpoppen (Plenum, New York), p. 207.
- Behmenburg, W., 1964, J. Quant. Spectrosc. Radiat. Transfer **4**, 177.
- Behmenburg, W., 1968, Z. Astrophys. **69**, 368.
- Behmenburg, W., 1979, "Line shapes" in *Progress in Atomic Spectroscopy*, edited by W. Hanle and H. Kleinpoppen (Plenum, New York), p. 1187.
- Bergeon, R., 1954, C. R. Acad. Sci. **238**, 2507.
- Bergeon, R., S. Robin, and B. Vodar, 1952, C. R. Acad. Sci. **235**, 360.
- Berman, P. R., 1975, Comments At. Mol. Phys. **5**, 19.

- Bernabeu, E., and J. M. Alvarez, 1980, Phys. Rev. A **22**, 2690.
- Besombes, F., J. Granier, and R. Granier, 1969, Opt. Commun. **1**, 161.
- Bevington, P. R., 1969, *Data Reduction and Error Analysis for the Physical Sciences* (McGraw-Hill, New York).
- Bezzerides, B., 1969a, Phys. Rev. **181**, 379.
- Bezzerides, B., 1969b, Phys. Rev. **186**, 239.
- Bieniek, R. J., 1977, Phys. Rev. A **15**, 1513.
- Biraben, F., B. Cagnac, E. Giacombino, and G. Grynberg, 1977, J. Phys. B **10**, 2369.
- Blouke, M. M., M. W. Cowens, J. E. Hall, J. A. Westphal, and A. B. Christensen, 1980, Appl. Opt. **19**, 3318.
- Bondarev, A. F., 1962, Opt. Spectrosc. **12**, 282.
- Bosquet, C., and N. Bras, 1977, J. Phys. (Paris) **38**, 139.
- Bottcher, C., 1971, J. Phys. B **4**, L99.
- Bottcher, C., 1973, Chem. Phys. Lett. **18**, 457.
- Bottcher, C., T. C. Cravens, and A. Dalgarno, 1975, Proc. R. Soc. London, Ser. A **346**, 157.
- Bottcher, C., and A. Dalgarno, 1974, Proc. R. Soc. London, Ser. A **340**, 187.
- Bottcher, C., A. Dalgarno, and E. L. Wright, 1973, Phys. Rev. A **7**, 1606.
- Bowman, N. J., and E. L. Lewis, 1978, J. Phys. B **11**, 1703.
- Breene, R. G., Jr., 1957, Rev. Mod. Phys. **29**, 94.
- Breene, R. G., Jr., 1961, *The Shift and Shape of Spectral Lines* (Pergamon, Oxford).
- Brigham, E. O., 1974, *The Fast Fourier Transform* (Prentice-Hall, Englewood Cliffs), p. 164.
- Brillet, Wan-Ü L., and A. Gallagher, 1980, Phys. Rev. A **22**, 1012.
- Brueckner, K. A., 1971, Astrophys. J. **169**, 621.
- Burgess, D. D. and J. E. Grindlay, 1970, Astrophys. J. **161**, 343.
- Burnett, K., and J. Cooper, 1980a, Phys. Rev. A **22**, 2027.
- Burnett, K., and J. Cooper, 1980b, Phys. Rev. A **22**, 2044.
- Burnett, K., J. Cooper, R. J. Ballagh, and E. W. Smith, 1980, Phys. Rev. A **22**, 2005.
- Butaux, J., and R. Lennuier, 1965, C. R. Acad. Sci., Ser B **261**, 671.
- Callaway, J., and E. Bauer, 1961, Phys. Rev. **140**, 1072A.
- Carlsten, J. L., and A. Szöke, 1976a, Phys. Rev. Lett. **36**, 667.
- Carlsten, J. L., and A. Szöke, 1976b, J. Phys. B **9**, L231.
- Carlsten, J. L., A. Szöke, and M. G. Raymer, 1977, Phys. Rev. A **15**, 1029.
- Carrington, C. G., D. Drummond, A. Gallagher, and A. V. Phelps, 1973, Chem. Phys. Lett. **22**, 511.
- Carrington, C. G., and A. Gallagher, 1974, Phys. Rev. A **10**, 1464.
- Chandrasekhar, S., 1943, Rev. Mod. Phys. **15**, 1.
- Chatham, R. H., A. Gallagher, and E. L. Lewis, 1980, J. Phys. B **13**, L7.
- Chen, C. L., and A. V. Phelps, 1973, Phys. Rev. A **7**, 470.
- Ch'en, S. Y., and R. B. Bennett, 1960, Phys. Rev. **119**, 1029.
- Ch'en, S. Y., and C. W. Fountain, 1964, J. Quant. Spectrosc. Radiat. Transfer **4**, 323.
- Ch'en, S. Y., and R. O. Garrett, 1966, Phys. Rev. **144**, 59.
- Ch'en, S. Y., and R. O. Garrett, 1970, Phys. Rev. A **1**, 975.
- Ch'en, S. Y., and R. O. Garrett, 1971, Phys. Rev. A **4**, 412.
- Ch'en, S. Y., D. E. Gilbert, and D. K. L. Tan, 1969, Phys. Rev. **184**, 51.
- Ch'en, S. Y., and P. K. Henry, 1973, J. Quant. Spectrosc. Radiat. Transfer **13**, 385.
- Ch'en, S. Y., E. C. Looi, and R. O. Garrett, 1967, Phys. Rev. **155**, 38.
- Ch'en, S. Y., and W. J. Parker, 1955, J. Opt. Soc. Am. **45**, 22.
- Ch'en, S. Y., A. Smith, and M. Takeo, 1960, Phys. Rev. **117**, 1010.
- Ch'en, S. Y. and M. Takeo, 1957, Rev. Mod. Phys. **29**, 20.
- Ch'en, S. Y., and R. A. Wilson, Jr., 1961, Physica (Utrecht) **27**, 497.
- Cheron, B., R. Scheps, and A. Gallagher, 1976, J. Chem. Phys. **65**, 326.
- Cheron, B., R. Scheps, and A. Gallagher, 1977, Phys. Rev. A **15**, 651.
- Chiu, H. Y., 1977, Appl. Opt. **16**, 237.
- Collins, B. S., A. D. Petford, and D. E. Blackwell, 1970, Appl. Opt. **9**, 1606.
- Condon, E. U., and G. H. Shortley, 1964, *The Theory of Atomic Spectra* (Cambridge University, Cambridge, England/London), p. 117.
- Cooley, J. W., and J. W. Tukey, 1965, Math. Computation **19**, 296.
- Cooper, J., 1966, Rep. Prog. Phys. **29**, 35.
- Cooper, J., 1967, Rev. Mod. Phys. **39**, 167.
- Cooper, J., 1973, "Comments on the theory of satellite bands," JILA Report No. 111 (Joint Institute for Laboratory Astrophysics, University of Colorado, Boulder).
- Cooper, J., 1979, Astrophys. J. **228**, 339.
- Copley, G. H., and D. M. Camm, 1973, Astron. Astrophys. **24**, 239.
- Cowley, C. R., 1970, *The Theory of Stellar Spectra* (Gordon and Breach, New York).
- Crosswhite, H. M., 1975, J. Res. Natl. Bur. Stand. Sect. A **79**, 17.
- Czuchaj, E., 1976, Z. Phys. A **276**, 85.
- Czuchaj, E., and J. Sienkiewicz, 1979, Z. Naturforsch. Teil A **34**, 694.
- Dakhil, M., and J. F. Kielkopf, 1977, J. Opt. Soc. Am. **67**, 844.
- Dalgarno, A., 1975, "Model and pseudo potential calculations" in *Atomic Physics 4* (Plenum, New York), p. 325.
- Dalgarno, A., and K. M. Sando, 1973, Comments At. Mol. Phys. **4**, 29.
- Davison, W. D., 1968, J. Phys. B **1**, 139.
- Day, R. A., 1970, Appl. Opt. **9**, 1213.
- Deleage, J. P., D. Kunth, G. Testor, F. Rostas, and E. Roueff, 1973, J. Phys. B **6**, 1892.
- Delhoume, M., W. Brillet, F. Masnou-Seeuws, N. Feautrier, and F. Rostas, 1981, J. Phys. B **14**, 3857.
- Demtröder, W., 1973, Phys. Rep. C **7**, 223.
- Demtröder, W., 1981, *Laser Spectroscopy* (Springer, Berlin).
- Deridder, G., and W. van Rensbergen, 1974, Sol. Phys. **34**, 77.
- Deridder, G., and W. van Rensbergen, 1976, Astron. Astrophys. Suppl. **23**, 147.
- de Sa, A., and D. G. McCartan, 1972, J. Phys. E **5**, 1183.
- Dicke, R. H., 1953, Phys. Rev. **89**, 472.
- Dravins, D., 1978, Appl. Opt. **17**, 404.
- Drayson, S. R., 1976, J. Quant. Spectrosc. Radiat. Transfer **16**, 611.
- Driver, R. D., and G. Lombardi, 1977, Astron. Astrophys. **59**, 299.
- Drummond, D., and A. Gallagher, 1973, Rev. Sci. Instrum. **44**, 396.
- Drummond, D. L., and A. Gallagher, 1974, J. Chem. Phys. **60**, 3426.
- Düren, R., 1980, "Experiments and model calculations to determine interatomic potentials" in Adv. At. Mol. Phys. **16**, 55.
- Düren, R., and W. Gröger, 1978, Chem. Phys. Lett. **56**, 67.
- Düren, R., and W. Gröger, 1979, Chem. Phys. Lett. **61**, 6.

- Düren, R., and G. Moritz, 1980, *J. Chem. Phys.* **73**, 5155.
 Düren, R., G. P. Raabe, and Ch. Schlier, 1968, *Z. Phys.* **214**, 410.
 Edmonds, A. R., 1968, *Angular Momentum in Quantum Mechanics* (Princeton University, Princeton, N. J.) revision of the 2nd edition. Note that the 1st (1957) edition has an error in Eq. (4.1.12).
 Edmunds, M. G., 1975, *Astron. Astrophys.* **38**, 137.
 Erickson, G. J., and K. M. Sando, 1979, *Bull. Am. Phys. Soc.* **24**, 1190.
 Erickson, G. J., and K. M. Sando, 1980, *Phys. Rev. A* **22**, 1500.
 Evans, J. M., and J. Cooper, 1972, *J. Quant. Spectrosc. Radiat. Transfer* **12**, 259.
 Evdokimov, Y. V., 1968, *Opt. Spectrosc.* **24**, 448.
 Exton, R. J., 1976, *J. Quant. Spectrosc. Radiat. Transfer* **16**, 309.
 Exton, R. J., and W. L. Snow, 1978, *J. Quant. Spectrosc. Radiat. Transfer* **20**, 1.
 Fano, U., 1957, *Rev. Mod. Phys.* **29**, 74.
 Farr, J. M., and W. R. Hindmarsh, 1971, *J. Phys. B* **4**, 568.
 Fermi, E., 1934, *Nuovo Cimento* **11**, 157.
 Ferray, M., J. P. Visticot, J. Lozingot, and B. Sayer, 1981, *J. Phys. B* **14**, 3875.
 Flusberg, A., R. Kachru, T. Mossberg, and S. R. Hartmann, 1979, *Phys. Rev. A* **19**, 1607.
 Foley, H. M., 1946, *Phys. Rev.* **69**, 616.
 Foley, H. M., 1948, *Phys. Rev.* **73**, 259.
 Ford, W. K., Jr., 1979, *Annu. Rev. Astron. Astrophys.* **17**, 189.
 Fox, R. L., and H. C. Jacobson, 1969, *Phys. Rev.* **188**, 232.
 Füchtbauer, C., 1934, *Phys. Z.* **35**, 975.
 Füchtbauer, C., and F. Gössler, 1935, *Z. Phys.* **93**, 648.
 Füchtbauer, C., and H. J. Reimers, 1935, *Z. Phys.* **95**, 1.
 Füchtbauer, C., and P. Schulz, 1935, *Z. Phys.* **97**, 699.
 Fuhr, J. R., W. L. Wiese, and L. J. Roszman, 1972, *Bibliography on Atomic Line Shapes and Shifts* (U. S. GPO, Washington, D. C.) and Supplements 1973, 1975, 1978.
 Gallagher, A., 1968, *Phys. Rev.* **172**, 88.
 Gallagher, A., 1975, *Phys. Rev. A* **12**, 133.
 Gallagher, A., 1979, "Metal vapor excimers" in *Excimer Lasers* edited by Ch. K. Rhodes (Springer, Berlin), p. 135.
 Gallagher, A., and T. Holstein, 1977, *Phys. Rev. A* **16**, 2413.
 Garrett, R. O., and S. Y. Ch'en, 1966, *Phys. Rev.* **144**, 66.
 Garrett, R. O., S. Y. Ch'en and E. C. Looi, 1967, *Phys. Rev.* **156**, 48.
 Gersten, J. I., and H. M. Foley, 1968, *J. Opt. Soc. Am.* **58**, 933.
 Gerstenkorn, S., and P. Luc, 1978, *Atlas du spectre d'absorption de la molecule d'iode* (CNRS, Paris).
 Giachetti, A., R. W. Stanley, and R. Zalubas, 1970, *J. Opt. Soc. Am.* **60**, 474.
 Gilbert, D. E., N. F. Allard, and S. Y. Ch'en, 1980, *J. Quant. Spectrosc. Radiat. Transfer* **23**, 201.
 Gilbert, D. E., and S. Y. Ch'en, 1969, *Phys. Rev.* **188**, 40.
 Gingerich, O., R. W. Noyes, W. Kalkofen, and Y. Cuny, 1971, *Sol. Phys.* **18**, 347.
 Goble, J. H., and J. S. Winn, 1979, *J. Chem. Phys.* **70**, 2051.
 Gombas, P., 1967, *Pseudopotentiale* (Springer, Berlin).
 Granier, J., R. Granier, and F. Schuller, 1975, *J. Quant. Spectrosc. Radiat. Transfer* **15**, 619.
 Granier, R., and J. Granier, 1966b, 1965a, *C. R. Acad. Sci., Ser. B* **260**, 92.
 Granier, R., and J. Granier, 1965b, *C. R. Acad. Sci., Ser. B* **260**, 3025.
 Granier, R., and J. Granier, 1966a, *C. R. Acad. Sci., Ser. B* **262**, 605.
 Granier, R., and J. Granier, 1966b, *C. R. Acad. Sci., Ser. B* **262**, 761.
 Granier, R., and J. Granier, 1966c, *C. R. Acad. Sci., Ser. B* **262**, 1502.
 Granier, R., J. Granier, and E. De Croutte, 1963a, *C. R. Acad. Sci., Ser. B* **256**, 3622.
 Granier, R., J. Granier and E. De Croutte, 1963b, *J. Phys. (Paris)* **24**, 349.
 Granier, R., J. Granier, and B. Vodar, 1966, *J. Quant. Spectrosc. Radiat. Transfer* **6**, 741.
 Griem, H. R., 1964, *Plasma Spectroscopy* (McGraw-Hill, New York), p. 63.
 Griem, H. R., 1974, *Spectral Line Broadening by Plasmas* (Academic, New York).
 Grynberg, G., and B. Cagnac, 1977, *Rep. Prog. Phys.* **40**, 79.
 Gwinn, J. A., P. M. Thomas, and J. F. Kielkopf, 1968, *J. Chem. Phys.* **48**, 568.
 Happer, W., 1972, *Rev. Mod. Phys.* **44**, 169.
 Happer, W., G. Moe, and A. C. Tam, 1975, *Phys. Lett. A* **54**, 405.
 Harima, H., Y. Fukuzo, K. Tachibana, and Y. Urano, 1981, *J. Phys. B* **14**, 3069.
 Harima, H., K. Tachibana, and Y. Urano, 1980, *Appl. Phys.* **49**, 16.
 Hedges, R. E. M., D. L. Drummond, and A. Gallagher, 1972, *Phys. Rev. A* **6**, 1519.
 Herget, W. F., W. E. Deeds, N. M. Gilar, R. J. Lovrel, and A. H. Nielsen, 1962, *J. Opt. Soc. Am.* **52**, 1113.
 Herman, P. S., and K. M. Sando, 1977, *J. Chem. Phys.* **68**, 1153.
 Hernandez, G., 1966, *Appl. Opt.* **5**, 1745.
 Hernandez, G., 1970, *Appl. Opt.* **9**, 1591.
 Herzberg, G., 1950, *Molecular Spectra and Molecular Structure I. Spectra of Diatomic Molecules* (Van Nostrand, Princeton), p. 219.
 Hindmarsh, W. R., 1963, *Phys. Lett.* **7**, 115.
 Hindmarsh, W. R., A. N. DuPlessis, and J. M. Farr, 1970, *J. Phys. B* **3**, L5.
 Hindmarsh, W. R., and J. M. Farr, 1969, *J. Phys. B* **2**, 1388.
 Hindmarsh, W. R., and J. M. Farr, 1972, *Prog. Quantum Electron.* **2**, 141.
 Hindmarsh, W. R., A. D. Petford, and G. Smith, 1967, *Proc. R. Soc. London, Ser. A* **297**, 296.
 Holmes, Q. A., S. Y. Ch'en, and M. Takeo, 1969, *J. Quant. Spectrosc. Radiat. Transfer* **9**, 749.
 Holmes, Q. A., M. Takeo, and S. Y. Ch'en, 1969a, *J. Quant. Spectrosc. Radiat. Transfer* **9**, 761.
 Holmes, Q. A., M. Takeo, and S. Y. Ch'en, 1969b, *J. Quant. Spectrosc. Radiat. Transfer* **9**, 769.
 Holstein, T., 1950, *Phys. Rev.* **79**, 744; also often referenced in the literature is the unpublished monograph "Pressure broadening of spectral lines," Report of the University of Pittsburgh, 1953.
 Holtsmark, J., 1919, *Ann. Phys. (Leipzig)* **58**, 577.
 House, L., 1970, *J. Quant. Spectrosc. Radiat. Transfer* **10**, 909.
 Huber, D. L., 1969a, *Phys. Rev.* **178**, 93.
 Huber, D. L., 1969b, *Phys. Rev.* **187**, 392.
 Hui, A. K., B. H. Armstrong, and A. A. Wray, 1978, *J. Quant. Spectrosc. Radiat. Transfer* **19**, 509.
 Huldt, L., and E. Knall, 1954, *Z. Naturforsch. Teil A* **9**, 663.
 Hummer, D. G., and G. Rybicki, 1971, *Annu. Rev. Astron. Astrophys.* **9**, 237.
 Hund, F., 1926, *Z. Phys.* **36**, 657.
 Hund, F., 1927, *Z. Phys.* **42**, 93.
 Hunten, D. M., B. E. Nelson, and C. J. Stump, Jr., 1976, *Appl. Opt.* **15**, 2264.

- Irwin, A. W., 1979, Mon. Not. R. Astron. Soc. **188**, 707.
- Ivanov, V. N. and I. S. Fishman, 1973, Opt. Spectrosc. **35**, 679.
- Jablonski, A., 1931, Z. Phys. **70**, 723.
- Jablonski, A., 1937, Acta Phys. Pol. **6**, 371.
- Jablonski, A., 1938, Acta Phys. Pol. **7**, 196.
- Jablonski, A., 1939, Acta Phys. Pol. **8**, 71.
- Jablonski, A., 1940, Physica (Utrecht) **7**, 541.
- Jablonski, A., 1945, Phys. Rev. **68**, 78.
- Jablonski, A., 1948, Phys. Rev. **73**, 258.
- Jablonski, A., 1965, Acta Phys. Pol. **27**, 49.
- Jablonski, A., 1968, in *Proceedings of the International Conference on Optical Pumping and Atomic Line Shapes* (Warsaw), 323.
- Jacquinot, P., 1960, Rep. Prog. Phys. **23**, 267.
- Jansson, P. A., 1970, J. Opt. Soc. Am. **60**, 184.
- Jefimenko, O., and S. Y. Ch'en, 1957, J. Chem. Phys. **26**, 913.
- Jefimenko, O., and W. Curtis, 1957, J. Chem. Phys. **27**, 953.
- Jefimenko, O., and G. M. Williams, 1965, J. Chem. Phys. **42**, 207.
- Jones, A. F., and D. L. Misell, 1970, J. Phys. A **3**, 462.
- Judd, B. R., 1963, *Operator Techniques in Atomic Spectroscopy* (McGraw-Hill, New York).
- Judd, B. R., 1975, *Angular Momentum Theory for Diatomic Molecules* (Academic, New York), p. 111.
- Kielkopf, J. F., 1972, Phys. Rev. **5**, 484.
- Kielkopf, J. F., 1973, J. Opt. Soc. Am. **63**, 987.
- Kielkopf, J. F., 1974, J. Chem. Phys. **61**, 4733.
- Kielkopf, J. F., 1975a, J. Chem. Phys. **62**, 4809.
- Kielkopf, J. F., 1975b, J. Chem. Phys. **62**, 3784.
- Kielkopf, J. F., 1976a, J. Phys. B **9**, 1601.
- Kielkopf, J. F., 1976b, J. Phys. B **9**, L547.
- Kielkopf, J. F., 1978, J. Phys. B **11**, 25.
- Kielkopf, J. F., 1979, J. Opt. Soc. Am. **89**, 482.
- Kielkopf, J. F., 1980, J. Phys. B **13**, 3813.
- Kielkopf, J. F., 1981a, "Multiple perturber satellites" in *Proceedings of the 5th International Conference on Spectral Line Shapes*, edited by B. Wende (de Gruyter, Berlin).
- Kielkopf, J. F., 1981b, Appl. Opt. **20**, 3327.
- Kielkopf, J. F., 1982, J. Phys. B **15**, 915.
- Kielkopf, J. F., and N. F. Allard, 1979, Phys. Rev. Lett. **43**, 196.
- Kielkopf, J. F., and N. F. Allard, 1980, J. Phys. B **13**, 709.
- Kielkopf, J. F., and J. A. Gwinn, 1968, J. Chem. Phys. **48**, 5570.
- Kielkopf, J. F., and R. B. Knollenberg, 1975, Phys. Rev. A **12**, 559.
- Kielkopf, J. F., and R. B. Knollenberg, 1981, J. Phys. B. **14**, 1263.
- Kielkopf, J. F., and R. A. Miller, 1974, J. Chem. Phys. **61**, 3304.
- Klapisch, M., 1969, These d'Etat (University of Paris) (unpublished).
- Kratz, H. R., 1949, Phys. Rev. **75**, 1844.
- Kreye, W., 1982, J. Phys. B **15**, 371.
- Kuhn, H. G., 1934, Philos. Mag. **18**, 987.
- Kuhn, H. G., 1937a, Phys. Rev. **52**, 133.
- Kuhn, H. G., 1937b, Proc. R. Soc. London, Ser. A **158**, 212.
- Kuhn, H. G., 1937c, Proc. R. Soc. London, Ser. A **158**, 230.
- Kuhn, H. G., 1961, *Atomic Spectra* (Academic, New York), p. 391.
- Kuhn, H. G., and F. London, 1934, Philos. Mag. **18**, 983.
- Kuhn, H. G., and O. Oldenburg, 1932, Phys. Rev. **41**, 72.
- Kunth, D., F. Masnou-Seeuws, F. Rostas, and E. Roueff, 1975, J. Phys. B **8**, 203.
- Langhoff, P. W., and R. P. Hurst, 1965, Phys. Rev. **139**, 1415.
- Lapp, M., 1966, Phys. Lett. **23**, 553.
- Larson, H. P., and K. L. Andrew, 1967, Appl. Opt. **6**, 1701.
- Lee, R. W., 1971, J. Phys. B **4**, 1640.
- Lemaire, J. L., 1980, private communication.
- Lenz, W., 1924, Z. Phys. **25**, 299.
- Lenz, W., 1933, Z. Phys. **80**, 423.
- Lewis, E. L., 1980, Phys. Rep. **58**, 1.
- Lewis, E. L., and L. F. McNamara, 1972, Phys. Rev. A **5**, 2643.
- Lewis, E. L., L. F. McNamara, and H. H. Michels, 1971, Phys. Rev. A **3**, 1939.
- Lewis, E. L., J. M. Salter, and M. Harris, 1981, J. Phys. B **14**, L173.
- Lindholm, E., 1945, Ark. Fys. A **32**, No. 17, 1.
- London, F., 1930a, Z. Phys. **63**, 245.
- London, F., 1930b, Z. Phys. Chem. (Leipzig) B **11**, 222.
- Lorentz, H. A., 1906, K. Akad. Wet. (Amsterdam), Proc. **8**, 591.
- Lorenzen, J., and K. Niemax, 1977, Z. Naturforsch. Teil A **32**, 853.
- Lorenzen, J., and K. Niemax, 1979, J. Quant. Spectrosc. Radiat. Transfer **22**, 247.
- Lorre, J. J., 1973, Astrophys. J. **78**, 67.
- Lwin, N., and D. G. McCartan, 1978, J. Phys. B **11**, 3841.
- Lwin, N., D. G. McCartan, and E. L. Lewis, 1976, J. Phys. B **9**, L161.
- Lwin, N., D. G. McCartan, and E. L. Lewis, 1977, Astrophys. J. **213**, 599.
- Mack, J. E., 1950, Phys. Rev. **77**, 745.
- Mack, J. E., 1952, Phys. Rev. **85**, 716.
- Mahan, G. D., 1968, J. Chem. Phys. **48**, 950.
- Mahan, G. D., 1969, J. Chem. Phys. **50**, 2755.
- Mahan, G. D., 1972, Phys. Lett. A **39**, 145.
- Marek, J., and K. Niemax, 1976a, Phys. Lett. A **57**, 414.
- Marek, J., and K. Niemax, 1976b, J. Phys. B **9**, L483.
- Margenau, H., 1932, Phys. Rev. **40**, 387.
- Margenau, H., 1935, Phys. Rev. **48**, 755.
- Margenau, H., 1939, Rev. Mod. Phys. **11**, 1.
- Margenau, H., 1951, Phys. Rev. **82**, 156.
- Margenau, H., and W. W. Watson, 1936, Rev. Mod. Phys. **8**, 22.
- Masnou-Seeuws, F., 1973, These d'Etat (University of Paris) (unpublished).
- Masnou-Seeuws, F., 1981, "Model potential calculations for alkali—rare-gas systems: comparison with experiments" in *Proceedings of the 5th International Conference on Spectral Line Shapes*, edited by B. Wende (de Gruyter, Berlin).
- Masnou-Seeuws, F., and R. McCarroll, 1974, J. Phys. B **7**, 2230.
- Masnou-Seeuws, F., M. Phillippe and P. Valiron, 1978, Phys. Rev. Lett. **41**, 395.
- Massey, H. S. W., and E. H. S. Burhop, 1952, *Electronic and Ionic Impact Phenomena* (Oxford, London), p. 179.
- Mazing, M. A., and N. A. Vrublevskaya, 1966, Sov. Phys.—JETP **23**, 228.
- Mazing, M. A., and P. D. Serapinas, 1971, Sov. Phys.—JETP **33**, 294.
- McCartan, D. G., 1972, Phys. Lett. A **42**, 155.
- McCartan, D. G., and J. M. Farr, 1976, J. Phys. B **9**, 985.
- McCartan, D. G., J. M. Farr, and W. R. Hindmarsh, 1974, J. Phys. B **7**, 208.
- McCartan, D. G., and W. R. Hindmarsh, 1969, J. Phys. B **2**, 1396.
- McCartan, D. G., and N. Lwin, 1977, J. Phys. B **10**, L17.
- McCord, T. B., and J. Frankston, 1975, Appl. Opt. **14**, 1437.
- Michelson, A. A., 1895, Astrophys. J. **2**, 251.
- Mies, F. H., 1968, J. Chem. Phys. **48**, 482.

- Mies, F. H., and A. L. Smith, 1966, *J. Chem. Phys.* **45**, 994.
- Minkowski, R., 1935, *Z. Phys.* **93**, 731.
- Mitchell, A. C. G., and M. W. Zemansky, 1934, *Resonance Radiation and Excited Atoms* (Cambridge University, Cambridge/London), p. 113.
- Moore, C. E., 1971, *Atomic Energy Levels Volumes 1–4*, NSRDS-NBS35 (U. S. GPO, Washington, D. C.).
- Morris, M. B., and I. J. McIlrath, 1979, *Appl. Opt.* **18**, 4145.
- Mossberg, T. W., R. Kachru, and S. R. Hartmann, 1981, "Collision broadening of two-photon ground-to-Rydberg state transitions," in *Proceedings of the 5th International Conference on Spectral Line Shapes*, edited by B. Wende (de Gruyter, Berlin).
- Mott, N. F., and H. S. W. Massey, 1965, *The Theory of Atomic Collisions* (Oxford University, London).
- Myint, H., R. M. Hill, and W. R. Hindmarsh, 1979, *J. Quant. Spectrosc. Radiat. Transfer* **22**, 489.
- Niemax, K., 1977, *J. Quant. Spectrosc. Radiat. Transfer* **17**, 125.
- Niemax, K., 1980, *J. Phys. B* **13**, 1791.
- Nienhuis, G., and F. Schuller, 1977, *Physica (Utrecht)* **C 92**, 397.
- Nikitin, E. E., 1965, *J. Chem. Phys.* **43**, 744.
- Nikitin, E. E., and B. M. Smirnov, 1978, *Usp. Fiz. Nauk* **124**, 201 (Sov. Phys.—Usp. **21**, 95).
- Ny, T. Z., and S. Y. Ch'en, 1937a, *Phys. Rev.* **51**, 567.
- Ny, T. Z., and S. Y. Ch'en, 1937b, *Phys. Rev.* **51**, 1158.
- Ny, T. Z., and S. Y. Ch'en, 1938, *Phys. Rev.* **54**, 1045.
- Oldenberg, O., 1928, *Z. Phys.* **74**, 184.
- Oldenberg, O., 1929, *Z. Phys.* **55**, 1.
- O'Malley, T. F., 1963, *Phys. Rev.* **130**, 1020.
- O'Mara, B. J., 1976, *Mon. Not. R. Astron. Soc.* **177**, 551.
- Omont, A., 1977, *J. Phys. (Paris)* **38**, 1343.
- Omont, A., E. W. Smith, and J. Cooper, 1972, *Astrophys. J.* **175**, 185.
- Omont, A., E. W. Smith, and J. Cooper, 1973, *Astrophys. J.* **182**, 283.
- O'Neill, J. A., and G. Smith, 1980a, *Astron. Astrophys.* **81**, 100.
- O'Neill, J. A., and G. Smith, 1980b, *Astron. Astrophys.* **81**, 108.
- Ottinger, Ch., R. Scheps, G. W. York, and A. Gallagher, 1975, *Phys. Rev. A* **11**, 1815.
- Pagel, B. E. J., 1971, *J. Phys. B* **4**, 279.
- Palmer, B. A., R. A. Keller, and R. Engleman, Jr., 1980, *An Atlas of Uranium Emission Intensities in a Hollow Cathode Discharge*, LA-8251-MS (Los Alamos Scientific Laboratory, Los Alamos).
- Palmer, E. W., M. Chutley, A. Franks, J. F. Verrill, and G. Gale, 1975, *Rep. Prog. Phys.* **38**, 975.
- Papoulis, A., 1962, *The Fourier Integral and Its Application* (McGraw-Hill, New York), p. 246.
- Parsons, R. G., and V. G. Weisskopf, 1967, *Z. Phys.* **202**, 492.
- Pascale, J., 1977, *J. Chem. Phys.* **67**, 204.
- Pascale, J., and J. Vandéplanque, 1974, *J. Chem. Phys.* **60**, 2278; also unpublished tables of alkali—noble-gas potentials.
- Peach, G., 1978, *J. Phys. B* **11**, 2107.
- Phillipe, M., F. Masnou-Seeuw, and P. Valiron, 1979, *J. Phys. B* **12**, 2493.
- Pierluissi, J. H., P. C. Vanderwood, and R. B. Gomez, 1977, *J. Quant. Spectrosc. Radiat. Transfer* **18**, 555.
- Ramsey, J. V., 1970, *Sol. Phys.* **12**, 492.
- Raymer, M. G., and J. L. Carlsten, 1977, *Phys. Rev. Lett.* **39**, 1326.
- Raymer, M. G., J. L. Carlsten, and G. Pichler, 1979, *J. Phys. B* **12**, L119.
- Reichel, A., 1968, *J. Quant. Spectrosc. Radiat. Transfer* **8**, 1601.
- Rhodes, Ch. K., 1979, *Excimer Lasers* (Springer, Berlin).
- Robin, S., and S. Robin, 1957a, *C. R. Acad. Sci.* **244**, 2375.
- Robin, S., and S. Robin, 1957b, *C. R. Acad. Sci.* **245**, 1056.
- Roesler, F. L., 1974, "Fabry-Perot instruments for astronomy" in *Astrophysics, Part A: Optical and Infrared, Methods of Experimental Physics 12*, edited by L. Marton (Academic, New York), p. 531.
- Roesler, F. L., 1980, private communication.
- Rostas, F., 1981, "Alkali-rare gas excimers", in *Proceedings of the 5th International Conference on Spectral Line Shapes*, edited by B. Wende (de Gruyter, Berlin).
- Rostas, F., and J. L. Lemaire, 1971, *J. Phys. B* **4**, 555.
- Roueff, E., 1970, *Astron. Astrophys.* **7**, 4.
- Roueff, E., 1972, *J. Phys. B* **5**, L79.
- Roueff, E., 1974, *J. Phys. B* **7**, 185.
- Roueff, E., 1975, *Astron. Astrophys.* **38**, 41.
- Royer, A., 1971a, *Phys. Rev. A* **3**, 2044.
- Royer, A., 1971b, *Phys. Rev. A* **4**, 499.
- Royer, A., 1978, *Acta Phys. Pol. A* **54**, 805.
- Royer, A., 1980, *Phys. Rev. A* **22**, 1625.
- Ruhmkorf, H. A., 1938, *Ann. Phys. (Leipzig)* **33**, 21.
- Sahal-Brechot, S., 1969, *Astron. Astrophys.* **1**, 91.
- Sando, K. M., 1974, *Phys. Rev. A* **9**, 1103.
- Sando, K. M., G. J. Erickson, and R. C. Binning, Jr., 1979, *J. Phys. B* **12**, 2697.
- Sando, K. M., and J. Wormhoudt, 1973, *Phys. Rev. A* **7**, 1889.
- Saxon, R. P., R. E. Olson, and B. Liu, 1977, *J. Chem. Phys.* **67**, 2692.
- Sayer, B., M. Ferray, and J. Lozingot, 1979, *J. Phys. B* **12**, 227.
- Sayer, B., M. Ferray, J. P. Visticot, and J. Lozingot, 1980, *J. Phys. B* **13**, 177.
- Sayer, B., J. P. Visticot, and J. Pascale, 1978, *J. Phys. (Paris)* **39**, 361.
- Scheps, R., and A. Gallagher, 1976, *J. Chem. Phys.* **65**, 859.
- Scheps, R., Ch. Ottinger, G. York, and A. Gallagher, 1975, *J. Chem. Phys.* **63**, 2581.
- Schuessler, H. A., K. J. Dietz, P. Dabkiewicz, H. J. Kluge, and T. Kühl, 1981, "Pressure broadening and pressure shift of the cadmium intercombination line," in *Proceedings of the 5th International Conference on Spectral Line Shapes*, edited by B. Wende (de Gruyter, Berlin).
- Schuhmann, L., D. Wildman, and A. Gallagher, 1980, *J. Chem. Phys.* **72**, 6081.
- Schuller, R., and W. Behmenburg, 1974, *Phys. Rep.* **12**, 273.
- Seaton, M., 1958, *Mon. Not. R. Astron. Soc.* **118**, 504.
- Shakeshaft, R., 1972, *J. Phys. B* **5**, 559.
- Sidell, N., and S. Y. Ch'en, 1977, *J. Quant. Spectrosc. Radiat. Transfer* **17**, 117.
- Simons, G., 1974, *J. Chem. Phys.* **60**, 645.
- Smalley, R. E., D. A. Auerbach, P. S. H. Fitch, D. H. Levy, and L. Wharton, 1977, *J. Chem. Phys.* **66**, 3778.
- Smirnov, B. M., 1967, *Sov. Phys.—JETP* **24**, 314.
- Smith, B., and B. S. Collins, 1976, *J. Phys. B* **9**, L117.
- Smith, E. W., J. Cooper, and L. J. Roszman, 1973, *J. Quant. Spectrosc. Radiat. Transfer* **13**, 1523.
- Smith, E. W., J. Cooper, and C. R. Vidal, 1969, *Phys. Rev.* **185**, 140.
- Smith, E. W., C. R. Vidal, and J. Cooper, 1969a, *J. Res. Natl. Bur. Stand. Sect. A* **73**, 389.
- Smith, E. W., C. R. Vidal, and J. Cooper, 1969b, *J. Res. Natl. Bur. Stand. Sect. A* **73**, 405.
- Smith, G., 1972, *J. Phys. B* **5**, 2310.
- Smith, G., 1975, *J. Phys. B* **13**, 2273.
- Smith, G., and D. St. J. Raggett, 1981, *J. Phys. B* **14**, 4015.
- Snow, W. L., 1976, Ph.D. thesis (West Virginia University) (unpublished).

- Speer, D. T., S. Von Laven, A. H. Karp, and M. Stocton, 1980, *Appl. Opt.* **19**, 2757.
- Spielfiedel, A., D. Gilbert, E. Roueff, and F. Rostas, 1979, *J. Phys. B* **12**, 3693.
- Spitzer, L., 1940, *Phys. Rev.* **58**, 348.
- Stacey, D. N., and J. Cooper, 1971, *J. Quant. Spectrosc. Radiat. Transfer* **11**, 1271.
- Stoicheff, B. P., and E. Weinberger, 1980, *Phys. Rev. Lett.* **44**, 733.
- Szudy, J., 1979, "Quasimolecular treatment of pressure broadening," an invited paper given at the Colloque sur l'influence des processus collisionnels sur le profil des raies spectrales (Orleans) (unpublished).
- Szudy, J., and W. E. Baylis, 1975, *J. Quant. Spectrosc. Radiat. Transfer* **15**, 641.
- Szudy, J., and W. E. Baylis, 1977, *J. Quant. Spectrosc. Radiat. Transfer* **17**, 681.
- Takeo, M., 1970, *Phys. Rev. A* **1**, 1143.
- Tam, A. C., and G. W. Moe, 1976, *Phys. Rev. A* **14**, 528.
- Tan, D. K. L., and S. Y. Ch'en, 1970, *Phys. Rev. A* **2**, 1124.
- Teachout, R. R., and R. T. Pack, 1971, *At. Data* **3**, 195.
- Thomann, P., K. Burnett, and J. Cooper, 1980, *Phys. Rev. Lett.* **45**, 1325.
- Thorne, A. P., 1974, *Spectrophysics* (Chapman and Hall, London), p. 193.
- Traving, G., 1960, *Über die Theorie der Druckverbreiterung von Spektrallinien* (G. Braun, Karlsruhe).
- Tull, R. G., J. P. Choisser, and E. H. Snow, 1975, *Appl. Opt.* **14**, 1182.
- Unsöld, A., 1968, *Physik der Sternatmosphären* (Springer, Berlin), p. 269.
- Vallée, O., P. Ranson, P. Combis, and J. Chapelle, 1977, *J. Phys. B* **10**, L589.
- Vaughan, J. M., and G. Smith, 1968, *Phys. Rev.* **166**, 17.
- Visticot J. P., J. Szudy, M. Ferray, and B. Sayer, 1981, *J. Phys. B* **14**, 4755.
- Visticot, J. P., J. Szudy, and B. Sayer, 1981, *J. Phys. B* **14**, 2329.
- Vogt, S. S., R. G. Tull, and P. Kelton, 1978, *Appl. Opt.* **17**, 574.
- Voslamber, D., 1969, *Z. Naturforsch. Teil A* **24**, 1458.
- Walkup, R. E., A. Spielfiedel, and D. E. Pritchard, 1980, *Phys. Rev. Lett.* **45**, 986.
- Wang, S. Y., and S. Y. Ch'en, 1979, *J. Quant. Spectrosc. Radiat. Transfer* **22**, 87.
- Ward, J., J. Cooper, and E. W. Smith, 1974, *J. Quant. Spectrosc. Radiat. Transfer* **14**, 555.
- Weber, E. W., 1979, *Phys. Rev. A* **20**, 2278.
- Weber, E. W., 1981, "Collision studies of H-alpha fine structure lines with high resolution laser spectroscopy," in *Proceedings of the 5th International Conference on Spectral Line Shapes*, edited by B. Wende (de Gruyter, Berlin).
- Weber, E. W., and K. Jungman, 1981, *Phys. Lett. A* **81**, 223.
- Weber, K. H., and K. Niemax, 1979a, *Opt. Commun.* **28**, 317.
- Weber, K. H., and K. Niemax, 1979b, *Opt. Commun.* **31**, 52.
- Webster, C. R., and F. Rostas, 1978, *Chem. Phys. Lett.* **59**, 57.
- Weisskopf, V., 1932a, *Z. Phys.* **75**, 287.
- Weisskopf, V., 1932b, *Z. Phys.* **77**, 398.
- Weisskopf, V., 1933, *Phys. Z.* **34**, 1 [translated in *Atomic Spectra*, by W. R. Hindmarsh (Pergamon, London), p. 328].
- Weller, W., W. Herbst, and S. Jeffers, 1977, *Publ. Astron. Soc. Pac.* **89**, 935.
- West, W. P., and A. Gallagher, 1978, *Phys. Rev.* **17**, 1431.
- West, W. P., P. Shuker, and A. Gallagher, 1978, *J. Chem. Phys.* **68**, 3864.
- Whiting, E. E., 1968, *J. Quant. Spectrosc. Radiat. Transfer* **8**, 1374.
- Wilson, A. D., and Y. Shimoni, 1975, *J. Phys. B* **8**, 2415.
- Yabuzaki, T., A. C. Tam, S. M. Curry, and W. Happer, 1978, *Phys. Rev. Lett.* **41**, 543.
- Yelnik, J. B., and D. Voslamber, 1979, *Astrophys. J.* **230**, 184.
- York, G., R. Scheps, and A. Gallagher, 1975, *J. Chem. Phys.* **63**, 1052.